The synthesis and characterisation of water soluble polymers and biomimetic applications.

Megson, Joanna Louise

The Synthesis and Characterisation of Water Soluble Polymers and Biomimetic Applications.

by

Joanna Louise Megson

A thesis submitted for the Degree of Doctor of Philosophy to the

University of Durham

September 1997

ABSTRACT

The Synthesis and Characterisation of Water Soluble Polymers and their Biomimetic Applications.

The first steps towards the long term objective of building entirely synthetic organic/inorganic composite materials in a biomimetic manner have been achieved. Following an introduction and discussion of the background to the work (Chapter 1), the syntheses and characterisation of various molecular weights of both poly(*exo,exo*-1,4-cyclopentenylene-5,6-ethylidene-2,3-sodium dicarboxylate) and poly(*exo,endo*-1,4-cyclopentenylene-5,6-ethylidene-2,3-sodium dicarboxylate) and model compounds of their repeat units have been described (Chapters 2 and 4). These compounds were used as additives in the crystallisation of $CaCO_3$ from supersaturated aqueous solutions of $Ca(HCO_3)_2$ (Chapters 3 and 5). The work described in Chapter 3 showed that the diacid model compounds used as additives controlled the morphology of calcite crystals grown from supersaturated solutions of $Ca(HCO_3)_2$ over a large range of concentrations of model compound; $[Ca^{2+}]$: [model compound] 10 to 1000:1. The polymers of these monomers appeared to give the same type of crystal morphology as the isolated model repeat units, however, modification was observed on only one face of the $CaCO_3$ crystals. This observation, and the relatively small crystal size distributions measured, indicated that the calcite crystallisation was nucleated beneath the polymer films at the truncated modified face and growth continued down into the solution.

ACKNOWLEDGEMENTS

There are so many people whom I wish to thank for helping me through the last three years. Firstly, my supervisor, Jim Feast, to whom I am indebted for his guidance, patience, English lessons and general pearls of wisdom! Thank you Jim. I must also mention Brigid Heywood, my mentor whilst at Keele, whose enthusiasm, encouragement and patience contributed to my enjoyment during the task of trying to understand crystal chemistry! My work would have progressed much more slowly without her help. Thank you also to Steve Rannard, my supervisor from Courtaulds, for the enthusiasm he showed, even when, at first, results were a little slow in appearing! The financial support from Courtaulds is also very much acknowledged.

In the early days both Erwin Herzog and David Snowden really helped me out in the lab. Thankyou also to; Ezat Khosravi who made the initiator used in this work, Alan Kenwright and Julia Say for all the help with NMR spectrometry, Gordon Forrest for carrying out GPC characterisation, Gordon Haswell and Ray Hart the master glass blowers, Stuart Williams and other members of the crystal science group at Keele for help with crystal characterisation, Joe Peel and Jimmy Lincoln in the stores and Hazel and Jean for keeping the environment immaculate and for the chats.

To people in the IRC, the "girlies", the "foreign contingency" and the "lads", you're all lovely, I cannot imagine working in a more friendly, supportive atmosphere.

Thank you also to my personal physio, Sharon for proof reading my thesis and for being the most caring lodger in the world! Thank you to my wonderful

parents for the love, support and encouragement that they have always shown throughout my 25 years of education, without you I would not have achieved anything. Also to my gifted brother, J.C., who has the ability of making the sun glow on the dreariest of days, I love you all. Finally, to Bas, who over the last three years and especially over the last few months has done everything for me except for doing my Ph.D! What more can I say? "Ik hou van jou" perhaps.

MEMORANDUM

The work reported in this thesis was carried out in the chemistry laboratories of the Interdisciplinary Research Centre in Polymer Science and Technology, Durham University and the chemistry laboratories of the Crystal Science Group in Keele. This work has not been submitted for any other degree and is the original work of the author except where acknowledged by references.

Aspects of the work have been presented by the author at the following meetings:

ISOM 11, University of Durham, July, 1995.

ISOM 12, St. Augustine, Florida, July, 1997.

COPYRIGHT

ABBREVIATIONS, ACRONYMNS AND SYMBOLS

( )	Crystal face
{ }	Set of crystal faces
FTIR	Fourier Transform Infrared Spectrometry
br	broad
s	strong
m	medium
w	weak
Model compound	Compound used as a model of the repeat units of the polymers
PDI	Polydispersity index
PEO	Poly(ethylene oxide)
Poly 1S	Starting polymer of monomer 1, poly(*exo.exo*-bicyclo [2.2.1] hept-5-ene-2,3-dicarboxylic acid dimethyl ester), highest Mn (182,000)
Poly 1P	Precursor to final polymer, monomer 1 poly(*exo,exo*-1,4-cyclopentenylene-5,6-ethylidene-2,3-dicarboxylic acid dimethyl ester), highest Mn
Poly 1F	Final polymer of monomer 1, poly(*exo,exo*-1,4-cyclopentenylene-5,6-ethylidene-2,3-sodium dicarboxylate). highest Mn
Poly 1S''	Starting polymer of monomer 1, lowest Mn (6,000).
Poly 1S'	Starting polymer of monomer 1, middle Mn (71,400)
ROMP	Ring Opening Metathesis Polymerisation.

CONTENTS

Appendices -

Appendix A - ^{1}H NMR spectra

Appendix B - ^{13}C NMR spectra

Appendix C - FTIR spectra

Appendix D - GPC traces

Appendix E - Crystallographic data

Appendix F - Calcite crystal data

Colloquia Attended

CHAPTER 1

An Introduction to Biomineralisation, Biomimetics and Ring Opening Metathesis Polymerisation

1.1 GENERAL INTRODUCTION

Natural inorganic/organic composites serve a variety of functions and are frequently remarkable materials (*e.g.* bones, teeth, endo- and exo-skeletons). One of the mechanisms by which they are believed to be produced involves the deposition of a polymer matrix which is subsequently covered with mineral. A question which this study begins to address is the possibility of building entirely synthetic organic/inorganic composite materials in an analogous way. In order to be successful in synthetically mimicking these natural composites it is necessary to obtain an understanding of the mechanisms of mineral deposition in biological systems. This topic, biomineralisation, is introduced in the following section, along with a review of the field of biomimetics.

1.2 BIOMINERALISATION AND BIOMIMETICS

1.2.1 Biomineralisation and Biomimetics

A vast array of organisms form minerals both extracellularly and intracellularly.[1] More than 60 different inorganic solids formed in such processes have been identified.[2] The major types and functions of biominerals are summarised in Table 1.2.1. The most abundant mineral is calcium carbonate which is found as calcite, aragonite, vaterite, monohydrocalcite or amorphous calcium carbonate.[3] Calcite and aragonite are a major constituent of many shells. Calcium phosphate, in the form of hydroxyapatite ($Ca_{10}(PO_4)_6(OH)_2$), forms a large proportion of bones and teeth in vertebrates. In bones, teeth and shells the minerals are in combination with a complex organic macromolecular matrix of proteins, polysaccharides, lipids and their combinations such as glycoproteins.

Mineral	Formula	Organism/ function
Calcium carbonate:		
Calcite	$CaCO_3$	Mollusc/ exoskeleton
		Algae/ exoskeletons
		Trilobites/ eye lens
Aragonite	$CaCO_3$	Fish/ gravity device
		Molluscs/ exoskeleton
Vaterite	$CaCO_3$	Ascidians/ spicules
Amorphous	$CaCO_3.nH_2O$	Plants/ Ca store
Calcium phosphate:		
Hydroxyapatite	$Ca_{10}(PO_4)_6(OH)_2$	Vertebrates/ endoskeletons
		teeth, Ca store
Octa-calcium phosphate	$Ca_8H_2(PO_4)_6$	Vertebrates/ precursor phase in bone?
		Mussels/ Ca store
Amorphous	?	Vertebrates/ precursor phase in bone?
Calcium oxalate:		
Whewellite	$CaC_2O_4.H_2O$	Plants/ Ca store
Weddellite	$CaC_2O_4.2H_2O$	Plants/ Ca store
Group IIA metal sulphates:		
Gypsum	$CaSO_4$	Jellyfish larvae/ gravity device
Barite	$BaSO_4$	Algae/ gravity device
Celestine	$SrSO_4$	Acantharia/ cellular support
Silicon dioxide:		
Silica	$SiO_2.nH_2O$	Algae/ exoskeleton
Iron oxides:		
Magnetite	Fe_3O_4	Bacteria/ magnetotaxis
		Chitons/ teeth
Goethite	α-FeO(OH)	Limpets/ teeth
Lepidocrocite	γ- FeO(OH)	Chitons/ teeth
Ferrihydrite	$5Fe_2O_3.9H_2O$	Animals and plants/
		Fe storage proteins

Table 1.2.1. The types and functions of the main inorganic solids found in biological systems, after Mann.[2]

Other extensively formed biogenic minerals are opal ($SiO_2.xH_2O$) which is used in invertebrate exoskeletons, of diatoms for example, and ferrihydrite ($5Fe_2O_3.9H_2O$), the mineral formed in ferritin during iron storage.

The process of biomineral deposition can be classified as either *biologically induced* or *biologically controlled.* The former process occurs in some bacterial

species and various green and brown algae. It is characterised by bulk extracellular and/or intercellular mineral formation without the use of organic matrices. The resulting mineral phases have crystal habits similar to those produced by precipitation from inorganic solutions. The second process is a matrix-mediated process and is found in plants and animals where, in general, the formation of crystals is regulated more closely by the organism. These materials are organic/inorganic composites that often exhibit order at the nanometer scale. In this instance crystal nucleation, phase, morphology and growth are directed by the organic biopolymers and interfacial molecular processes. Usually the inorganic phase is crystalline, in which case the sub units have preferred orientations and unusual shapes and sizes. There is much interest in understanding the mechanisms of biologically controlled mineralisation as the range of control over mineral growth exhibited is desirable for materials engineering.[4] Two particularly extensively studied examples are human bone and mollusc shells.

Human compact bone will be the first natural composite to be discussed. On the microstructural level (~200μm diameter) of this hierarchical material are osteons. These are hollow fibres composed of concentric lamellae and pores. The lamellae are built from fibres which are made up of many fibrils. There are ellipsoidal and cylindrical pores within the osteons. The ellipsoidal pores, lancunae, provide space for the osteocytes, the living cells of the bone and the cylindrical pores, Haversian canals, contain blood vessels which nourish the tissue. Canaliculi are fine channels radiating from the lancunae. At the

nanoscale the fibrils are an inorganic/organic composite of hydroxyapatite and the protein, collagen [Fig. 1.2.1].

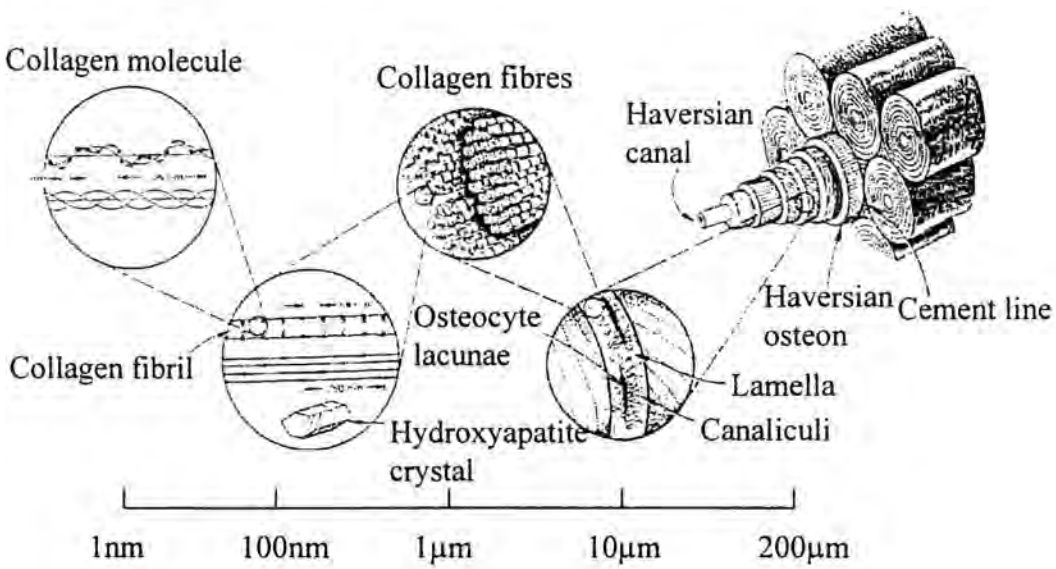

Fig. 1.2.1. The hierarchical structure of compact bone, after Lakes.[4]

The collagen molecule which is approximately 300nm long and 1.5nm in diameter contains three chains of amino acids which form a 'rope like' triple helical structure. The polypeptides are rich in glycine, proline, hydroxyproline and alanine; the small glycine residues at every third amino acid residue allow close packing of the polypeptides.

As the platelike calcium phosphate crystals, which are formed within the fibrils of collagen, are extremely small (~45nm x 20nm x 3nm) the overall ultrastructure of bone is complex. Determining the precise orientation of the crystals with respect to the matrix is a very difficult task. Mineralised tendons of large land birds are better organised and more easily studied. To date, most information on apatite/collagen interactions have come from this source.[1] The

collagen found in calcified turkey tendon is similar to that of compact bone although the exact fidelity of the comparison is unknown. The strongest intermolecular attractions between triple helical molecules occur when the neighbouring molecules are shifted by ~68nm. A widely accepted model for the structure of collagen within a fibril is the quarter staggered model [Fig. 1.2.2].[2] In this arrangement the collagen molecule is separated into five zones, four of the zones are equal in length (~68nm) and one is shorter (~28nm). On stacking the molecules in the staggered arrangement the resulting holes which occur between the ends of the molecules are of the dimensions 30-40nm x 3-5nm, these are shown in Fig. 1.2.2, the position being marked as a 'Hole zone'. Several models of the collagen fibril arrangement predict that grooves are organised in parallel rows at the same height as the fibrils. As the hydroxyapatite crystals have the dimension of ~45nm x 20nm x 3nm they can fit into the "slot like" hole zones with the *a* axis of the crystal perpendicular to the long fibre axis of the collagen fibrils and the *c* axis parallel to it.[5]

It is thought that the function of the hydrophobic, collagen matrix is to provide the spatial architecture, via the formation of holes and grooves, for the crystallisation of hydroxyapatite and that hydrophilic constituents, such as glyco and phospho proteins are responsible for the control of mineral nucleation. This concept for the construction of organic/inorganic composite materials using an essentially 'inert' framework macromolecule working in contact with water soluble macromolecules which determine the structure of the mineral to be inserted into the inert framework has been applied to a range of biomineralised

structures. Much of the present information comes from investigations on mollusc shells.

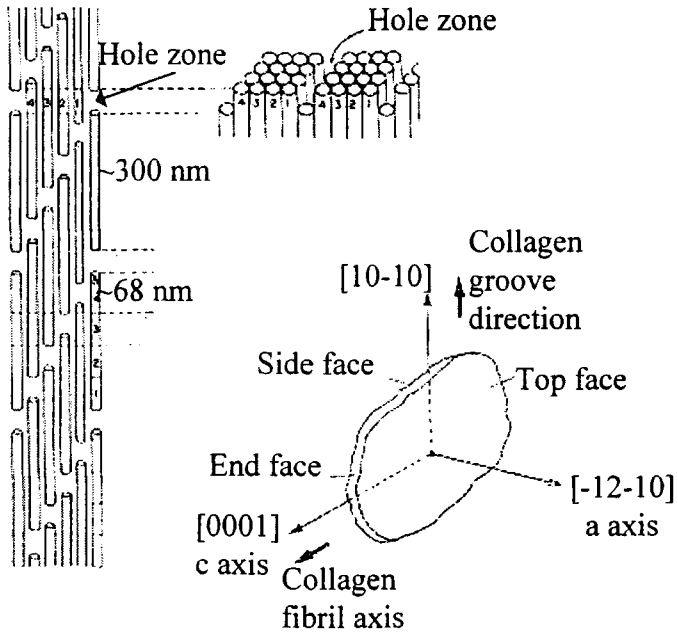

Fig. 1.2.2. A diagram showing the relationship between the crystallographic properties of calcium phosphate crystals of bone and the collagen fibrils, after Mann[2] and Weiner.[1]

The nacreous layers of bivalves, gastropods and the cephalopod *Nautilus* have been studied extensively. The inner layers of these shells consist of polygonal blocks, usually six sided, of aragonite sandwiched between thin sheets (30-300nm) of a protein-polysaccharide organic matrix.[2] The organic component of the composite constitutes between 1 and 5% of the weight of the dry shell. Two main types of macromolecule are present in these structures, the framework organic matrix and water soluble acidic macromolecules. The sheets within the framework structure of many of these mollusc shells have a thin core layer of the

polysaccharide, β-chitin sandwiched between two layers of silk fibroin-like proteins. The protein layers are rich in the amino acids, glycine and alanine and are hydrophobic. The conformation adopted is that of an antiparallel, β-pleated sheet and the chains lie perpendicular to the long axis of the chitin fibrils giving a three layer "plywood" structure. The acidic, hydrophilic proteins can be divided into at least two categories, those rich in aspartic acid, associated with small amounts of polysaccharide and those rich in serine and glutamic acid which are often associated with relatively large amounts of polysaccharides. The acidic macromolecules are present in the surface layers of the matrix sheets.

For a given species the thickness of the aragonite crystals is remarkably uniform ranging from 0.4 - 1.2μm. It is thought that the thickness is determined by the location of a prepositioned matrix layer with acidic macromolecules on the surface which act to inhibit the crystal growth. The diameters of the crystal polygons are much more variable and a large range is observed within a single mineral layer. This could indicate a lack of control of crystal growth parallel to the polymer sheets. However, the boundaries between the polygons are linear and smooth.[6] This is in contrast to the boundaries between calcite crystals in formaniferal shells where the interface is serrated or sinuous suggesting that intergrowth between crystals has occurred. This is evidence of some degree of control in the horizontal direction of the aragonite crystals in the nacre. It has been observed by the use of SEM and TEM that the *c* axes of the aragonite crystals lie perpendicularly to the plane of the organic sheets. The alignment of the *a* and *b* axes with respect to the matrix sheets depends upon the species considered. In the gastropod, no preferred orientation occurs between the *a* and *b*

axes and the chitin fibrils or protein chains, whereas the orientation is virtually perfect in the bivalves, *Pinctada magaratifera* and *Neotrigonia magaratifera*, such that the X-ray diffraction pattern is close to that of a single crystal. Figure 1.2.3a. shows an SEM micrograph of the aragonitic layer of the bivalve *Mytilus californianus* the orientation of the *a* and *b* axes are barely discernible. It may be inferred from the above information that crystal nucleation is well controlled by the organic matrix. The specific spatial relations between the core macromolecules and the *c* axes and in some cases the *a* and *b* axes of the associated crystals strongly suggests that nucleation is an epitaxial process. It can also be concluded that nucleation occurs at specific sites on the matrix surface. Perhaps the best evidence being the 'stack-of-coins' mode of growth of the gastropod nacre in which, as the name suggests, the aragonite crystals have the appearance of coins stacked vertically with gradually decreasing diameter giving a conical shape with the smaller more immature crystals at the top.

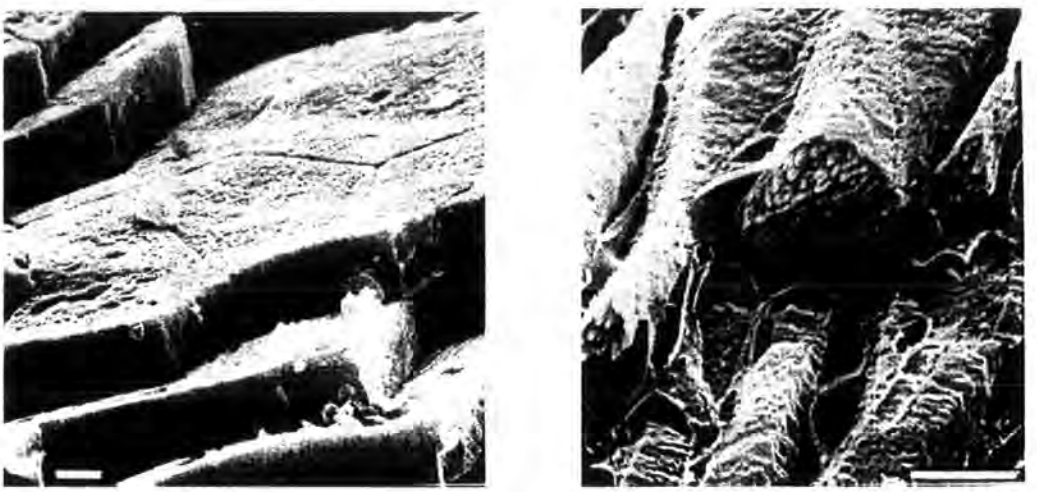

a. b.

Fig. 1.2.3. Scanning electron micrographs showing the two forms of calcium carbonate found in the shell of the mollusc *Mytilus californianus*. a. aragonitic layer. b. calcitic layer. Scale bar = 1×10^{-6}m.

This structure is a result of the fact that nucleation of crystals occurs in successive layers at the same location. A speculative discussion of the nucleation site is given by Weiner and Traun[7] in which it is proposed that acidic proteins are constituents of the nucleation site. These adopt the β-sheet conformation and bind calcium in such a way as to induce oriented aragonite crystals to form by epitaxy.

Evidence for the control of inorganic crystallisation by organic macromolecules in mollusc shell deposition has been obtained independently by two groups. Work carried out in a collaboration between Stucky and Mann *et al.* [8 9 10] consisted of inserting preformed discs *e.g.* glass cover slips and mica discs, between the mantle and shell of the gastropod *Halitotis references* (Red Albanone) for measured periods of time, removal of the discs and analysis of the mineral deposition. The deposition of the mineral which leads to the formation of 'flat pearls' was analogous to the process which occurs within the shell. An organic sheet was initially laid down on the disc followed by the growth of calcite layers with preferred {104} orientation, followed by the growth of the nacreous aragonite. Significant observations from this work were that mineralisation occurred on all abiotic substrates only after the deposition of an organic macromolecular layer and that the calcite-aragonite transition was always abrupt. *In vitro* calcium carbonate growth experiments, with $CaCO_3$ grown from supersaturated $Ca(HCO_3)_2$ solution, revealed that a similar calcite-aragonite transition could be induced on discs having nucleated protein layers, by the addition of soluble proteins extracted from the aragonitic and calcitic layers.[10] Analogous observations were made by Falini and Weiner,[11] who found that

macromolecules extracted from the aragonitic shell layers of molluscs induced aragonite formation *in vitro* when preadsorbed in a substrate of β-chitin and silk fibroin protein. Water soluble macromolecules from calcite shell layers induced mainly calcite under the same conditions. Work carried out by both groups indicates that the framework macromolecule is necessary for controlled crystallisation but it is the acidic macromolecules which are responsible for the precipitation of aragonite or calcite.

In addition to the use of living organisms and biomolecules to mimic biological processes, scientists are using biological concepts as inspiration for new ideas in the synthesis of organic/inorganic composite materials. The aim of these studies is to synthesise materials with controlled properties, such as uniform particle size, polymorph selectivity, tailored morphology, oriented nucleation and organised assembly.

Biomineralisation can be viewed as four separate constructional processes, as described by Mann;[12] supramolecular preorganisation, interfacial molecular recognition, vectorial processing and cellular processing. Before discussing the work undertaken in the field of materials chemistry the stages of biomineralisation will be described .

The first stage involves the construction of an organised reaction environment. This can be in the form of lipid vesicles *e.g.* coccolith mineralisation in marine algae,[12] magnetite deposition in magnetotactic bacteria[13] and mineralisation within the spherical cages of the iron storage protein, ferritin.[1] The alternative reaction environment is a protein/polysaccharide matrix *e.g.* in bone[1] and mollusc

shells[6] where *in situ* mineralisation of the polymers result in host-guest composites.[14]

The controlled nucleation of inorganic clusters from aqueous solutions is the second constructional stage in biomineralisation. The nucleation occurs within the confines of the preformed organic supramolecular assemblies. It is generally accepted that the preorganised architectures have functional surfaces which affect the nucleation of the mineral phase. In order to induce nucleation the surfaces of the organic phase must either lower the activation energy of nucleation or influence the collision frequency between the organic and inorganic components. One possible way in which this could occur is by chemical complementarity. It has been observed that carbonate and phosphate minerals tend to be associated with carboxylate rich (aspartate, glutamate) and phosphorylated (phosphoserine) proteins respectively *eg.* in mollusc shell and bone. It is possible that functional groups on these polymers can mimic the oxyanion stereochemistry and cation coordination geometry of certain mineral surfaces and induce nucleation on specific crystal planes.

The third stage of biomineralisation involves the assembly of the mineral phase with vectorial regulation of crystal growth and termination. The final stage is associated with a variety of constructional processes involving larger scale cellular activity and the production of higher-order architectures with elaborate ultra and microstructural properties. This area of biomineralisation is probably the most difficult to mimic due to the complexity of the static and dynamic processes used in nature.

There are four main types of synthetic preorganised reaction environments currently used by materials chemists working in the field of biomimetics *i.e.* vesicles[15,16] and protein cages, monolayers,[17 18 19 20] microemulsions[21 22] and gels, and polymeric films. The presence of water soluble organic additives is also known to have significant effect upon the morphology of crystals grown from supersaturated solutions. Work published in 1990 by Mann *et al.* discusses the effect of additives on calcite crystal growth from supersaturated bicarbonate solutions.[23] The molecules investigated had the structure $^{-}O_2C(CH_2)_nCO_2^{-}$ where n = 1-7, the effect of the unsaturated molecules, maleate and fumarate were also examined. It was observed that crystals of $CaCO_3$ grown with malonate, $^{-}O_2C(CH_2)CO_2^{-}$, as additive were modified at $[Ca^{2+}]$:[additive] molar ratios between 2-8:1. At these concentrations the calcite crystals appeared rounded in the direction parallel to the c-axis [001] faces. At higher concentration (2-3:1) the crystals exhibited a spindle shaped morphology. On increasing the length of the aliphatic chain the morphological effect was significantly reduced. On addition of maleate, $^{-}O_2C(CH)_2CO_2^{-}$, the effect upon crystal morphologies appeared to be the same as observed with malonate as additive, only to a lesser extent. Fumarate had no influence on the morphology of calcite. It was concluded from this that an increased conformational freedom led to a greater morphological change. Both maleate and malonate had a desired geometrical match between functional group distance and the ions in the modified faces, *i.e.* 4 Angstrom distances. The larger effect of malonate was attributed to the fact that it is more flexible than maleate, thus increasing the ability of the molecule to adopt a suitable stereochemical match to the carbonate anions of the modified

face. Work discussed later in this thesis disputes this argument as the effect of the more rigid 1,2-dicarboxylate monomers investigated in this work on the morphology of $CaCO_3$ crystals was much greater than that discussed above and occurred at much lower concentrations of additive, ranging from $[Ca^{2+}]$:[additive] 1000:1 - 10:1.

Over the last few years studies carried out by Mann and Heywood on mineral deposition beneath Langmuir monolayers have shown that monolayers are capable of inducing the nucleation and growth of the inorganic phase. The advantage of surfactant monolayers is that they act as two dimensional organised templates whose dimensions may be altered at will by compression of the molecules at the air/water interface on a Langmuir trough. The monolayers are formed by insoluble amphiphilic molecules which self assemble at the air-solution interface.[17] The effects of changing the headgroup, polarity and packing conformations of the amphiphiles on the crystallisation of minerals has been investigated.[24] A mineral grown extensively in these studies is $CaCO_3$, which is usually grown from a supersaturated solution of $Ca(HCO_3)_2$.[19] These studies have shown that the choice of headgroup used can determine the polymorph of crystals grown. When crystallisation of $CaCO_3$ was carried out beneath a neutral octadecanol monolayer mineralisation was inhibited, whilst neutral cholesterol layers gave similar results to those observed in control experiments with no monolayer. The negatively charged stearate monolayer induced oriented calcite and vaterite formation depending upon the concentration of the $Ca(HCO_3)_2$ solution, 9mmol dm^{-3} giving calcite and 4.5mmol dm^{-3} giving vaterite. Positively charged octadecylamine monolayers gave vaterite. In more recent work

phosphonate and sulphate functionalised *n*-alkyl monolayers gave different crystallographic orientations. This was attributed to stereochemical complementarity between monolayer and mineral.[19]

Recently, microemulsions have been used as templates for mineralisation resulting in control of structure on the mesoscopic scale. The approach carried out by Ozin *et al.* has been to grow alumino phosphates within microemulsions of alkyl ammonium surfactants in tetraethylene glycol.[21 25] The resulting inorganic spheres exhibit various surface structures which are described as bowl like, honeycomb and quilted and are attributed to a 'vesicle type' templating which occurs within the microemulsion. A complementary strategy used by Mann *et al.* is the growth of calcium phosphate in the nanometer sized water conduits of frozen oil/water emulsions. The oils used were dodecane, tetradecane and hexadecane.[22 26 27] Reticulated frameworks of calcium phosphates were constructed, however, little or no control was observed on a smaller scale.

The use of polymers as organised reaction environments has been studied by various groups. The approach that Brisdon took was to mediate crystallisation of inorganic solids from cross-linked polymer films. The crystallisation of $CaCO_3$ from supersaturated solutions of $Ca(HCO_3)_2$ has been carried out in the presence of functionalised and unfunctionalised polysiloxane membrane films mounted on glass rods.[28 29] Yields of $CaCO_3$, in the form of calcite, were significantly greater on the functionalised membranes *e.g.* esters, ethers and fluoroaromatic groups. It was concluded that the polymer films were reducing the activation energy to calcite nucleation. The disadvantage of this approach was reported to be that the catalysts used in the polymer synthesis could not be fully removed and may have

had an influence on the crystallisation observed. Bianconi *et al.* undertook similar experiments in which sheets of PEO were used in attempts to control the crystallisation of CdS.[30] In this work CdS was grown on the polyethylene oxide film giving spherical particles, however, the aggregation and lack of orientation of the mineral phase indicated a lack of controlled nucleation. Another piece of work, by Falini *et al.*, involved the crystallisation of calcite, by slow diffusion of $(NH_4)_2CO_3$ vapour in a closed box containing dishes of $CaCl_2$ solutions.[31] A range of added polyelectrolytes containing carboxylate and/or sulphate functional groups *e.g.* poly-L-aspartate, were studied due to the fact that these charged groups are often found in proteins and glycoproteins involved in biomineralisation. The electrolytes were incorporated into gelatin films which were then cross linked to make them insoluble. The films containing poly-L-aspartate induced discrete, oriented calcite crystal growth. More recent work involves a complementary strategy, again using the poly-L-aspartate film, to grow an organised array of magnesium calcite crystals with up to 12% Mg content. This unusual stabilisation of the calcite with such a high magnesium content is analogous to that found in radial calcitic ooids, small spheres made from concentric shells.

The work discussed above involves mineralisation on the polymer films. Another process which occurs in biomineralisation is the controlled growth of crystals within a polymer matrix. However, it has been demonstrated that the distinction between growth in and on polymers is not always clear. [32]

Studies by Calvert *et al.* indicate that crystals of calcium oxalate are nucleated within cast films of a series of hydroxylated acrylate polymers. The polymers

used were partly hydrophilic but not soluble in aqueous solutions, their surfaces were swollen by water and diffuse. Nucleation was thought to occur within the polymer and the crystal growth continued outwards from the surface. In most cases the polymer did not take an active part in the precipitation but controlled the process through phase behaviour, diffusion effects and matrix orientation.

Perhaps the best example, to date, of alignment of inorganic crystals beneath a polymeric film was reported by Charych in 1995.[33] The work discussed in this article involved the growth of $CaCO_3$ from a supersaturated solution of $Ca(HCO_3)_2$ beneath polymeric films of 10,12-pentacosadiynoic acid. The polymer was synthesised on the supersaturated solution by spreading and compressing the monomer 10,12-pentacosadiynoic acid, on the surface of a Langmuir trough and polymerisation was initiated by a radical mechanism, using u.v. irradiation. Crystals of calcite appeared to be nucleated at the (012) face and in certain areas of the film appeared to be coaligned with the polymer backbone.

Many aspects of the effect of polymers upon crystal growth have not yet been studied. No work has been reported in which the molecular weight distribution, conformation and microstructure of the polymers are known. Polymers have been synthesised by techniques in which complete control over the polymer properties is not possible and irregular polymers often result. The effect of specific functionalisation also remains unclear, although Brisdon *et al.*[28] have shown that systematic functionalisation of polysiloxanes can affect crystallisation. Ideally, polymers with known molecular weight distribution and conformation should be used. In order to understand the effect of a polymer it is also necessary to know how the individual repeat units when used as additive

control the inorganic crystal growth. The approach taken in the work discussed in this thesis was to synthesise model compounds with well defined structure and stereochemistry and observe the effect of these as additives on crystal growth from supersaturated solutions of $Ca(HCO_3)_2$. Then, to synthesise polymers, in a well defined manner, with repeat units analogous to the model compounds and observe the effect of the polymers upon crystallisation of the inorganic salt. The advantage of this approach is that the degree of control of the polymers on inorganic crystallisation might be more fully understood if the effects of the monomers were already established. Also, the effect of molecular weight which is controlled by living polymerisation and to some extent the stereochemical relationships of carboxylate anions along the polymer backbone can be investigated. The technique used for polymer synthesis is Ring Opening Metathesis Polymerisation (ROMP), which is introduced in the following section, Section 1.2.3.

1.2.2 References for Section 1.2

[1] ' On Biomineralisation', Lowenstam H.A. and Weiner S., Oxford University Press Inc., New York, 1989

[2] Mann S., *Nature,* **332**, 119-124, 1988.

[3] Lowenstam H.A., *Science*, **221**, 1126-1131, 1981.

[4] Lakes R., *Nature*, **361**, 511-514, 1993.

[5] Heywood B. R., *Micr.Res.Tech.*,**27**, 376-388, 1994.

[6] Weiner S., *Crit. Rev. Biochem.*, **20**, 365-408, 1986.

[7] Weiner S. and Traub W., *Phil.Trans.R.Soc.Lond.*, B304, 425, 1984.

[8] Fritz M., Belcher A. M., Radmacher M., Walters D. A., Hansma P. K., Stucky G. D., Morse D. E. and Mann S., *Nature*, **371**, 49-51, 1994.

[9] Zaremba C. M., Belcher A. M., Fritz M., Li Y., Mann S., Hansman P.K., Morse D. E., Speck J. S. and Stucky G. D., *Chem. Mater.*, **8**, 679-690, 1996.

[10] Belcher A. M., Wu X. H., Christensen R. J., Hansman P. K., Stucky G. D. and Morse D. E., *Nature*, **381**, 56-69, 1996.

[11] Falini G., Albeck S., Weiner S. and Addadi L., *Science*. **271**, 67-69, 1996.

[12] Mann S., *J.Mater.Chem.*, **5**(7), 935-946, 1995.

[13] Mann S., Archibald D. D., Didymus J. M., Douglas T., Heywood B. R., Meldrum F. C. and Reeves N. J., *Science*, **261**, 1286-1292, 1993.

[14] Mann S. in: ' Biomimetic Materials Chemistry', Mann S. (Ed), 143, VCH, New York, 1996.

[15] Kresge C. T., Leonowicz M. E., Roth W. J., Vartuli J. C. and Beck J. S., *Nature*, **359**, 710, 1992.

[16] Burkett S. L. And Mann S., *Chem.Commun.*, 321-322, 1996.

[17] Heywood B. R. and Mann S., *Adv.Mater.***6**, No.1, 9-20, 1994.

[18] Litvin A. L., Valiyaveettil S., Kaplan D. L. and Mann S., *Adv.Mater.*, **9**, No.2, 1997.

[19] Heywood B. R. and Mann S., *Chem.Mater.*, **6**, 311-318, 1994.

[20] Ward M. And Frostman L. M., *Langmuir*, **13**, 330-337, 1997.

[21] Oliver S., Kuperman A., Coombs N., Lough A. and Ozin G. A., *Nature*, **378**, 47, 1995.

[22] Walsh D. and Mann S., *Chem.Mater.*, **8**, 1944-1953, 1996.

[23] Mann S., Didymus J. M., Sanderson N. P., Heywood B. R. and Samper E. J. A., *J.Chem.Soc.Faraday Trans.*, **86**(10), 1873-1880, 1990.

[24] Rajam S., Heywood B. R., Walker J. B. A., Mann S., Davey R. and Birchall J. D., *J.Chem.Soc.Faraday Trans.*, **87**(5), 727-734, 1991.

[25] Oliver S., Coombs N. And Ozin G. A., *Adv.Mater.*, 7, No.11, 931-935, 1995.

[26] Walsh D. and Mann S., *Nature*, **377**, 320-323, 1995.

[27] Walsh D., Hopwood J. D. and Mann S., *Science*, **264**, 1576-1578, 1994.

[28] Brisdon B. J., Heywood B. R., Hodson A. G. W., Mann S. and Wong K. K. W., *Adv.Mater.*, **5**, No.1, 49-51, 1993.

[29] Wong K. K. W., Brisdon B. J., Heywood B. R., Hodson A. G. W. and Mann S., *J.Mater.Chem.*, **4**(9), 1387-1392, 1994.

[30] Bianconi P A., Lin J. and Strzelecki A. R., *Nature*, **349**, 315-317, 1991.

[31] Falini G., Gazzano M. And Ripamonti, *Adv.Mater.*, **6**, No. 1, 46-48, 1994.

[32] Burdon J., Oner M. and Calvert P., *Mater.Sci.Eng.*, part C, Oct. 1995.

[33] Berman A., Ahn D. J., Lio A., Salmeron M., Reichert A. and Charych D., Science, **269**, 515-518, 1995.

1.3 RING OPENING METATHESIS POLYMERISATION

1.3.1 Ring opening metathesis polymerisation

The olefin disproportionation reaction was discovered by Banks and Bailey in the early 1950s[1] and may be represented by the scheme shown below [Fig. 1.3.1].

Fig. 1.3.1. The olefin disproportionation reaction.

Ring Opening Metathesis Polymerisation (ROMP) was first observed by Anderson and Merkling in the polymerisation of norbornene [Fig. 1.3.2].[2]

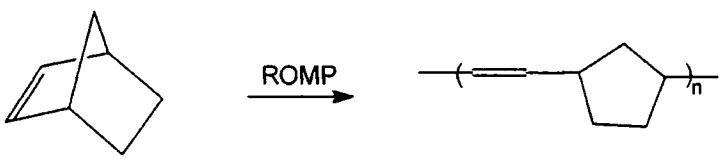

Fig. 1.3.2. ROMP of norbornene.

Calderon noted the similarity between the two reactions and used the term 'olefin metathesis' to describe them both.[3]

The widely accepted mechanism for ROMP is the Chauvin/Herrison mechanism in which the reactive species is a metallacarbene [Fig. 1.3.3.].[4] In this mechanism the metallacarbene coordinates to a double bond to give a π complex. This then forms a metallacyclobutane which cleaves, as shown, to give a new double bond and the reactive metallacarbene is attached to the chain end. The

latter then reacts with a new monomer unit to form another metallacyclobutane and the reaction proceeds. There is no net making and breaking of bonds during ROMP, the reaction is therefore essentially thermoneutral. The driving force for the reaction is provided by the use of strained cycloalkene monomer units.

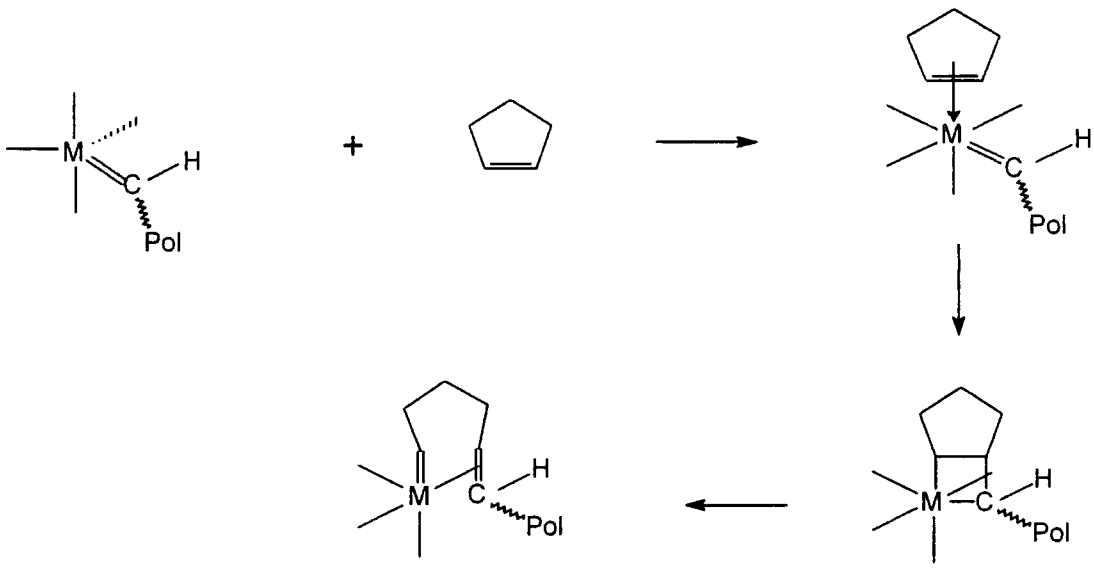

Fig. 1.3.3. The Chauvin/Herrisson mechanism for ROMP.

Metathesis can be terminated by a reaction of the propagating metal with oxygen of oxygenated species (water, alcohol, *etc.*) with the metal carbene complex. Alternatively, well defined metathesis can be terminated by a Wittig type reaction, typically with an oxygen containing molecule, which leads to the formation of an unreactive organometallic compound [Fig. 1.3.4].[5]

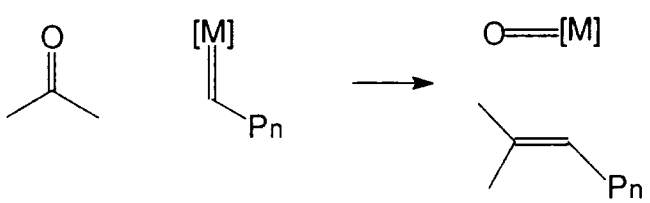

Fig. 1.3.4. Termination of metathesis by a Wittig type reaction.

Chain transfer reactions can occur between the propagating metal carbene and a C=C bond in the backbone of another chain. This competes with the reaction in which the metal carbene interacts with the monomer units, leading to propagation. A similar intermolecular reaction is possible between the active metal carbene and the C=C bonds from the same polymer chain. This results in the formation of cyclic oligomers and is known as "back biting". This reaction can lead to the polymer having a lower molecular weight and larger polydispersity than is found in well regulated species.

Effective ROMP requires a low energy barrier between the metal carbene and metallacyclobutane and a negative Gibbs free energy. The Gibbs free energy can be expressed by the following equation,

$$\Delta G = \Delta H - T\Delta S$$

where T, ΔH and ΔS are the temperature (K), enthalpy and entropy of ring opening respectively. The entropy for polymerisation is always negative due to the fact that separate monomers are much more disordered than if they are linked to each other within a polymer chain. Therefore, the entropy term ($-T\Delta S$) is always positive and for a favourable reaction the magnitude of the ΔH term must be negative and greater than the magnitude of $-T\Delta S$. As the temperature is increased the $T\Delta S$ term increases positively and the Gibbs Free Energy eventually becomes positive. The temperature at which $\Delta G = 0$, namely $T = \Delta H/\Delta S$, is known as the ceiling temperature, above which polymerisation does not occur.

Ring strain and ring size are important factors in determining whether monocyclic or bicyclic olefins undergo metathesis polymerisation. Three and

four membered rings are strained due to deformation of the normal bond angles and larger rings containing eight or more carbon atoms are strained due to torsional or transannular effects. For all of these monomers, ring opening is thermodynamically feasible and generally occurs readily. For five, six and seven membered rings the strain is lower and the situation becomes delicately balanced with other physical factors such as temperature, concentration and pressure affecting polymerisability. Lower temperature and higher monomer concentration lead to a smaller entropy term, thus, making the polymerisation favourable.

A significant advantage of norbornene, bicyclo[2.2.1]hept-2-ene, derivatives is that they have a greatly reduced tendency to undergo secondary metathesis (back biting) with the vinylene units in the polymer backbone due to the steric inhibition of the olefinic moiety by branching at the α-carbons.[6] In general, polymerisations with 5-*exo* substituted and 5,6-di-*exo* substituted-2-norbornene compounds have been more successful than with the corresponding *endo* isomers. This could be due to stabilising interaction between the *endo* substituent and the double bond or due to slightly larger ring strain of the *exo* isomer.

In the early days of ROMP, a large variety of initiator systems was used which are now often referred to as classical catalysts. These initiators were ill defined *i.e.* the actual structure of the reactive species was unknown and were often based on molybdenum, tungsten or rhenium. One of the more successful systems contained WCl_6, $EtAlCl_2$ (4 eq) and ethanol (1 eq)[7 8] Alkylidene complexes were generated *in situ* from the halides, oxides or oxyhalides of the transition metals.

It was usual to use a co-catalyst *eg.* R_4Sn, R=Me[9] and/or accelerator *eg.* H_2O[10], EtOH[11] to aid the generation of the carbene.

$$WCl_6 + (CH_3)_4Sn \rightarrow WCl_5CH_3 + (CH_3)_3SnCl$$

$$WCl_5CH_3 \rightarrow WCl_4{=}CH_2 + HCl$$

Fig. 1.3.5. Formation of a tungsten carbene in a 'classical' catalyst system using a co-catalyst.

One problem with the classical initiators was that decomposition was often observed over the course of a typical polymerisation reaction. Although many catalysts were highly reactive their nature was not known and reactivity could not be controlled. Also, the tolerance towards electron donating functionalities present in the monomer was very poor or non-existent. The high reactivity led to reactions with the acyclic double bonds of the polymer backbone and often large amounts of cyclic side products were obtained. Due to all the above factors, molecular weight distributions were broad and well defined or block co-polymers could not be synthesised.

Far more control over the reactivity of ROMP catalysts is possible by the use of well defined alkylidene complexes. These well defined initiators enable the synthesis of polymers with narrow molecular weight distribution (<1.01). The first isolated metal carbene species, the Fischer carbene, was a heteroatom stabilised complex and was shown to be reactive in olefin metathesis.[12] It was found to react with highly strained olefins such as cyclobutene and norbornene derivatives. The diphenyl complex, first synthesised by Casey and Burkhardt in

1973 was not stabilised by a heteroatom and was much more reactive, initiating the polymerisation of less strained olefins.[13]

Fischer carbene Casey carbene

Fig. 1.3.6. Metal carbenes used to initiate metathesis.

Grubbs and co-workers first isolated well defined metallacyclobutane complexes which were active as metathesis catalysts.[14] The reaction of Tebbe reagent with various olefins in the presence of nitrogen bases resulted in the formation of titanacyclobutane complexes. It has been shown that these titanacycles readily exchange with olefins[15] via a rate determining loss of olefin from the titanacyclobutane ring to generate the transition metal methylidene species $Cp_2Ti{=}CH_2$ which is active in metathesis [Fig. 1.3.7]. This type of catalyst is able to polymerise norbornene in a living manner.

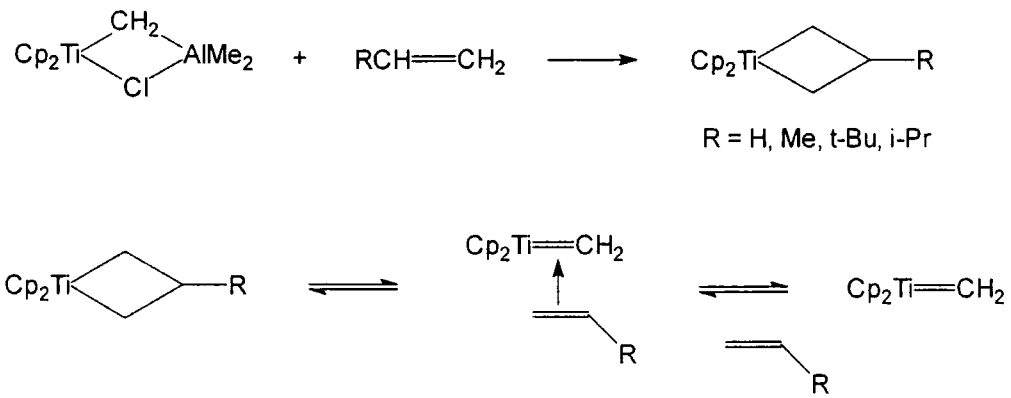

Fig. 1.3.7. Formation of metallacyclobutane and methylidene species.

In the mid 1980s four co-ordinate alkylidene complexes of tungsten and molybdenum were isolated which were highly active in olefin metathesis.[16] The general structure of these complexes is $[M(HBu)(NAr)(OR)_2]$ and they possess the bulky imido ligand (2,6-diisopropylphenyl imido) and alkoxide groups as well as the active alkylidene [Fig. 1.3.8].

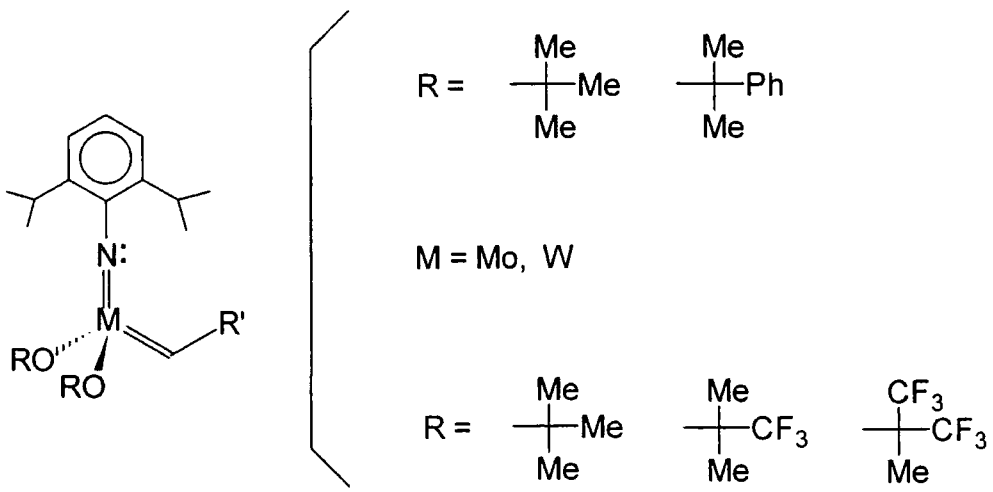

Fig. 1.3.8. Some Schrock-type metal carbene complexes used for metathesis

Four co-ordination allows small substrates to attack the metal centre and give five co-ordinate intermediate metallacyclobutane. The bulky alkoxide groups and the imido ligand prevent intermolecular reactions which could result in inactive complexes or decomposition of the catalyst. The bulky ligands also slow down bimolecular decomposition reactions. Substitution of the methyl groups on the alkoxides with the more electronegative trifluoromethyl groups makes the complex more active since the trifluoro groups draw electron density away from the metal centre. This makes the metal centre of the complex more electrophilic and a better acceptor for the incoming olefin which can be regarded as a π donor.[17] This effect is demonstrated by the observation that when OR is

$O(C(CH_3)(CF_3)_2)$ the tungsten complex will readily metathesise acyclic olefins, whereas, when OR is OBu^t it does not react with acyclic olefins. As a consequence of the high reactivity of tungsten, alkylidenes of this metal do not polymerise monomers that contain a variety of functionalities. Molybdenum catalysts, in contrast, tolerate a large number of functionalities, a few of which are shown in Fig. 1.3.9.

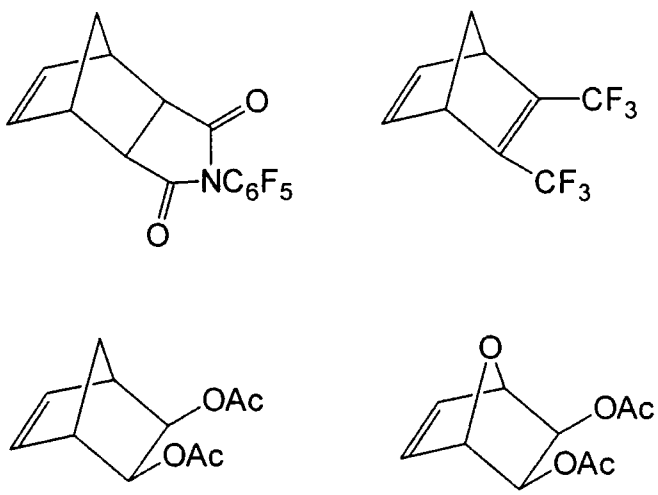

Fig. 1.3.9. Some monomers with functionalities tolerated by the molybdenum initiator.

Although molybdenum catalysts work in the presence of many functionalities a search for catalysts that tolerate more functional groups continues. It was observed that as the central atom of the alkylidene complex moves to the right of the periodic table of elements the catalyst becomes more tolerant towards functionalities [Table 1.3.1]. The aim was to find a catalyst that was selective enough to complex and react with a soft C=C bond in the presence of hard carbonyls like ester groups and ketones.

Titanium	Tungsten	Molybdenum	Ruthenium
Alcohols, Water	Alcohols, Water	Alcohols, Water	Olefins
Acids	Acids	Acids	Alcohols, Water
Aldehydes	Aldehydes	Aldehydes	Acids
Ketones	Ketones	Olefins	Aldehydes
Esters, Amides	Olefins	Ketones	Ketones
Olefins	Esters, Amides	Esters, Amides	Esters, Amides

Table. 1.3.1. As the central atom moves to the right in the periodic table of elements, it becomes softer and contains more d-electrons. Complexation and reaction of olefins is favoured over the complexation and reaction of the harder, oxygen containing double bonds.

After it was shown that $RuCl_3$ can function as a ROMP catalyst in water further investigations were made into the development of ruthenium-based, well defined initiators. The initiator shown in Fig. 1.3.10 is a very effective initiator in aqueous environments and is highly tolerant of functional groups.[18,19]

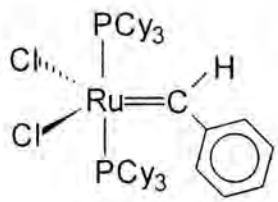

Fig. 1.3.10. Ruthenium carbene, tolerant of many functionalities and water.

There are several ways of incorporating monomer repeat units into a polymer chain leading to a range of microstructures and potentially control over the

physical properties of the polymer. The microstructure can be controlled in favourable cases by changing the catalyst system and the reaction conditions. Three main factors which define the microstructure of polymers synthesised by ROMP are:

1. the *cis/trans* vinylene ratios and distribution
2. tacticity effects
3. the head/head, tail/head and tail/tail frequency and distribution

1. *Cis/trans* double bond isomerism

The backbone of a polymer prepared by ROMP contains unsaturated bonds which can be either *cis* or *trans* [Fig. 1.3.11].

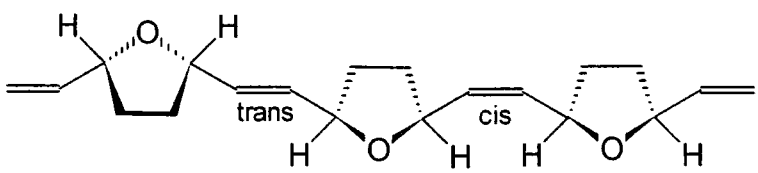

Fig. 1.1.11. *Cis* and *trans* double bonds in poly(2,5(furanylene)vinylene).

The proportion of *cis* double bonds in a particular polymer, denoted by σ_c, is primarily determined by the catalyst system, concentration, solvent and temperature, the nature of the monomer may also affect the outcome.

2. Tacticity effects

Monomers such as bicyclo[2.2.1]hept-2-enes may not have chiral centres but give polymers containing chiral centres. There is the possibility of two centres

adjacent to the double bond having the same chiralities resulting in a racemic dyad or different chiralities, giving a meso dyad. Sequences of racemic dyads give syndiotactic polymers and sequences of meso dyads provide isotactic polymers. Polymers with a random distribution of meso and racemic dyads are known as atactic. As each C=C bond can have *cis* or *trans* geometry there are four possible microstructural arrangements for pure homosteric polymers [Fig.1.3.12].

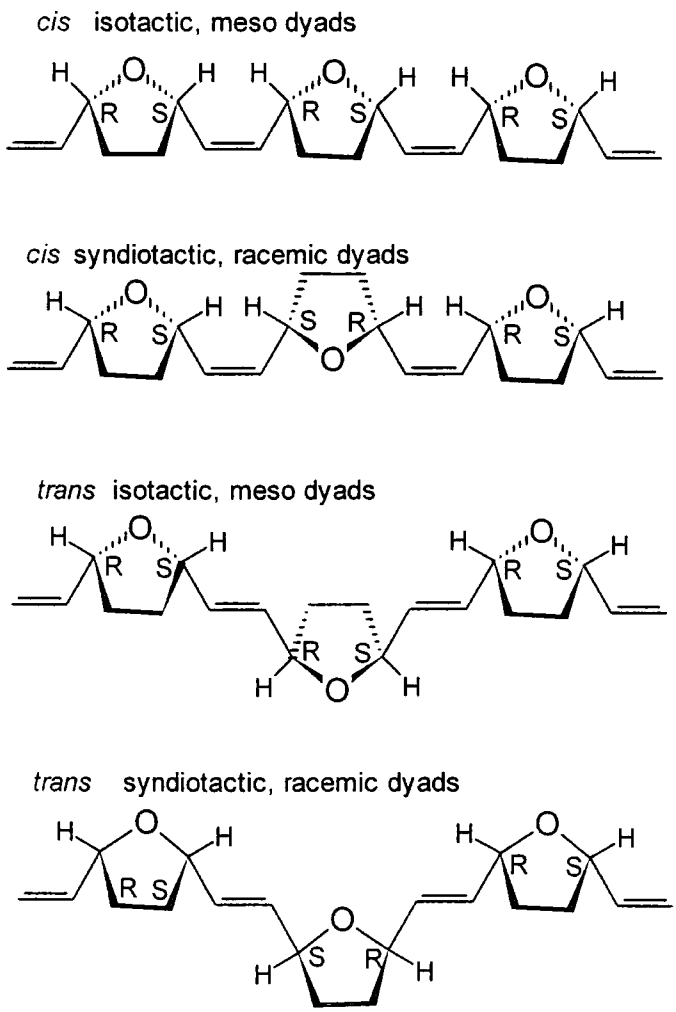

Fig. 1.3.12. The four possible configurations of homosteric poly(2,5(furanylene)vinylene).

3. Head and tail effects

In the case of unsymmetrically substituted monomers such as 5,5-dimethylbicyclo[2.2.1]hept-2-ene, polymers can form with head-head (HH), head-tail (HT) or tail-tail (TT) structures [Fig. 1.3.13].

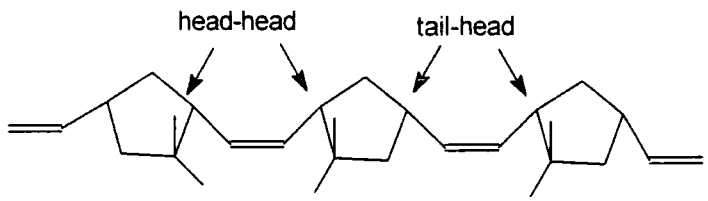

Fig. 1.3.13. Head-tail effects in poly(5,5-dimethylbicyclo[2.2.1]hept-2-ene).

Furthermore, each of these structures can have meso or racemic dyads and *cis/trans* isomerism, so a large number of configurations becomes possible. Most of the polymers prepared in this thesis are made from symmetrically substituted bicyclo[2.2.1]hept-2-ene and 7-oxabicyclo[2.2.1]hept-2-ene monomers. Symmetrical monomers, such as *exo,exo*- and *endo,endo*-bicyclo[2.2.1]hept-5-ene-2,3-dicarboxylic acids, cannot give rise to HH, HT or TT addition modes.

References for Section 1.3.1

[1]Banks R. L. and Bailey G. C., *Ind.Eng.Chem.Prod.Res.Div.*, **3**, 170, 1964.

[2] Anderson A. W. And Merckling N. G., *Chem.Abs.*, **50**, 3008, 1955.

[3] Calderon N. e*t al*, *Chem.Eng.News*, **45**, 52, 1967.

[4] Herrison J. L. and Chauvin Y., *Macromol.Chem.*, **141**, 161, 1970.

[5] Schrock R. R., *Acc.Chem.Res.*, **23**, 158, 1990.

[6] Ofstead E. A. and Wagener K. B., in "New Methods of Polymer Synthesis", W. J. Mijs (Ed.), 237, Plenium Press, New York, 1992.

[7] Calderon N., Ofstead E. A., Ward J. P., Judy W. A. and Scott K. W., *J.Am.Chem.Soc.*, **90**, 4133, 1986.

[8] Calderon N., Lawrence J. P. And Ofstead E. A., *Adv.Organomet.Chem.*, **17**, 449, 1979.

[9] Thorn-Csanyi E. and Timm H., *J.Mol.Cat.*, **28**, 37, 1985.

[10] Thorn-Csanyi E. and Kessler M., *J.Mol.Cat.*, **36**, 31, 1986.

[11] Ivin K. J., Laverty D. T. and Rooney J. J., *Makromol.Chem.*, **178**, 1545, 1977.

[12] Fischer E. O. and Maasbol A., *Angew.Chem.Inter.Ed.*, **3**, 580, 1964.

[13] Casey C. P. And Burkhardt T. S., *J.Am.Chem.Soc.*, **95**, 5833, 1973.

[14] Howard T. R., Lee J. B. and Grubbs R. H., *J.Am.Chem.Soc.*, **102**, 6876, 1980.

[15] Straus P. A. and Grubbs R. H., *Organometallics*, **1**, 1658, 1982.

[16] Murdzek J. S. and Schrock R.R., *Organometallics*, **6**, 1373, 1987.

[17] Schrock R. R., *Acc.Chem.Res.*, **23**, 158, 1990.

[18] Lynn D. M., Kanaoka S. and Grubbs R. H., *J.Am.Chem.Soc.*, **118**, 784, 1996.

[19] Fraser C. and Grubbs R. H., *Macromolecules*, **28**, 7248, 1995.

CHAPTER 2

Dicarboxylic acid Model Compound Synthesis and Characterisation

2.1 INTRODUCTION

2.1.1 General introduction

The objectives of work discussed in this chapter are the syntheses and characterisation of a series of 2,3-dicarboxylic acid derivatives of bicyclo[2.2.1]hept-5-ene and 7-oxabicyclo[2.2.1]hept-5-ene. The use of these model compounds as the organic additives in crystal growth experiments is described in Chapter 3. The most convenient synthetic route for any of these derivatives involves the formation of the polycyclic structure via a Diels-Alder cycloaddition reaction followed by derivatisation of the adduct.

2.1.2 The Diels-Alder cycloaddition reaction

In a typical Diels-Alder reaction an olefin or acetylene derivative (dienophile) adds 1,4 to a 1,3-diene to give a six membered ring [Fig. 2.1.1].[1]

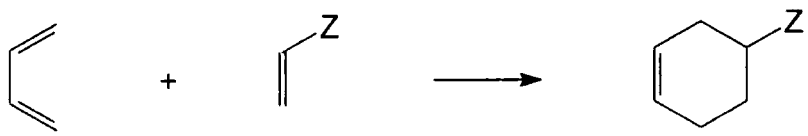

Fig. 2.1.1. The Diels Alder reaction between a conjugated diene and an olefin.

Z = an electron withdrawing group.

The reaction takes place most rapidly and in the highest yield if the dienophile is substituted by an electron withdrawing group (conventional Diels-Alder) or with electron donating groups on the olefin and electron withdrawing groups on the diene (Diels-Alder with inverse electron demand).[2] The diene can react only in the *cis* conformation and therefore cyclic dienes react faster than acyclic dienes;

five membered ring dienes are particularly favoured due to the coplanarity of the diene double bonds and the ideal distance between the termini.

With the substituted cyclic dienophiles used in this work and a cyclic diene the reaction produces either *exo* or *endo* adducts depending upon the conditions. Under moderate temperature conditions the addition is predominantly *endo*, the kinetically favoured product. This is usually attributed to the fact that the dienophile is added so as to give a maximum of "secondary overlap" of π-molecular orbitals in the transition state [Fig. 2.1.2].[3]

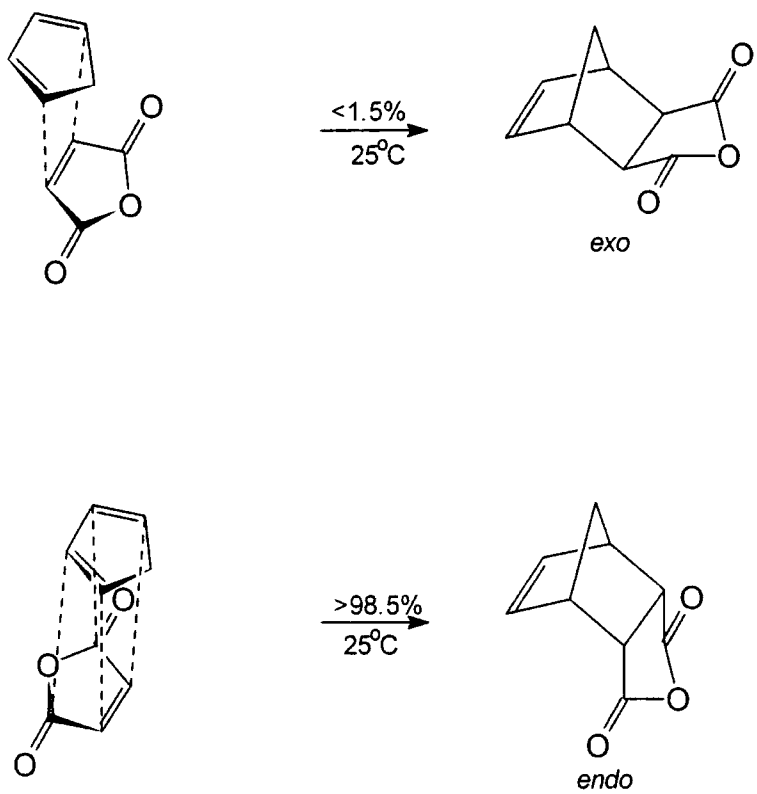

Fig. 2.1.2. A schematic representation of the orientation of the reactants in the approach to the transition state and the products of the Diels-Alder cycloaddition between cyclopentadiene and maleic anhydride.

However, the *endo*-adduct is invariably the kinetic product whether or not there is the possibility of "secondary overlap" of π-molecular orbitals, for example,

cyclopentene gives the *endo*-adduct as the kinetic product in reactions with cyclopentadiene. In order to obtain the more thermodynamically stable *exo* adduct, severe temperature conditions, longer reaction times and repeated recrystallisation are usually necessary.

The reaction of the cyclic diene, furan with the cyclic dienophile maleic anhydride is one of the few examples where the *exo* product forms at room temperature.[3] In this case the first formed *endo* adduct, the kinetic product, dissociates very easily at room temperature allowing the thermodynamically more stable *exo* isomer to become the predominant product even under mild conditions [Fig. 2.1.3]. Thus, after 1 min the *endo*:*exo* ratio is 50:50 whereas after 1 hour it is 1:99.

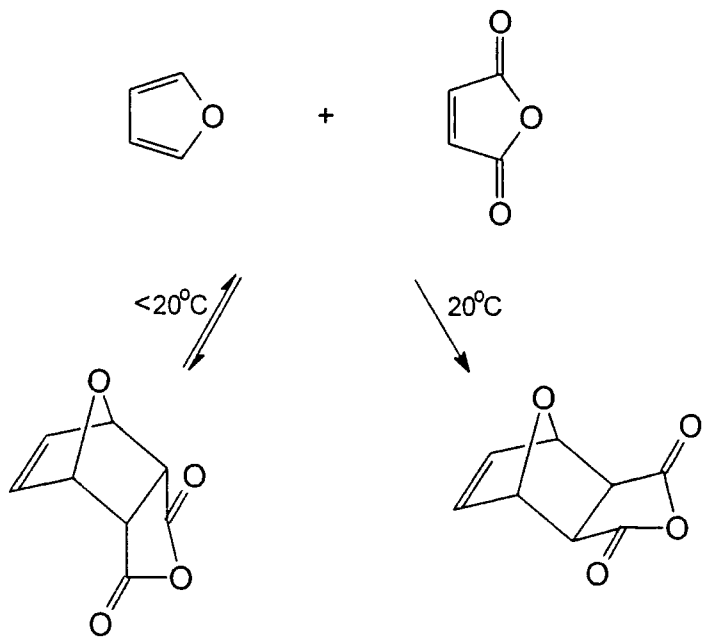

Fig. 2.1.3. A diagram showing the conversion the of the *endo* to the *exo* adduct for the Diels-Alder cycloaddition between furan and maleic anhydride.

2.2 RESULTS AND DISCUSSION

2.2.1 The synthesis and characterisation of bicyclo[2.2.1]hept-5-ene-2,3-dicarboxylic acids

Both *exo,exo* (model compound 1b) and *endo,endo* (model compound 2b) bicyclo[2.2.1]hept-5-ene-2,3-dicarboxylic acids were synthesised by hydrolysis of the corresponding anhydride adducts, model compounds 1a and 2a respectively [Fig. 2.2.1]. The synthesis of each diacid model compound involved placing the model compound in doubly distilled water and stirring. In the case of model compound 1a, the reaction was carried out at reflux temperature, whereas model compound 2a was simply stirred at room temperature. The crude products crystallised as colourless, transparent solids which were recovered by filtration and recrystallised from water. The yields of both model compounds, with respect to the anhydride precursor compounds, were high (87 and 92% respectively) and the melting points agreed with values reported in literature.

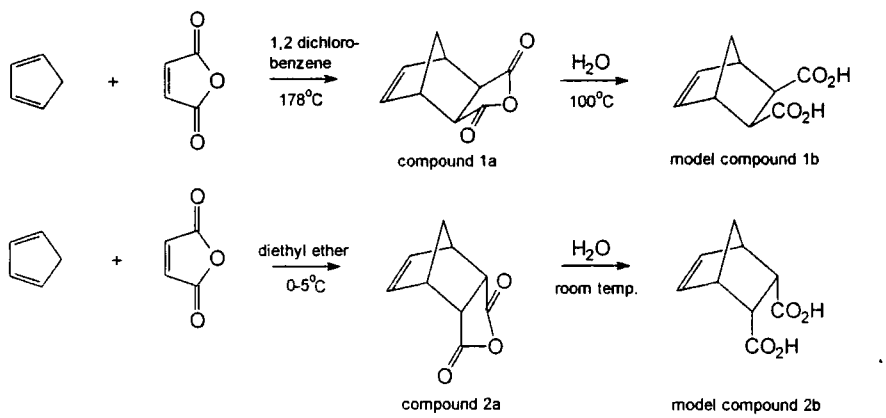

Fig. 2.2.1. A schematic diagram of the synthesis of model compounds 1b and 2b.

Evidence that the hydrolyses of model compounds 1a and 2a have been carried out successfully can be seen on comparison of their ^1H NMR spectra with the

spectra of model compounds 1b and 2b. The chemical shifts of the peaks corresponding to the methylene ABq, H_7 and $H_{7'}$, show a pattern which is consistent with the assigned structures [Fig. 2.2.2].

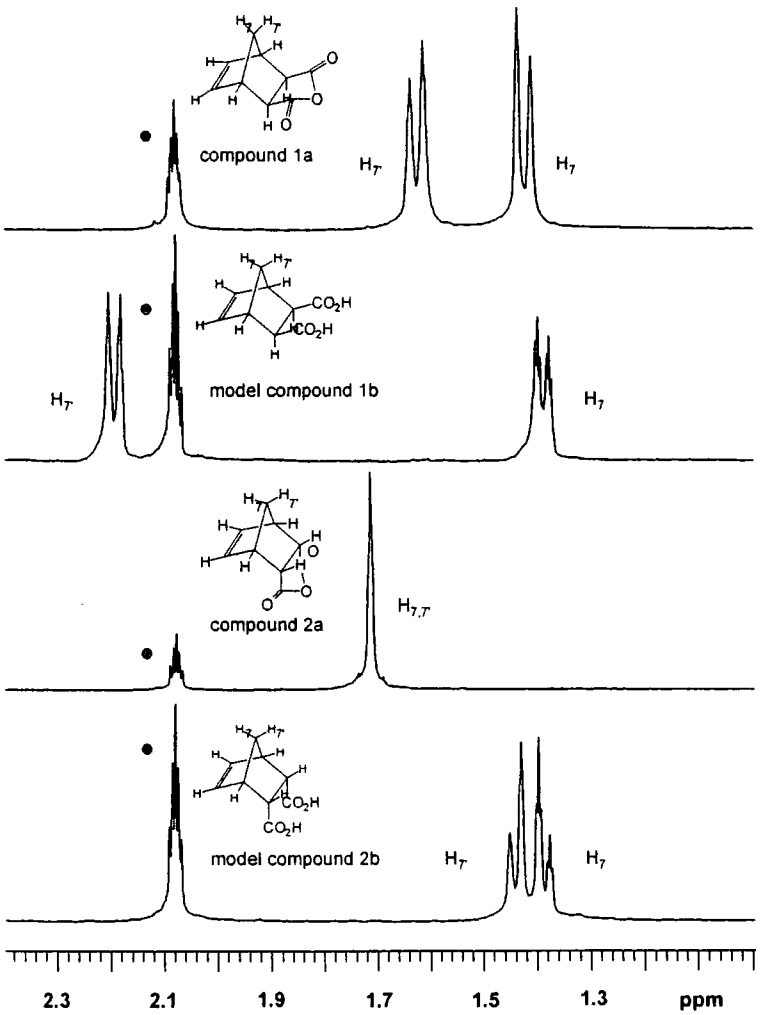

Fig. 2.2.2. ^{1}H NMR spectra of model compounds, 1a, 1b, 2a and 2b.

- residual hydrogens in acetone-d_6

The difference between chemical shifts for H_7 and $H_{7'}$ is greater in the carboxylic acids than in the corresponding anhydrides. The chemical shift in the spectrum of the *exo*-anhydride model compound, model compound 1a, is 0.2ppm with $H_{7'}$

at 1.6 ppm and H_7 at 1.4ppm whereas the difference in the dicarboxylic acid model compound, model compound 1b is (0.8ppm) with $H_{7'}$ at 2.2ppm and H_7 at 1.4ppm. In the ^1H NMR spectrum of the *endo*- anhydride model compound, model compound 2a, the peaks corresponding to H_7 and $H_{7'}$ are overlapping at 1.7ppm whereas the bridge hydrogen atoms in the carboxylic acid model compound, model compound 2b, differ in chemical shift by 0.03ppm with $H_{7'}$ at 1.41ppm and H_7 at 1.37ppm. These differences are reasonable and can be explained on the basis that the movement of the carbonyl groups in the anhydride model compounds is more restricted due to the ring structure of the anhydride, by contrast in the dicarboxylic acid the carbonyl groups have less restricted movement and are in closer proximity to $H_{7'}$ leading to a larger interaction. The adduct, 2-*endo*-3-*exo*-bicyclo[2.2.1]hept-5-ene-2,3-dicarboxylic acid (model compound 3a) was synthesised in one step from the Diels-Alder reaction between cyclopentadiene and fumaric acid [Fig. 2.2.3]. As the reaction was carried out at room temperature it was necessary to pre-crack dicyclopentadiene under severe temperature conditions (>170°C) to yield the cyclopentadiene required (93%yield).

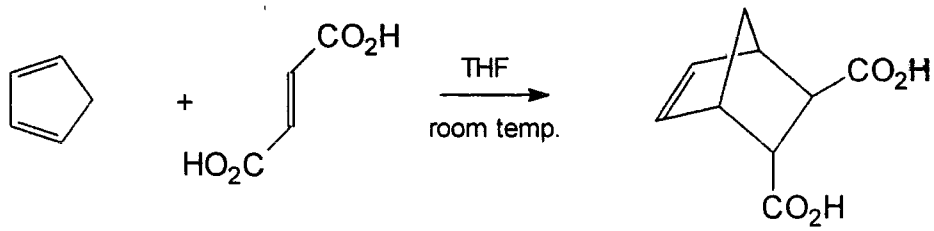

Fig. 2.2.3. A schematic representation of the synthesis of model compound 3a.

The infrared spectra of model compounds 1b, 2b and 3a [see appendices C2,C5 and C7 respectively] were recorded as KBr discs and were all consistent with the assigned structures displaying O-H stretching at 3200-3100cm^{-1}, carboxylic acid dimer modes at 2618-2739cm^{-1} and carboxylic acid carbonyl stretching modes in the 1691-1716cm^{-1} region. Further indication of correct assignment was seen in the chemical ionisation mass spectra of the model compounds as each spectrum showed a strong molecular ion peak at 200 ($M + NH_4^+$).

Comparison of the ^{1}H NMR spectra of the dicarboxylic acid model compounds 1b, 2b and 3a revealed differences in chemical shifts and fine structures of the resolved signals [Fig. 2.2.4]. Detailed analysis of the set of spectra allowed complete unambiguous assignment of the structures of 1b, 2b and 3a. Broad signals corresponding to the hydroxyl hydrogen of the dicarboxylic acids can be seen in the spectra for model compound 2b and 3a at 10.4 and 10.7ppm respectively. The corresponding peak for model compound 1b is not observed, this is probably due to the fact that the line broadening is so large that it is concealed within the base line. Although no hydroxyl hydrogen peak is seen in the spectrum of model compound 1b other spectral evidence, which is discussed below, allows unambiguous assignment of the structure. In the spectrum of

model compound 1b the triplet arising from the olefinic, $H_{5,6}$ hydrogens is found at 6.25ppm, 0.09ppm downfield from that in model compound 2b which occurs at 6.16ppm. This small difference in chemical shift is in the expected direction, in model compound 1b the carboxylic acid functionalities are *exo* leading to less shielding of $H_{5,6}$ whereas in model compound 2b the *endo* position of the acid functionalities leads to greater shielding. As expected, in the *exo,endo* model compound, model compound 3a, both the olefinic signals (at 6.10ppm and 6.30ppm) can be seen. The chemical shifts of the peaks corresponding to the methylene ABq, H_7 and $H_{7'}$, show a pattern which is consistent with the assigned structures. The difference between chemical shifts for H_7 and $H_{7'}$ is largest in model compound 1b, (0.8ppm) with $H_{7'}$ at 2.2ppm and H_7 at 1.4ppm. This difference is expected due to the carbonyl groups of the *exo* acid functionalities and $H_{7'}$ being in close proximity in a similar plane leading to a large interaction between the two. The difference between chemical shifts in model compound 2b is the smallest of the three isomers at 0.03ppm with $H_{7'}$ at 1.41ppm and H_7 at 1.37ppm, this small difference is due to the *endo* acid functionalities having the least interaction with $H_{7'}$. In model compound 3a, the *exo.endo* model compound, the chemical shift is intermediate between the the values of the *exo* and *endo* model compounds at 0.2ppm as expected. In Fig.2.2.4 the peak at 2.08ppm is due to the residual hydrogens in the solvent, acetone-d_6. Other ^1H NMR assignments are given in the experimental section of this chapter.

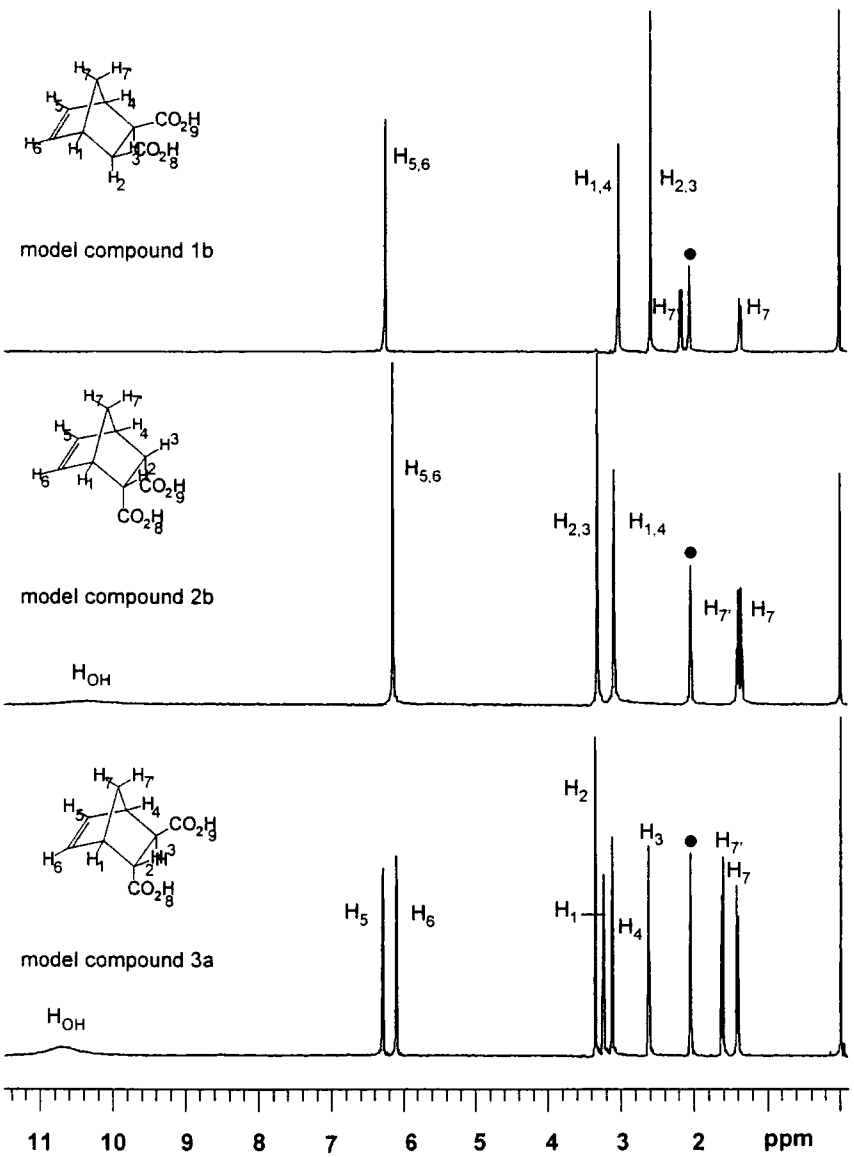

Fig. 2.2.4. ^{1}H NMR spectra of model compounds 1b, 2b and 3a.

• residual hydrogens in acetone-d_6

2.2.2 The synthesis and characterisation of *exo,exo*-7-oxabicyclo[2.2.1]hept-5-ene-2,3-dicarboxylic acid (model compound 4b).

Exo,exo-7-oxabicyclo[2.2.1]hept-5-ene-2,3-dicarboxylic acid (model compound

4b) was synthesised by the hydrolysis of *exo*-7-oxabicyclo[2.2.1]hept-5-ene-2,3-dicarboxy anhydride (model compound 4a) [Fig. 2.2.5].

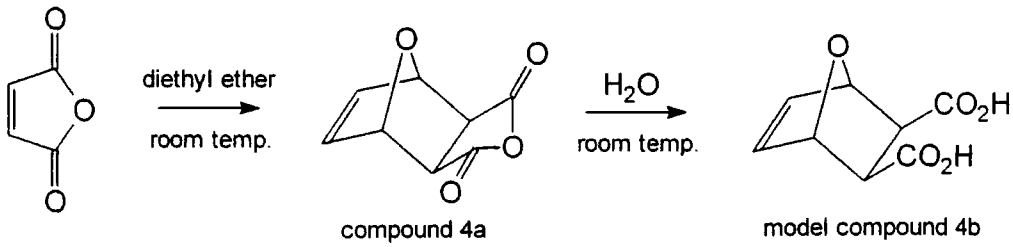

Fig. 2.2.5. A schematic representation of the synthesis of model compound 4b.

When the Diels-Alder reaction between furan and maleic anhydride was carried out in diethyl ether at room temperature the *exo* adduct crystallised from the solution and was the sole product after two days. The product was a transparent, colourless, crystalline solid with a m.pt. of 118°C and was recovered in a 74% yield. The infrared spectrum was recorded as a KBr disc and was consistent with the assigned structure, displaying anhydride carbonyl stretches at 1866 and 1790cm^{-1} and anhydride C-O stretches at 1232 and 1091cm^{-1}. The chemical ionisation mass spectrum showed a base peak at 68 ($C_4H_4O^{+\bullet}$) resulting from a retro Diels-Alder reaction, although no corresponding maleic anhydride peak was observed. The molecular ion was detected as a peak of low intensity at 184 (M + NH_4^+), which is consistent with the instability of this Diels-Alder adduct.

The hydrolysis of model compound 4a was carried out in doubly distilled water in an analogous reaction to the synthesis of model compound 2b. The diacid product, model compound 4b, was recovered as a colourless, crystalline solid in a 68% yield with respect to model compound 4a. The melting point was measured

at 137°C which is consistent with published values (see pp). The infrared spectrum was recorded as a KBr disc and is consistent with the assigned structure with an O-H stretch at 3150cm^{-1}, carboxylic acid dimer modes at 2672cm^{-1} and carboxylic acid carbonyl stretch, 1708cm^{-1}. The chemical ionisation mass spectrum contained a base peak at 134 ($C_4H_4O_4.NH_4^+$) and was consistent with the assigned structure.

The ^1H and ^{13}C NMR spectra of model compound 4b were recorded in solution in D_2O and referenced with respect to D_2O at 4.68ppm. Both spectra are consistent with the assigned structure [Fig.2.2.6.], the detailed assignment is recorded in the experimental section of this chapter.

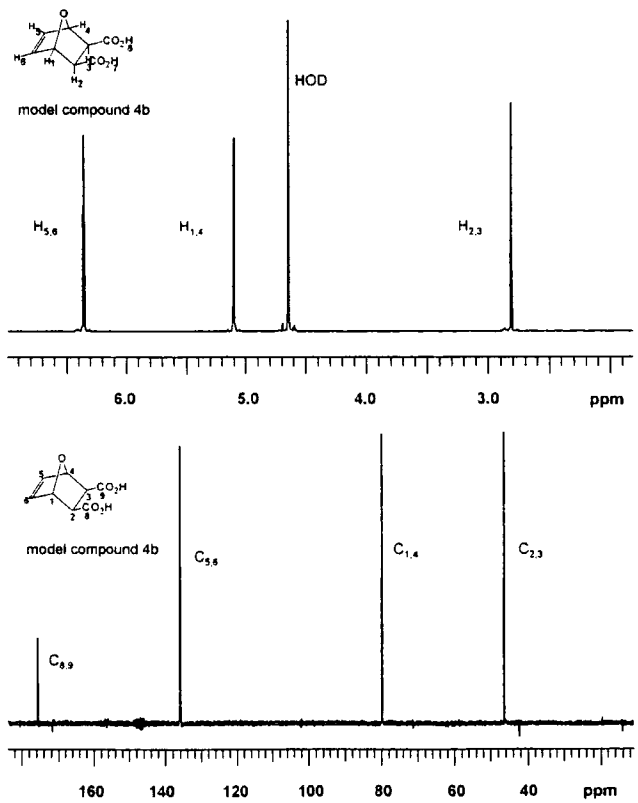

Fig. 2.2.6. ^1H and ^{13}C NMR spectra of model compound 4b

2.2.3 The synthesis and characterisation of bicyclo[2.2.1]heptane-2,3-dicarboxylic acids and *exo,exo*-7-oxabicyclo[2.2.1]heptane-2,3-dicarboxylic acid.

The olefinic moieties in model compounds 1b, 2b, 3a and 4b were hydrogenated catalytically using palladium on carbon in acetic acid at atmospheric pressure and room temperature [Fig. 2.2.7].

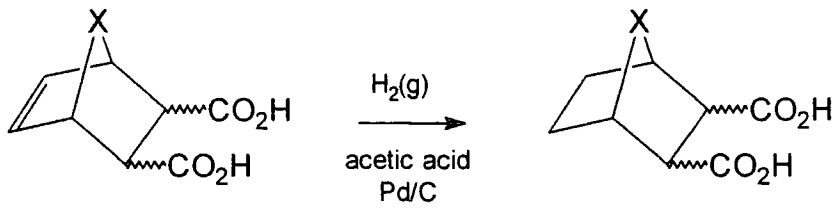

Fig. 2.2.7. A schematic diagram of the hydrogenation of model compounds 1b, 2b, 3a and 4b. X = CH_2 or O.

The Pd/C catalyst residue was separated from the model compound solutions by filtration and the solvent removed *in vacuo* to give the crude, solid products which were recrystallised from doubly distilled water to give the expected products. The products were colourless, transparent crystals obtained in yields from 81-88%. The infrared spectrum of each model compound was recorded as a KBr disc and all were consistent with the assigned structures, none contained olefinic stretches and all contained O-H stretches between 2966 and 3220cm^{-1}, carboxylic acid dimer modes were seen at 2625 and 2727cm^{-1} and carboxylic acid carbonyl stretches between 1708 and 1713cm^{-1}. The chemical ionisation mass spectra of 1c, 2c and 3b showed a strong peak at 202 ($M + NH_4^+$) and were consistent with assigned structures.

The ^{1}H NMR spectra of model compounds 1c, 2c, 3b and 4c proved a useful tool for determining whether successful hydrogenation has occurred. Comparison of the ^{1}H NMR spectra reveals that all model compounds were fully hydrogenated. It can be seen from the loss of signals corresponding to olefinic hydrogen atoms ($6.1<\delta H_{5,6}<6.3$ppm) and the subsequent gain of methylene hydrogen signals ($1.26<\delta H_{5,5',6,6'}<1.7$ppm) that hydrogenation has taken place as illustrated for model compounds 1b and 1c below [Fig. 2.2.8]

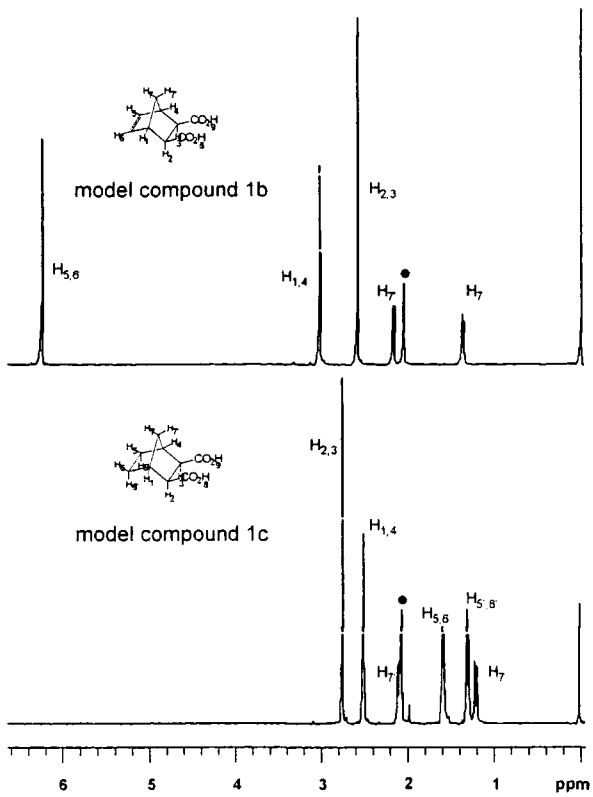

Fig. 2.2.8. A comparison of the ^{1}H NMR spectra of model compound 1b and

• residual hydrogens in acetone-d_6

A signal, found between 10 and 11ppm, corresponding to the carboxylic acid hydroxy hydrogen atom, $H_{8,9}$, can be seen in all hydrogenated model compound

spectra. In model compounds 1c, 2c and 3b the chemical shifts of the peaks corresponding to the methylene ABq of H_7 and $H_{7'}$ are more difficult to assign due to the overlap with signals due to $H_{5,5',6,6'}$, however, the pattern revealed is, as found for model compounds 1b, 2b and 3a, consistent with assigned structures [Fig. 2.2.9]. The difference between the chemical shifts of H_7 and $H_{7'}$ is the largest in model compound 1c, the *exo,exo* model compound, (0.9ppm) with $H_{7'}$ at 2.1ppm and H_7 at 1.2ppm. As in the case of the unhydrogenated adducts this is reasonable since the carbonyl groups of the carboxylic acid functionalities and $H_{7'}$ are in relatively close proximity, in a similar plane, leading to a large interaction. The difference in chemical shifts in model compound 2c is the smallest of the three model compounds (~0.03ppm). The small splitting is due to the small interaction between H_7 and the *endo* carbonyl functional groups. Due to a large amount of overlapping of the H_7 and $H_{7'}$ signals with the methylene hydrogen atoms it is not possible to assign, unambiguously, the chemical shifts of the bridge hydrogen atoms. In model compound 3b, the *exo,endo* model compound, the difference in chemical shifts between H_7 and $H_{7'}$ is intermediate between the *exo,exo* and *endo,endo* model compounds (~0.2ppm), again, overlap with of signals arriving from $H_{5,5',6,6'}$ results in an inability to unambiguously assign the chemical shifts for the bridge hydrogen atoms [Fig. 2.2.10].

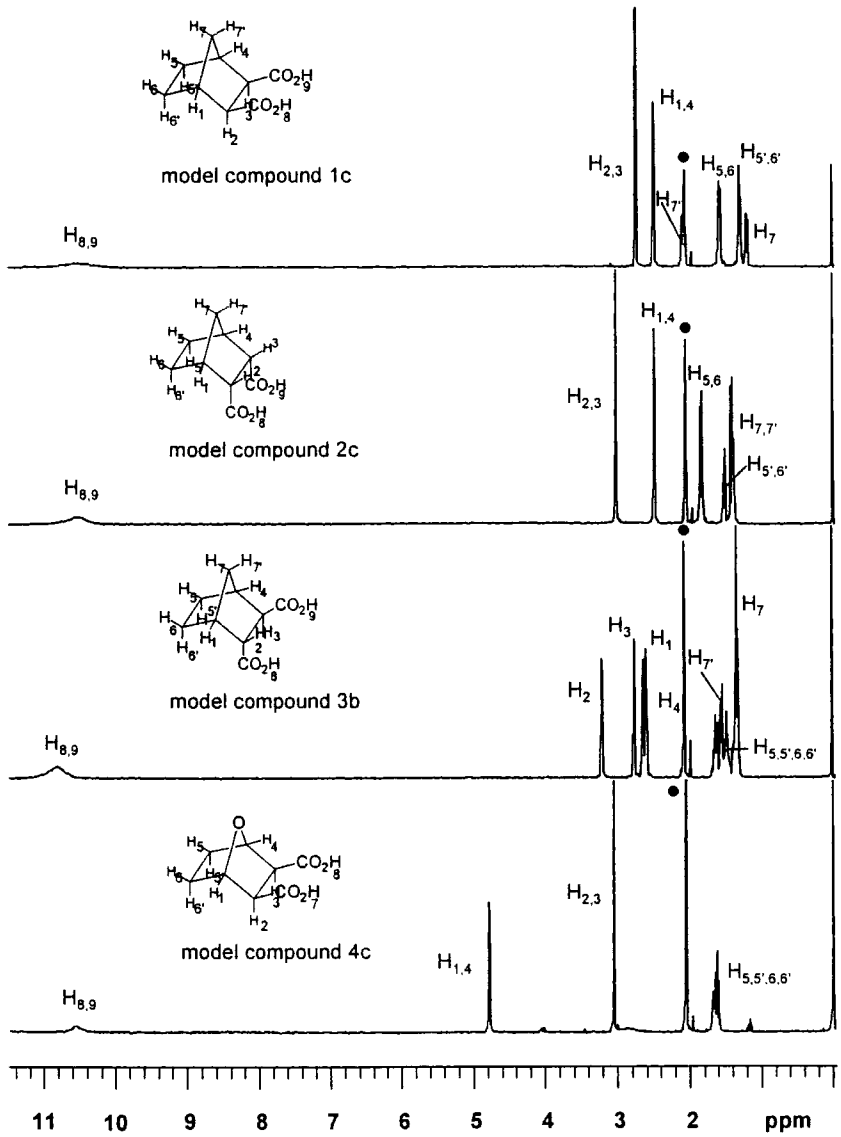

Fig. 2.2.9. A comparison of ^{1}H NMR for model compounds 1c, 2c, 3b and 4c.

• residual hydrogens in acetone-d_6

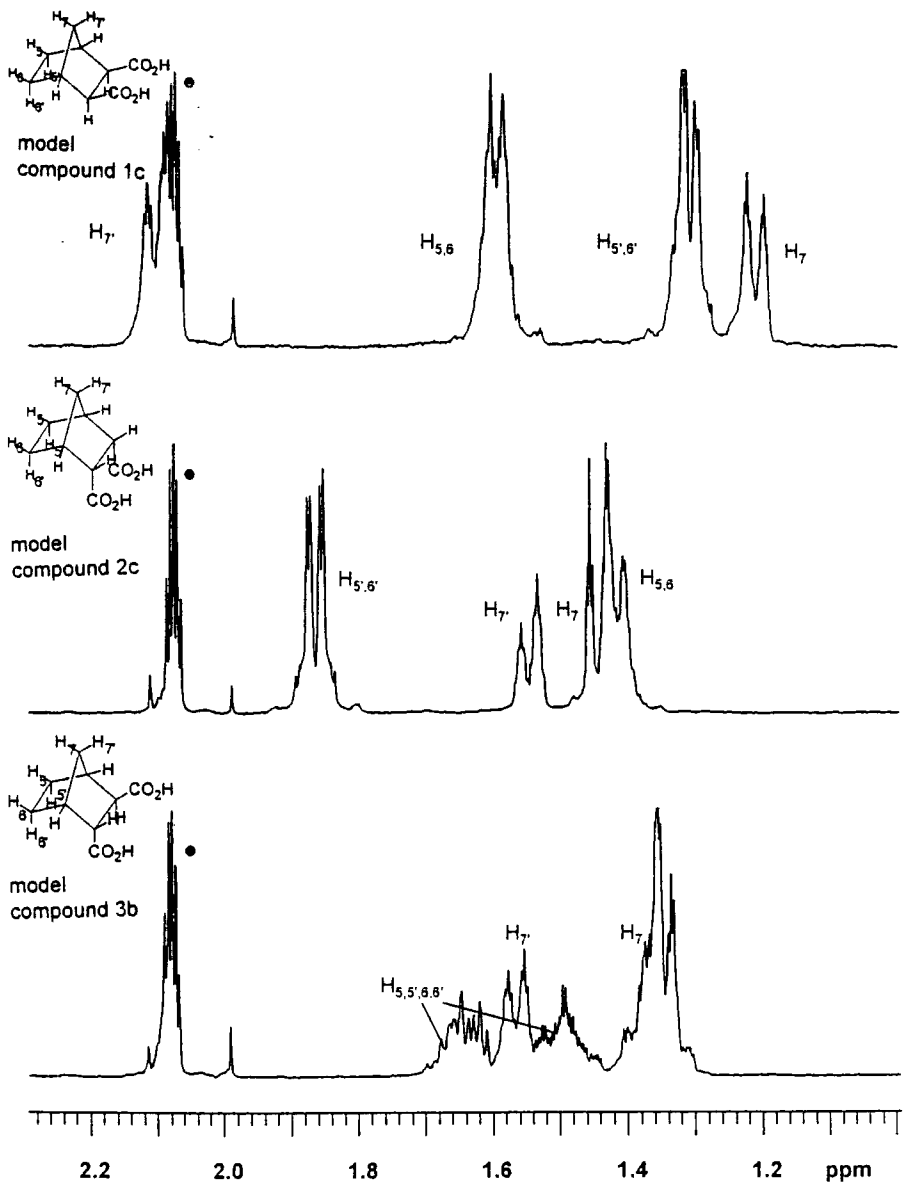

Fig. 2.2.10: ^{1}H NMR spectra of model compounds 1c, 2c and 3b.

An expansion of the region, 1.0 - 2.3 ppm.

•residual hydrogens in acetone-d_6

2.3 EXPERIMENTAL

Reagents and apparatus

All organic reagents were reagent grade, purchased from Aldrich Chemical Co. and used as recieved unless otherwise stated. The ^{1}H and ^{13}C NMR spectra were recorded using a Varian VXR 400 spectrometer operating at 400MHz for ^{1}H and 100MHz for ^{13}C NMR spectra. Chemical shifts are recorded in parts per million (δ) and referenced to internal TMS at 0 ppm. Coupling constants are listed in Hertz. A Perkin-Elmer 1600 series FTIR spectrometer was used to record infra-red spectra. Chemical ionisation mass spectra were recorded on a VG Analytical 7070E spectrometer using ammonia as the reagent gas. Melting points were obtained on an Electrothermal digital melting point apparatus and are recorded without correction. Elemental analyses (C, H, N) were performed using a Carlo-Elba-446 elemental analyser produced by Exeter Analytical Inc.

The synthesis and characterisation of *exo*-bicyclo[2.2.1]hept-5-ene-2,3-dicarboxy anhydride (model compound 1a).

Maleic anhydride (91.67g, 0.93 mol) and 1,2-dichlorobenzene ($100cm^3$) were placed in a 3-necked, round bottomed flask ($500cm^3$) fitted with a condenser, thermometer and dropping funnel. The mixture was stirred and heated to 178°C.[4] Dicyclopentadiene (75ml, 73.88g, 0.56mol) was added to the flask via the dropping funnel over a period of 2hrs to give a clear, yellow solution. The mixture was heated to reflux for 6hrs, giving a brown solution, which was allowed to cool overnight. The resulting light yellow crystals were recovered by filtration from the brown solution and recrystallised five times from acetone to

give transparent, colourless, lath-like crystals (13.53g, 0.064mol, 7% yield; m.pt 142.9-143.2°C, Lit.[5] 143°C). Found C, 65.57%, H, 4.92%; Calculated for $C_9H_9O_5$: C, 65.85%, H, 4.91%. ^1H NMR[6,7] [see appendix A1], (d_6-acetone, 400MHz) δ(ppm): 6.37 (pseudo t, $1.6 \leq J_{6,1} \sim J_{6,7'} < 2.4$Hz, 2H, $H_{5,6}$), 3.34 (p, $J_{1,6} \sim J_{1,5} \sim J_{1,7} \sim J_{1,7'}$, 2H, $H_{1,4}$), 3.14 (d, $J_{1,2}$ = 1.2Hz, 2H, $H_{2,3}$), ABq δ_B 1.6 (b, 1H, $H_{7'}$), δ_A 1.4 (q, 1H, H_7) J_{AB} = 10.4Hz. ^{13}C NMR [see appendix B1], (d_6-acetone, 100MHz) δ(ppm): 172.94 (s, $C_{8,9}$), 138.63 (s, $C_{5,6}$), 49.72 (s, $C_{2,3}$), 47.33 (s, $C_{1,4}$), 44.54 (s, C_7). FTIR[6] [see appendix C1], (KBr disc), (cm^{-1}): 3064 - 2884 (s, CH stretches), 1831, 1772 (br, s, C=O stretch), 1214, 1085 (s, C-O stretch). CI Mass Spec. (m/z), (M = $C_9H_8O_3$) : 182 (100%, B, MNH_4^+), 120 (16%, C_8H_8O, M-CO_2,), 91 (20%, C_7H_7, MH^+-CO_2-H_2O), 66 (9%, C_5H_6, M-$C_4H_2O_3$).

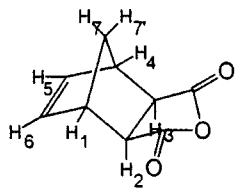

IUPAC assignment of hydrogen atoms within model compound 1a.

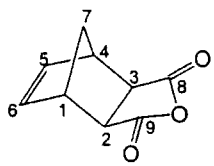

IUPAC assignment of carbon atoms within model compound 1a.

The synthesis and characterisation of *exo,exo*-bicyclo[2.2.1]hept-5-ene-2,3-dicarboxylic acid (model compound 1b).

Model compound 1a (3.17g, 0.019mol) and doubly distilled water (40ml) were placed in a one necked-round bottomed flask ($50cm^3$) fitted with a condenser and stirrer bar. The mixture was heated to reflux[8] for 2hrs, after which the model compound had fully dissolved, to give a clear, colourless solution, which was allowed to cool overnight. The solid deposited was recovered by filtration from

the solution to give colourless crystals (3.01g, 0.016mol, 87% yield; m.pt 150 - 151°C, Lit.[8] 148 - 149°C, decomp.). Found C, 59.40%, H, 5.66%; Calculated for $C_9H_{10}O_4$: C, 59.33%, H, 5.53%. ^1H NMR [see appendix A2], (d_6-acetone, 400MHz) δ(ppm): 6.25 (t, $1.6 \leq J_{6,1} \sim J_{6,7'} > 2.0$Hz, 2H, $H_{5,6}$), 3.03 (p, $1.6\text{Hz} < J_{1,6} \sim J_{1,5} \sim J_{1,7} \sim J_{1,7'} > 2\text{Hz}$, 2H, $H_{1,4}$), 2.59 (d, $J_{2,1}$ = 2Hz, 2H, $H_{2,3}$), ABq δ_B 2.18 (b, 1H, $H_{7'}$), δ_A 1.37 (q, 1H, H_7) J_{AB} = 8.4Hz. ^{13}C NMR [see appendix B2], (d_6-acetone, 100MHz) δ(ppm): 172.93 (s, $C_{8,9}$), 138.72 (s, $C_{5,6}$), 47.55 (s, $C_{1,4}$), 46.41 (s, $C_{2,3}$), 45.74 (s, C_7). FTIR [see appendix C2], (KBr disc), (cm^{-1}): 3200, (br, s, h-bonded O-H stretch), 2739 (s, O-H), 1716 (br, s, C=O). CI Mass Spec. (m/z), (M = $C_9H_{10}O_4$) : 200 (100%, B, MNH_4^+), 183 (36%, $C_9H_{11}O_4$, MH^+), 165 (11%, $C_9H_8O_3$, $MH^+ - H_2O$), 91 (18%, C_7H_7, $MH^+-2CO_2-2H_2O$), 66 (12%, C_5H_6, $M-C_4H_4O_4$). Approximately 0.3g of the product was recrystallsed from ethyl acetate, the resulting crystals were suitable for use in single crystal X-ray diffraction. The crystal structures were determined by Dr. A.S. Batsanov. Crystallographic data is given in appendix E1.

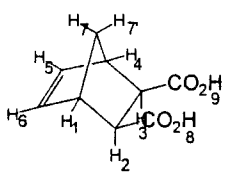

IUPAC assignment of hydrogen atoms within model compound 1b.

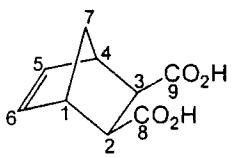

IUPAC assignment of carbon atoms within model compound 1b.

The synthesis and characterisation of *exo,exo*-bicyclo[2.2.1]heptane-2,3-dicarboxylic acid (model compound 1c).

Model compound 1b (0.65g, 0,004mol), palladium on carbon (5% Pd, 100mg) and acetic acid (10ml) were placed in an ampule (50ml) fitted with a stirrer bar. The mixture was stirred and hydrogen admitted. The uptake of hydrogen was measured using the manometer of standard water filled hydrogenation apparatus. The Pd/C catalyst was separated from the colourless solution by filtration and the solvent removed from the filtrate using a rotary evaporator. The crude product was recrystallised from doubly, distilled water to give a colourless crystalline solid. (0.58g, 0.003mol, 88% yield; m.pt 151 - 153°C, Lit.[8] 152 - 153°C decomp.). Found C, 58.73%, H, 6.57%; Calculated for $C_9H_{12}O_4$: C, 58.69%, H, 6.61%. ^{1}H NMR [see appendix A3], (d_6-acetone, 400MHz) δ(ppm): 11.94 (b, H_{OH}), 2.74 (dm, $J_{6,1}$=1.6Hz, 2H, $H_{2,3}$), 2.49 (bt, $J_{1,7}$ = $J_{1,7'}$ 2.8Hz, 2H, $H_{1,4}$), 2.10 (bm, 1H, $H_{7'}$), 1.57 (dm, 2H, $H_{5,6}$), 1.29 (dm, 2H, $H_{5',6'}$), 1.19 (dm, 1H, $H_{7'}$). ^{13}C NMR [see appendix B3], (d_6-acetone, 100MHz) δ(ppm): 174.53 (s, $C_{8,9}$), 51.80 (s, C), 40.80 (s, C), 36.06 (s, C), 29.15 (s, C). FTIR [see appendix C3], (KBr disc), (cm^{-1}): 2966, (br, s, h-bonded O-H stretch), 2625 (s, O-H), 1713 (br, s, C=O). CI Mass Spec. (m/z), (M = $C_9H_{12}O_4$) : 200 (100%, B, MNH_4^+), 184 (24%, $C_9H_{12}O_4$, $M^{+\cdot}$), 167 (4%, $C_9H_{10}O_3$, MH^+ - H_2O), 94 (2%, C_7H_9, MH^+-$2CO_2$-$2H_2O$). Approximately 0.3g of the product was recrystallised from ethyl acetate, the resulting crystals were suitable for use in single crystal X-ray diffraction. The crystal structures were determined by Dr. A.S. Batsanov. Crystallographic data is given in appendix E2.

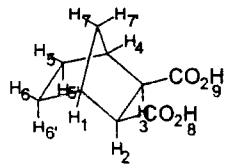

IUPAC assignment of hydrogen atoms within model compound 1c.

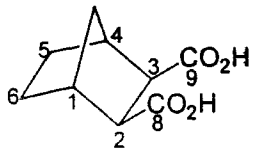

IUPAC assignment of carbon atoms within model compound 1c.

The synthesis and characterisation of *endo*-bicyclo[2.2.1]hept-5-ene-2,3-dicarboxy anhydride (model compound 2a).

Maleic anhydride (63.9g, 0.65mol) and anhydrous diethyl ether (400cm^3) were placed in a 3-necked round bottomed flask (1 litre) fitted with a thermometer, condenser dropping funnel and magnetic stirrer, the mixture was stirred. Cyclopentadiene (52.47g, 0.79mol) was added [6] dropwise via a dropping funnel over a period of $1^1/_6$ hrs. The stirring mixture was cooled using an ice/salt bath and the temperature did not rise above 7°C during the addition of the cyclopentadiene. The mixture was stirred with cooling for a further 2hrs after which all the solids had fully dissolved the ice/salt bath was removed and a white powder precipitated. The diethyl ether was decanted off and the product dried *in vacuo* to give a colourless crystalline solid which was recrystallised once from acetone (97.61g, 0.59mol, 93% yield; m.pt 164°C, Lit.[5] 165°C). Found C, 65.65%, H,4.87%; Calculated for $C_9H_9O_5$: C, 65.85%, H, 4.91%. ^{1}H NMR,[6] [see appendix A4], (d_6-acetone, 400MHz) δ(ppm): 6.29 (t, 1.6≤ $J_{6,1}$ ~ $J_{6,7'}$ >2.4Hz, 2H, $H_{5,6}$), 3.79 (m, 2H, $H_{2,3}$), 3.43 (m, 2H, $H_{1,4}$), 1.69 (m, 2H, $H_{7,7'}$). ^{13}C NMR [see appendix B4], (d_6-acetone, 100MHz) δ(ppm): 172.72 (s, $C_{8,9}$), 136.31 (s, $C_{5,6}$), 53.28 (s, C_7), 47.98 (s, $C_{2,3}$), 46.62 (s, $C_{1,4}$). FTIR[6] [see appendix C4],

(KBr disc), (cm^{-1}): 3064 - 2884 (s, CH stretches), 1849, 1772 (br, s, C=O stretch), 1226, 1085 (s, C-O stretch). CI Mass Spec. (m/z) (M = $C_9H_8O_3$) : 182 (100%, B, MNH_4^+), 120 (8%, C_8H_8O, M-CO_2,), 91 (13%, C_7H_7, MH^+-CO_2-H_2O), 66 (7%, C_5H_6, M-$C_4H_2O_3$).

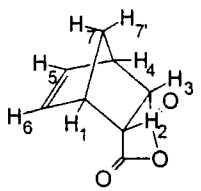

IUPAC assignment of hydrogen atoms within model compound 2a.

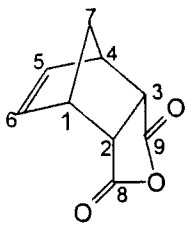

IUPAC assignment of carbon atoms within model compound 2a.

The synthesis and characterisation of *endo,endo*-bicyclo[2.2.1]heptene-2,3-dicarboxylic acid (model compound 2b).

Model compound 2a (5.5g, 0.03mol) and doubly distilled water (60ml) were placed in a one necked-round bottomed flask ($100cm^3$) fitted with a condenser and stirrer bar. The mixture stirred for 2hrs, after which the model compound had fully dissolved, to give a clear, colourless solution which was left to stand overnight. The resulting solid was recovered by filtration from the solution to give colourless crystals (5.02g, 0.027mol, 92% yield; m.pt 179-183°C, Lit.[9] 177-179°C, decomp.).

Found C, 59.16%, H, 5.48%;Calculated for $C_9H_{10}O_4$: C, 59.33%, H, 5.53%.

^{1}H NMR [see appendix A5], (d_6-acetone, 400MHz) δ(ppm): 10.41 (b, $H_{8,9}$), 6.16 (t, 1.6Hz<$J_{6,1}$ ~ $J_{6,7'}$>2Hz, 2H, $H_{5,6}$), 3.33 (t, 2H, $H_{2,3}$), 3.10 (q, $J_{1,7}$=$J_{1,7'}$=$J_{1,2}$=$J_{1,6}$=$J_{1,5}$=1.6Hz, 2H, $H_{1,4}$), ABq δ_B 1.41 (b, 1H, $H_{7'}$), δ_A 1.37 (q, 1H, H_7) J_{AB} = 8.4Hz. ^{13}C NMR [see appendix B5], (d_6-acetone, 100MHz) δ(ppm):

173.74 (s, $C_{8,9}$), 135.50 (s, $C_{5,6}$), 49.02 (s, $C_{1,4}$), 48.49 (s, $C_{2,3}$), 47.15 (s, C_7). FTIR [see appendix C5], (KBr disc), (cm^{-1}): 3100, (br, s, h-bonded O-H stretch), 2661 (s, O-H), 1707 (br, s, C=O). CI Mass Spec. (m/z), (M = $C_9H_{10}O_4$) : 200 (100%, B, MNH_4^+), 183 (91%, $C_9H_{11}O_4$, MH^+), 165 (14%, $C_9H_8O_3$, $MH^+ - H_2O$), 91 (12%, C_7H_7, $MH^+-2CO_2-2H_2O$), 66 (11%, C_5H_6, $M-C_4H_4O_4$).

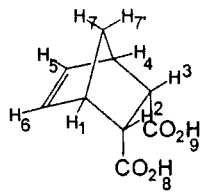

IUPAC assignment of hydrogen atoms within model compound 2b.

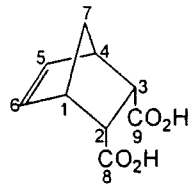

IUPAC assignment of carbon atoms within model compound 2b.

The synthesis and characterisation of *endo,endo*-bicyclo[2.2.1]heptane-2,3-dicarboxylic acid (model compound 2c).

Model compound 2b (0.66g, 0,004mol), palladium on carbon (5% Pd, 100mg) and acetic acid (10ml) were placed in an ampule (50ml) fitted with a stirrer bar. The mixture was stirred and hydrogen admitted. The uptake of hydrogen was measured using a manometer of standard water filled hydrogenation apparatus. The Pd/C catalyst was separated from the colourless solution by filtration and the solvent removed from the filtrate using a rotary evaporator. The crude product was recrystallised from doubly, distilled water to give a colourless solid. (0.57g, 0.003mol, 87% yield; m.pt 150 - 152°C, Lit.[10] 150 - 151°C). Found C, 58.52%, H, 6.57%;Calculated for $C_9H_{12}O_4$: C, 58.69%, H, 6.61%. ^1H NMR [see appendix A6], (d_6-acetone, 400MHz) δ(ppm): 11.86 (b, H_{OH}), 3.02 (dm, $J_{6,1}$=0.8Hz, 2H, $H_{2,3}$), 2.49 (bt, $1.6<J_{1,7} \sim J_{1,7}>2.8$Hz, 2H, $H_{1,4}$), 2.10 (bm, 1H,

$H_{7'}$), 1.57 (dm, 2H, $H_{5,6}$), 1.29 (dm, 2H, $H_{5',6'}$), 1.19 (m, 2H, $H_{7,7'}$). ^{13}C NMR [see appendix B6], (d_6-acetone, 100MHz) δ(ppm): 173.81 (s, $C_{8,9}$), 47.06 (s, $C_{1,4 \text{ or } 2,3}$), 41.07 (s, $C_{1,4 \text{ or } 2,3}$), 40.10 (s, $C_{5,6 \text{ or } 7}$), 24.59 (s, $C_{5,6 \text{ or } 7}$). FTIR [see appendix C6], (KBr disc), (cm^{-1}): 3200, (br, s, h-bonded O-H stretch), 2727 (s, O-H), 1710 (br, s, C=O). CI Mass Spec. (m/z), (M = $C_9H_{12}O_4$) : 200 (74%, $C_9H_{16}NO_4$, MNH_4^+), 184 (100%, B, M^+), 167 (8%, $C_9H_{10}O_3$, $MH^+ - H_2O$), 94 (8%, C_7H_9, $MH^+-2CO_2-2H_2O$). Approximately 0.3g of the product was recrystallised from ethyl acetate, the resulting crystals were suitable for use in single crystal X-ray diffraction. The crystal structures were determined by Dr. A.S. Batsanov. Crystallographic data is given in appendix E3.

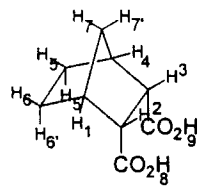

IUPAC assignment of hydrogen atoms within model compound 2c.

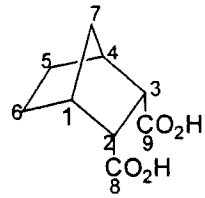

IUPAC assignment of carbon atoms within model compound 2c.

The synthesis and characterisation of 2-*endo*-3-*exo*-bicyclo[2.2.1]hept-5-ene-2,3-dicarboxylic acid (model compound 3a).

Fumaric acid (3.08g, 0.027mol), cyclopentadiene (2.3ml, 2.3g, 0.035mol) and dry THF (50ml) were placed in a one necked round bottomed flask fitted with a condenser and stirrer bar. The solution was stirred at room temperature for 48hrs and the solvent removed using a rotary evaporator. The solid was recrystallised from doubly distilled water and the solvent removed by filtration to give colourless crystals. (4.41g, 0.024mol, 93% yield; m.pt 185-186°C, Lit.[11] 186°C,

decomp.). Found C, 59.20%, H, 5.55%; Calculated for $C_9H_{10}O_4$: C, 59.33%, H, 5.53%. ^1H NMR [see appendix A7], (d_6-acetone, 400MHz) δ(ppm): 10.73 (b, $H_{8,9}$), 6.31 (q, 1H, H_5), 6.11 (q, 1H, H_6), 3.36 (t, 1H, H_2), 3.25 (b, 1H, H_1), 3.14 (b, 1H, H_4), 2.64 (dd, 1H, H_3) ABq δ_B 1.62 (bd, 1H, $H_{7'}$), δ_A 1.42 (bd, 1H, H_7) J_{AB} = Hz. ^{13}C NMR [see appendix B7], (d_6-acetone, 100MHz) δ(ppm): 179.88 (s, C_9), 178.56 (s, C_8), 142.42 (s, C_5), 140.03 (s,C_6) 52.52 (s, C_2), 52.42 (s, C_4), 52.07 (d, C_7), 51.74 (s, C_3), 50.39 (s, C_1). FTIR [see appendix C7], (KBr disc), (cm^{-1}): 3100, (br, s, h-bonded O-H stretch), 3000 - 2800 (s, CH stretch), 2618 (s, O-H), 1691 (s, C=O). CI Mass Spec. (m/z), (M = $C_9H_{10}O_4$) : 200 (100%, B, MNH_4^+), 183 (9%, $C_9H_{11}O_4$, MH^+), 165 (3%, $C_9H_8O_3$, MH^+ - H_2O), 91 (8%, C_7H_7, MH^+-$2CO_2$-$2H_2O$), 66 (13%, C_5H_6, M-$C_4H_4O_4$). Approximately 0.3g of the product was recrystalli sed from ethyl acetate, the resulting crystals were suitable for use in single crystal X-ray diffraction. The crystal structures were determined by Dr. A.S. Batsanov. Crystallographic data is given in appendix E4.

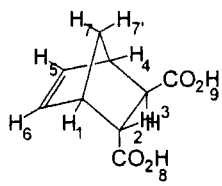

IUPAC assignment of hydrogen atoms within the model compound 3a.

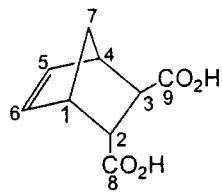

IUPAC assignment of carbon atoms within the model compound 3a.

The synthesis and characterisation of 2-*endo*-3-*exo*-bicyclo[2.2.1]heptane-2,3-dicarboxylic acid (model compound 3b).

Model compound 3a (0.59g, 0,003mol), palladium on carbon (5% Pd, 100mg) and acetic acid (10ml) were placed in an ampule (50ml) fitted with a stirrer bar. The mixture was stirred and hydrogen admitted. The uptake of hydrogen was measured using the manometer of standard water filled hydrogenation apparatus. The Pd/C catalyst was separated from the colourless solution by filtration and the solvent removed from the filtrate using a rotary evaporator. The crude product was recrystallised from doubly, distilled water to give a colourless crystalline solid. (0.52g, 0.003mol, 86% yield; m.pt 162-163°C, Lit. 161-163°C). Found C, 58.73%, H, 6.61%,Calculated for $C_9H_{12}O_4$: C, 58.69%, H, 6.61%.

^{1}H NMR[12] [see appendix A8], (d_6-acetone, 400MHz) δ(ppm): 11.94 (b, H_{OH}), 3.19 (m, 1H, H_2), 2.75 (dm, $J_{2,3}$ = 5.2Hz, 2H, H_3), 2.63 (m, 1H, H_1), 2.59 (m, 1H, H_4), 1.7-1.3 (m, 6H, $H_{3,3',2,2',7,7'}$). ^{13}C NMR [see appendix B8], (d_6-acetone, 100MHz) δ(ppm): 175.76 (s, C_9), 174.56 (s, C_8), 49.87 (s, C_{2or3}), 49.20 (s, C_{2or3}), 42.48 (s, C_{1or4}), 40.80 (s, C_{1or4}), 38.57 (s, $C_{5,6or7}$), 29.51 (s, $C_{5,6or7}$) (peak concealed by acetone peaks in shown spectrum, assigned by running spectrum in DMSO), 24.73 (s, $C_{5,6or7}$). FTIR[12] [see appendix C8], (KBr disc), (cm^{-1}): 3220, (br, s, h-bonded O-H stretch), 2996 - 2850 (s, CH stretch), 2649 (s, O-H), 1708 (s, C=O). CI Mass Spec. (m/z), (M = $C_9H_{12}O_4$) : 200 (100%, B, MNH_4^+), 184 (19%, $C_9H_{12}O_4$, $M^{+\cdot}$), 167 (4%, $C_9H_{10}O_3$, $MH^+ - H_2O$).

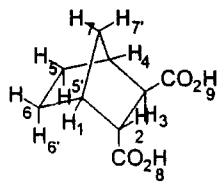

IUPAC assignment of hydrogen atoms within the model compound 3b.

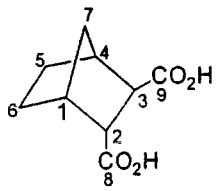

IUPAC assignment of carbon atoms within the model compound 3b.

The synthesis and characterisation of *exo*-7-oxabicyclo[2.2.1]hept-5-ene-2,3-dicarboxy anhydride (model compound 4a).

Maleic anhydride (128g, 1.3mol) was dissolved in diethyl ether (500ml) and the solution poured into a one necked, round bottomed, flask fitted with a condenser and stirrer bar. Furan (89.1g, 1.3mol) was added and the solution[13] stirred at room temperature for 12hrs. The resulting white solid was recovered by filtration and washed with a small amount of diethyl ether. The product was a transparent, colourless, crystalline solid. (160.7g, 0.96mol, 74% yield; m.pt 118°C, Lit.[14] 125°C). Found C, 57.79%, H, 3.61%, Calculated for $C_8H_6O_4$: C, 57.83%, H, 3.64%. ^{1}H NMR [see appendix A9], (d_6-acetone, 400MHz) δ(ppm): 6.65 (t, $J_{6,1} \sim J_{6,4} \sim$ 1Hz, 2H, $H_{5,6}$), 5.38 (t, $J_{1,6} \sim J_{1,5} \sim$ 1Hz, 2H, $H_{1,4}$), 3.39 (s, 2H, $H_{2,3}$). ^{13}C NMR [see appendix B9], (d_6-acetone, 100.58MHz) δ(ppm): 172.94 (s, $C_{8,9}$), 137.74 (s, $C_{5,6}$), 83.05 (s, $C_{1,4}$), 49.92 (s, $C_{2,3}$). FTIR [see appendix C9], (KBr disc), (cm^{-1}): 3105 - 3001 (m, CH stretches), 1860, 1790 (s, C=O stretch), 1232, 1091 (s, C-O stretch). CI Mass Spec. (m/z), (M = $C_8H_6O_4$) : 184 (1%, $C_8H_{12}NO_5$, MNH_4^+), 68 (100%, B, M-$C_4H_2O_3$).

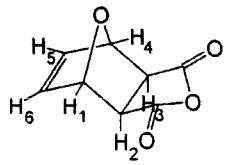

IUPAC assignment of hydrogen atoms within model compound 4a.

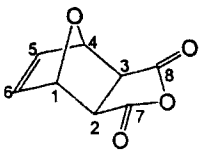

IUPAC assignment of carbon atoms within model compound 4a.

The synthesis and characterisation of *exo,exo*-7-oxabicyclo[2.2.1]hept-5-ene-2,3-dicarboxy anhydride (model compound 4b).

Model compound 4a (50g, 0.30mol) and doubly distilled water (200ml) were placed in a one necked-round bottomed flask (50cm^3) fitted with a condenser and stirrer bar. The solution was stirred for 1hr and allowed to stand for 48hrs. The resulting solid was recovered by filtration and washed with a small amount of doubly distilled water to give a colourless, crystalline solid. (38.0g, 0.2mol, 68% yield; m.pt 137°C, Lit.[15] 134°C). Found C, 52.14%, H, 3.26%, Calculated for $C_8H_8O_4$: C, 52.18%, H, 3.28%. ^{1}H NMR [see appendix A10], (D_2O, 400MHz) δ(ppm): 6.38 (bs, 2H, $H_{5,6}$), 5.12 (bs, 2H, $H_{1,4}$), 2.83 (bs, 2H, $H_{2,3}$). ^{13}C NMR [see appendix B10], (D_2O, 100.58MHz) δ(ppm): 175.78 (s, $C_{7,8}$), 136.13 (s, $C_{5,6}$), 80.14 (s, $C_{1,4}$), 46.61 (s, $C_{2,3}$). FTIR [see appendix C10], (KBr disc), (cm^{-1}): 3150, (br, s, h- bonded O-H stretch), 2672 (s, O-H), 1708 (s, C=O). CI Mass Spec. (m/z), (M = $C_8H_8O_5$) : 202 (2%, $C_8H_{12}NO_5$, MNH_4^+), 134 (100%, B, $C_4H_4O_4NH_4^+$). Approximately 0.3g of the product was recrystallsed from ethyl acetate, the resulting crystals were suitable for use in single crystal X-ray diffraction. The crystal structures were determined by Dr. A.S. Batsanov. Crystallographic data is given in appendix E5.

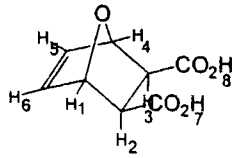

IUPAC assignment of hydrogen atoms within model compound 4b.

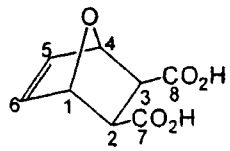

IUPAC assignment of carbon atoms within model compound 4b.

The synthesis and characterisation of *exo, exo*-7-oxabicyclo-[2.2.1]heptane-2,3-bis(carboxylic acid) (model compound 4c).

Model compound 4a (0.61g, 0,003mol), palladium on decolourising carbon (5% Pd, 100mg) and acetic acid (10ml) were placed in an ampule (50ml) fitted with a stirrer bar. The mixture was stirred and hydrogen admitted. The uptake of hydrogen was measured using standard water filled hydrogenation apparatus. The Pd/C catalyst was separated from the colourless solution by filtration and the solvent removed from the filtrate using a rotary evaporator. The crude product was recrystallised from doubly, distilled water to give a colourless crystalline solid. (0.50g, 0.003mol, 81% yield; m.pt 122°C, Lit. [16]122-123°C). Found C, 51.58%, H, 5.40%, Calculated for $C_8H_8O_4$: C, 51.62%, H, 5.41%. ^{1}H NMR [see appendix A11], (d_6-acetone, 400MHz) δ(ppm): 4.79 (m, 2H, $H_{1,4}$), 3.05 (bs, 2H, $H_{2,3}$) 165.05 (m, 4H, $H_{5,5',6,6'}$). ^{13}C NMR [see appendix B11], (d_6-acetone, 100.58MHz) δ(ppm): 172.66 (s, $C_{7,8}$), 79.12 (s, $C_{5,6}$), 52.55 (s, $C_{1,4}$), 29.60 (s, $C_{2,3}$).

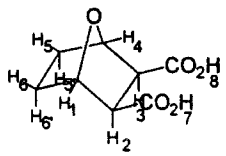

IUPAC assignment of H atoms

in model compound 4c.

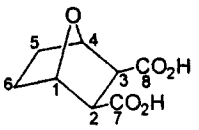

IUPAC assignment of C atoms

in model compound 4c.

2.4 REFERENCES FOR CHAPTER 2

[1] 'Organic Chemistry', 2nd Ed., Mc.Murray J., publ. by Brooks/Cole, 1988.

[2] 'Advanced Organic Chemistry: Reactions, Mechanisms and Structure', March J., 4th Ed., John Wiley and Sons, Inc., 1992.

[3] Sauer. J., *Angew.Chem.Internat.Edit.*, **6**, No.1, 16-32, 1967.

[4] Castner, K.F. and Calderon, N., *J.Mol.Catal.*, **15**, 47-59, 1982.

[5] Craig, D., *J.Am.Chem.Soc.*, **73**, 4889, 1951.

[6] Canonne, P., Belanger, D., Lemay, G., *J.Org.Chem.* **47**, 3953-3959, 1982.

[7] Berning, W., Hunig, S., Prokschy, F., *Chem.Ber.*, **117**, 1455-1464, 1984.

[8] Alder, Stein, *Justus Liebigs Ann.Chem.*, **504**, 216-248, 1933.

[9] Diels, Alder, *Justus Liebigs Ann.Chem.*, **460**, 103-112, 1928.

[10] Moriconi, Crawford, *J.Org.Chem.* **33**, 370-376, 1968.

[11] Brace, *J.Org.Chem.*, **44**, 1964-1969, 1979.

[12] Waldmann, H., *Justus Liebigs Ann.Chem.*, 7, 671-680, 1990.

[13] Woodward, R.B., Baer, H., *J.Am.Chem.Soc.*, **70**, 1161-1166, 1948.

[14] Stockmann, H., *J.Org.Chem.*, **26**, 2025-2029, 1961.

[15] Jolivet, J., *Ann.Chim.*, **5**, 1165-1217, 1960.

[16] Alder, Backendorf, *Justus Liebigs Ann.Chem.*, **117**, 113-119, 1938.

CHAPTER 3

Crystallisation of Calcium Carbonate in the Presence of Dicarboxylic acid Model Compounds

3.1 INTRODUCTION

The objectives of the work discussed in this chapter were to determine the effects of the bicyclo-dicarboxylic acid model compounds upon the crystallisation of $CaCO_3$ from supersaturated aqueous solutions of $Ca(HCO_3)_2$. The synthesis and characterisation of all model compounds used in the crystallisation experiments described in this chapter have been discussed in Chapter 2.

3.2 EXPERIMENTAL

3.2.1 Introduction

Calcium carbonate was purchased from Aldrich Ltd and the source and quality of the reactants used in model compound synthesis is given in the experimental section of Chapter 2. All other chemicals and solvents were purchased from Aldrich Ltd and used as supplied unless otherwise stated, the water used was doubly distilled and deionised (conductivity < 0.06μS) using Elga UHQ apparatus. All glassware was washed thoroughly with hot soapy ('Super detergent', purchased from Coventry Chemicals Ltd.) tap water, deionised water, fresh dilute nitric acid, deionised water, methanol and finally deionised water.

3.2.2 Preparation of supersaturated $Ca(HCO_3)_{2(aq)}$

Calcium carbonate (6g), suspended in deionised water (3l) was added to a 5l, one necked, round bottomed flask with a teflon coated magnetic stirrer bar. The mixture was stirred rapidly to prevent $CaCO_3$ sedimentation. Carbon dioxide gas from a vapour withdrawal cylinder was bubbled through the reaction solution via a hollow glass tube with a bulbous end of about 1.5cm diameter, containing

approximately ten holes of 1mm diameter. Water filled Dreschel bottles were placed between the CO_2 cylinder and the 5l round bottomed flask to ensure the removal of all soluble organic and/or inorganic contaminants and also after the flask in order to monitor the flow of gas through the mixture [Fig. 3.2.1]. Carbon dioxide was bubbled through the mixture for $1^1/_2$ hours. Excess $CaCO_{3(s)}$ was filtered from the mixture using a Buchner funnel fitted with two fine, hardened, purified, ashless filter papers produced by W. and R. Balston Ltd., No.542, 11cm diameter. The CO_2 gas was bubbled through the resulting clear, colourless supersaturated calcium hydrogen carbonate solution for a further $^1/_2$ hour to dissolve any nascent crystallites.

3.2.3 Introduction of additives

The supersaturated solution (100ml aliquots) was placed in crystallisation dishes each labelled and containing three glass microscope coverslips (13mm dia.). The dishes were placed in a plastic tray filled to a height of approximately 1cm with tap water, in order to stabilise the ambient temperature (19°C), and covered loosely with plasticiser free cling film [Fig. 3.2.2].

After 12hrs crystals had formed at the surface of the solution, these were collected on a glass microscope coverslip. Crystals were found at the bottom of the crystallising dishes, these tended to appear more slowly than those at the surface and were collected after 2 days. In order to collect the crystals from the bottom of the dish the remaining surface crystals and solution were removed by the use of a plastic micropipette funnel attached to a water pump. It was then possible to collect the microscope slides from the base of the dishes.

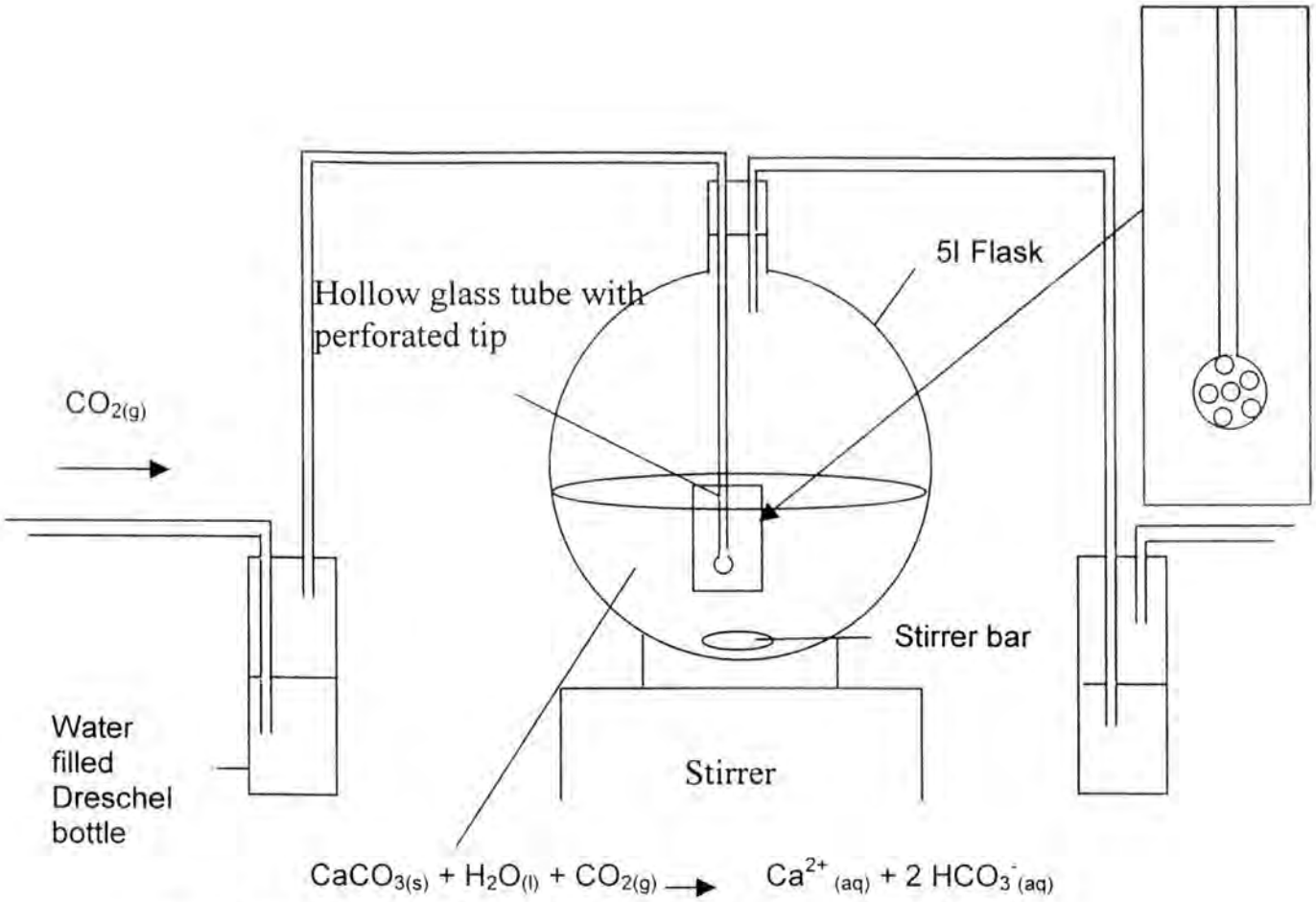

Fig. 3.2.1. A diagrammatic representation of the apparatus used to produce supersaturated solutions of $Ca(HCO_3)_2$.

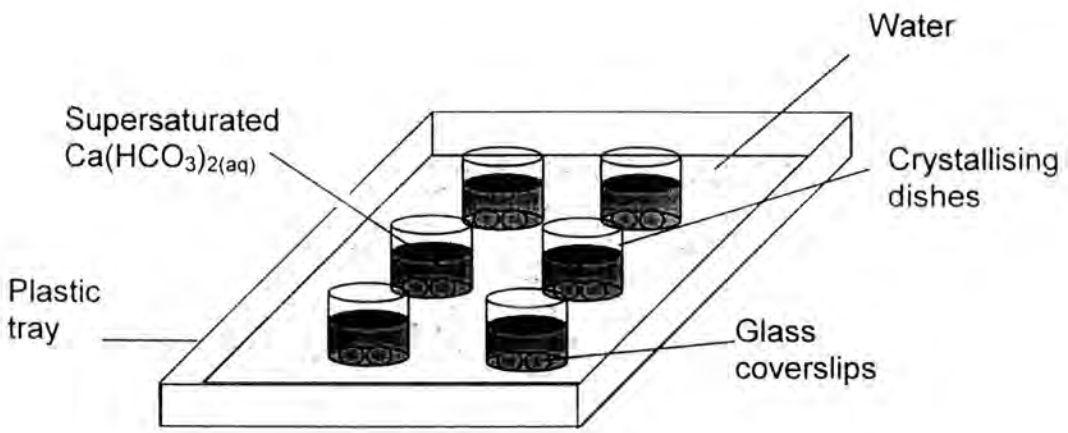

Fig. 3.2.2. A diagram of the crystal growth experiment.

To each dish a solution (1ml, 0.1ml or 0.01ml) of the model compound in water (0.1M) was added. This gave $[Ca^{2+}]$: [model compound] molar ratios of 10:1, 100:1 and 1000:1 respectively. Three control dishes, containing no additive, were used in each experiment for comparison.

Crystals were examined initially by optical microscopy using a Zeiss Axiophot Optical Microscope with a par focalised, *i.e.* the camera is in focus if the image seen through the eyepiece is in focus, M80 camera system. Mounting the coverslips on microscope slides allowed the concurrent analysis of both bulk and surface crystals. Crystal size measurements and nucleation densities were determined from the optical micrographs. Scanning Electron microscopy was used for more detailed morphological examinations. The microscope coverslips with crystals were attached to microscope stubbs by carbon discs (*ca.* 8mm dia.) with adhesive on both faces and in certain cases were gold sputtered in order to reduce charging effects. The SEM had a field emission electron gun and accelerating voltages ranging from 500V - 20kV. The accelerating voltage used in these studies was approximately 1kV. Polymorph determination of air dried surface and bulk grown crystals was carried out using IR spectroscopy as KBr discs or X-Ray powder diffraction by comparison of the d spacings with standard values from Joint Committee on Powder Diffraction Standards (JCPDS) tables; see JCPDS (1974) table numbers: for calcite, 24-27A; for vaterite; 24-30A. The nucleation densities, mean sizes and standard distribution values of the crystals were measured with the aid of Imagen 2 data analysis equipment. The longest physical axis of the crystals were measured. All molecular modelling was

carried out using the Cerius© (copyright of MSI) 2 version 3.0 software using a universal forcefield.

3.3 RESULTS AND DISCUSSIONS

3.3.1a Control system

Control crystals were collected from both the air/water interface and the base of the dishes. Virtually all crystals observed were rhombohedral with six smooth, well defined {1 0 4} faces [Fig. 3.3.1]. A 3D molecular projection of the structure of calcite rhombs and {1 0 4} crystal faces see appendices F4 and F5. XRD studies confirmed the polymorph to be calcite. Approximately 10% of the rhombohedra were truncated; in general, these morphological modifications occurred along non specific planes. Traces of vaterite were seen occasionally but aragonite was never seen in the controls.

Fig. 3.3.1. Scanning electron micrographs showing control rhombs grown from bulk solution.

The crystals collected at the air/water interface were mainly intergrown and dendritic whereas those collected at the base were much more discrete. [Fig.3.3.2].

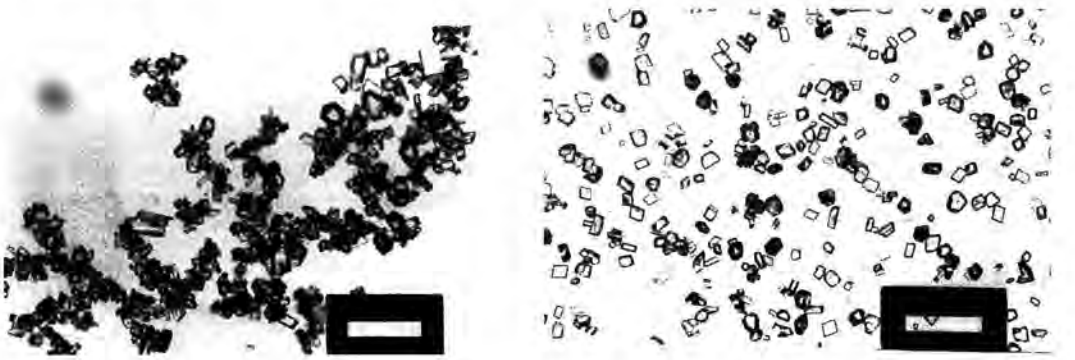

a. b.

Fig. 3.3.2. Optical micrographs showing, a. Control crystals of $CaCO_3$ grown at the air/water interface. Scale bar = 100μm. b. Control crystals of $CaCO_3$ grown in the bulk solution and collected on coverslips. Scale bar = 200μm.

Crystal sizes from the base sample ranged from 20-80μm, with a mean value of 30μm for the longest axis and a standard deviation ± 10μm. The large size distribution indicated that crystal nucleation was episodic.

3.3.1b Effect of mono-*exo*-acid model compound

Model compound 5, *exo*-bicyclo[2.2.1]hept-5-ene-2-dicarboxylic acid provided by Dr. Erwin Herzog, was used as the additive in the crystallisation of $CaCO_3$ from a supersaturated solution of $Ca(HCO_3)_2$ at $[Ca^{2+}]$:[model compound] molar ratios of 10:1, 100:1 and 1000:1. The resulting crystals were modified in a non specific manner at either the edges or corners of a {1 0 4} rhombic form [Fig. 3.3.3]. The crystals appeared very similar to those grown from the control

solution showing little or no effect of the mono-acid model compound additive on the inorganic crystallisation.

Fig. 3.3.3. Scanning electron micrographs showing $CaCO_3$ crystals grown from bulk solution in presence of model compound 5. a. $[Ca^{2+}]$:[model compound 5] 10:1.

3.3.2 Effect of model compounds 1b, 1c, 2b, 2c, 3a and 3b

The structures of the model compounds discussed in this section are given in the experimental section of Chapter 2 (pp 49-62) and are shown on the bookmark. The influence of model compound 1b, *exo,exo*-bicyclo[2.2.1]hept-5-ene-2,3-dicarboxylic acid, on the crystallisation of $CaCO_3$ at $[Ca^{2+}]$:[model compound] molar ratios of 10:1, 100:1 and 1000:1 was evident in the unique morphology of crystals and the associated data for nucleation density and size. The nucleation density of crystals grown in the bulk was noticeably larger at the highest concentration of model compound at an average of 340 crystals/cm^2 compared to less than half this value for the lower two concentrations. In comparison the nucleation density for the control (no model compound) assay was 136

crystals/cm^2. Crystals grown at the air/water interface were modified in the same way as those in the bulk, however, crystals at the surface were more intergrown and not suitable for detailed morphological studies or determination of nucleation densities and crystal sizes. The effect upon bulk nucleation at high dosage suggests that the influence of high model compound concentration may be related to the cation binding function of the additive; this would affect the supersaturation with respect to $CaCO_3$(s). The effect might be to reduce the relative supersaturation at the air/water interface with CO_2(g) out gassing and favour precipitation in bulk solution.

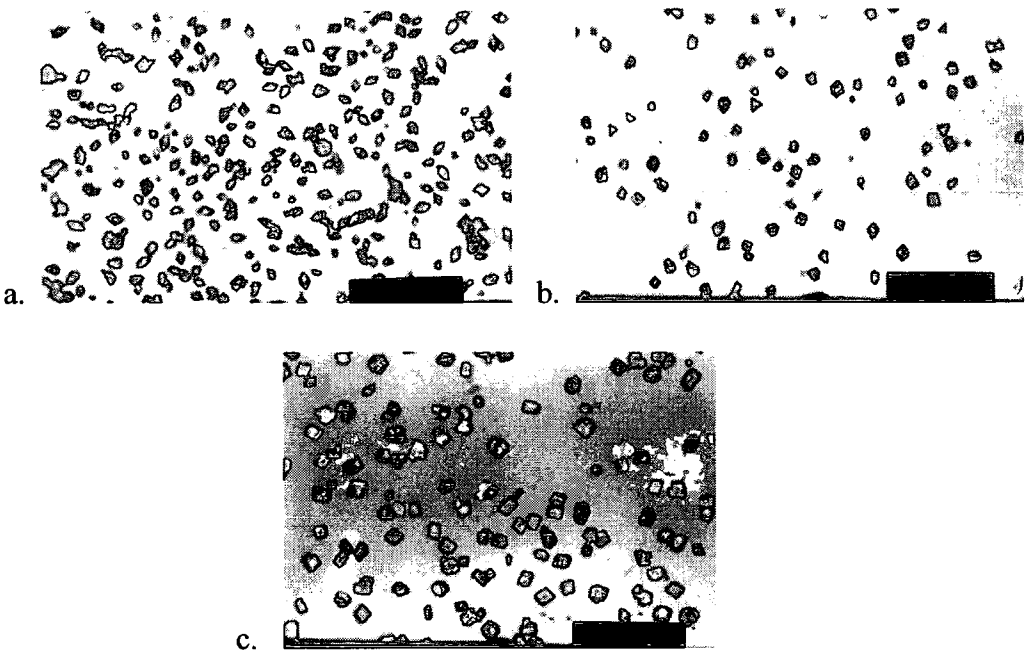

Fig. 3.3.4. Optical micrographs showing crystals of $CaCO_3$ grown from bulk solution with model compound 1b as additive [Ca^{2+}]:[model compound 1b] a. 10:1. b. 100:1. c. 1000:1. Scale bars = 100μm

Both surface and bulk grown calcite crystals were modified extensively at the highest additive concentration , less so, but in the same manner, at intermediate

concentration and to a significantly lesser extent at the lowest model compound concentration. The most modified crystals had an essentially rhombohedral structure with elongated appendages which gave the crystals the appearance of spearheads when viewed in projection [Fig. 3.3.5a]. On observation using SEM, all crystal surfaces were roughened and slightly rounded. The crystals grown at the intermediate model compound concentration had a similar appearance, however, the appendages were shorter [Fig. 3.3.5.b] and the crystals more rhombohedral in form [Fig. 3.3.5.c]. In addition to the roughened faces, narrow strips of smooth faces were observed. At the lowest concentration of additive, crystals appeared essentially rhombohedral and were distinguished by the perturbations of growth at the vertices (not reproduced here).

The shapes of the calcite crystals grown from solution containing intermediate concentration of model compound were compared with molecular models of calcite where the expression of specific faces was determined on the basis of relative stabilities of the different forms. From these investigations it became apparent that the crystal morphologies resembled the structure of a highly modified calcite rhomb with preferentially expressed {1 0 2} faces. The specific stabilised faces can be defined to be a subset of the {1 0 2} family. These data suggest that the stable faces are the (1 0 -2) and the symmetrical equivalent (-1 0 2) face. Further evidence that the crystals were modified in such a manner was obtained from a comparison of the observed interfacial angles with theoretical values. These also confirmed the unique stabilisation of the (1 0 -2) and (-1 0 2) faces [compare Fig. 3.3.5c with Fig. 3.3.6]. One reason for the selective interaction of model compound 1b with the nominally homopolar, (1 0 -2) and

(-1 0 2) faces of calcite could be due to geometric matching

a.

b.

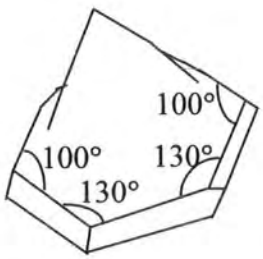

c.

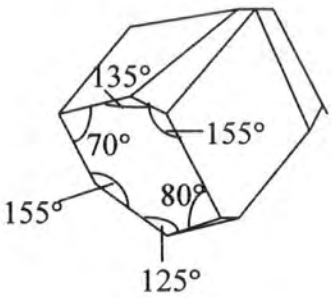

Fig. 3.3.5. Scanning electron micrographs showing $CaCO_3$ crystals grown from bulk solution in presence of model compound 1b a. $[Ca^{2+}]$:[model compound 1b] 10:1, b. and c. $[Ca^{2+}]$:[model compound 1b] 100:1 and diagrams of certain crystals including angles.

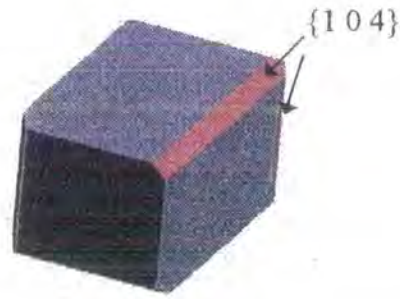

Fig. 3.3.6. A theoretical calcite crystal with preferential expression of (1 0 -2) and (-1 0 2) faces (shown in blue). This structure was calculated using Cerius© 2, version 3.0 molecular modelling software.

between the Ca^{2+} ions of the crystal lattice [Fig. 3.3.7] and distances between the carboxylate oxygens of the model compound see Fig. 3.3.18a, p 88. Molecular modelling data for the model compound showed that there are three oxygen-oxygen distances of ~4 angstroms which could interact with Ca^{2+} ions in the preferentially stabilised faces which are also 4 angstroms apart. The fact that the (0 0 1) face, another homopolar face, is not expressed can be explained by the fact that there are no Ca^{2+} ion distances of 4 angstroms in this face, only of 5 and 6 angstroms. Hence, the carboxylate oxygens of the model compound which are approximately 3 to 4 angstroms apart do not match geometrically with the Ca^{2+} ion separations in the face. Additional support for the fact that this model compound modified the (1 0 -2) and (-1 0 2) faces could be that there is a good

stereochemical match between the carboxylate groups of the *exo,exo* model compound and the carbonate groups of the faces *i.e.* the carboxylate groups can adopt a configuration in which the groups are essentially parallel to each other as is found between carbonate groups in the face [see Fig.3.3.8].

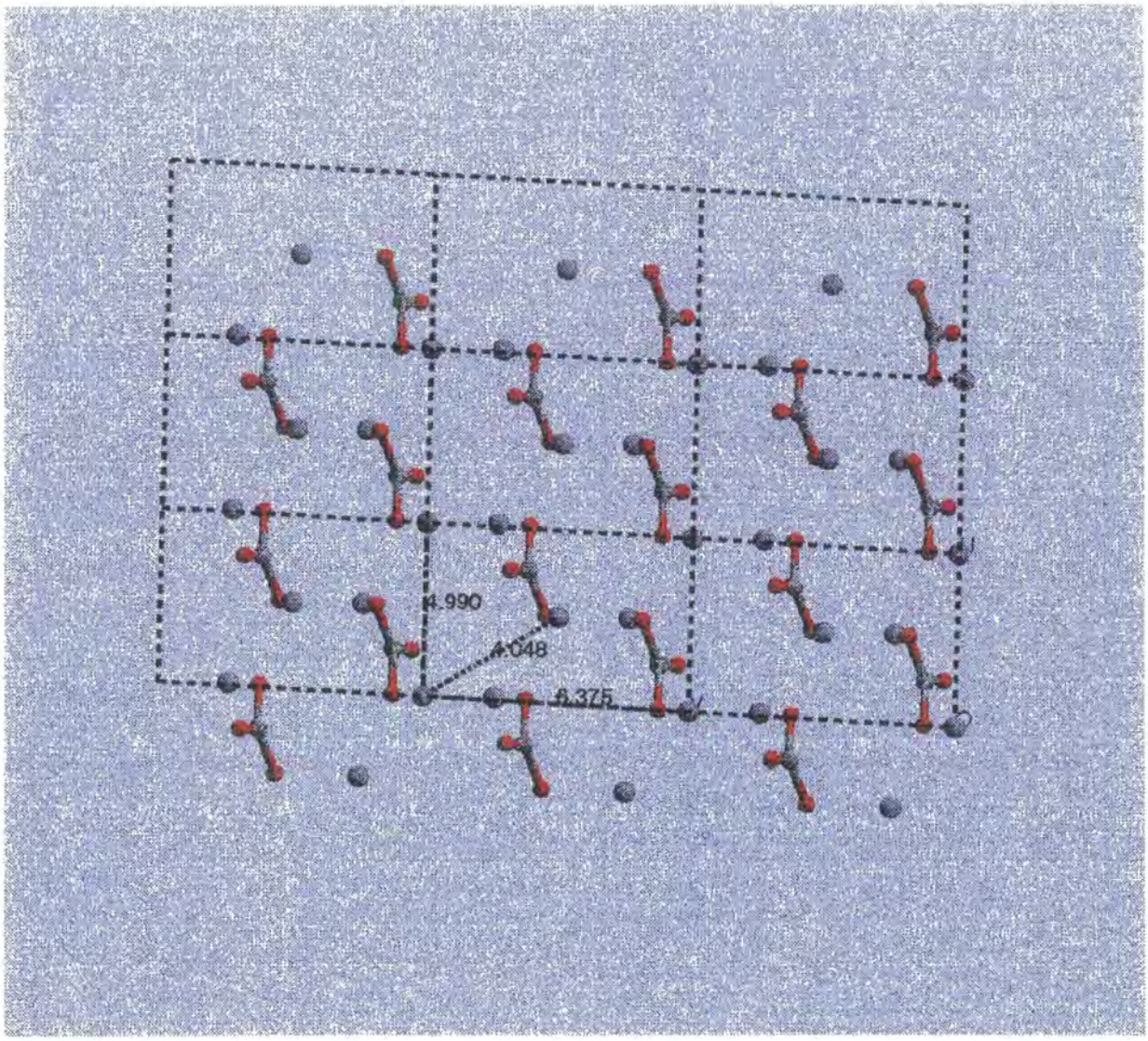

Fig. 3.3.7. A molecular model of the (1 0 -2) showing distances between adjacent calcium ions within the face.

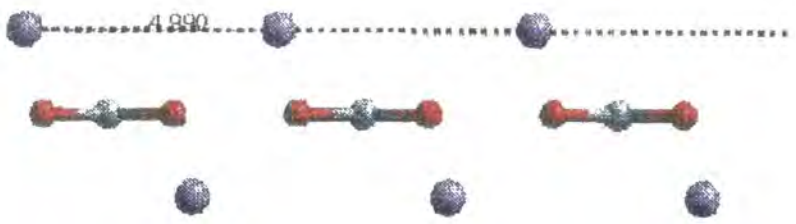

The (001) face of Calcite

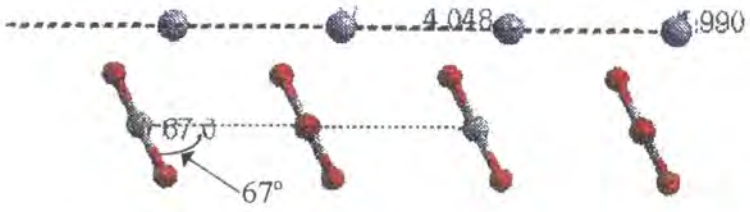

The (10.-2) face of Calcite

Fig. 3.3.8. A comparison of the crystal lattices of the (0 0 1) and the (1 0 -2) faces of calcite. Notice the 4.048 angstrom separation between ions in (1 0 -2) and the fact that the (1 0 0) face does not contain an ~ 4 Angstrom separation between calcium ions. Also note the parallel arrangement of carbonate anions in (1 0 -2) which may be mimicked well by the carboxylate groups in the *exo,exo* and *endo,endo* model compounds, again, this is not seen in (0 0 1).

It must be noted that the ions in the other faces belonging to the {1 0 2} family have also a favourable geometrical and stereochemical arrangement for interaction with the model compounds, although they are not expressed to the same extent as the (1 0 -2) and (-1 0 2) faces. This could be due to the fact that they are not homopolar *i.e.* the layers of carbonate and calcium ions in the face are not discrete. The fact the (1 0 -2) and (-1 0 2) faces are more preferentially expressed could be due to the fact that the faces are homopolar, hence providing favourable attraction between the functionalities of the model compound and the crystal faces.

The influence of model compound 1c, the hydrogenated analogue of model compound 1b, on the crystallisation of $CaCO_3$ was also observed at [Ca^{2+}]:[repeat unit] 10:1 and 100:1. On addition of the model compound solution in the higher concentration two types of crystal were collected from the air/water interface, the 'spearhead' shaped crystals as seen in the experiments with model compound 1b as additive and long, narrow, flat, transparent crystals which were probably crystals of the calcium salt of the model compound [Fig. 3.3.9]. The crystals from the bulk solution were of the same morphology as seen with model compound 1b, however, the crystals were smaller (~10μm), this is consistent with the idea that the long, flat 'lath like' crystals are calcite salts of the model compound, hence, less Ca^{2+} ions are free to form $CaCO_3$ in the bulk.

a.  b. 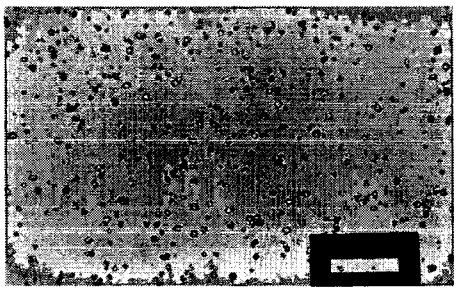

Fig. 3.3.9. Optical micrographs showing crystals of $CaCO_3$ grown from bulk solution with model compound 1c as additive $[Ca^{2+}]$:[model compound 1c] 10:1 a. Crystals grown at the air/water interface. Scale bar = 100μm b. Crystals grown in bulk solution. $[Ca^{2+}]$:[model compound 1c] 100:1. Scale bar = 200μm

At lower concentration of model compound 1c no 'lath like' crystals were observed at the air/water interface and the crystals grown from bulk solution were larger (~20μm) the nucleation density was also higher at 712 crystals/cm^2 compared to 516 crystals/cm^2 at the higher concentration of model compound 1c. Both concentrations of model compound 1c gave crystals with the same type and degree of morphological change as model compound 1b at $[Ca^{2+}]$:[model compound 1b] molar ratio, 100:1 (pp 69-72). The only difference seen was that the modified faces appeared rougher in texture [Fig. 3.3.10].

Fig. 3.3.10. Scanning electron micrographs showing $CaCO_3$ crystals grown from bulk solution in presence of model compound 1c. a. $[Ca^{2+}]$:[model compound 1c] 10:1, b. $[Ca^{2+}]$:[model compound 1c] 100:1.

These observations are not surprising due to the fact that, like model compound 1b, the hydrogenated analogue contains carboxylate groups with three oxygen-oxygen distances of ~ 4 angstroms. Therefore the {1 0 -2} can be stabilised in the same way as discussed above. The reason why the degree of habit modification is less for the hydrogenated model compound could be due to the fact that one of the oxygen-oxygen distances deviates slightly further from the 4 angstrom value at 3.7 angstroms [Fig. 3.3.18b, p 89]. This might be enough to compromise the geometrical match between the carboxylate oxygen distances and the Ca^{2+} ions in the crystal face. Again, the reason why the model compound modified the (1 0 -2) and (-1 0 2) faces could be that there is a good stereochemical match between the carboxylate groups of the model compound and the carbonate groups of the faces.

Both model compound 2b, *endo,endo*-bicyclo[2.2.1]heptene-2,3-dicarboxylic acid, and the hydrogenated model compound 2c at $[Ca^{2+}]$:[model compound 2b or 2c] 10:1, also led to the same type of habit modification, to the same extent, as effected by model compound 1b at a $[Ca^{2+}]$:[model compound 1b] of 100:1.

The faces of crystals grown in the presence of model compound 2b were analogous in texture to those modified by model compound 1b [Fig. 3.3.11] but those faces controlled by addition of model compound 2c were rougher with larger stepping observed on the {1 0 -2} faces [Fig. 3.3.12]. Crystal sizes and nucleation densities were similar to those discussed for model compounds 1b and 1c.

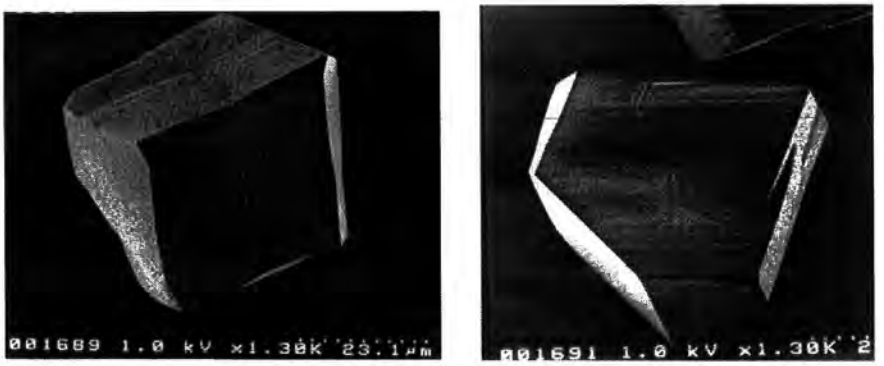

Fig. 3.3.11. Scanning electron micrographs showing $CaCO_3$ crystals grown from bulk solution in presence of model compound 2b a. $[Ca^{2+}]$:[model compound 2b] 10:1, b. $[Ca^{2+}]$:[model compound 2b] 100:1.

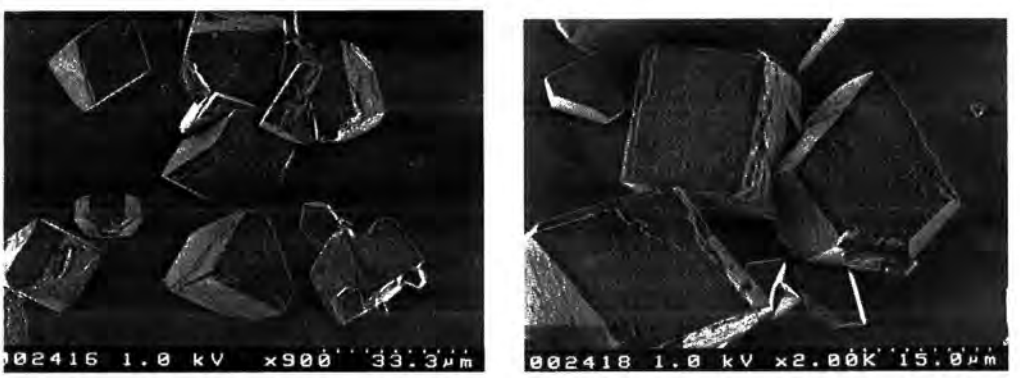

Fig. 3.3.12. Scanning electron micrographs showing $CaCO_3$ crystals grown from bulk solution in presence of model compound 2c at $[Ca^{2+}]$:[model compound 2c] 10:1.

Crystals grown from supersaturated $Ca(HCO_3)_2$ solutions in the presence of model compounds 3a, 2-*endo*-3-*exo*-bicyclo[2.2.1]hept-5-ene-2,3-dicarboxylic acid and 3b were much less modified than crystals grown in the presence of the *exo,exo* (model compounds 1) or *endo,endo* (model compounds 2) model compounds. Unambiguous measurement of angles between the faces was not possible due to the irregularity of their edges. It was apparent that the crystals were modified in the same manner as discussed previously, but to a much lesser extent. This can be best seen by comparing the crystals shown in Fig. 3.3.12. with those shown below in Fig. 3.3.13. This observation is consistent with the importance of the distances between carboxylate oxygens in the model compound in controlling $CaCO_3$ crystallisation. In the case of these *exo,endo* model compounds there is only one possible oxygen-oxygen distance of ~4 angstroms hence the probability of a modifying interaction is reduced. Another reason why the *exo,endo* model compound did not modify the (1 0 -2) or (-1 0 2) faces to the same extent as the *exo,exo* and *endo,endo* model compounds could be that in this case there is only a limited stereochemical match between the carbonate groups for the model compound and the carbonate groups of the faces. It can be seen from the molecular modelling diagrams for model compounds 3a and 3b [Fig. 3.3.19a and b] that the carboxylate groups are much less likely to adopt a configuration in which they are parallel to each other, as in (1 0 -2) and (-1 0 2), than in the case of either the *exo,exo* or the *endo,endo* model compounds.

Fig. 3.3.13. Scanning electron micrographs showing $CaCO_3$ crystals grown from bulk solution in presence of a. Model compound 3a $[Ca^{2+}]$:[model compound 3a] 10:1, b. Model compound 3b $[Ca^{2+}]$:[model compound 3b] 10:1.

3.3.3 Effect of model compounds 4b and 4c

Crystallisation experiments using model compound 4b, *exo,exo*-7-oxabicyclo[2.2.1]hept-5-ene-2,3-dicarboxy anhydride, as the additive were carried out at $[Ca^{2+}]$:[model compound 4b] molar ratios of 10:1, 100:1 and 1000:1. The nucleation density of $CaCO_3$ crystals grown in the bulk was noticeably larger at the highest concentration of model compound, at an average of 210 crystals/cm^2 compared to 124 and 60 crystals/cm^2 for the intermediate and lower concentrations respectively. Once again this observation implies that the model compound induces crystal nucleation.

The mean size of the crystals is larger than measured in the previous section, at 50μm compared to between 10 and 30μm. This is explained by the fact that crystal sizes were measured along the longest axis of each crystal and the crystals in this study were preferentially elongated along one growth axis. However, little change in the range of sizes of crystals compared to control crystals [see appendix F1] indicates that nucleation is episodic. This observation supports the

view that nucleation events are affected by the Ca^{2+} complexation, lowering of supersaturation and possible surface tension effects of the model compound. Crystals grown at the air/water interface were modified in the same way as those in the bulk; however, crystals at the surface were more intergrown. Both surface and bulk calcite crystals were modified extensively at the highest additive concentration, less so, but in the same manner, at intermediate concentration and to a significantly lesser extent at the lowest model compound concentration. From optical studies, the most modified crystals appeared to be long, narrow, cylindrical shaped crystals arranged in random orientations. The crystal length being approximately twice the value of the width [Fig. 3.3.14]. Observations using SEM revealed that the crystals were cylinders, capped at each end with three smooth {1 0 4} faces [Fig. 3.3.14b]. The faces along the length of the crystals were rougher in texture and faces in the direction parallel to the c-axis were straight. Observation of the crystal down the c-axis showed an essentially circular shape [Fig. 3.3.14c].

The crystals grown at the intermediate model compound concentration had a similar appearance. In this case the growth was not as extended along the long dominant growth axis, with a ratio of length to width of ~ 7 : 5 [Fig. 3.3.15]. At the lowest concentration of additive, crystals appeared less extended in the direction parallel to the c-axis. The crystals were, however, modified in the same manner.

a.

b.

c.

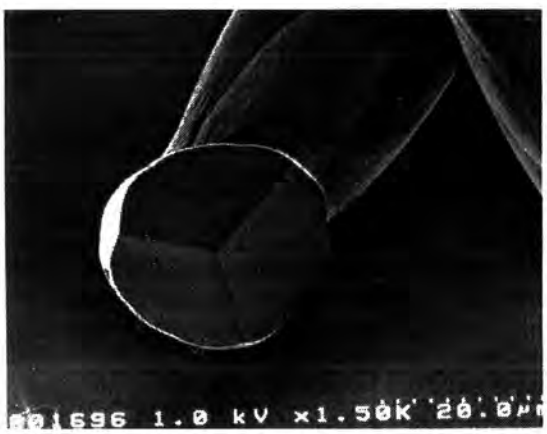

d.

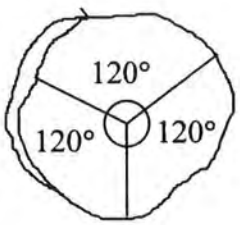

Fig. 3.3.14. Optical and scanning electron micrographs showing $CaCO_3$ crystals grown from bulk solution at $[Ca^{2+}]$:[model compound 4b] 10:1, a. Optical micrograph, scale bar = 200µm. b and c. Scanning electron micrographs. d.

Diagram of a calcite crystal modified by model compound 4b at highest concentration, showing angles between faces viewed down the c-axis.

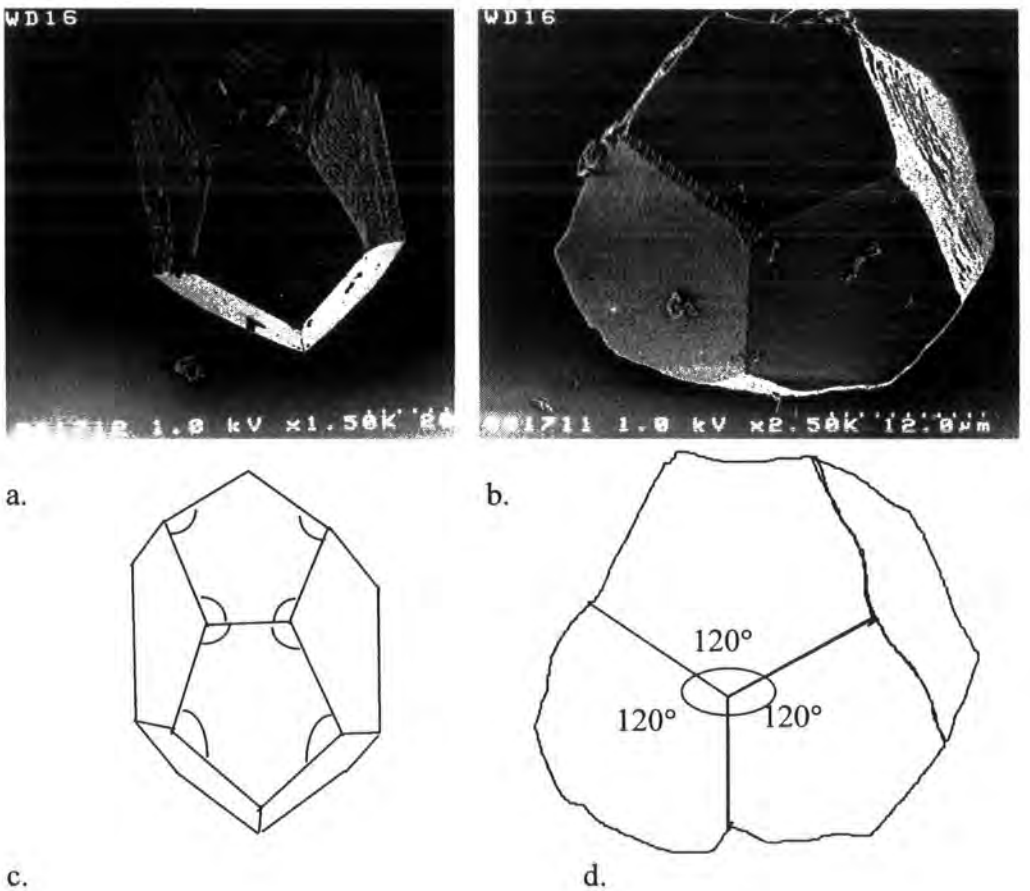

Fig. 3.3.15. Scanning electron micrographs showing $CaCO_3$ crystals grown from bulk solution in presence of Model compound 4a $[Ca^{2+}]$:[model compound 4a] 100:1 a. A crystal viewed approximately perpendicular to the c-axis. b. A crystal viewed approximately down the c-axis. c. A diagrammatic representation of the crystal seen in a. All angles marked = 110°. d. A diagrammatic representation of the crystal seen in b, angles are marked.

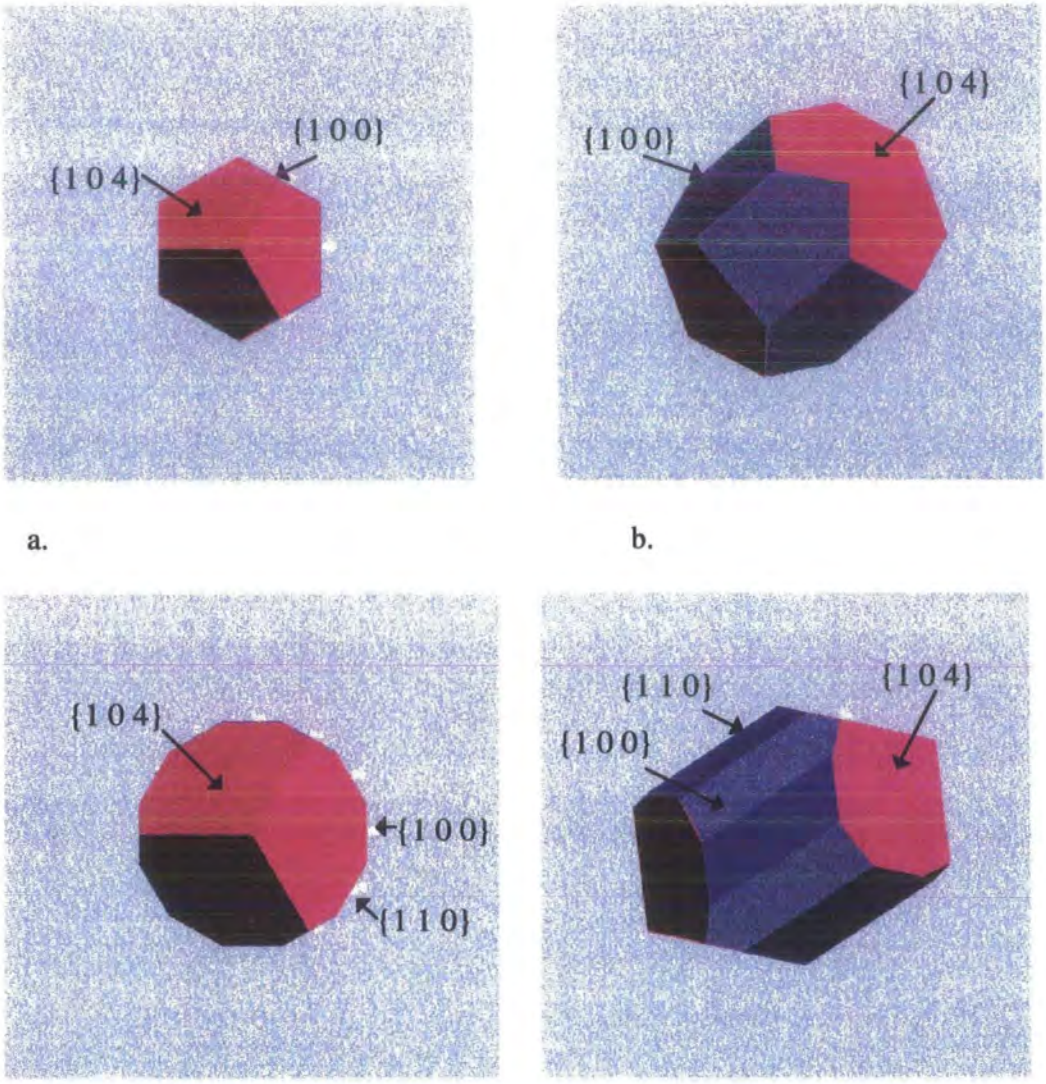

Fig. 3.3.16. Theoretical calcite crystal morphologies, calculated using Cerius© 2, version 3.0 molecular modelling software using a universal forcefield. a. Preferential expression of {1 0 0} viewed down the c-axis of calcite. b. Preferential expression of {1 0 0} viewed approximately perpendicularly to the c-axis of calcite. c. Preferential expression of {1 0 0} and {1 1 0} viewed down the c-axis of calcite. d. Preferential expression of {1 0 0} and {1 1 0} viewed approximately perpendicularly to the c-axis of calcite.

The calcite crystals grown at intermediate concentration were compared with molecular models of the calcite form. From these investigations it was apparent that the crystals were preferentially expressing {1 0 0} faces. Further evidence that the crystals were modified in such a manner was provided by interfacial measurements which matched those of theoretical crystals [compare Fig. 3.3.15 with Fig. 3.3.16a and b]

The more modified crystals, grown at a $[Ca^{2+}]$:[model compound 3a] molar ratio of 10:1, had a much more circular cross section when viewed down the c-axis. This could be due to the fact that both the {1 0 0} and the {1 1 0} faces of the calcite crystal were preferentially expressed (compare Fig. 3.3.14d and Fig. 3.3.16c,d).

The influence of the hydrogenated model compound 4c on the crystallisation of $CaCO_3$ at a $[Ca^{2+}]$:[model compound 4c] molar ratio of 100:1 was observed. The crystal morphology was the same as that of $CaCO_3$ crystals grown in the presence of model compound 4b at the same concentration but the extent of modification was less [Fig. 3.3.17].

Fig. 3.3.17. Scanning electron micrographs showing $CaCO_3$ crystals grown from bulk solution in presence of model compound 4c $[Ca^{2+}]$:[model compound 4c] 100:1.

3.4 GENERAL COMMENTS

It is evident that all diacid model compounds discussed in this chapter which were used as additives in the crystallisation experiments controlled the morphology of $CaCO_3$ crystals grown from supersaturated solutions of $Ca(HCO_3)_2$. *Exo,exo, endo,endo* and *exo,endo* bicyclo[2.2.1]hept-5-ene dicarboxylic acids controlled the morphology of the crystals in the same way *i.e.* interaction with the (1 0 -2) and (-1 0 2) faces, but to different extents. Both the *exo,exo* and *endo,endo* model compounds had a much greater effect upon the morphology of the grown calcite crystals than the *exo,endo* model compound. This was attributed to the preferential geometrical and stereochemical matching between the *exo,exo* and *endo,endo* carboxylate groups and the distances and stacking of Ca^{2+} and CO_3^{2-} ions in the preferentially expressed faces. *Exo,exo*-7-oxabicyclo[2.2.1]hept-5-ene-2,3-dicarboxy anhydride, when used as an additive, led to a different morphology of calcite. In this case, at lower model compound concentrations {1 0 0} faces and at the highest model compound concentration both {1 0 0} and {1 1 0} faces were preferentially expressed. The resulting crystals were anisotropic and cylindrical with preferential elongation along the c-axis.

The work described in this chapter showed that the model compounds used as additives controlled the morphology of $CaCO_3$ crystals grown from supersaturated solutions of $Ca(HCO_3)_2$ at a large range of concentrations, $[Ca^{2+}]$: [model compound] 10-1000:1. The model compounds did not seem to control the sizes of the crystals of $CaCO_3$ indicating that episodic nucleation had occurred. The polymers of these model compounds, resulted in

control of crystal size distribution which could be due to nucleation of crystals by the polymers. The synthesis and characterisation of the polymers used are discussed in the next chapter, Chapter 4.

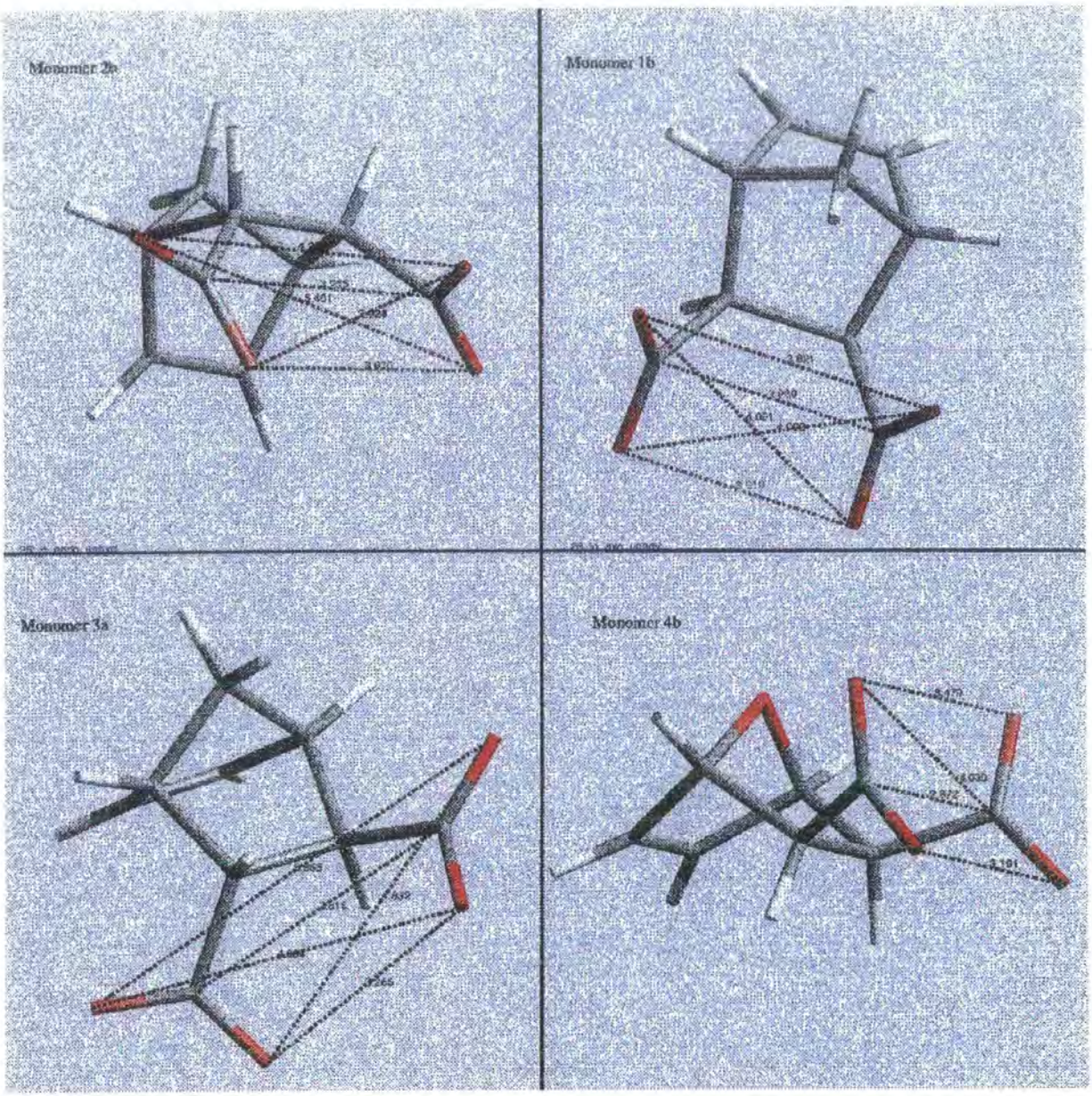

Fig. 3.3.18a. Molecular model diagrams of the unsaturated monomers.

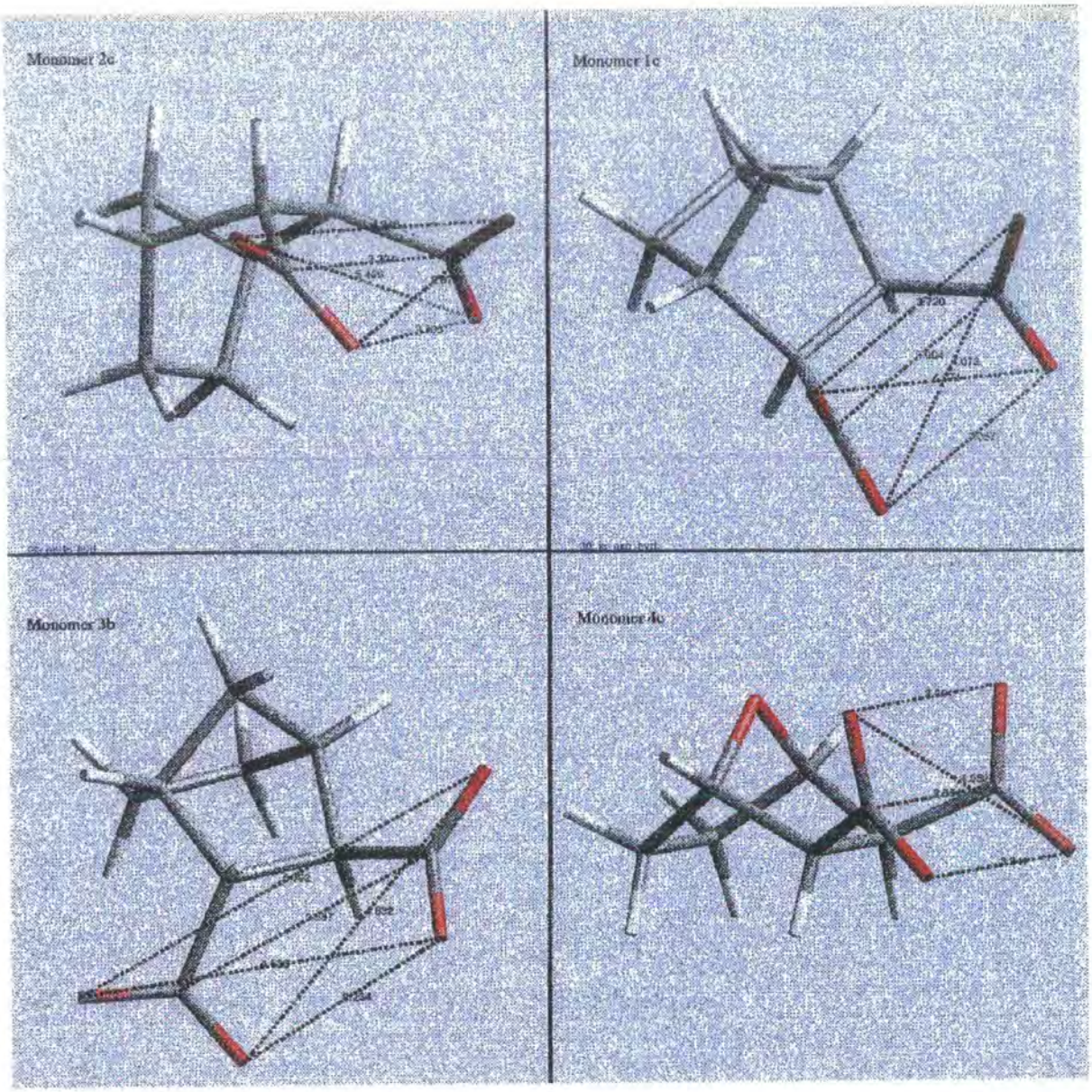

Fig. 3.3.18b. Molecular model diagrams of the saturated monomers.

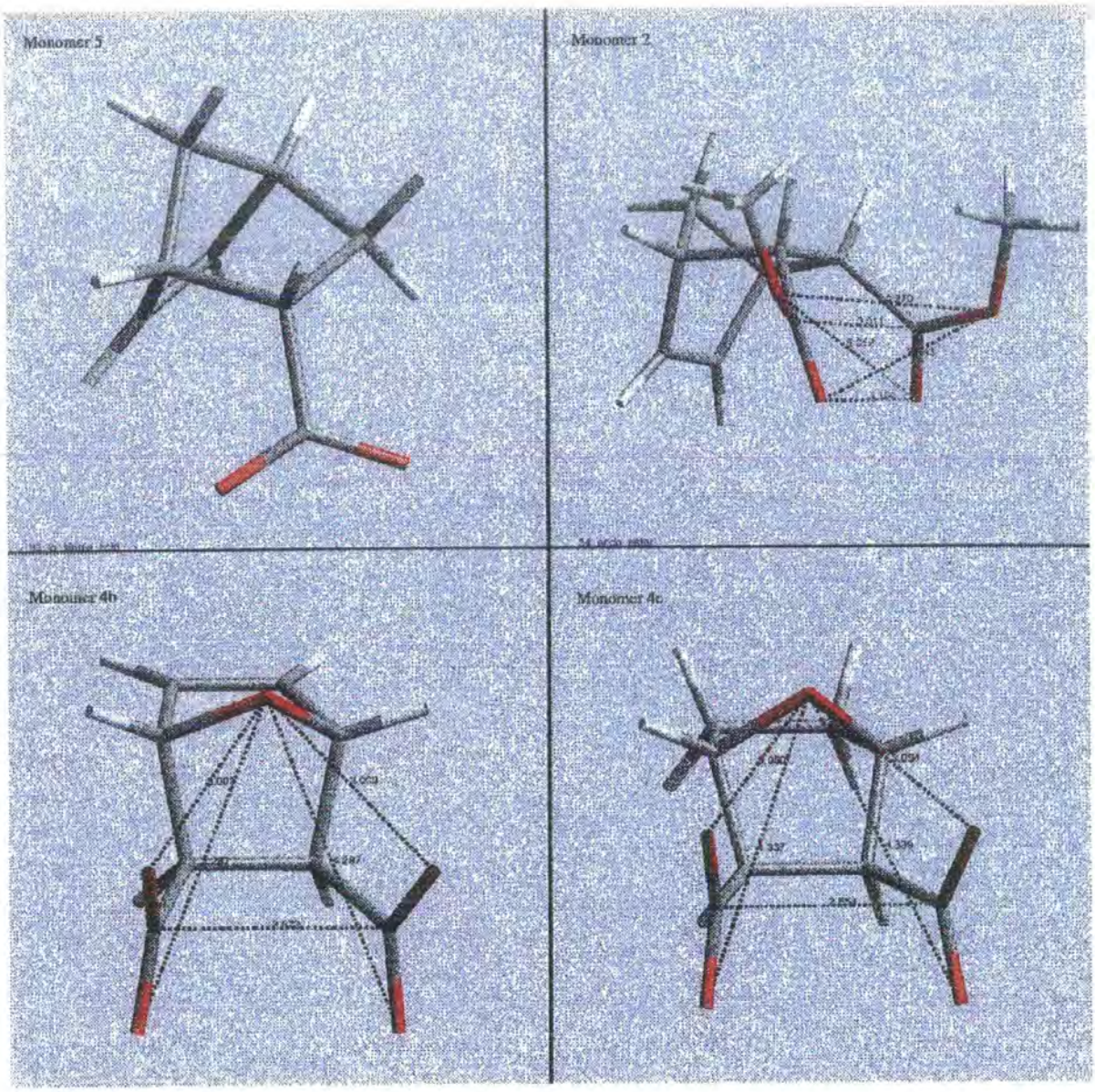

Fig. 3.3.18c. Molecular model diagrams of monomers.

CHAPTER 4

Polymer Synthesis and Characterisation

4.1 INTRODUCTION

The objectives of the work described in this chapter are the synthesis and characterisation of water soluble polymers of controlled stereochemistry with sodium carboxylate pendant functional groups. The syntheses of the monomers *exo,exo, endo,endo* and *endo,exo* -bicyclo[2.2.1]hept-5-ene-2,3-bis(carboxy methyl ester), monomers 1, 2 and 3 respectively, are the first topics discussed. The ROMP of these monomers using the well defined initiator, Mo(CH-^{t}Bu)(NAr)(O-^{t}Bu)$_2$, (initiator 1), to give unsaturated polymers with a range of Mn values (200K, 50K and 5K) and low PDI values (~ 1.01) is also described. A review of the final two steps in the polymer synthesis is also included. These steps involved the hydrogenation of the backbone double bonds and base catalysed hydrolysis of the dimethyl ester functional groups to yield the target water soluble polymer.

4.2 RESULTS AND DISCUSSION

4.2.1 Monomer synthesis and characterisation

Introduction

The three substituted norbornene monomers were synthesised by literature proceedures.[1,2,3,4] *Exo,exo*-bicyclo[2.2.1]hept-5-ene-2,3-dicarboxylic acid dimethyl ester (monomer 1) and *endo,endo*-bicyclo[2.2.1]hept-5-ene-2,3-dicarboxylic acid dimethyl ester (monomer 2) were both prepared by two step syntheses. In each case a Diels Alder [4+2] cycloaddition reaction was carried out between cyclopentadiene and maleic anhydride to give the acid anhydride adduct which was then esterified to give the diester. When carried out at

temperatures between 0 and 5°C the Diels Alder reaction led almost exclusively to the *endo* anhydride, the kinetic product, and temperatures above 178°C were necessary to obtain the more thermodynamically favoured *exo* product in yields greater than 60%. Both adducts were purified by recrystallisation and then esterified in methanol using *p*-toluene sulphonic acid as catalyst to give the dimethyl esters. *Endo,exo*-bicyclo[2.2.1]hept-5-ene-2,3-dicarboxylic acid dimethyl ester (monomer 3) was synthesised in a one step [4+2] Diels-Alder cycloaddition reaction between cyclopentadiene and dimethyl fumarate. The reaction was carried out at room temperature. Optimisation of reaction conditions, reaction schemes and some ^{1}H NMR data are discussed below. Other ^{1}H NMR, ^{13}C NMR, FTIR and chemical ionisation mass spectra are shown in appendices A14, B14 and C13 respectively and are consistent with the structures assigned. Full spectral assignments are given in the experimental section (pp 115-116). All NMR spectra were recorded for solutions in d_6-acetone. Monomer spectra were recorded in $CDCl_3$ solution as well, in order to compare chemical shifts directly with the literature values. Assignments were consistent with the literature values and all ambiguous assignments were confirmed by the use of DEPT, ^{1}H COSY and HETCOR NMR spectra.

Monomer Synthesis

Synthesis of *exo,exo*-bicyclo[2.2.1]hept-5-ene-2,3-bis(carboxymethyl ester) (monomer 1).

Monomer 1 was synthesised in a two step reaction. The first step was a Diels Alder reaction between maleic anhydride and cyclopentadiene[1]. Reaction

conditions were optimised inorder to increase the percentage of the more thermodynamically stable exo adduct. The amount of exo:endo adduct was increased from 60:40 to 75:25 by increasing the temperature from 173°C to 178 - 204°C and increasing the reaction time from 1.5hrs to 7hrs. Dicyclopentadiene was cracked *in situ* under the severe temperature conditions to yield the cyclopentadiene required. The product was recrystallised from acetone (x6) to obtain the pure 100% exo anhydride in low yield. The anhydride was then esterified using methanol and *p*-toluene sulphonic acid as catalyst to give the dimethyl ester monomer in a 90% yield [Fig. 4.2.1].

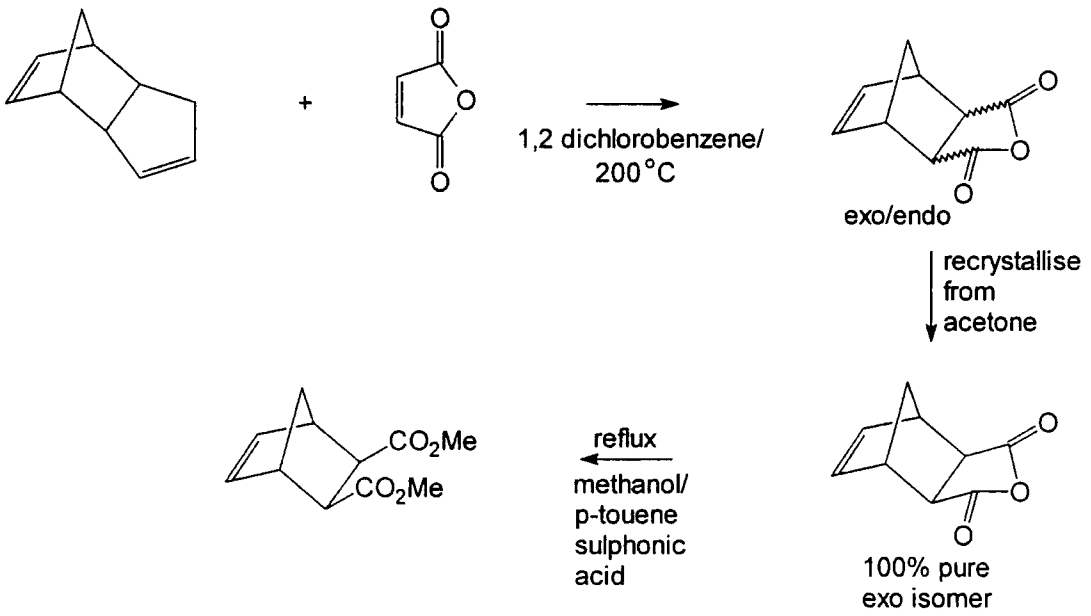

Fig. 4.2.1. A Schematic Representation of the Synthesis of *exo,exo*-bicyclo[2.2.1] hept-5-ene-2,3-bis(carboxymethyl ester) (monomer 1).

Synthesis of *endo,endo*-bicyclo[2.2.1]hept-5-ene-2,3-bis(carboxymethyl ester) (monomer 2).

In this experiment, the temperature conditions for the Diels-Alder cycloaddition reaction were mild (0-5°C). Due to the low reaction temperatures, it was

necessary to pre-crack dicyclopentadiene under severe temperature conditions (>170°C) to yield the cyclopentadiene required. At all times during addition of the dicyclopentadiene to the stirring solution of maleic anhydride the temperature was maintained between 0 and 5°C. The crude product contained a high content of the endo isomer (~98%) and after one recrystallisation the pure 100% endo isomer was recovered in a high yield (93%). The anhydride was then esterified using methanol and *p*-toluene sulphonic acid to yield the dimethyl ester monomer in 90% yield. A schematic representation of the two step reaction to give monomer 2 is shown below [Fig. 4.2.2].

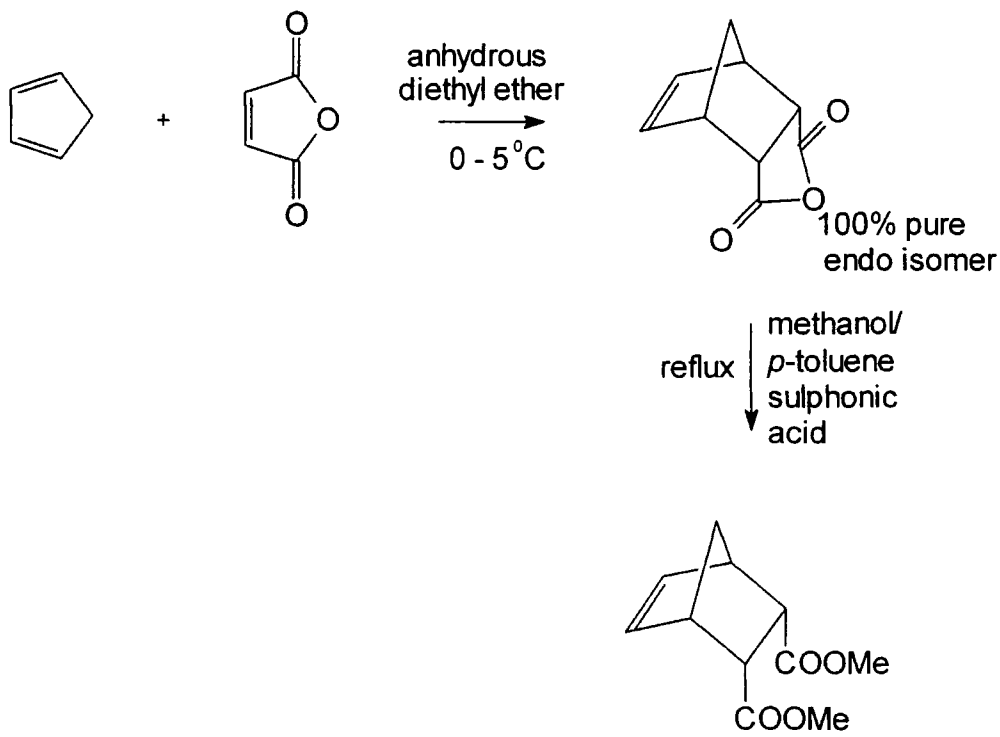

Fig. 4.2.2. A Schematic Representation of the Synthesis of *endo,endo*-bicyclo[2.2.1]hept-5-ene-2,3-bis(carboxymethyl ester) (monomer 2).

Synthesis of *exo,endo*-bicyclo[2.2.1]hept-5-ene-2,3-bis(carboxymethyl ester) (monomer 3).

Dicyclopentadiene was pre-cracked, under the same conditions used in the synthesis of monomer 2, to yield the cyclopentadiene required. Monomer 3 was synthesised in a simple one step reaction at room temperature and recovered as a light yellow, clear, liquid. The crude product was purified by distillation under reduced pressure to give a clear, colourless liquid [Fig. 4.2.3]. The product was used in polymerisation reactions as the, as made, racemic mixture.

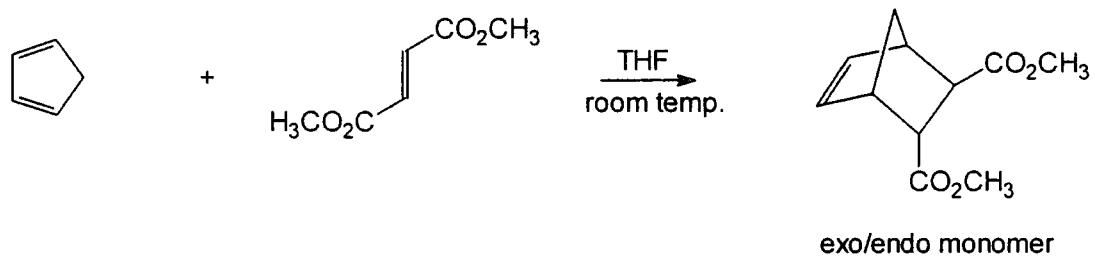

Fig. 4.2.3. A Schematic Representation of the Synthesis of *exo,endo*-bicyclo[2.2.1]hept-5-ene-2,3-bis(carboxymethyl ester) (monomer 3).

Monomer Characterisation

Comparison of the ^1H NMR spectra of monomers 1, 2 and 3 (see respective appendices) revealed differences in chemical shifts and fine structures of the resolved signals. Detailed analysis of the set of spectra allowed complete unambiguous assignment of the structures of 1, 2 and 3. The assignments and IUPAC numbering for the monomers are given in the experimental section. In the spectrum of monomer 1 the triplet peak corresponding to the olefinic hydrogens $H_{5,6}$ is found at 6.23ppm, 0.09ppm downfield from that in monomer 2

which occur at 6.14ppm. This small difference in chemical shift is in the expected direction, in monomer 1 the ester functionalities are *exo* leading to less shielding of $H_{5,6}$ whereas in monomer 2 the *endo* position of the ester functionalities leads to greater shielding. As expected, both the olefinic signals (at 6.10 and 6.27ppm) can be seen in the *exo.endo* monomer 3. The chemical shifts of the peaks corresponding to the methylene ABq, H_7 and $H_{7'}$, show a pattern which is consistent with the assigned structures and can be seen in Fig. 4.2.4. The difference between chemical shifts for H_7 and $H_{7'}$ is largest in monomer 1, (0.7ppm) with $H_{7'}$ at 2.1ppm and H_7 at 1.4ppm. This difference is expected as the carbonyl groups of the *exo* ester functionalities and $H_{7'}$ are in close proximity and in a similar plane which leads to a large interaction between the two. The difference between chemical shifts in monomer 2 is the smallest of the three isomers at 0.03ppm with $H_{7'}$ at 1.40ppm and H_7 at 1.36ppm. The small difference is due to the *endo* ester functionalities having the least interaction with $H_{7'}$. In monomer 3, the *exo.endo* monomer, the chemical shift is intermediate between the *exo* and *endo* monomers (0.2ppm) with $H_{7'}$ at 1.6ppm and H_7 at 1.4ppm. In Fig.4.2.4 the peak at 2.05ppm is due to the solvent, acetone- d_6. Other ^{1}H NMR assignments are given in the experimental section.

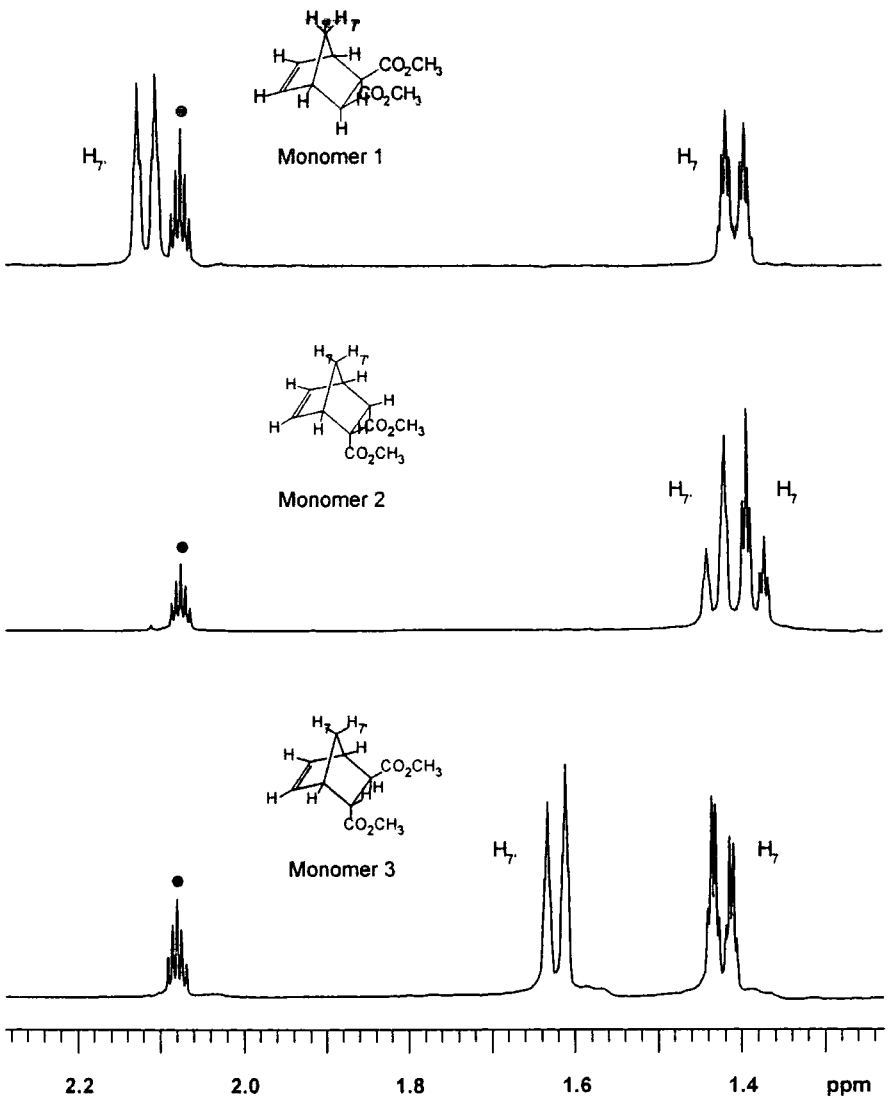

Fig. 4.2.4. A Comparison of the ^{1}H NMR spectra from 1.1-2.3ppm of monomers 1, 2 and 3.

- residual hydrogens in acetone-d_6

4.2.2 Polymer synthesis and characterisation

Introduction

Polymers with saturated backbones and sodium carboxylate pendant functional groups were synthesised in a three step process [Fig. 4.2.5]. The initial reaction involved the living ring opening metathesis polymerisation of monomers 1, 2 and 3 using the well defined initiator, Mo(CH-^{t}Bu)(NAr)(O-^{t}Bu)$_2$, (initiator 1), as reported by R.R.Schrock in 1991.[5,6] The resulting polymers had olefinic moieties in the backbone and dimethyl ester pendant functional groups. The unsaturated polymer backbones were hydrogenated, using *p*-toluene sulphonylhydrazide as a convenient precursor to diimide, an effective reducing agent for vinylenes.[7] This reduced the possibility of side reactions in the final hydrolysis step. The dimethyl ester pendant functional groups of the precursor polymer were hydrolysed under basic conditions (NaOH(aq) 10%w/w) to give the target polymer.

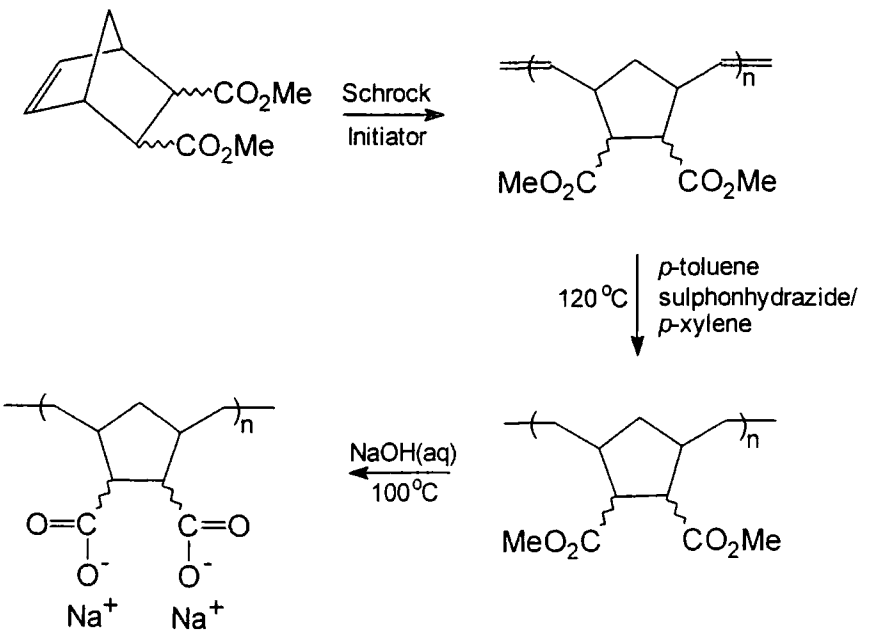

Fig. 4.2.5. A schematic representation of the polymer synthesis.

Step 1: The synthesis and characterisation of poly(bicyclo[2.2.1]hept-5-ene-2,3-dicarboxylic acid dimethyl esters) (Poly-*x*S).

The ROMP of monomers 1, 2 and 3, using initiator 1 in benzene, yields polymers with unsaturated backbones and dimethyl ester pendant functional groups. All polymerisations were carried out at room temperature, under a nitrogen atmosphere in benzene with the catalyst concentrations being typically 0.4 - 40mM. Polymer synthesis could be followed by the colour change of the solution. The colour of the propagating polymer solutions ranged from yellow to orange depending upon initiator concentration. A greater amount of initiator led to a darker, more orange appearance. The polymerisations were terminated by addition of excess benzaldehyde, in a Wittig-type reaction which cleaved the polymer from the metal. On addition of benzaldehyde, the colour of the solutions became considerably darker. The polymers were precipitated (x2 - x4) from benzene into methanol and recovered as white solids. All of the polymers made were soluble in benzene, toluene and dichloromethane in the molecular weight range investigated.

In the majority of cases, the monomers were polymerised in a living manner (PDI≤1.1) to give polymers with Mn target values of approximately 200,000, 50,000 and 5,000 [Table 4.2.1]. The PDI values of the *exo,exo*- and *endo,exo*-dimethyl ester polymers with Mn target values of 200,000 are 1.21 and 1.12 respectively. The higher values are probably due to the fact that, within the first 5mins of polymerisation, the solutions became very viscous resulting in less efficient mixing. Although the addition of more solvent after 5mins decreased the solution viscosity, allowing vigorous stirring, the PDI values remained high.

The PDI of the corresponding *endo,endo-* polymer (Poly-2S) is low due to the fact that polymerisation conditions were optimised by using more solvent. The polymers were synthesised on a relatively small scale (0.2 - 1.1g) as this minimised the use of the expensive initiator. The percentage yields decrease with decreasing Mn, this is due to the repeated reprecipitation (x4) which was necessary to remove the larger amounts of initiator used. Characterisation of these polymers using NMR spectrometric data is discussed separately (p104).

Polymer	Mn	PDI	Mass (g)	% yield
exo/exo	182,000	1.21	0.87	88
	71,400	1.12	0.35	69
	7,700	1.10	0.44	52
endo/endo	174,000	1.01	1.10	92
	57,700	1.02	0.81	78
	6,005	1.12	0.17	34
exo/endo	275.400	1.12	0.52	61
	68,600	1.03	0.34	68
	4,900	1.07	0.23	23

Table 4.2.1. Characterisation data for the ROMP, Poly-*x*S.

Step 2: The hydrogenation of poly(bicyclo[2.2.1]hept-5-ene-2,3-dicarboxylic acid dimethyl ester) (Polys-*x*P).

The polymers synthesised in step 1 were hydrogenated by refluxing with *p*-toluene sulphonylhydrazide in *p*-xylene (bpt. 138°C). The duration of heating was varied according to the amount of polymer used. Polymers were precipitated from methanol and recovered as colourless, transparent, adhesive solids. The Mn

of all the hydrogenated polymers, with one exception are, within experimental error, the same as the values for the corresponding polymers made in step 1. From this information it can be deduced that the polymers were not degraded in the hydrogenation process. The *endo,endo-* polymer, Poly-2P is the only example where the Mn of the step 2 polymer (89,100) was significantly lower than that of it's precursor (174,100). The SEC trace [appendix D8] showed a broad peak, indicating a large proportion of lower Mn polymer was present, the PDI (1.5) is considerably larger than that of the precursor (1.01). This evidence indicates that the polymer decomposed during hydrogenation. The PDI values for all other hydrogenated polymers were, within experimental error, generally the same as the precursor values, indicating in most cases little or no polymer decomposition took place.

Polymer	Mn	PDI	Mass (g)	% yield
exo/exo	184,900	1.21	0.29	57
	68,200	1.11	0.16	52
	~7,700	*	0.02	1
endo/endo	89,100	1.51	0.49	88
	52,000	1.05	0.42	76
	-	-	-	-
exo/endo	220,500	1.34	0.40	98
	65,500	1.04	0.17	56
	5,900	1.08	0.04	40

Table 4.2.2. Characterisation data for the hydrogenated, Polys-*x*P.

* Insufficient polymer recovered - polymer not synthesised

The reason why the *endo,endo-* polymer underwent fragmentation on hydrogenation is not clearly understood but nevertheless merits some comment. We know (see later, pp 108-110) that the *exo,exo-* polymers had a high *trans* vinylene content whereas both the *endo,endo-* and *exo,endo-* polymers had an essentially 50:50 distribution of *cis* and *trans* vinylenes. A *trans* dyad give minimal steric strain and greater flexibility in the backbone of the polymer [Fig.4.2.6]

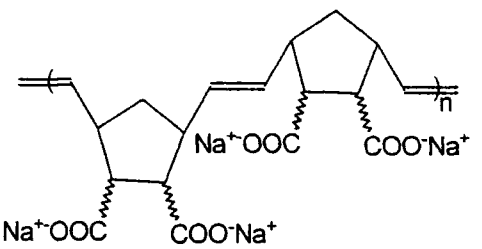

Fig. 4.2.6. A diagrammatic representation of a *trans* dyad.

Whereas, the *cis* dyad results in greater non bonded interactions and hence potentially more steric strain and a marginally stiffer backbone [Fig.4.2.7].

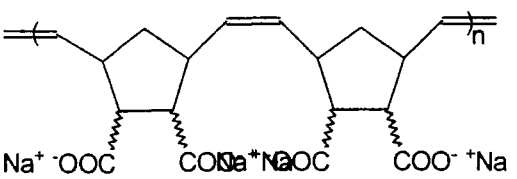

Fig.4.2.7. A diagrammatic representation of a *cis* dyad.

The conditions for diimide hydrogenation are quite severe, boiling xylene at 126°C and a large stiff and stressed polymer molecule may experience sufficient

stress to lead to fragmentation under these condition. This rationalisation is necessarily speculative but is consistent with our observations.

Step 3: The hydrolysis of poly(1,4-cyclopentenylene-5,6-ethylidene-2,3-dicarboxylic acid dimethyl ester) (Polys -xF).

The polymers were hydrolysed in refluxing aqueous NaOH (10% w/w), reactions were terminated when full dissolution of the polymer had occurred. The products were precipitated into methanol and recovered as white solids. In the instances where the Mn was measured the values for the hydrolysed polymers were, within experimental error, the same as the values for the corresponding polymers made in step 2. From this information it can be deduced that these polymers were not substantially degraded in the hydrolysis process.

Polymer	Mn	PDI	Mass (g)	% yield
exo/exo	160,000	1.47	0.20	80
	~68,200	*	0.90	90
	-	-	-	-
endo/endo	73,000	1.70	0.35	92
	48,400	1.22	0.21	68
	-	-	-	-
exo/endo	147,200	1.54	0.28	82
	~65,500	*	0.34	68
	~5,900	*	0.03	40

Table 4.2.3. Characterisation data for the hydrogenated, hydrolysed, Poly-*x*F.

* Aqueous GPC analysis not carried out on this polymer. - not synthesised.

Polymer characterisation using ^{1}H and ^{13}C NMR spectrometry:

Both ^{1}H and ^{13}C NMR spectroscopic analyses were used in characterising the polymers. Full assignment of the spectra was carried out with the aid of DEPT, ^{1}H COSY and HETCOR spectra and the analyses of polymers synthesised in step 1 were consistent with literature data.[5] Full spectral assignments are given in the experimental section 4.3. All NMR spectra of polymers with dimethyl ester functional groups were recorded as solutions in $CDCl_3$ and polymers with sodium carboxylate groups, as solutions in D_2O. All signals in the ^{1}H NMR spectra are broad, this is a characteristic of most polymer spectra. The observed broadening is due to the fact that a specific type of hydrogen atom in the basic repeat unit within the polymer chain is found in many slightly different chemical environments, this leads to a certain type of hydrogen atom resonating over a range of frequencies. The hydrogenation and hydrolysis of all polymers can be followed by both ^{1}H and ^{13}C NMR spectrometry.

Successful hydrogenation is indicated in the ^{1}H NMR spectrum [Fig. 4.2.8] by the loss of signals corresponding to the vinylic hydrogen atoms ($H_{5,6,}$~ 5.5ppm) and in the ^{13}C NMR spectrum [Fig. 4.2.9] by the loss of vinylic carbon atom resonances ($C_{5,6}$ ~ 130ppm). These signals are replaced by peaks corresponding to hydrogen and carbon atoms in a saturated environments $1ppm \leq \delta H_{5,5',6,6'} \leq 3ppm$ for ^{1}H NMR and 33.48ppm and 29.96ppm for ^{13}C NMR. Therefore the evidence for hydrogenation is clear and unambiguous from both ^{1}H and ^{13}C NMR spectroscopic analyses. By contrast it is not possible to say conclusively, from a consideration of the ^{1}H NMR spectrum, that full hydrolysis has taken place. There is a residual methanol peak (3.2ppm) which could possibly conceal an

ester methyl signal. Long periods of drying (4 weeks, under vacuum, 69°C) did not remove the last traces of the solvent. The reason for the difficulty in removal is probably due to hydrogen bonding between the anionic functional groups and the methanol. Conclusive evidence of full hydrolysis comes from the ^{13}C NMR spectra in which no methoxy methyl carbon atom peaks ($29ppm \leq \delta C_{5,6} < 39ppm$) can be seen. [Figs. 4.2.9 and 4.2.10]

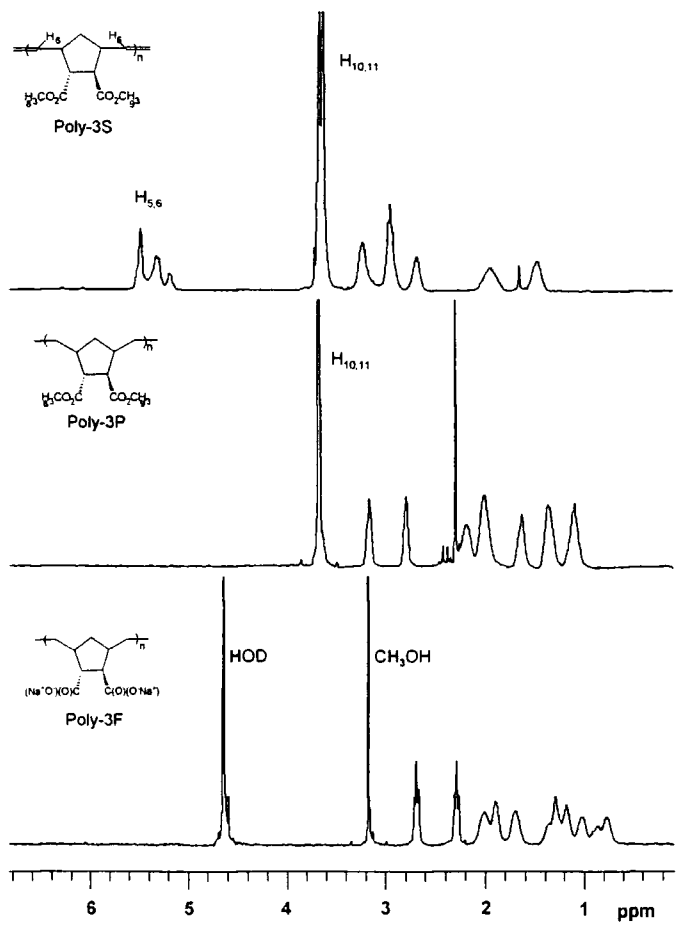

Fig. 4.2.8. A comparison of ^{1}H NMR spectra for Poly-3S, Poly-3P and Poly3F.

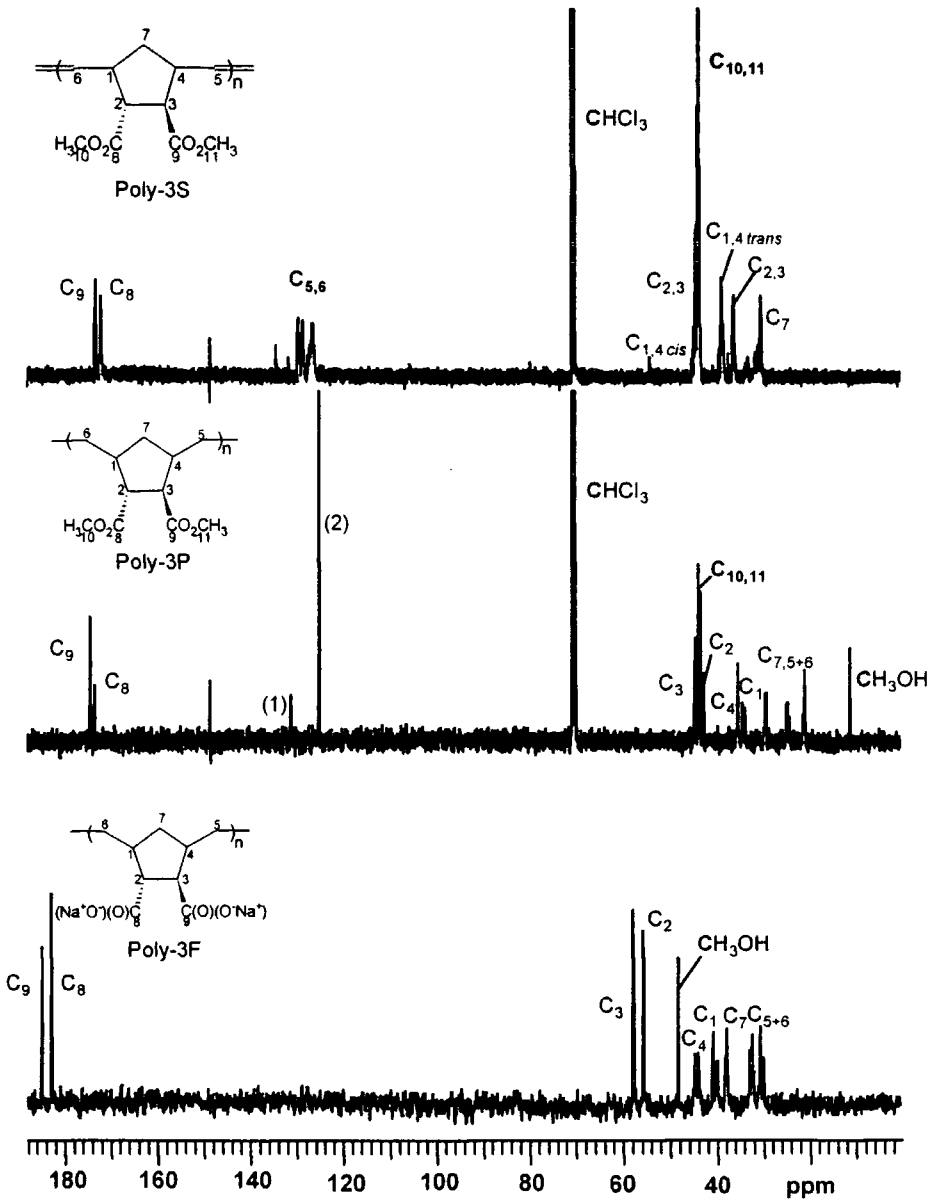

Fig. 4.2.9. A comparison of ^{13}C NMR spectra for Poly-3S, Poly-3P and Poly3F.

(1) Residual solvent, *p*-xylene, $C_{1,4}$ (2) Residual solvent, *p*-xylene, $C_{2,3,5,6}$

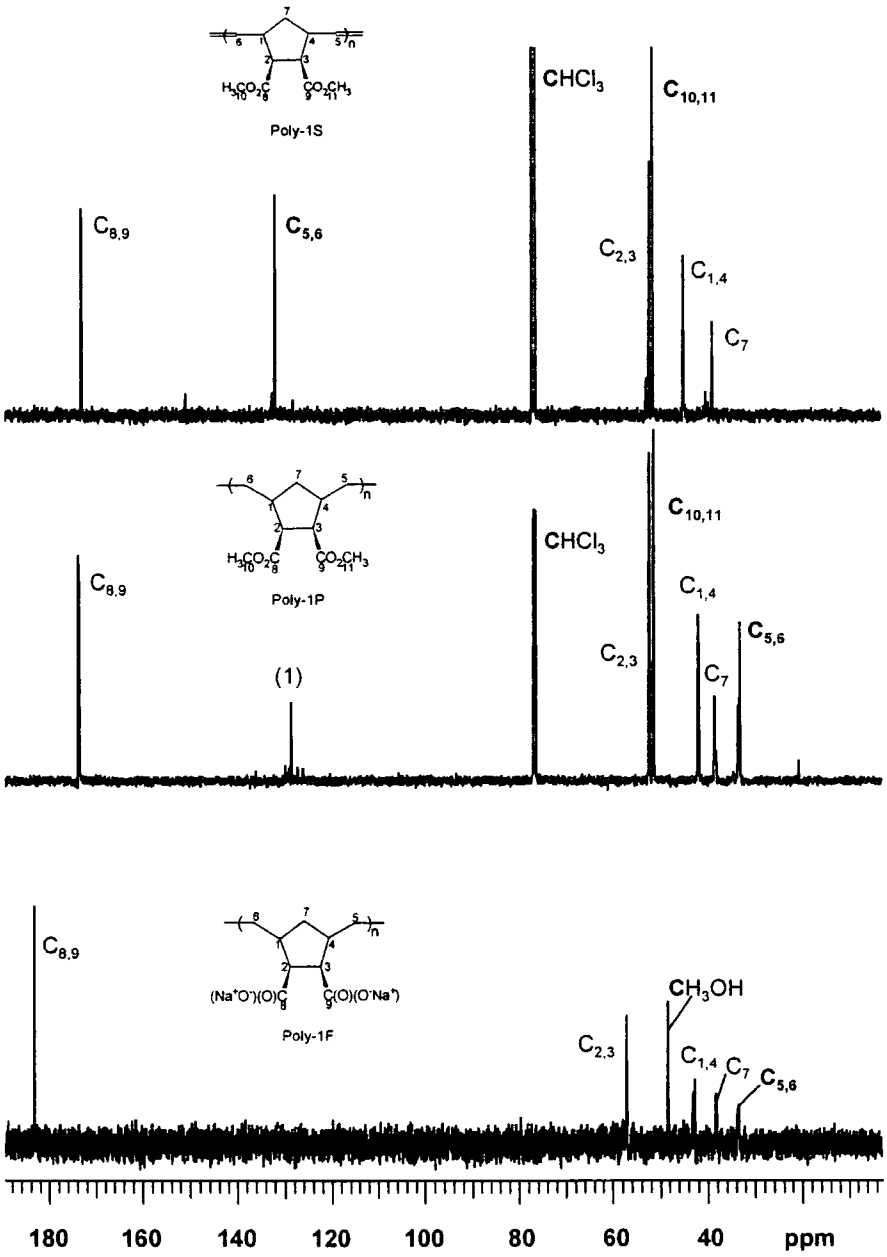

Fig. 4.2.10. A comparison of ^{13}C NMR spectra for Poly-1S, Poly-1P and Poly1F.

(1) Residual solvent, *p*-xylene, $C_{2,3,5,6}$

Unambiguous determination of the cis:trans content of the double bonds in the backbone of the unsaturated polymers is only possible for the *exo,exo* dimethyl

ester polymers (Poly-1S^{x}). Analysis is carried out by averaging the integral values of the previously assigned discrete trans and cis vinylic signals (5.39 and 5.22ppm) in the ^{1}H NMR spectrum [Fig. 4.2.7]. The polymers were found to contain 12% cis and 88% trans olefinic carbons.

In order to determine the *cis/trans* microstructure of a polymer it is necessary to obtain the integrated intensities for the *cis/cis, cis/trans, trans/trans* and *trans/cis* signals for the vinylic and/or allylic carbons and compute the *cis/trans* frequency and distribution. This requires well resolved spectra. In favourable cases further fine structure can be interpreted in terms of frequency and distribution of meso and racemic dyads giving a complete picture of the microstructure.[8] As the trans content of these polymers is high, the trans/cis, cis/trans and especially the cis/cis peaks are difficult to resolve, in the case of the cis/cis peaks impossible. Therefore the microstructure in terms of *cis/trans* distribution and meso/racemic frequency and distribution cannot be deduced from the available spectroscopic data.

The unambiguous assignment of the cis:trans content of double bonds in the *endo,endo*- ROMP polymers (Poly-2S^{x}) was not possible. In both the ^{1}H and ^{13}C NMR spectra, line broadening resulted in a lack of discrete cis and trans peaks. However, it can be estimated from the overlapping vinylic signals in the ^{1}H NMR spectrum [Fig. 4.2.11] that the cis:trans content is approximately 50:50. The large amount of fine structure in the ^{13}C NMR spectrum [appendix B18] indicates that the polymers are probably atactic.

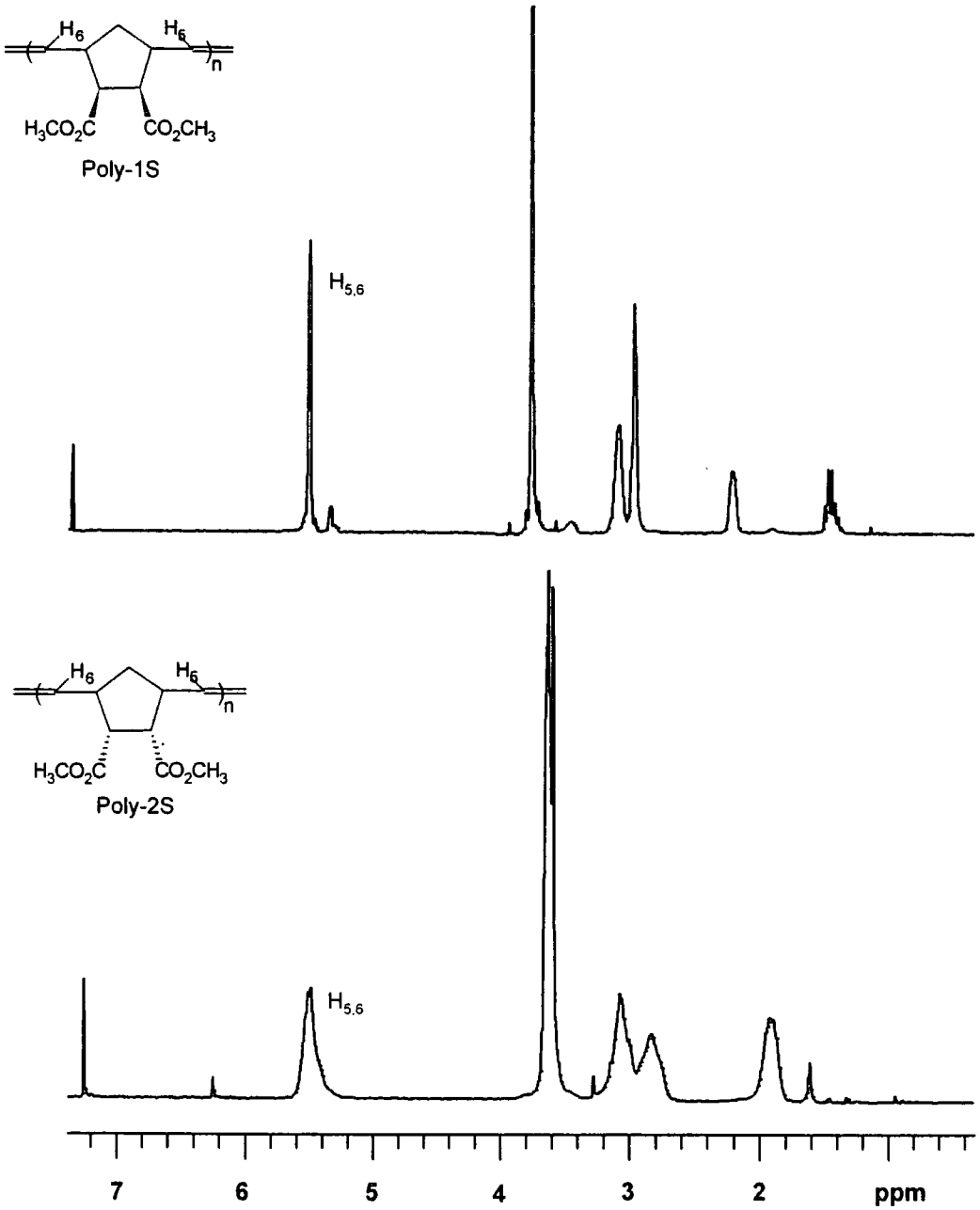

Fig. 4.2.11. ^{1}H NMR spectra of Poly-1S and Poly-2S, with vinylic hydrogen atoms marked.

The discrete vinylic carbon signals in the ^{13}C NMR spectrum of the *exo,endo-* polymers give the best indication of cis:trans content. The areas below the resolved peaks are approximately equal, indicating that the polymers are ~50:50, cis:trans [Fig. 4.2.9.]. As signals have a large amount of fine structure it is probable that the polymer is atactic, some proportion of the fine structure may also be due to head, tail effects.

The hydrogenated polymers (Poly-*x*P) do not contain double bonds in the backbone, therefore, there are no cis or trans considerations and multiplicities in the ^{13}C spectra disappear to give simpler spectra [Fig. 4.2.8].

It is evident from the ^{13}C NMR spectra of the *endo,endo-* polymer (Poly-2P) and it's hydrolysis product (Poly-2F) that hydrolysis results in the isomerisation of the functional groups to give a polymeric product with 50:50 *endo,exo-* pendant functional group content [Fig. 4.2.12] since the spectrum of Poly-2F is identical with Poly-3F. This epimerization at the CH alpha to the ester is consistent with our earlier hypothesis that the *endo,endo-* polymer experienced steric stress (pp 102-103). Only the *endo,endo-* polymer undergoes this epimerization process on hydrolysis, the *exo,exo-* and *exo,endo-* isomers are totally unaffected.

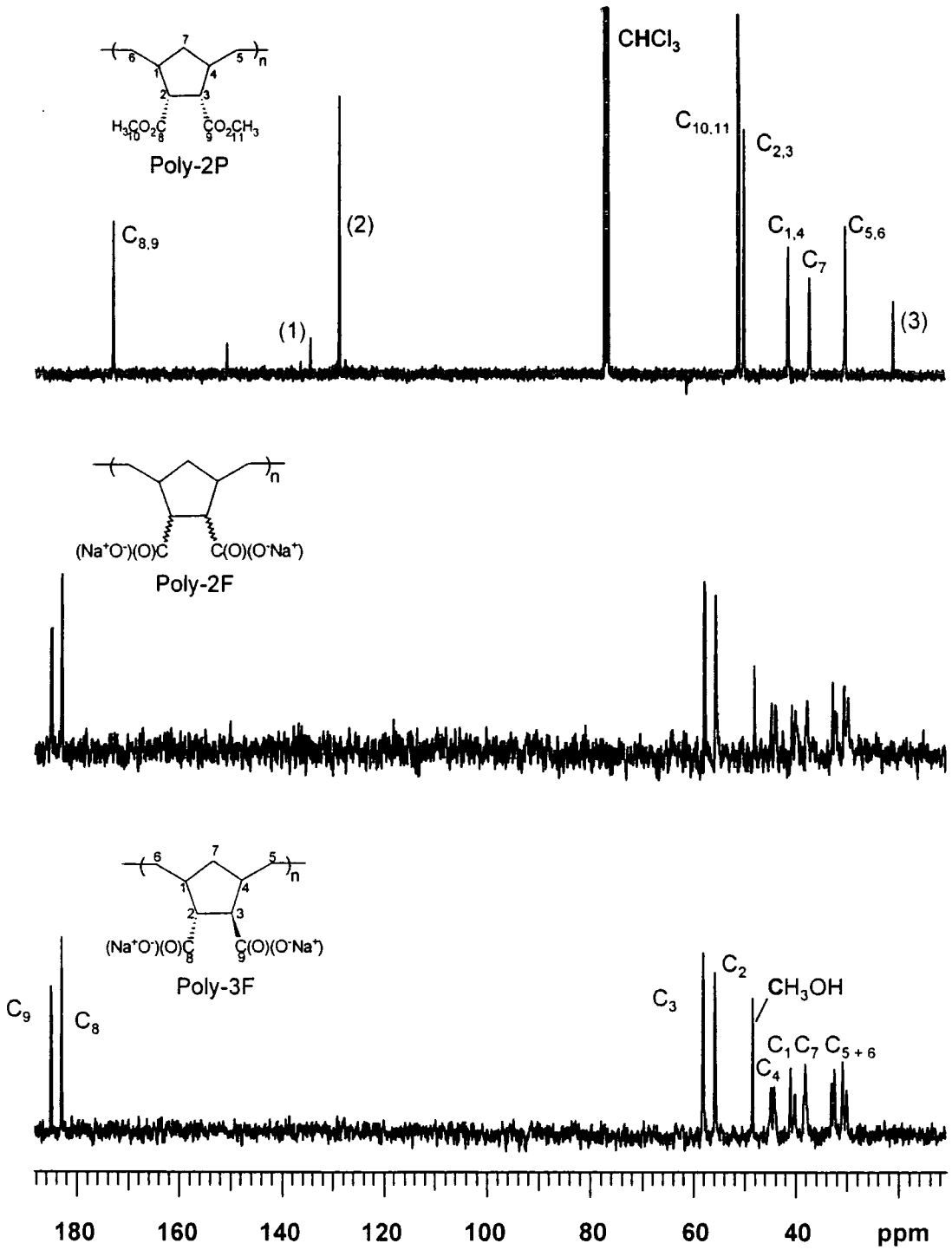

Fig. 4.2.12. A comparison of ^{13}C NMR spectra for Poly-2P, Poly-2F and Poly-3F. (1) Residual solvent, *p*-xylene, $C_{1,4}$ (2) Residual solvent, *p*-xylene, $C_{2,3,5,6}$

4.3 EXPERIMENTAL

4.3.1 Reagents and apparatus.

All organic reagents were reagent grade, purchased from Aldrich Chemical Co. and used as received unless otherwise stated. All polymerisation reactions and manipulations were carried out in a MBraun 150B-G glove box under dry nitrogen atmosphere or by standard Schlenk techniques unless otherwise specified. Benzene was dried over CaH_2 and distilled onto potassium with benzophenone radical anion as indicator of dryness. Polymerisation grade solvent was vacuum transferred from this flask as required. The well defined molybdenum initiator, $Mo(CH\text{-}^tBu)(NAr)(O\text{-}^tBu)_2$, which was used, was synthesised by Dr. Ezat Khosravi. The ^1H and ^{13}C NMR spectra were recorded using a Varian VXR 400 MHz spectrometer run at 400MHz and 100 MHz respectively. Chemical shifts are recorded in parts per million (δ) and referenced to TMS at 0 ppm in those spectra where $CDCl_3$ was used as NMR solvent and to the HOD peak at 4.75ppm in spectra where D_2O was used. Coupling constants are listed in Hertz. Size exclusion chromatography measurements of the saturated dimethyl ester polymers were carried out in $CHCl_3$ solution using a refractive index detector. Size exclusion chromatography measurements of the unsaturated polymers were carried out in THF solution using a Viscotek Differential Refractometer/Viscometer dual detector (Model 200). The use of the viscometer detector leads to this system being regarded as the most reliable for the determination of molecular weight values by SEC. All samples were prepared by dissolving in filtered, degassed GPR grade THF (concentration 0.1%w/w) and filtered through a 0.2μm polypropylene-backed PTFE filter.

Sample solutions were pumped through styrene/divinyl benzene gel columns (10μm mixed) at 308K. The instrument was calibrated using set of polystyrene molecular weight standards, columns and calibrants were purchased from Polymer Laboratories.

4.3.2 Monomer synthesis and characterisation:

The synthesis and characterisation of *exo,exo*-bicyclo[2.2.1]hept-5-ene-2,3-dicarboxylic acid dimethyl ester (monomer 1).

Exo-bicyclo[2.2.1]hept-5-ene-2,3-dicarboxy anhydride (13.50g, 0.064mol) was dissolved in methanol (50ml) and placed in a single necked, round bottomed flask (250ml) fitted with a stirrer bar and condenser. *p*-Toluene sulphonic acid (0.154g, 0.82 mmol) was added and the stirring mixture was heated[3] to reflux for 7hrs. The bulk of the solvent was removed using a rotary evaporator and the residue dissolved in diethyl ether (30ml) and washed successively with water (40ml), aqueous $NaHCO_3$ (40ml, 10%w/w) and water (40ml). The diethyl ether was removed under reduced pressure to leave a white, crystalline solid which was sublimed to give, *exo,exo*-bicyclo[2.2.1]hept-5-ene-2,3-dicarboxylic acid dimethyl ester, a clear, colourless crystalline solid (4.70g, 0.018mol, 27.5% yield; b.pt. 70°C, 0.1mmHg[1]). Found C, 62.89%, H, 6.75% (calculated for $C_{10}H_6O_4$: C, 62.85, H, 6.71%.). ^{1}H NMR[1] [see appendix A12], (d_6-acetone, 400MHz) δ(ppm): 6.23 (t, $J_{6,1} = J_{6,7'}$=2.0Hz, 2H, $H_{5,6}$), 3.59 (s, 6H, $H_{8,9}$), 3.02 (p, $J_{1,6}$~$J_{1,5}$~$J_{1,7}$~$J_{1,7'}$~2Hz, 2H, $H_{1,4}$), 2.60 (d, $J_{6,1}$ = 2Hz, 2H, $H_{2,3}$), ABq δ_B 2.06 (b, 1H, $H_{7'}$) δ_A 1.39 (b, 1H, H_7), J_{AB} = 8.8Hz. ^{13}C NMR [see appendix B12] (d_6-acetone, 100MHz) δ(ppm): 174.22 (s, $C_{8,9}$), 138.66 (s, $C_{5,6}$), 51.81 (s, $C_{10,11}$), 47.60 (s,

$C_{1,4}$), 46.17 (s, $C_{2,3}$), 45.75 (s, C_7). NMR spectra were also run in $CDCl_3$ and were consistant with literature values.[8] FTIR [see appendix C11], (KBr disc), (cm^{-1}): 3060 - 2950 (s, CH stretches), 2878 (m, O-CH_3 stretch), 1742, 1729 (s, C=O stretch), 1255, 1191 (s, C-O stretch). EI Mass Spec. (m/z), (M = $C_{11}H_{14}O_4$) : 210 (0.5%, $C_{11}H_{14}O_4$, $M^{+\bullet}$), 179 (5%, $C_{10}H_{11}O_3$, M - OCH_3) 145 (17%, $C_6H_9O_4$, MH^+ - C_5H_6), 66 (100%, C_5H_6, M - $C_6H_9O_4$) .

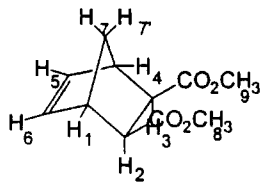

IUPAC assignment of hydrogen atoms within monomer 1.

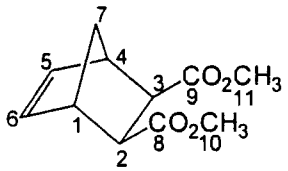

IUPAC assignment of carbon atoms within monomer 1.

The synthesis and characterisation of *endo,endo*-bicyclo[2.2.1]hept-5-ene-2,3-dicarboxylic acid dimethyl ester (monomer 2).

Endo-Bicyclo[2.2.1]hept-5-ene-2,3-dicarboxy anhydride (48.78g, 0.30mol) was dissolved in methanol (120ml) and placed in a one necked, round bottomed flask (500ml) fitted with a condenser and stirrer bar, to this, *p*-toluene sulphonic acid (0.76g, 0.004mol) was added. The solution was refluxed for 4hrs and the bulk of the solvent removed using a rotary evaporator. The residue was then dissolved in diethyl ether (180ml) and washed successively with water (180ml), $NaHCO_3$ (aq) (10% w/w, 180ml) and water (180ml). After drying for 2 days over anhydrous $MgSO_4$ the solution was filtered, the diethyl ether removed on a rotary evaporator and the product purified by distillation onto molecular sieves (70-84°C, 0.03mmHg[1]). Found C, 62.68%, H, 6.71%, (Calculated for $C_{10}H_6O_4$: C, 62.85, H, 6.71%). ^1H NMR[1] [see appendix A13], (d_6-acetone, 400MHz) δ(ppm):

6.14 (t, $J_{6,1} = J_{6,7} = 1.6$ Hz, 2H, $H_{5,6}$), 3.52 (s, 6H, $H_{8,9}$), 3.34 (t, 2H, $H_{2,3}$), 3.09 (m, 2H, $H_{1,4}$), ABq δ_B 1.40 (b, 1H, $H_{7'}$) δ_A 1.36 (b, 1H, H_7), $J_{AB} = 8.4$Hz.. ^{13}C NMR [see appendix B13], (d_6-acetone, 100MHz) δ(ppm): 172.97 ($C_{8,9}$), 135.50 ($C_{5,6}$), 51.37 ($C_{10,11}$), 48.90 (C_7), 48.49 ($C_{2,3}$), 46.94 ($C_{1,4}$). FTIR [see appendix C12], (KBr disc), (cm^{-1}): 3080 - 2884 (s, CH stretches), 2844 (m, O-CH_3 stretch), 1731 (br, s, C=O stretch), 1337, 1196 (s, C-O stretch). CI Mass Spec. (m/z), (M = $C_{11}H_{14}O_4$) : 228 (14%, $C_{11}H_{18}NO_4$, MNH_4^+), 211 (100%, $C_{11}H_{15}O_4$, MH^+), 196 (69%, $C_{10}H_{12}O_4$, $MH^+ - CH_3$), 179 (38%, $C_{10}H_{11}O_3$, M - OCH_3).

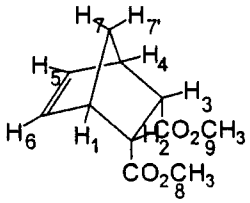

IUPAC assignment of hydrogen atoms within monomer 2.

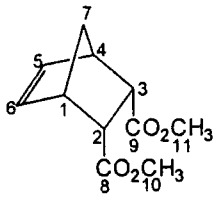

IUPAC assignment of carbon atoms within monomer 2.

The synthesis and characterisation of *2-endo-3-exo*-bicyclo[2.2.1]hept-5-ene-2,3-dicarboxylic acid dimethyl ester (monomer 3).

A solution of dimethyl fumarate (18.8g, 0.13mol) in tetrahydrofuran (320ml) was placed in a round bottomed flask (500ml) fitted with a condenser, dropping funnel and stirrer bar. Cyclopentadiene (11.6g, 0.18mol) was added dropwise to the solution with stirring. The reaction proceeded for 24 hrs at room temperature after which the solvent was removed on a rotary evaporator. The light yellow, clear, liquid product was dried over CaH_2 and then purified by distillation under reduced pressure to give a clear, colourless liquid (77°C, 0.005mmHg[1]). Found C, 62.54%, H, 6.75% (Calculated for $C_{10}H_6O_4$: C, 62.85, H, 6.71%). ^{1}H NMR[1] [see appendix A14], (d_6-acetone, 400MHz) δ(ppm): 6.27 (dd, $J_{5,4} = 5.6$Hz, $J_{5,7'} =$

3.2Hz, 1H, H_5), 6.05 (dd, $J_{6,1}$ = 5.6Hz, $J_{6,7'}$ = 3.2Hz, 1H, H_6), 3.68 (s, 1H, H_9), 3.60 (s, 1H, H_8), 3.32 (t, $J_{2,1} \sim J_{2,3} \sim 4.4$Hz, 1H, H_2), 3.23 (bm, 1H, H_1), 3.08 (bm, 1H, H_4), 2.61 (dd, $J_{2,3}$ = 4.4Hz, $J_{3,7}$ = 1.6Hz, 1H, H_3), ABq δ_B 1.60 (b, 1H, $H_{7'}$) δ_A 1.40 (q, 1H, H_7), J_{AB} = 8.4Hz. ^{13}C NMR [see appendix B14], (d_6-acetone, 100MHz) δ(ppm): 174.08 (s, C_9). 172.69 (s, C_8), 137.25 (s, C_5), 134.85 (s, C_6), 51.24 (d, C_{11}), 50.93 (d, C_{10}), 47.48, 47.28, 46.78, 46.66, 45.29, (all s, $C_{1,4,5,6,7}$). FTIR [see appendix C13], (KBr disc), (cm^{-1}): 3081 - 2886 (s, CH stretches), 2820 (m, O-CH_3 stretch), 1737 (br, s, C=O stretch), 1249, 1196 (s, C-O stretch). EI Mass Spec. (m/z), (M = $C_{11}H_{14}O_4$) : 210 (3%, $C_{11}H_{14}O_4$, $M^{+\bullet}$), 179 (11%, $C_{10}H_{11}O_3$, M - OCH_3), 145 (31%, $C_6H_9O_4$, MH^+ - C_5H_6), 66 (100%, C_5H_6, M - $C_6H_9O_4$) .

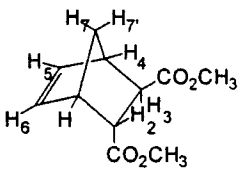

IUPAC assignment of hydrogen atoms within monomer 3.

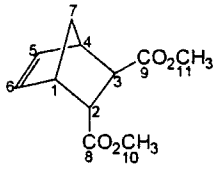

IUPAC assignment of carbon atoms within monomer 3.

4.3.3 Polymer synthesis and characterisation:

Preparation of poly(*exo,exo*-bicyclo[2.2.1]hept-5-ene-2,3-dicarboxylic acid dimethyl ester)[5] Mn = 182,000, (Poly-1S)

A solution of initiator 1 (3.2mg, 6.5 x 10^{-6} mol) in benzene (3ml) was stirred vigorously in a sample vial (20ml) fitted with stirrer bar. Monomer 1 (1.01g, 0.005mol) in benzene (3ml) was added quickly but dropwise to the stirring solution. After 10 mins the solution became very viscous and more solvent was

added (10ml) until vigorous stirring was again possible. The reaction proceeded for a further 50 mins, during which time the initial light yellow colouration did not change. The reaction was then quenched with benzaldehyde (2 drops) to give an orange solution and stirred for a further 20 mins. The reaction vessel was removed from the glove box and the polymer precipitated by addition of the benzene solution to excess methanol and reprecipitated twice from THF into methanol. The product was isolated by decantation and dried *in vacuo* to give a white, fibrous polymer (0.89g, 88% yield). Found C, 62.33%, H, 6.75% (Calculated for $(C_{10}H_6O_4)_n$: C, 62.85, H, 6.71%). Mn = 182,000, PDI = 1.24 [see appendix D1]. ^{1}H NMR [see appendix A15], ($CDCl_3$, 400MHz) δ(ppm): 5.39 (s, 1.7H, $H_{5,6\ trans}$), 5.22 (m, 0.3H, $H_{5,6\ cis}$), 3.61 (s, 6H, $H_{8,9}$), 3.30 (bm, 0.3H, $H_{1,4\ cis}$), 2.93 (bm, 1.7H, $H_{2,3\ trans}$), 2.81 (bm, 1.7H, $H_{1,4\ trans}$), 2.81 (bm, 0.3H, $H_{2,3\ cis}$, assigned from COSY spectrum) 2.04 (bm, 1H, $H_{7\ or\ 7'}$), 1.26 (bm, 1H, $H_{7\ or\ 7'}$). ^{13}C NMR [see appendix B15], ($CDCl_3$, 100MHz) δ(ppm): 173.09 (s, $C_{8,9\ trans}$), 172.92 (s, $C_{8,9\ cis}$), 132.80 (s, $C_{5,6\ trans/cis}$), 131.96 (s, $C_{5,6\ trans/trans}$), 128.28 (s, $C_{5,6\ cis/trans}$), 53.07 (s, $C_{2,3\ cis/trans}$), 52.42 (s, $C_{2,3\ trans/trans}$), 51.74 (s, $C_{10,11}$), 45.22 (s, $C_{1,4\ trans/cis}$), 45.16 (s, $C_{1,4\ trans/trans}$), 40.58 (s, $C_{1,4\ cis/trans}$), 39.15 (s, C_7).

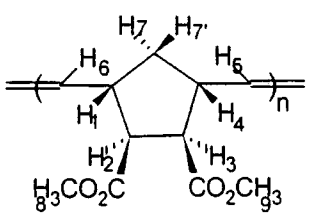

IUPAC assignment of hydrogen atoms within Poly-1S.

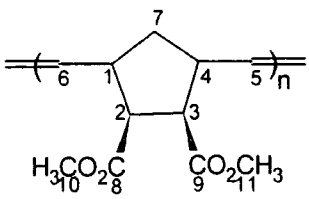

IUPAC assignment of carbon atoms within Poly-1S.

Hydrogenation of poly(*exo,exo*-bicyclo[2.2.1]hept-5-ene-2,3-dicarboxylic acid dimethyl ester). Mn = 185,000, (Poly-1P)

Poly-1S (0.5g), *p*-toluene sulphonylhydrazide[7] (5g, 0.027mol) and *p*-xylene (50ml) were placed in a one necked, round bottomed flask (100ml) fitted with a condenser and stirrer bar and then heated, with stirring to 120°C for 4hrs.

The hot solution was added dropwise to vigorously stirring methanol (500ml) in a beaker (600ml) to give a precipitate which was isolated by decantation. The resulting polymer (0.29g, 57% yield) was a colourless, transparent, adhesive solid. Mn = 184,900, PDI = 1.28 [see appendix D2]. ^{1}H NMR [see appendix A16], ($CDCl_3$, 400MHz) δ(ppm): 3.68 (bm, 6H, $H_{8,9}$), 2.67 (bd, 2H, $H_{2,3}$), 2.21 (2bm, 2H, $H_{1,4}$), 1.55 (bm, 2H, $H_{5,6}$), 1.17 (bt, 1H, H_7), 0.80 (bm, 1H, $H_{7'}$). ^{13}C NMR [see appendix B16], ($CDCl_3$, 100MHz) δ(ppm): 173.95 (m, $C_{8,9}$), 134.51 (s, *p*-xylene, C_1), 128.74 (s, *p*-xylene, C_2), 52.52 (s, $C_{10,11}$), 51.68 (s, $C_{2,3}$), 42.27 (d, $C_{1,4}$), 38.69 (s, $C_{7 \text{ or } 6 \text{ and } 5}$), 33.73 (s, $C_{7 \text{ or } 6 \text{ and } 5}$), 20.82 (s, *p*-xylene, CMe).

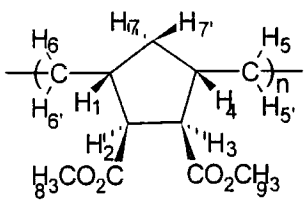

IUPAC assignment of hydrogen atoms within Poly-1P.

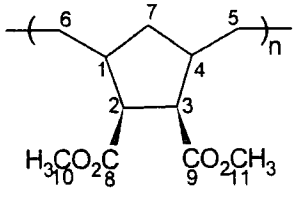

IUPAC assignment of carbon atoms within Poly.-1P.

Base hydrolysis of poly(*exo,exo*-1,4-cyclopentenylene-5,6-ethylidene-2,3-dicarboxylic acid dimethyl ester). Mn = 159,900, (Poly-1F)

Poly-1P (250mg) and NaOH(aq) (3ml, 10% w/w) were placed in a one necked, round bottomed flask (6ml) fitted with a condenser and stirrer bar. The suspension was stirred vigorously and heated to reflux for 10hrs after which the majority of the polymer had dissolved. The solution was decanted from the undissolved polymer and the resulting, white, powdery, water soluble polymer (200mg, 80% yield), was precipitated into methanol (30ml). Mn = 159,900, PDI = 1.47 [see appendix D3]. ^{1}H NMR [see appendix A17] (D_2O, 400MHz) δ(ppm): 2.36 (bm, 2H, $H_{2,3}$), 1.91 (bm, 3H), 1.31, 1.25, 1.04, 0.96, 0.60 (bm, 5H). ^{13}C NMR [see appendix B17], (D_2O, 100MHz) δ(ppm): 183.46 (s, $C_{8,9}$), 57.21 (s, $C_{2,3}$), 43.00 (d, $C_{1,4}$), 38.34 (s, C_7), 33.55 (bd, $C_{5,6}$).

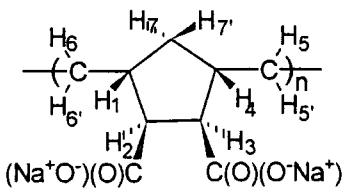

IUPAC assignment of hydrogen atoms within Poly-1F.

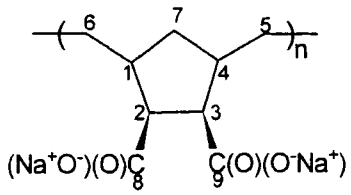

IUPAC assignment of carbon atoms within Poly-1F.

Preparation of poly(*exo,exo*-bicyclo[2.2.1]hept-5-ene-2,3-dicarboxylic acid dimethyl ester).[5] Mn=71,400, (Poly 1S')

A solution of initiator 1 (6.5mg, 0.013mmol) in benzene (2.5ml) was stirred vigorously in a sample vial (20ml). Monomer 1 (0.679g, 0.003mol) in benzene (2.5ml) was added quickly but dropwise to the solution with stirring. The reaction proceeded for one hour during which the solution became more viscous

and the initial light yellow colouration did not change. The reaction was then quenched with benzaldehyde (2 drops), to give an orange solution, and stirred for a further 20 mins. The reaction vessel was removed from the glove box and the polymer precipitated by addition of the benzene solution in excess methanol and reprecipitated twice from THF into methanol. The product was isolated by decantation and dried *in vacuo* to give a white, powdery polymer (350mg, 69% yield). Found C, 62.22%, H, 6.55% (Calculated for $(C_{10}H_6O_4)_n$: C, 62.85%, H, 6.71%). Mn = 71,400, PDI = 1.12 [see appendix D4]. ^{1}H NMR ($CDCl_3$, 400MHz) δ(ppm): 5.39 (s, 1.8H, $H_{5,6\ trans}$), 5.22 (d, 0.2H, $H_{5,6\ cis}$), 3.61 (s, 6H, $H_{8,9}$), 3.30 (bm, 0.2H, $H_{1,4\ cis}$), 2.94 (bm, 1.8H, $H_{2,3\ trans}$), 2.81 (bm, 1.8H, $H_{2,3\ trans}$), 2.81 (bm, 0.2H, $H_{2,3\ cis}$, assigned from COSY spectrum), 2.05 (bm, 1H, $H_{7\ or\ 7'}$), 1.26 (bm, 1H, $H_{7'}$). ^{13}C NMR ($CDCl_3$, 100MHz) δ(ppm): 173.00 (s, $C_{8,9\ trans}$), 172.83 (s, $C_{8,9\ cis}$), 132.80 (s, $C_{5,6\ trans/cis}$), 131.87 (s, $C_{5,6\ trans/trans}$), 52.98 (s, $C_{2,3\ cis/trans}$), 52.32 (s, $C_{2,3\ trans}$), 51.65 (s, $C_{10,11}$), 45.13 (s, $C_{1,4\ trans}$), 40.49 (s, $C_{1,4\ cis}$), 39.06 (s, C_7).

Hydrogenation of poly(*exo,exo*-bicyclo[2.2.1]hept-5-ene-2,3-dicarboxylic acid dimethyl ester). Mn = 68,200, (Poly 1P')

Poly-1S' (0.31g), *p*-toluene sulphonylhydrazide[3] (3g, 0.016mol) and *p*-xylene (50ml) were placed in a one necked, round bottomed flask (100ml) fitted with a condenser and stirrer bar and then heated, with stirring to 120°C for 4hrs. The hot solution was added dropwise to vigorously stirring methanol (500ml) in a beaker (600ml) to give a precipitate which was isolated by decantation. The resulting polymer was a colourless, transparent, adhesive solid (0.16g, 52%

yield). Mn =68,200, PDI = 1.11 [see appendix D5]. No NMR analysis was carried out on this precursor polymer, however, full analysis on the final polymer, Poly-1F', was carried out and the results are given in the next section.

Base hydrolysis of poly(*exo,exo*-1,4-cyclopentenylene-5,6-ethylidene-2,3-dicarboxylic acid dimethyl ester). Mn = ~68,200, (Poly-1F')

Poly-1P' (100mg) and NaOH (aq) (1.5ml, 10% w/w) were placed in a one necked, round bottomed flask (5ml) fitted with a condenser and stirrer bar. The suspension was stirred vigorously and heated to reflux for 4hrs after which the polymer had dissolved. The hot solution was added dropwise to methanol (15ml) in a beaker (25ml) with vigorous stirring to give a precipitate which was isolated by centrifugation and decantation. The resulting polymer was a white, powdery solid (0.9g, 90% yield). ^{1}H NMR (D_2O, 400MHz) δ(ppm): 2.36 (bm, 2H, $H_{2,3}$), 1.91 (bm, 3H), 1.31, 1.25, 1.04, 0.96, 0.60 (bm, 5H). ^{13}C NMR (D_2O, 100MHz) δ(ppm): 183.44 (s, $C_{8,9}$), 57.20 (s, $C_{2,3}$), 43.00 (s, $C_{1,4}$), 40.49 (s, C_7), 33.51 (s, $C_{5,6}$).

Preparation of poly(*exo,exo*-bicyclo[2.2.1]hept-5-ene-2,3-dicarboxylic acid dimethyl ester).[5] Mn = 7,700, (Poly 1S'')

A solution of initiator 1 (81mg, 1.7x10^{-4}mol) in benzene (2.5ml) was stirred vigorously in a sample vial (20ml). Monomer 1 (0.836g, 0.004mol) in benzene (2.5ml) was added quickly but dropwise to the stirring solution. The reaction proceeded for one hour during which the solution became more viscous and the initial yellow/orange colouration did not change. The reaction was then

quenched with benzaldehyde (4 drops) to give an orange/brown solution and stirred for a further 20 mins. The reaction vessel was removed from the glove box and the polymer precipitated by addition of the benzene solution in excess methanol and reprecipitated three times from THF into methanol. The product was isolated by centrifugation, decantation and dried *in vacuo* to give a light green, powdery polymer (436mg, 52% yield). Mn = 7,700, PDI = 1.10 [see appendix D6]. Found C, 64.38%, H, 6.72% (Calculated for $(C_{10}H_6O_4)_n$: C, 62.85, H, 6.71%). ^{1}H NMR ($CDCl_3$, 400MHz) δ(ppm): 5.39 (bs, 1.8H, $H_{5,6\ trans}$), 5.22 (b, 0.2H, $H_{5,6\ cis}$), 3.61 (s, 6H, $H_{8,9}$), 3.30 (bm, 0.2H, $H_{1,4\ cis}$), 2.94 (bm, 1.8H, $H_{2,3\ trans}$), 2.81 (bm, 1.8H, $H_{2,3\ trans}$), 2.81 (bm, 0.2H, $H_{2,3\ cis}$, assigned from COSY spectrum), 2.05 (bm, 1H, $H_{7\ or\ 7'}$), 1.26 (bm, 1H, $H_{7\ or\ 7'}$). ^{13}C NMR ($CDCl_3$, 100MHz) δ(ppm): 173.10 (s, $C_{8,9\ trans}$), 172.92 (s, $C_{8,9\ cis}$), 132.79 (s, $C_{5,6\ trans/cis}$), 131.96 (s, $C_{5,6\ trans/trans}$), 53.06 (s, $C_{2,3\ cis/\ trans}$), 52.41 (s, $C_{2,3\ trans}$), 51.74 (s, $C_{10,11}$), 45.15 (s, $C_{1,4\ trans}$), 40.58 (s, $C_{1,4\ cis}$), 39.14 (s, C_7).

Attempted hydrogenation of poly(*exo,exo*-bicyclo[2.2.1]hept-5-ene-2,3-dicarboxylic acid dimethyl ester). (Poly 1P'')

Poly-1S'' (0.25g), *p*-toluene sulphonylhydrazide (2g, 0.01mol) and *p*-xylene (16ml) were placed in a one necked, round bottomed flask (50ml) and heated to 120°C for $1^1/_2$ hrs. The hot solution was added dropwise to vigorously stirring methanol (160ml) in a beaker (200ml) giving a small amount of viscous liquid (~2mg, 1% yield). No characterisation was carried out on this polymer due to the recovery of insufficient polymer.

Preparation of poly(*endo,endo*-bicyclo[2.2.1]hept-5-ene-2,3-dicarboxylic acid dimethyl ester).[5] Mn = 174,000, (Poly-2S)

A solution of initiator 1 (2.9mg, 0.0006mmol) in benzene (3ml) was stirred vigorously in a sample vial (20ml). Monomer 2 (1.192g, 0.006mol) in benzene (2ml) was added quickly via Pasteur pipette to the stirring solution. The reaction proceeded for one hour during which the solution appeared more viscous and the initial light yellow colouration did not change. The reaction was then quenched with benzaldehyde (2 drops) to give an orange solution and stirred for a further 20 mins. The reaction vessel was removed from the glove box and the polymer precipitated by addition of the benzene solution to excess methanol and reprecipitated twice from THF into methanol. The product was isolated by decantation and dried *in vacuo* to give a white, polymer with the texture of crepe paper (1.10g, 92%yield). Found C, 61.98%, H, 6.73% (Calculated for $(C_{10}H_6O_4)_n$: C, 62.85%, H, 6.71%). Mn = 174,000, PDI = 1.01 [see appendix D7]. ^{1}H NMR [see appendix A18] ($CDCl_3$, 400MHz) δ(ppm): 5.51 (bm, 2H, $H_{5,6}$), 3.64 (bm, 6H, $H_{8,9}$), 3.09 (bm, 2H, $H_{2,3}$), 2.84 (bm, 2H, $H_{1,4}$ assigned from COSY spectrum), 1.92 (bm, 2H, $H_{7,7'}$). ^{13}C NMR [see appendix B18] ($CDCl_3$, 100MHz) δ(ppm): 172.64 (m, $C_{8,9}$), 131.77 (m, $C_{5,6}$), 51.31 (s, $C_{10,11}$, assigned from COSY spectrum), 51.28 (m, $C_{2,3}$), 44.61 (m, $C_{1,4}$), 37.96 (m, C_7).

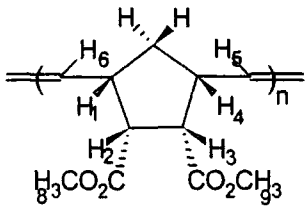

IUPAC assignment of hydrogen atoms within Poly-2S.

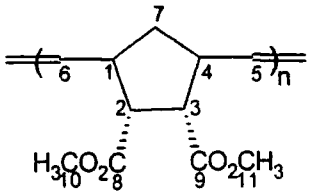

IUPAC assignment of carbon atoms within Poly-2S.

Hydrogenation of poly(*endo,endo*-bicyclo[2.2.1]hept-5-ene-2,3-dicarboxylic acid dimethyl ester). Mn = 90,000, (Poly-2P)

Poly-2S (0.55g), *p*-toluene sulphonhydrazide[3] (5g, 0.027mol) and *p*-xylene (50ml) were placed in a one necked, round bottomed flask (100ml) fitted with a condenser and stirrer bar and heated, with stirring to 120°C for 4hrs.

The hot solution was added dropwise to vigorously stirring methanol (500ml) in a beaker (600ml) to give a precipitate which was isolated by decantation. The resulting polymer was a colourless, transparent, adhesive solid (0.49g, 88% yield). Mn = 90,000, PDI = 1.5 [see appendix D8]. ^{1}H NMR [see appendix A19] ($CDCl_3$, 400MHz) δ(ppm): 3.68 (bm, 6H, $H_{8,9}$), 3.05 (bm, 2H, $H_{2,3}$), 2.08 (2bm, 4H, $H_{1,4\ cis\ and\ trans,\ 5,6}$), 1.40 (2bm, 4H, $H_{7,7',5,6}$) ^{13}C NMR [see appendix B19] ($CDCl_3$, 100MHz) δ(ppm): 173.10 (m, $C_{8,9}$), 134.51 (s, *p*-xylene, C_1), 128.74 (s, *p*-xylene, C_2), 51.12 (s, $C_{10,11}$), 50.07 (s, $C_{2,3}$), 41.20 (m, $C_{1,4}$), 37.05 (s, $C_{7\ or\ 6\ and\ 5}$), 30.18 (s, $C_{7\ or\ 6\ and\ 5}$), 20.82 (s, *p*-xylene, CMe).

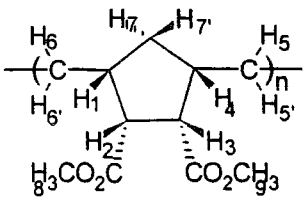

IUPAC assignment of hydrogen atoms within Poly-2P.

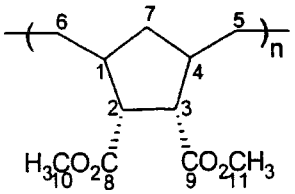

IUPAC assignment of carbon atoms within Poly-2P.

Base hydrolysis of poly(*endo,endo*-1,4-cyclopentenylene-5,6-ethylidene-2,3-dicarboxylic acid dimethyl ester). Mn = 73,000, (Poly-2F)

Poly-2P (380mg) and NaOH(aq) (6ml, 10% w/w) were placed in a one necked, round bottomed flask (10ml) fitted with a condenser and stirrer bar. The suspension was stirred vigorously and heated to reflux for 10hrs after which the the polymer had dissolved. The hot solution was added dropwise to vigorously stirring methanol (60ml) in a beaker (100ml) to give a precipitate which was isolated by centrifugation and decantation. The resulting polymer was a white, powdery solid (0.35g, 92% yield). Mn = 73,000, PDI = 1.70 [see appendix D9]. ^{1}H NMR [see appendix A20] (D_2O, 400MHz) δ(ppm): 2.70 (t, 1H, H_2), 2.30 (t, 1H, H_3), 2.01, 1.90, 1.70 (bm, 4H), 1.37, 1.30, 1.19, 1.03, 0.90, 0.78 (bm, 4H). ^{13}C NMR [see appendix B20] (D_2O, 100MHz) δ(ppm): 185.26 (s, C_9), 183.17 (m, C_8), 58.22 (s, C_3),55.97 (s, C_2), 44.75 (m, C_4), 40.69 (m, C_1), 38.23 (m, C_7), 32.94 (m, $C_{5\text{ or }6}$), 30.68 (m, $C_{5\text{ or }6}$).

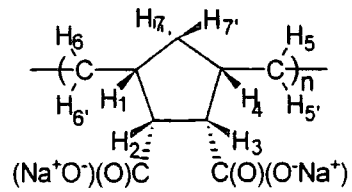

IUPAC assignment of hydrogen atoms within Poly-2F.

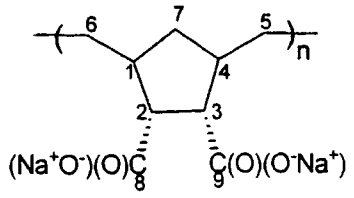

IUPAC assignment of carbon atoms within Poly-2F.

Preparation of poly(*endo,endo*-bicyclo[2.2.1]hept-5-ene-2,3-dicarboxylic acid dimethyl ester).[5] Mn = 57,700, (Poly-2S')

A solution of initiator 1 (9.9mg, 0.00002 mol) in benzene (2.5ml) was stirred vigorously in a sample vial (20ml). Monomer 2 (1.0200g, 0.0049mol) in benzene (2.5ml) was added quickly via Pasteur pipette to the stirring solution. The reaction proceeded for one hour during which the solution appeared more viscous and the initial light yellow colouration did not change. The reaction was then quenched with benzaldehyde (2 drops) to give an orange solution and left stirring for a further 20 mins. The reaction vessel was removed from the glove box and the polymer precipitated directly into methanol and reprecipitated three times from THF into excess methanol. The product was then isolated by centrifugation and decantation and dried *in vacuo* to give a white, polymer (0.81g, 78%yield). Mn = 57,700, PDI = 1.02 [see appendix D10]. Found C, 63.09%, H, 6.71% (Calculated for $(C_{10}H_6O_4)_n$: C, 62.85%, H, 6.71%). ^{1}H NMR ($CDCl_3$, 400MHz) δ(ppm): 5.51 (bm, 2H, $H_{5,6}$), 3.65 (bm, 6H, $H_{8,9}$), 3.09 (bm, 2H, $H_{2,3}$), 2.85 (bm, 2H, $H_{1,4}$ assigned from COSY spectrum), 1.94 (bm, 2H, $H_{7,7'}$). ^{13}C NMR ($CDCl_3$, 100MHz) δ(ppm): 172.63 (m, $C_{8,9}$), 131.77 (m, $C_{5,6}$),

51.30 (s, $C_{10,11}$, assigned from COSY spectrum), 51.27 (m, $C_{2,3}$), 44.60 ($C_{1,4}$), 37.92 (m, C_7).

Hydrogenation of poly(*endo,endo*-bicyclo[2.2.1]hept-5-ene-2,3-dicarboxylic acid dimethyl ester). Mn = 58,100, (Poly-2P')

Poly-1S' (0.55g), *p*-toluene sulphonylhydrazide[3] (5g, 0.027mol) and *p*-xylene (50ml) were placed in a one necked, round bottomed flask (100ml) fitted with a condenser and stirrer bar and then heated, with stirring to 120°C for 4hrs.

The hot solution was added dropwise to vigorously stirring methanol (500ml) in a beaker (600ml) to give a precipitate which was isolated by decantation. The resulting polymer was a more transparent and adhesive solid than poly-1S'. (0.42g, 76% yield). Mn = 52,000, PDI = 1.05 [see appendix D11].

^{1}H NMR ($CDCl_3$, 400MHz) δ(ppm): 3.68 (bm, 6H, $H_{8,9}$), 3.05 (bm, 2H, $H_{2,3}$), (2bm, 4H, $H_{1,4\ cis\ and\ trans,\ 5,6}$), 1.39 (2bm, 4H, $H_{7,7',5,6}$). ^{13}C NMR ($CDCl_3$, 100MHz) δ(ppm): 173.10 (m, $C_{8,9}$), 134.52 (s, *p*-xylene, C_1), 128.75 (s, *p*-xylene, C_6), 51.13 (s, $C_{10,11}$), 50.08 (s, $C_{2,3}$), 41.21 (m, $C_{1,4}$), 37.05 (s, $C_{7\ or\ 6\ and\ 5}$), 30.20 (s, $C_{7\ or\ 6\ and\ 5}$), 20.82 (s, *p*-xylene, CMe).

Base hydrolysis of poly(*endo,endo*-1,4-cyclopentenylene-5,6-ethylidene-2,3-dicarboxylic acid dimethyl ester). Mn = 48,400, (Poly-2F')

Poly-2P' (0.31mg) and NaOH(aq) (5ml, 10% w/w) were placed in a one necked, round bottomed flask (10ml) fitted with a condenser and stirrer bar. The suspension was stirred vigorously and heated to reflux for 10hrs after which the the polymer had dissolved. The hot solution was added dropwise to vigorously

stirring methanol (50ml) in a beaker (100ml) to give a precipitate which was isolated by centrifugation and decantation. The resulting polymer was a white, powdery solid (0.21g, 68% yield). Mn = 58,100, PDI =1.3 [see appendix D12]. ^{1}H NMR (D_2O, 400MHz) δ(ppm): 2.70 (t, 1H, H_2), 2.30 (t, 1H, H_3), 2.02, 1.90, 1.71 (bm, 4H), 1.30, 1.19, 1.03, 0.90, 0.78 (bm, 4H). ^{13}C NMR (D_2O, 100MHz) δ(ppm): 185.28 (s, C_9), 183.19 (m, C_8), 58.26 (s, C_3), 55.95 (s, C_2), 44.65 (m, C_4), 40.73 (m, C_1), 38.25 (m, C_7), 32.94 (m, $C_{5\text{ or }6}$), 30.69 (m, $C_{5\text{or }6}$).

Preparation of poly(*endo,endo*-bicyclo[2.2.1]hept-5-ene-2,3-dicarboxylic acid dimethyl ester).[2] Mn = 6,000, (Poly-2S'')

A solution of initiator 1 (48.3mg, 0.00010 mol) in benzene (2ml) was stirred vigorously in a sample vial (20ml). Monomer 2 (0.5g, 0.0024mol) in benzene (2ml) was added quickly via Pasteur pipette to the stirring solution. The reaction proceeded for one hour during which the initial orange colouration did not change. The reaction was then quenched with benzaldehyde (7 drops) to give an orange/brown solution and stirred for a further 20 mins. The reaction vessel was removed from the glove box and the polymer precipitated directly into methanol and reprecipitated three times from THF into excess methanol. The product was then isolated by centrifugation and decantation and dried *in vacuo* to give a slightly yellow polymer (0.17g, 34%yield). Found C, 62.44%, H, 6.60% (Calculated for $(C_{10}H_6O_4)_n$: C, 62.85%, H, 6.71%). Mn = 6,000, PDI = 1.12 [see appendix D13]. ^{1}H NMR ($CDCl_3$, 400MHz) δ(ppm): 5.51 (bm, 2H, $H_{5,6}$), 3.65 (bm, 6H, $H_{8,9}$), 3.09 (bm, 2H, $H_{2,3}$), 2.85 (bm, 2H, $H_{1,4}$ assigned from COSY spectrum), 1.94 (bm, 2H, $H_{7,7'}$). ^{13}C NMR ($CDCl_3$, 100MHz) δ(ppm): 172.41 (m,

$C_{8,9}$), 131.77 (m, $C_{5,6}$), 51.29 (s, $C_{10,11}$, assigned from COSY spectrum), 51.27 (m, $C_{2,3}$), 44.60 ($C_{1,4}$), 37.96 (m, C_7).

Preparation of poly(*2-endo-3-exo*-bicyclo[2.2.1]hept-5-ene-2,3-dicarboxylic acid dimethyl ester).[6] Mn = 275,400, (Poly-3S)

A solution of initiator 1 (1.8mg, 4 x 10^{-6} mol) in benzene (4ml) was stirred vigorously in a sample vial (20ml). Monomer 3 (0.815g, 0.004mol) in benzene (3ml) was added quickly via Pasteur pipette to the stirring solution. After 10mins the solution became very viscous and a further 8ml aliquot of solvent was added to reduce the viscosity. The reaction proceeded for a further 50mins. during which time the initial light yellow colouration did not change. The reaction was then quenched with benzaldehyde (2 drops) to give an orange solution and stirred for a further 20 mins. The reaction vessel was removed from the glove box and the polymer precipitated directly into hexane and reprecipitated twice from into excess methanol. The product was then isolated by centrifugation and decantation and dried *in vacuo* to give a white, fibrous polymer (0.52g, 61%yield). Found C, 62.49%, H, 6.80% (Calculated for $(C_{10}H_6O_4)_n$: C, 62.85%, H, 6.71%). Mn =275,400. PDI = 1.12 [see appendix D14]. ^{1}H NMR [see appendix A21] ($CDCl_3$, 400MHz) δ(ppm): 5.32 (3 x bm, 2H, $H_{5,6}$), 3.67 (dm, 6H, $H_{8,9}$), 3.24 (bm, 1H, $H_{2,3}$), 2.96 (bm, 2H, $H_{1,4 \text{ and } 2,3}$), 2.70 (bm, 1H, $H_{1,4}$), 1.97 (bm, 1H, H_7), 1.49 (bm, 1H, $H_{7'}$). ^{13}C NMR [see appendix B21] ($CDCl_3$, 100MHz) δ(ppm): 174.28 (m, $C_{8,9\ exo}$), 173.21 (m, $C_{8,9\ endo}$), 132.54 (dm, $C_{5,6\ cis\ or\ trans}$), 130.08 (m, $C_{5,6\ cis\ or\ trans}$), 52.50 (m, $C_{1,4\ cis}$), 52.31 (bd, $C_{2,3\ cis\ or\ trans}$), 51.75 (m, $C_{10,11}$), 46.74 (m, $C_{1,4trans}$), 44.43 (m, $C_{2,3\ cis\ or\ trans}$), 39.13 (m, C_7).

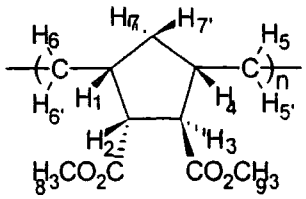

IUPAC assignment of hydrogen atoms within Poly-3S.

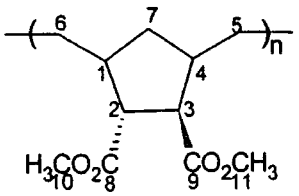

IUPAC assignment of carbon atoms within Poly-3S.

Hydrogenation of poly(*2-endo-3-exo*-bicyclo[2.2.1]hept-5-ene-2,3-dicarboxylic acid dimethyl ester). Mn = 220,500, (Poly-3P)

Poly-3S (0.41g), *p*-toluene sulphonylhydrazide[3] (4g, 0.022mol) and *p*-xylene (40ml) were placed in a one necked, round bottomed flask (50ml) fitted with a condenser and stirrer bar and then heated, with stirring to 120°C for 4hrs. The hot solution was added dropwise to vigorously stirring methanol (400ml) in a beaker (600ml) to give a precipitate which was isolated by decantation. The resulting polymer was a colourless, transparent and adhesive solid (0.40g, 98% yield). Mn = 220,500, PDI = 1.34 [see appendix D15]. ^{1}H NMR [see appendix A22] ($CDCl_3$, 400MHz) δ(ppm): 3.67 (dm, 6H, $H_{8,9}$), 3.15 (bm, 1H, $H_{2,3}$), 2.78 (bm, 1H, $H_{2,3}$), (bm, 1H, $H_{1,4}$), 1.20 (bm, 2H, $H_{1,4 \text{ and } 5,6}$), 1.63 (bm, 1H, $H_{6',5'}$), 1.35 (bm, 2H, $H_{5,6 \text{ and } 7}$), 1.09 (bm, 2H, $H_{5,6 \text{ and } 7'}$). ^{13}C NMR [see appendix B22] ($CDCl_3$, 100MHz) δ(ppm): 175.28 (s, C_9), 174.33 (m, C_8), 134.52 (s, *p*-xylene, C_1), 128.75 (s, *p*-xylene, C_2), 52.39 (s, C_3), 51.81 (s, $C_{10 \text{ or } 11}$), 51.37 (s, $C_{10 \text{ or } 11}$), 50.72 (s, C_2), 43.74 (m, C_4), 42.69 (m, C_1), 38.03 (m, C_7), 33.48 (m, $C_{5 \text{ or } 6}$), 29.96 (m, $C_{5 \text{ or } 6}$), 20.82 (s, *p*-xylene, CMe).

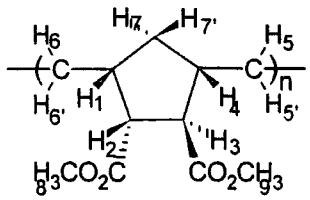

IUPAC assignment of hydrogen atoms within Poly-3P.

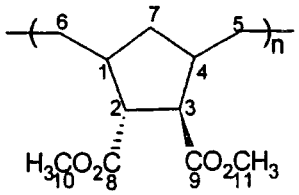

IUPAC assignment of carbon atoms within Poly-3P.

Base hydrolysis of poly(*2-endo-3-exo*-1,4-cyclopentenylene-5,6-ethylidene-2,3-dicarboxylic acid dimethyl ester). Mn = 147,200, (Poly-3F)

Poly-3P (340mg) and NaOH(aq) (5ml, 10% w/w) were placed in a one necked, round bottomed flask (10ml) fitted with a condenser and stirrer bar. The suspension was stirred vigorously and heated to reflux for 10hrs after which time the polymer had dissolved. The hot solution was added dropwise to vigorously stirring methanol (50ml) in a beaker (100ml) to give a precipitate which was isolated by centrifugation and decantation. The resulting polymer was a white, powdery solid (0.28g, 82% yield). Mn = 147,200, PDI = 1.54 [see appendix D16]. ^{1}H NMR [see appendix A23] (D_2O, 400MHz) δ(ppm): 2.70 (t, 1H, H_2), 2.30 (t, 1H, H_3), 2.01, 1.90, 1.70 (bm, 4H), 1.37, 1.30, 1.19, 1.03, 0.90, 0.78 (bm, 4H). ^{13}C NMR [see appendix B23] (D_2O, 100MHz) δ(ppm): 185.24 (s, C_9), 183.16 (m, C_8), 58.18 (s, C_3), 55.97 (s, C_2), 44.65 (m, C_4), 40.73 (m, C_1), 38.27 (m, C_7), 32.92 (m, $C_{5\text{ or }6}$), 31.01 (m, $C_{5\text{ or }6}$).

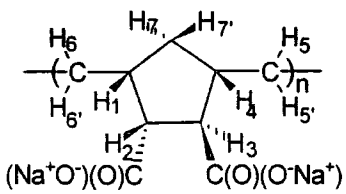

IUPAC assignment of hydrogen atoms within Poly-3F.

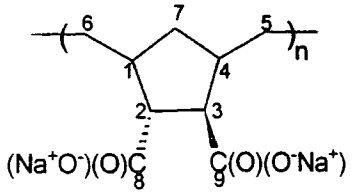

IUPAC assignment of carbon atoms within Poly-3F.

Preparation of poly(*2-endo-3-exo*-bicyclo[2.2.1]hept-5-ene-2,3-dicarboxylic acid dimethyl ester). Mn = 68,600, (Poly-3S')

A solution of initiator 1 (4.8mg, 9.9 x 10^{-6} mol) in benzene (1.5ml) was stirred vigorously in a sample vial (10ml). Monomer 3 (0.497g, 0.0024mol) in benzene (1.5ml) was added quickly via Pasteur pipette to the stirring solution. The reaction proceeded for one hour during which the solution became more viscous and the initial light yellow colouration did not change. The reaction was then quenched with benzaldehyde (2 drops) to give an orange solution and stirred for a further 20 mins. The reaction vessel was removed from the glove box and the polymer precipitated directly into methanol and reprecipitated twice from THF into excess methanol. The product was isolated by centrifugation and decantation and dried *in vacuo* to give a white polymer (0.337g, 68%yield). Mn = 68,600, PDI = 1.02 [see appendix D17]. Found C, 62.59%, H, 6.72% (Calculated for $(C_{10}H_6O_4)_n$: C, 62.85%, H, 6.71%). 68,600. PDI = 1.03. ^{1}H NMR ($CDCl_3$, 400MHz) δ(ppm): 5.32 (3 x bm, 2H, $H_{2,3}$), 3.70 (dm, 6H, $H_{8,9}$), 3.24 (bm, 1H, $H_{2,3}$), 2.96 (bm, 2H, $H_{1,4 \text{ and } 2,3}$), 2.70 (bm, 1H, $H_{1,4}$), 1.96 (bm, 1H, H_7), 1.50 (bm, 1H, $H_{7'}$). ^{13}C NMR ($CDCl_3$, 100MHz) δ(ppm): 174.29 (m, $C_{8,9\ exo}$), 173.22 (m, $C_{8,9\ endo}$), 132.52 (dm, $C_{5,6\ cis\ or\ trans}$), 130.10 (m, $C_{5,6\ cis\ or\ trans}$), 52.51 (m, $C_{1,4\ cis}$), 52.24

(bd, $C_{2,3\ cis\ or\ trans}$), 51.75 (m, $C_{10,11}$), 46.74 (m, $C_{1,4trans}$), 44.54 (m, $C_{2,3\ cis\ or\ trans}$), 39.14 (m, C_7).

Hydrogenation of poly(*2-endo-3-exo*-bicyclo[2.2.1]hept-5-ene-2, dicarboxylic acid dimethyl ester). Mn = 74,500, (Poly-3P')

Poly-1S' (0.30g), *p*-toluene sulphonylhydrazide (3g, 0.016mol) and *p*-xylene (30ml) were placed in a one necked, round bottomed flask (50ml) fitted with a condenser and stirrer bar and then heated, with stirring to 120°C for 4hrs.

The hot solution was added dropwise to vigorously stirring methanol (500ml) in a beaker (600ml) to give a precipitate which was isolated by decantation. The resulting polymer was a colourless, transparent, adhesive solid (0.17g, 56% yield). Mn = 65,500, PDI = 1.04 [see appendix D18]. ^{1}H NMR ($CDCl_3$, 400MHz) δ(ppm): 3.69 (dm, 6H, $H_{8,9}$), 3.18 (bm, 1H, $H_{2,3}$), 2.81 (bm, 1H, $H_{2,3}$), (bm, 1H, $H_{1,4}$), 2.03 (bm, 2H, $H_{1,4\ and\ 5,6}$), 1.63 (bm, 1H, $H_{6',5'}$), 1.39 (bm, 2H, $H_{5,6\ and\ 7}$), 1.11 (bm, 2H, $H_{5,6\ and\ 7'}$). ^{13}C NMR ($CDCl_3$, 100MHz) δ(ppm): 175.41 (s, C_9), 174.55 (m, C_8), 134.52 (s, *p*-xylene, C_1), 128.87 (s, *p*-xylene, C_2), 52.51 (s, C_3), 51.92 (s, $C_{10\ or\ 11}$), 51.49 (s, $C_{10\ or\ 11}$), 50.81 (s, C_2), 43.78 (m, C_4), 42.48 (m, C_1), 38.04 (m, C_7), 33.47 (m, $C_{5\ or\ 6}$), 30.18 (m, $C_{5\ or\ 6}$), 20.82 (s, *p*-xylene, CMe).

Base hydrolysis of poly(*2-endo-3-exo*-1,4-cyclopentenylene-5,6-ethylidene-2,3-dicarboxylic acid dimethyl ester). Mn = ~ 65,500, (Poly-3F')

Poly-3P' (100mg) and NaOH(aq) (1.5ml, 10% w/w) were placed in a one necked, round bottomed flask (6ml) fitted with a condenser and stirrer bar. The suspension was stirred vigorously and heated to reflux for 6hrs after which the

polymer had dissolved. The hot solution was added dropwise to vigorously stirring methanol (15ml) in a beaker (25ml) to give a precipitate which was isolated by centrifugation and decantation. The resulting polymer was a white, powdery solid (0.78g, 78% yield). Mn ~ 65,500. ^{1}H NMR (D_2O, 400MHz) δ(ppm): 2.70 (t, 1H, H_2), 2.30 (t, 1H, H_3), 2.01, 1.90, 1.70 (bm, 4H), 1.37, 1.30, 1.19, 1.03, 0.90, 0.78 (bm, 4H). ^{13}C NMR (D_2O, 100MHz) δ(ppm): 185.25 (s, C_9), 183.17 (m, C_8), 58.17 (s, C_3), 56.00 (s, C_2), 44.76 (m, C_4), 40.72 (m, C_1), 38.25 (m, C_7), 32.90 (m, $C_{5\text{ or }6}$), 30.99 (m, $C_{5\text{ or }6}$).

Preparation of poly(*2-endo-3-exo* -bicyclo[2.2.1]hept-5-ene-2,3-dicarboxylic acid dimethyl ester). Mn = 5,900. EX99. (Poly-3S'')

A solution of initiator 1 (96.2mg, 2 x 10^{-4} mol) in benzene (4ml) was stirred vigorously in a sample vial (20ml). Monomer 3 (0.985g, 0.0047mol) in benzene (3ml) was added quickly via Pasteur pipette to the stirring solution. The initial orange colouration became slightly darker on addition of the monomer to the initiator. The reaction proceeded for one hour during which the solution appeared slightly more viscous. The polymerisation was then quenched with benzaldehyde (7 drops) to give a brown solution and stirred for a further 20 mins. The reaction vessel was removed from the glove box and the polymer precipitated directly into methanol and reprecipitated three times from THF into excess methanol. The product was isolated by centrifugation and decantation and dried *in vacuo* to give a light yellow/green polymer (0.23g, 23%yield). Found C, 63.00%, H, 6.85% (Calculated for $(C_{10}H_6O_4)_n$: C, 62.85%, H, 6.71%). Mn = 4,900, PDI = 1.07 [see appendix D19]. ^{1}H NMR ($CDCl_3$, 400MHz)

δ(ppm): 5.32 (3 x bm, 2H, $H_{2,3}$), 3.70 (dm, 6H, $H_{8,9}$), 3.24 (bm, 1H, $H_{2,3}$), 2.96 (bm, 2H, $H_{1,4 \text{ and } 2,3}$), 2.70 (bm, 1H, $H_{1,4}$), 1.96 (bm, 1H, H_7), 1.50 (bm, 1H, $H_{7'}$). ^{13} C NMR ($CDCl_3$, 100MHz) δ(ppm): 174.19 (m, $C_{8,9\ exo}$), 173.27 (m, $C_{8,9\ endo}$), 132.41 (dm, $C_{5,6 \text{ cis or trans}}$), 130.50 (m, $C_{5,6 \text{ cis or trans}}$), 52.40 (m, $C_{1,4\ cis}$), 52.12 (bd, $C_{2,3\ cis \text{ or } trans}$), 51.65 (m, $C_{10,11}$), 46.63 (m, $C_{1,4trans}$), 44.43 (m, $C_{2,3 \text{ cis or trans}}$), 38.93 (m, C_7).

Hydrogenation of poly(*2-endo-3-exo*-bicyclo[2.2.1]hept-5-ene-2, dicarboxylic acid dimethyl ester). Mn = 5,900, (Poly-3P'')

Poly-3S''(0.10g), *p*-toluene sulphonylhydrazide (1g, 0.005mol) and *p*-xylene (8ml) were placed in a one necked, round bottomed flask (10ml) fitted with a condenser and stirrer bar and then heated, with stirring to 120°C for 1hr. The hot solution was added dropwise to vigorously stirring methanol (80ml) in a beaker (100ml) to give a precipitate which was isolated by centrifugation and decantation. The resulting polymer was a colourless, transparent, adhesive solid (0.04g, 40% yield). Mn = 5,900, PDI = 1.08 [see appendix D20].

Base hydrolysis of poly(*2-endo-3-exo*-1,4-cyclopentenylene-5,6-ethylidene-2,3-dicarboxylic acid dimethyl ester). Mn = ~ 5,900, (Poly-3F'').

Poly-3P'' (0.04mg) and NaOH(aq) (0.5ml, 10% w/w) were placed in a one necked, round bottomed flask (10ml) fitted with a condenser and stirrer bar. The suspension was stirred vigorously and heated to reflux for 4hrs after which time the polymer had dissolved. The hot solution was added dropwise to vigorously stirring methanol (5ml), in a beaker (25ml), to give a precipitate which was isolated by centrifugation and decantation. The resulting polymer was a white, powdery solid (0.030g, 75% yield).

4.4. REFERENCES FOR CHAPTER 4

[1] Castner, K.F. and Calderon, N., *J.Mol.Catal.*, **15**, 47-59, 1982.

[2] Craig, D., *J.Am.Chem.Soc.*, **73**, 4889, 1951.

[3] Gastel, F.J.C., Klunder, A.J.H. and Zwanenburg, B., *J. Trav. Chim.Pays-Bas,* **110,** 175-184, 1991.

[4] Berning, W., Hunig, S., Prokschy, F., *Chem. Ber.,* **117**, 1455-1464, 1984.

[5] Bazan, G.C., Schrock, R.R., Cho, H.N. and Gibson, V.C., *Macromolecules*, **24**, 4495-4502, 1991.

[6] O' Dell, R., McConville D.H., Hofmeister, G.,E. and Schrock, R.R., *J.Am.Chem.Soc.,* **116**, no.8, 3414-3423, 1994.

[7] Sohn, B.H., Gratt, J.A., Lee, J.K. and Cohen R.E., *J.Appl.Poly.Sci.,* **58**, 1041-1046, 1995.

[8] "Olefin Metethesis and Metathesis Polymerisation", Ivin K.J. and Mol J. C., Academic Press, London and California, 1997.

[9] Canonne, P., Belanger D. and Lemay G., *J.Org.Chem.*, **47**, 3953-3959, 1982.

CHAPTER 5

Crystallisation of Calcium Carbonate in the Presence of Functionalised Polymers

5.1 INTRODUCTION

The synthesis and characterisation of all polymers used in the crystallisation experiments described in this chapter have been discussed in Chapter 4. Polymers Poly1F^x and Poly3F^x, containing monomer units in which the carboxylate functional groups are *exo,exo* and *exo,endo* respectively have been used. The structures of these polymers can be seen in Chapter 4 and on the bookmark. The polymers Poly2F^x, containing repeat units in which the carboxylate functional groups are *endo,endo* were not synthesised. This was due to the fact that the severe hydrolysis conditions necessary for synthesis of the sodium salt of the polymer led to the isomerisation of the less thermodynamically stable *endo,endo* isomer to the *exo,endo* form.

5.2 MATERIALS AND METHODS

Calcium carbonate was purchased from Aldrich Ltd and the source and quality of the reactants used in monomer synthesis is given in the experimental section of Chapter 4. All other chemicals and solvents were purchased from Aldrich Ltd also and used as supplied unless otherwise stated, the water used was doubly distilled and deionised (conductivity < 0.06μS) using Elga UHQ apparatus. The procedure used for washing glassware and the preparation of supersaturated solutions of $Ca(HCO_3)_2$ ($[Ca^{2+}] \sim 10$ mol dm^{-3}, pH 5.8-6.0, temp. 293K) were carried out as described in Chapter 3 (pp 63-64).

The supersaturated solution was placed in crystallisation dishes (100ml aliquots), each labelled and containing three microscope coverslips (13mm dia.). To each dish a solution (1ml, 0.1ml or 0.01ml) of the polymer in water, 0.1M with respect

to repeat unit, was added *ie.* 23mg/ml for each polymer. This gave $[Ca^{2+}]$: [repeat unit] molar values of 10:1, 100:1 and 1000:1 respectively. Three control dishes, containing no polymer, were used in each experiment for comparison. The dishes were placed in a plastic tray filled to a height of approximately 1cm with water, in order to stabilise the temperature (19°C), and covered loosely with plasticiser free cling film. After 12hrs crystals had formed at the surface of the solution, these were collected on a glass microscope coverslip (13mm dia.). A few crystals were found at the bottom of the crystallising dishes, these tended to appear more slowly than those at the surface and were collected after 2 days. The base crystals were collected using the procedure described in Chapter 3 (p 64). Crystals were examined initially by optical microscopy using a Zeiss Axiophot Optical Microscope with a par focalised M80 camera system. Mounting the coverslips on microscope slides allowed examination of both base and surface crystals. Scanning Electron Microscopy was used for more detailed morphological examinations. The microscope coverslips with crystals were attached to microscope stubbs by carbon discs (*ca.* 8mm dia.) with adhesive on both faces and in certain cases were gold sputtered in order to reduce charging effects. The SEM had a field emission electron gun and possible accelerating voltages ranging from 500V - 20kV. The accelerating voltage used in these studies was approximately 1kV.

Polymorph determination of air dried surface and bulk grown crystals was carried out using IR spectroscopy as KBr discs or X-Ray powder diffraction by comparison of the d spacings with standard values from Joint Committee on Powder Diffraction Standards (JCPDS) tables; see JCPDS (1974) table numbers:

for calcite, 24-27A; for vaterite; 24-30A. The nucleation densities, mean sizes and standard distribution values of the crystals were measured with the aid of Imagen 2 data analysis software. The longest axes of the crystals were measured. All molecular modelling was carried out using Cerius© (copyright of MSI) 2 version 3.0 software using a universal forcefield.

5.3 RESULTS AND DISCUSSION

5.3.1 Control System

Crystals were collected from both the air/water interface and the base of the dishes. Virtually all crystals observed were rhombohedral with six smooth well defined {1 0 4} faces. For molecular modelling data on the structure of calcite rhombs and {1 0 4} face see appendices F4 and F5. XRD studies confirmed the polymorph to be calcite. The crystals collected at the air/water interface were mainly intergrown and dendritic whereas those collected at the base were much more individually grown. Crystal sizes ranged from 20-80μm with a mean size of 36.6 μm and standard deviation of ±14μm. The large size distribution indicated that crystal growth was episodic. Some rhombohedra were truncated along non specific planes. For examples of optical micrographs and scanning electron micrographs of these crystals see Ch 3 (pp 67-68).

5.3.2 Effect of Poly3F''

The influence of Poly3F'' (*exo,endo* monomer units, Mn ~ 6,000) on the crystallisation of $CaCO_3$ at a $[Ca^{2+}]$: [repeat unit] molar ratio of 10:1 was studied. Discrete, individual crystals were identified at the surface suggesting independent

nucleation had occurred. Crystals were also of a uniform size with a mean value of 39μm and standard deviation ± 8μm, this value is significantly lower than that of the control crystals. The relatively small crystal size distribution indicates that a reasonably controlled, fairly synchronous series of nucleation events had occurred. These features are different to the control and indicate that the added polymer influences the surface crystal growth. This is consistent with a surface active polymer and we might expect that a polycarboxylate might form an insoluble surface "skin" over an aqueous calcium salt solution.

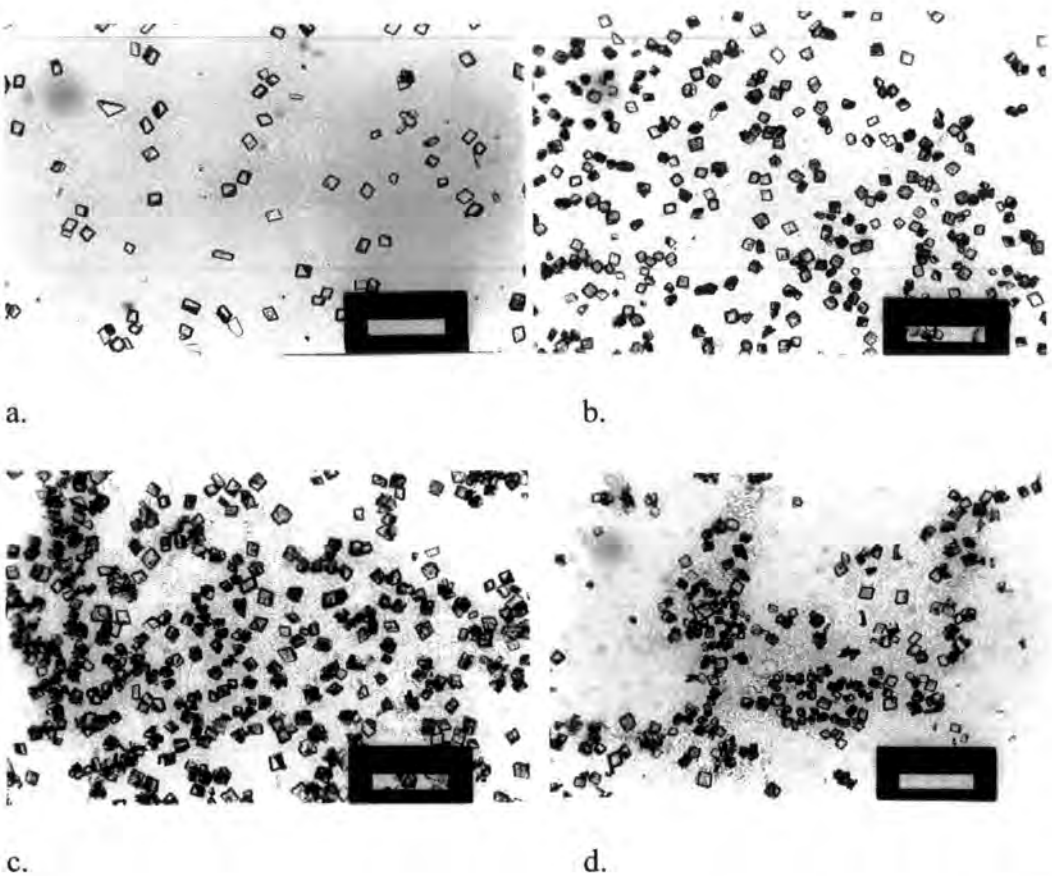

a. b.

c. d.

Fig. 5.3.1. Optical micrographs showing crystals of $CaCO_3$ grown at the air/polymer, water interface $[Ca^{2+}]$:[repeat units] molar ratios 10:1. a. Poly3F'' additive b. Poly3F' additive c. Poly3F additive d. Poly1F' additive. Scale bars = 200μm

The presence of such a film was confirmed by observation using optical microscopy and scanning electron microscopy [Figs. 5.3.1.]. This thin film was much easier to see in the raw sample than in the images reproduced in Fig. 5.3.1. Crystals grown at the air/water interface had a distinctive novel face with no symmetry related equivalent in the remainder of the crystal. This observation is consistent with the hypothesis that crystal nucleation occurred under a polymer film at the air/water interface and that this process generates the observed distinctive novel face. The new face was defined by the truncation of three of the {1 0 4} faces at angles of 45°, 50° and 85°. No modification of these symmetry related faces was seen, this was consistent with oriented nucleation of the crystal by the polymer film.

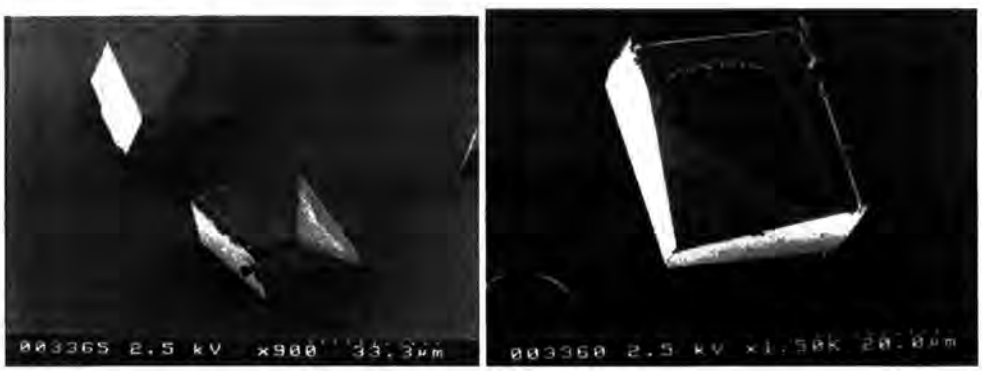

Fig. 5.3.2. Scanning electron micrographs showing $CaCO_3$ crystals grown at the air, polymer/water interface with Poly3F'' $[Ca^{2+}]$:[repeat unit] molar ratio 10:1.

5.3.3 Effect of Poly3F'

The influence of Poly3F' (*exo,endo* monomer units, Mn ~70,000) on the crystallisation of $CaCO_3$ at $[Ca^{2+}]$: [repeat unit] molar ratios of 10:1, 100:1 and 1000:1 was observed in the same manner. The crystals were again uniform in

size with mean size of 29μm and standard deviation of ±6μm, which again shows a significantly smaller distribution of crystal sizes than seen in the control. The nucleation density of these crystals at the highest concentration of the polymer, was larger than observed for the lower Mn polymer at the same concentration at 236 crystals/mm^2 compared to Poly 3F'' at 76 crystals/mm^2 polymer [Fig. 5.3.1. compare a and b]. The effect upon the morphology of the crystals was the same at each concentration but less modification occurred at lower concentrations of polymer. As with Poly3F'', a novel face was present, with no symmetry related equivalent in these surface grown modified rhombohedral crystals. Again, no truncation of the symmetry related faces was seen, this was consistent with the induction of crystal growth by the polymer film. The crystal surfaces which had been in contact with the polymer during growth were roughened. SEM studies showed this to be due to contamination of the crystal faces with excess polymer.

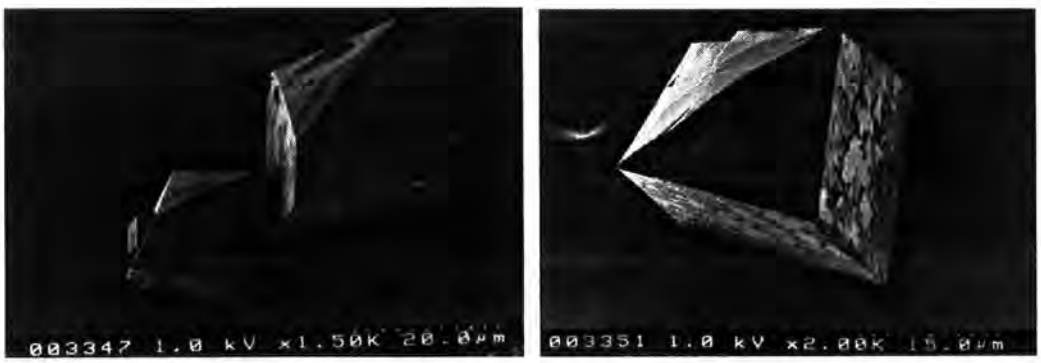

Fig. 5.3.3. Scanning electron micrographs showing $CaCO_3$ crystals grown at the air, polymer/water interface with Poly3F' [Ca^{2+}]:[repeat unit] 10:1.

5.3.4 Effect of Poly 3F

The influence of Poly3F (*exo,endo* monomer units, Mn = 147,000) on the crystallisation of $CaCO_3$ at $[Ca^{2+}]$: [repeat unit] molar ratios of 10:1, 100:1 and 1000:1 was observed. The nucleation density was larger than observed with the lower molecular weight polymers at 336 crystals/mm^2 compared to 236 for Poly 3F' crystals/mm^2 and 76 crystals/mm^2 for the polymer with lowest Mn Poly3F'' [Fig.5.3.1]. The same type of modification was observed at each concentration although the extent of modification was greater in the presence of the higher molecular weight polymer. A non-symmetry equivalent, trapezoidal truncation was seen to bisect the rhombic {1 0 4} faces of the crystal at 101°. A distinctive feature of this novel face was a slight central elevation and some degree of surface roughening [see Fig. 5.3.4.]

Fig. 5.3.4. Scanning electron micrographs showing $CaCO_3$ crystals grown at the air,polymer/water interface with Poly3F $[Ca^{2+}]$:[repeat unit] 10:1.

5.3.5 Effect of Poly 1F'

On studying the effect of Poly1F' (*exo,exo* monomer units, Mn 50K) on the crystallisation of $CaCO_3$ at $[Ca^{2+}]$: [repeat unit] molar ratios of 10:1 the

following effects were observed. The nucleation density of crystals grown at the air/water interface was 108 crystals/mm^2 with mean crystal size of 30μm along the longest axis and standard deviation ±7μm. As in the case of the polymers with *exo,endo* repeat units (Poly3F'') the small size distribution indicates that controlled, synchronous nucleation had occurred. The polymer film could be seen by both optical and scanning electron microscopy [Figs. 5.3.1, 5.3.5]. The modification of the crystals appeared to be the same as observed using Poly3F'' and Poly3F' as additive only the crystals had generally rougher surfaces.

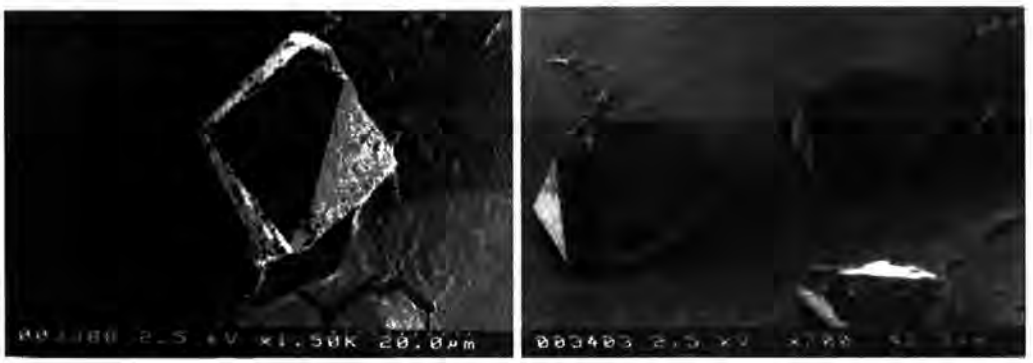

Fig. 5.3.5. Scanning electron micrographs showing $CaCO_3$ crystals grown at the air,polymer/water interface with Poly1F' [Ca^{2+}]:[repeat unit] 10:1.

5.3.5 Determination of Polymer Modified Crystal Faces

SEM studies allowed assignment of the polymer modified faces. Angles between the truncated faces of the calcite crystals and the {1 0 4} faces were measured from micrographs. As the angles between crystal faces are representative of the face, the information obtained was used to assign the faces. The truncated faces of crystals grown in the presence of Poly3F'', Poly3F' and Poly1F' appeared to be the same. From the measurement of angles between the

truncated triangular faces and {1 0 4} faces and comparison with the theoretical interfacial angles of calcite it was determined that the faces were of the type (1 0 ℓ) where ℓ = -1, -2 or -3 [Fig. 5.3.6 and Fig. 5.3.7]. On the basis of previous studies of oriented crystal growth under defined polymeric surfaces this suggests oriented nucleation in the <1 0 w> where w = 1,2 or 3.

a. b.

Fig. 5.3.6. A diagrammatic representation of modified calcite rhombs showing truncated (1 0 -ℓ) faces in grey and relevant angles a) $CaCO_3$ crystal, modified by poly3F'', see Fig. 5.3.2. b) $CaCO_3$ crystal, modified by poly3F', see Fig. 5.3.3.

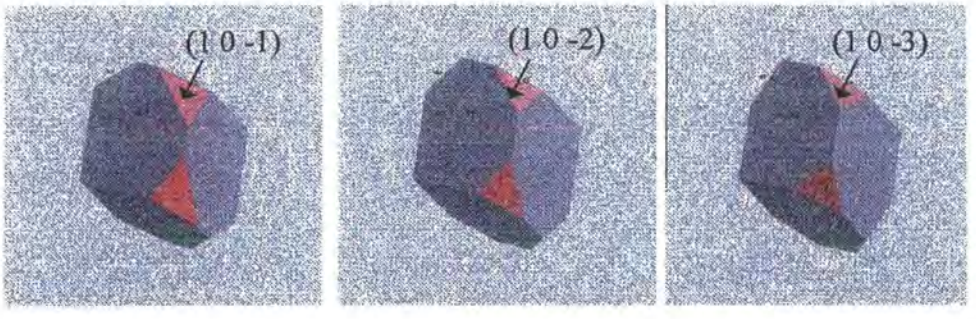

a. b. c.

Fig. 5.3.7. Theoretical calcite crystals with preferential expression of {1 0 ℓ}. a. ℓ = -1 b. ℓ = -2 c. ℓ = -3

The modification due to poly3F (*exo,endo* monomer units, 200K) was unlike that of the lower molecular weight polymers. In this case the rectangular, elevated face appeared to be of the type {1 1 1} based upon the same calculations used above [Fig. 5.3.8].

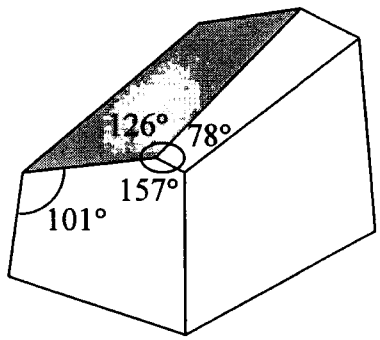

Fig.5.3.8. A diagrammatic representation of a typical calcite rhomb, modified by poly3F, showing the truncated (1 1 1) face in grey and relevant angles, see Fig. 5.3.4.

It has already been determined, from studies of the effect of the monomers on $CaCO_3$ crystal growth that the geometric matching of the 4 Angstrom distance between the carboxylate oxygens of the monomers and the same distance between Ca^{2+} ions in the (1 0 -2) and (-1 0 2) faces of the calcite lattice leads to preferential expression of these faces. It is not surprising that the polymers, which are constructed from these monomer units, in general, seem to interact with the same type of crystal faces. It is noticeable that the polymer containing *exo,endo* monomer units appear to modify the calcite crystals to a greater extent

flexibility around the carboxylate groups when the monomer has been ring opened. This gives a greater possibility of the functional groups being able to adopt a desirable geometric and stereochemical configuration for interaction with the Ca^{2+} ions in the crystal face *i.e.* oxygen-oxygen distances of 4 Angstroms and approximately parallel carbonate groups. The favoured stereochemistry of the carbonate groups can be achieved by treating two adjacent carboxylate groups from adjacent repeat units as the reactive motif [Fig. 5.3.9].

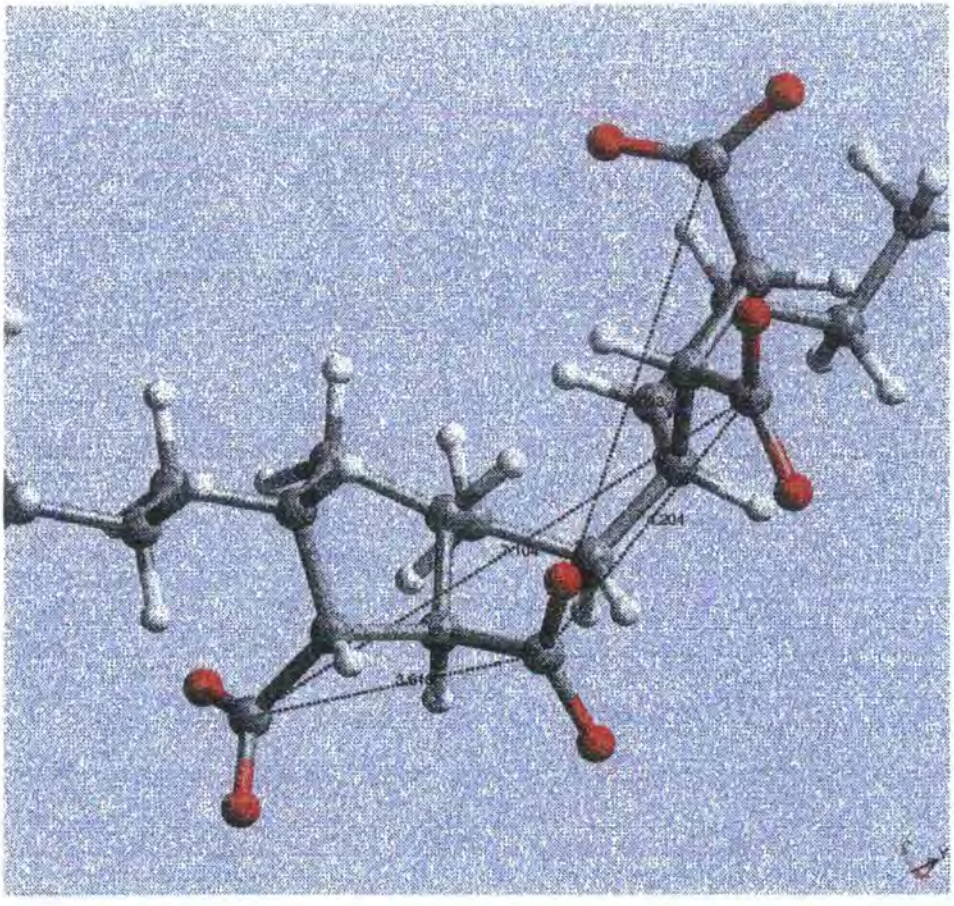

Fig. 3.3.9. A molecular model of a section of Poly3F^x (*exo,endo* monomers) showing a possible 4.2 angstrom distance between oxygen ions in adjacent carboxylate groups from different repeat units, notice the possible parallel relationship between the functional groups.

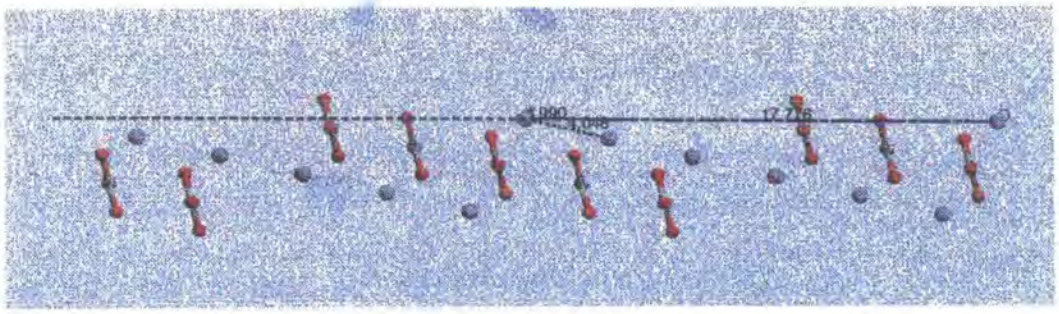

a.

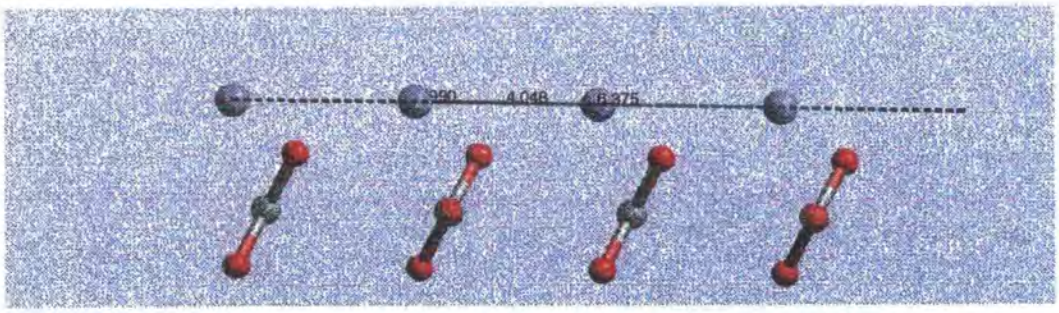

b.

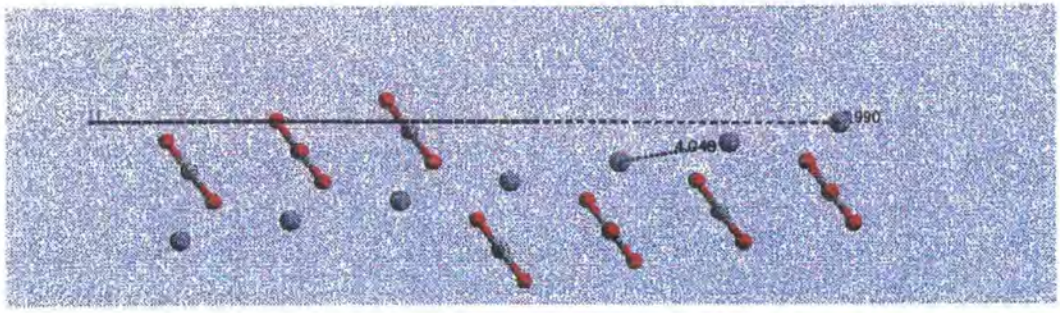

c.

Fig. 5.3.10. Molecular models of calcite faces; a. (1 0 -1) b. (1 0 -2)

c. (1 0 3)

Poly3F did not show modification of calcite as discussed above, in this case, the (1 1 1) face seemed to be preferentially expressed. This face has a lower density of ions than the (1 0 -*l*) set faces. [Fig. 5.3.10 a, b and c and Fig 5.3.11].

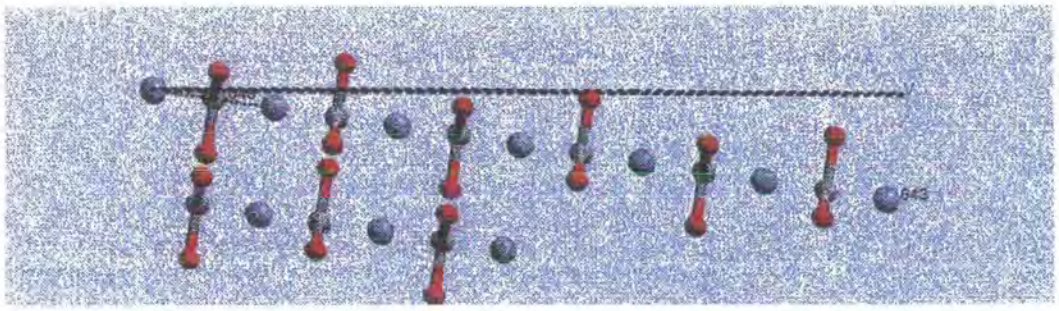

Fig. 5.3.11. A molecular model of (1 1 1).

5.4 GENERAL COMMENTS

All polymers used as additive in the crystallisation of $CaCO_3$ from the supersaturated solutions of $Ca(HCO_3)_2$ formed films at the air/water interface. These polymer films induced the nucleation and controlled the morphology of the $CaCO_3$ crystals grown beneath the film. Poly3F'' (*exo,endo* monomer units, Mn ~ 6,000), Poly3F' (*exo,endo* monomer units, Mn ~70,000) and Poly1F' (*exo,exo* monomer units, Mn 50K), at $[Ca^{2+}]$:[repeat unit], 100:1 and 10:1 led to the preferential expression of a single, triangular face of type (1 0 -*l*) with no symmetry related equivalents. Poly3F (*exo,endo* monomer units, Mn = 147,000) at the same concentrations led crystals with a single trapezoidal truncation, in this case the face was found to be (1 1 1). The fact that no symmetry related equivalent faces were observed indicates that the crystals grew from the polymer film with the truncated faces being in direct contact with the film at nucleation. The size distributions of the crystals grown in contact with the polymers were smaller than in the control experiments indicating that the polymers had controlled the nucleation of the $CaCO_3$.

CHAPTER 6

Conclusions and Proposals for Future Work

6.1 INTRODUCTION

The first steps towards the long term objective of building entirely synthetic organic/inorganic composite materials have been carried out in a biomimetic manner. Crystals of $CaCO_3$ with controlled morphology and size have been grown from aqueous, supersaturated solutions of $Ca(HCO_3)_2$ at the air/water interface, beneath carboxylate polymer films.

6.2 CONCLUSIONS

All of the dicarboxylic acid model compound and dimethyl ester monomer syntheses described in Chapters 2 and 4 were carried out successfully as indicated by the characterisation of the product. Polymers Poly1F^x and Poly3F^x, containing monomer units in which the carboxylate functional groups were *exo,exo* and *exo,endo* were synthesised successfully. The polymers Poly2F^x, containing repeat units in which the carboxylate functional groups are *endo,endo* were not synthesised. This was due to the fact that the severe hydrolysis conditions necessary for synthesis of the sodium salt of the polymer led to the isomerisation of the less thermodynamically stable *endo,endo* isomer to the *exo,endo* form.

The work described in Chapter 3 showed that the dicarboxylic acid model compounds used as additives controlled the morphology of calcite crystals grown from supersaturated solutions of $Ca(HCO_3)_2$ at a large range of concentrations, $[Ca^{2+}]$: [monomer] 10 -1000:1. The polymers of these monomers also controlled crystal growth and appeared to give the same type of crystal morphology as the repeat units (see Chapter 5), however, modification was only observed on one

face of the $CaCO_3$ crystals. This observation and the relatively small crystal size distributions indicate that the calcite crystallisation was nucleated beneath the polymer films at the truncated modified face and growth continued down into the solution.

6.3 PROPOSALS FOR FUTURE WORK

When 7-oxabicyclo[2.2.1]hept-5-ene was used as an additive in the crystallisation of $CaCO_3$ from supersaturated solutions of $Ca(HCO_3)_2$ the resulting calcite crystals were highly modified resulting in cylindrical shaped crystals. One possibility for future work would be to polymerise this monomer, in a way that allows full removal of the initiator used, perhaps by the use of the water tolerant initiator, $RuCl_2(PCy_3)_2(=CHPh)$ in an emulsion polymerisation. Then to use these polymers as additives in the crystallisation of $CaCO_3$.

To obtain further information upon how the polymers discussed in this thesis effect the crystallisation of $CaCO_3$, larger crystals of $CaCO_3$ could be grown in the presence of the polymers by the controlled diffusion of $(NH_4)_2CO_{3(g)}$ into solutions of $CaCl_2$ and polymer additive.

Although the polymers discussed in this thesis had considerable control on the crystallisation of $CaCO_3$, due to the high cost of initiator and the fact that the techniques used for polymer synthesis were time consuming and required great care in handling, it would be preferable to find cheaper, synthetically more accessible polymers which have the same level of control on $CaCO_3$ crystallisation as those already used.

The next stage in the strive towards an organic/inorganic biomimetic composite is to effectively "build" layers of polymer with attached crystals into a 3D structure. This could perhaps be achieved by the use of block co-polymers which could provide alternating sections of water soluble and water insoluble polymer allowing crystal growth from aqueous solutions only within the water soluble domains of the polymers. Removal of the solvent could then lead to organic/inorganic composites with alternating layers of water soluble polymer and inorganic crystals embedded between areas of hydrophobic polymer.

APPENDIX A

^{1}H NMR SPECTRA

Appendix A1 : ^{1}H NMR spectrum of *exo*-bicyclo[2.2.1]hept-5-ene-2,3-dicarboxy anhydride.
Recorded at 400MHz in d_6-acetone.

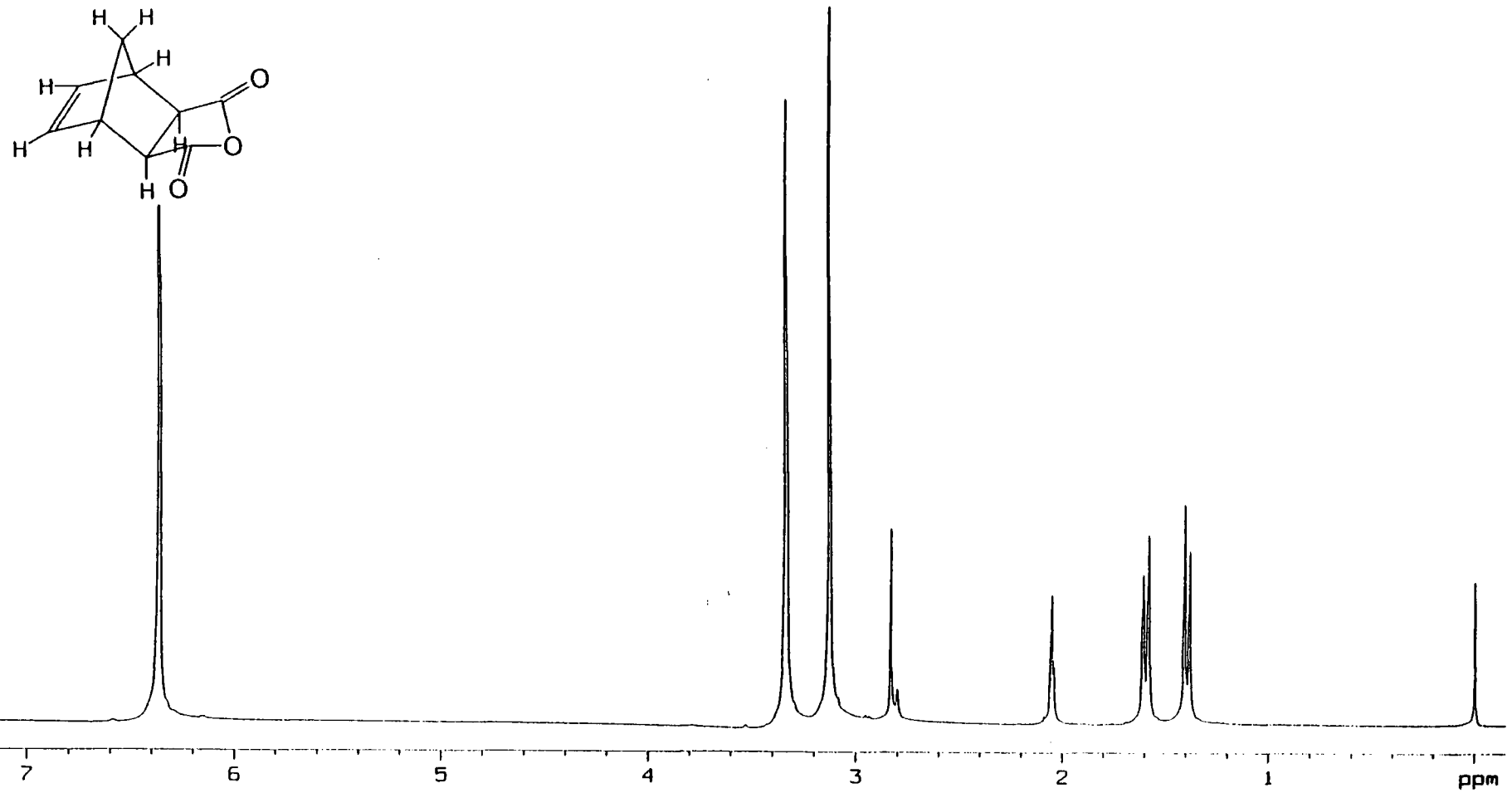

Appendix A2 : ^{1}H NMR spectrum of *exo,exo*-bicyclo[2.2.1]hept-5-ene-2,3-dicarboxylic acid.
Recorded at 400MHz in d_6-acetone.

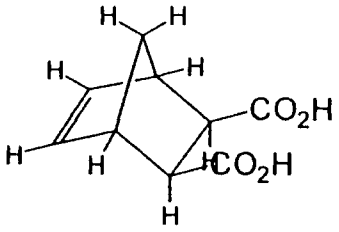

Appendix A3 : ^{1}H NMR spectrum of *exo,exo*-bicyclo[2.2.1]heptane-2,3-dicarboxylic acid.
Recorded at 400MHz in d_6-acetone.

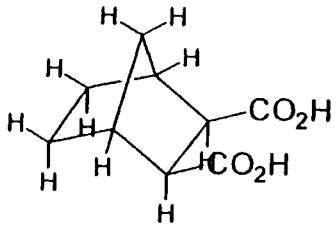

Appendix A4 : ^{1}H NMR spectrum of *endo*-bicyclo[2.2.1]hept-5-ene-2,3-dicarboxy anhydride.
Recorded at 400MHz in d_6-acetone.

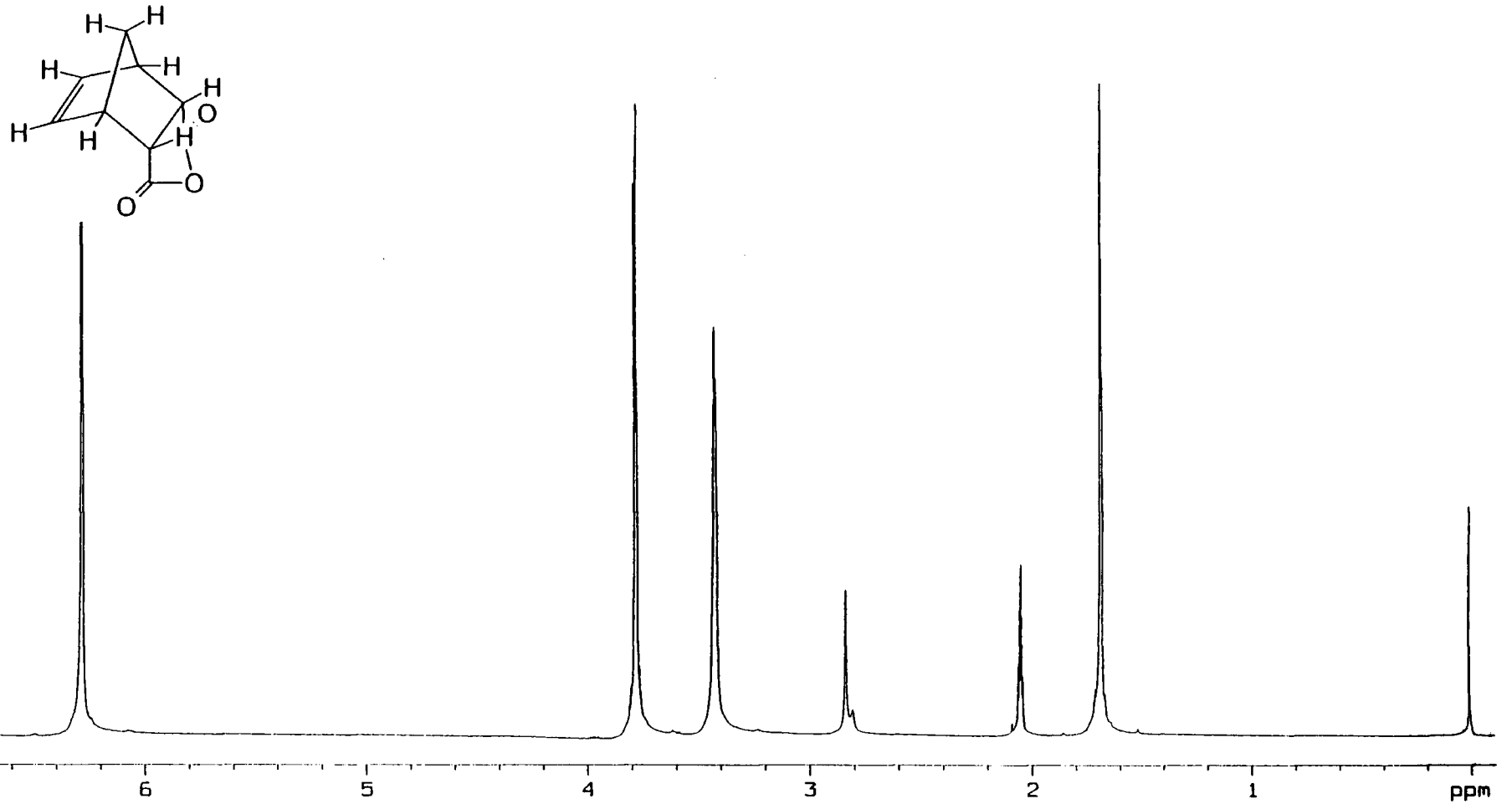

Appendix A5 : ^{1}H NMR spectrum of *endo,endo*-bicyclo[2.2.1]heptane-2,3-dicarboxylic acid.
Recorded at 400MHz in d_6-acetone.

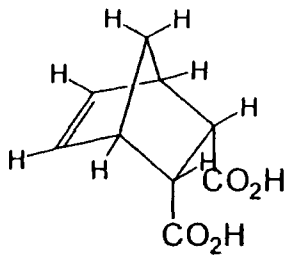

Appendix A6 : ^{1}H NMR spectrum of *endo,endo*-bicyclo[2.2.1]heptane-2,3-dicarboxylic acid.
Recorded at 400MHz in d_6-acetone.

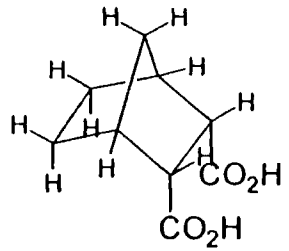

Appendix A7 : ^{1}H NMR spectrum of 2-*endo*-3-*exo*-bicyclo[2.2.1]hept-5-ene-2,3-dicarboxylic acid.
Recorded at 400MHz in d_6-acetone.

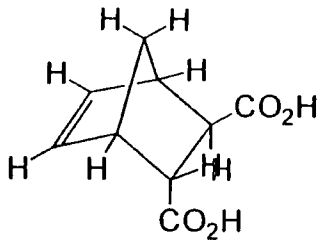

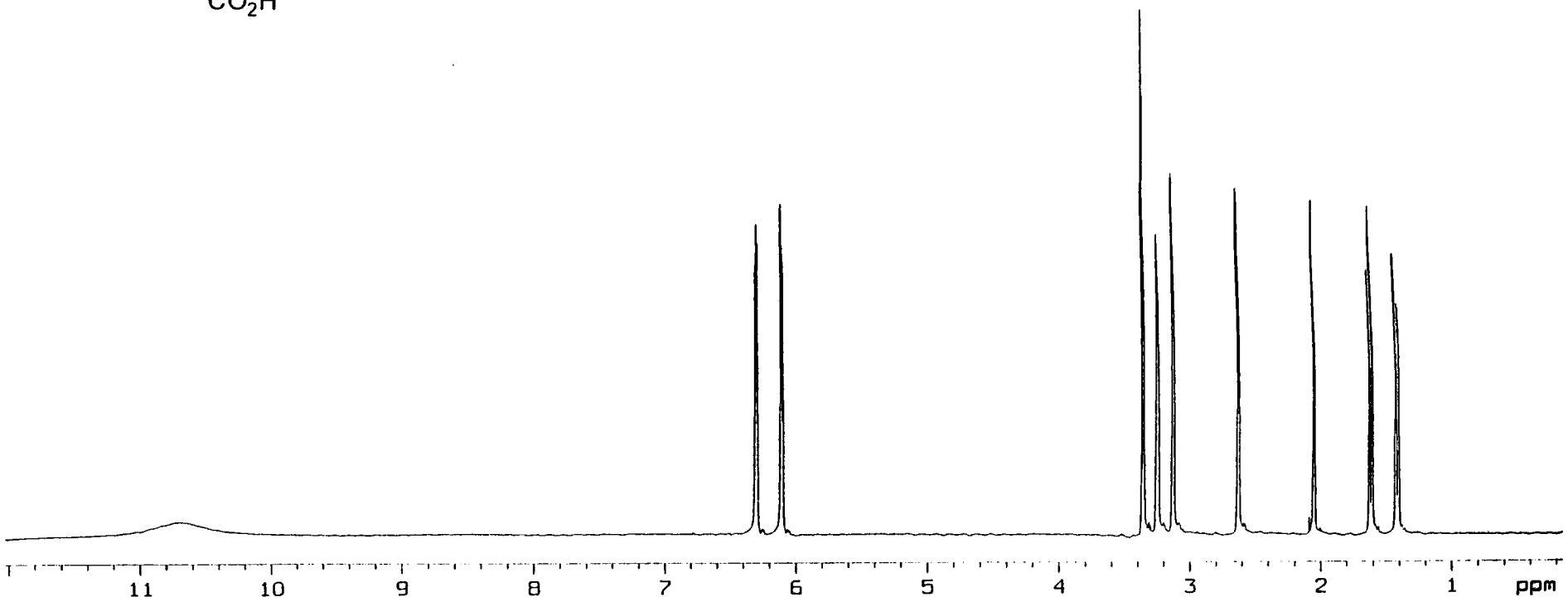

Appendix A8 : ^{1}H NMR spectrum of 2-*endo*-3-*exo*-bicyclo[2.2.1]heptane-2,3-dicarboxylic acid.
Recorded at 400MHz in d_6-acetone.

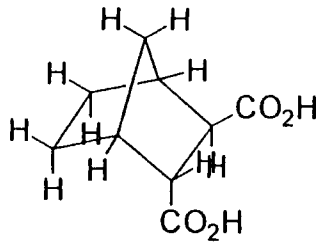

Appendix A9 : ^{1}H NMR spectrum of *exo*-7-oxabicyclo[2.2.1]hept-5-ene-2,3-dicarboxy anhydride.
Recorded at 400MHz in d_6-acetone.

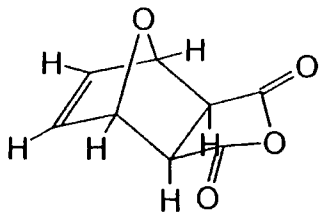

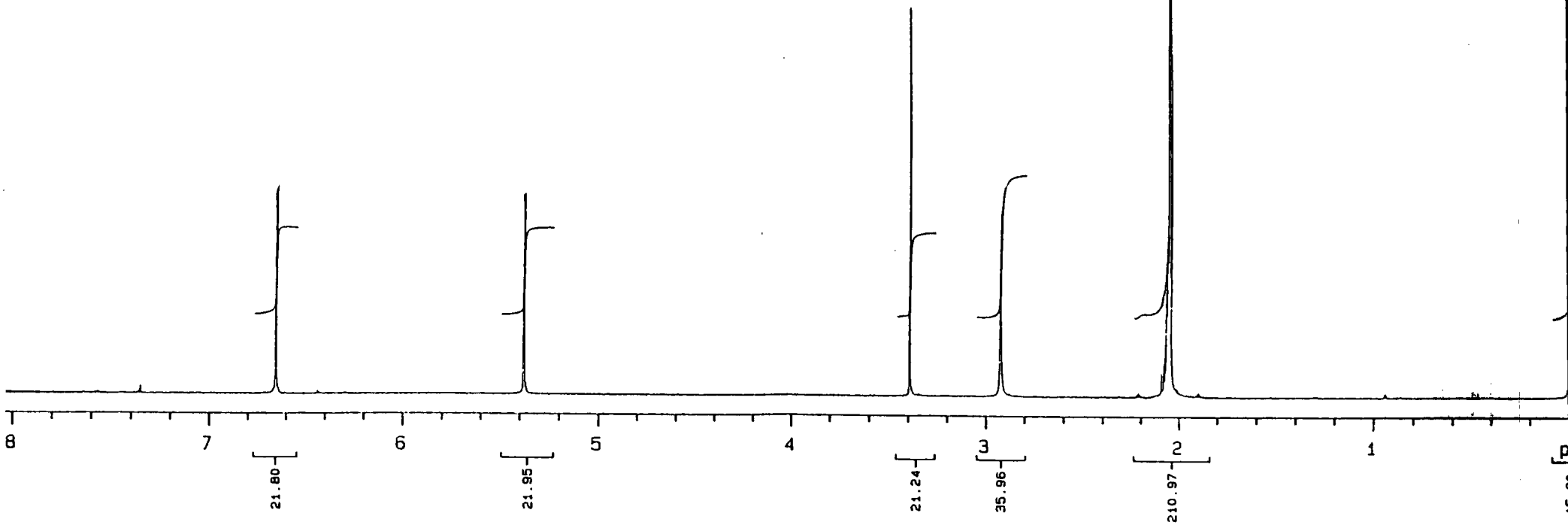

Appendix A10: ^{1}H NMR spectrum of *exo,exo*-7-oxabicyclo-[2.2.1]hept-5-ene-2,3-bis(carboxylic acid).
Recorded at 400MHz in D_2O.

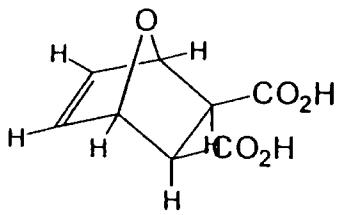

Appendix A11: ^{1}H NMR spectrum of *exo,exo*-7-oxabicyclo-[2.2.1]heptane-2,3-bis(carboxylic acid).
Recorded at 400MHz in d_6-acetone.

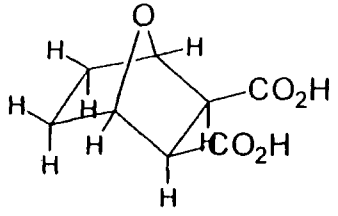

Appendix A12: ^{1}H NMR spectrum of *exo,exo*-bicyclo[2.2.1]hept-5-ene-2,3-dicarboxylic acid dimethyl ester. (monomer 1)
Recorded at 400MHz in d_6-acetone.

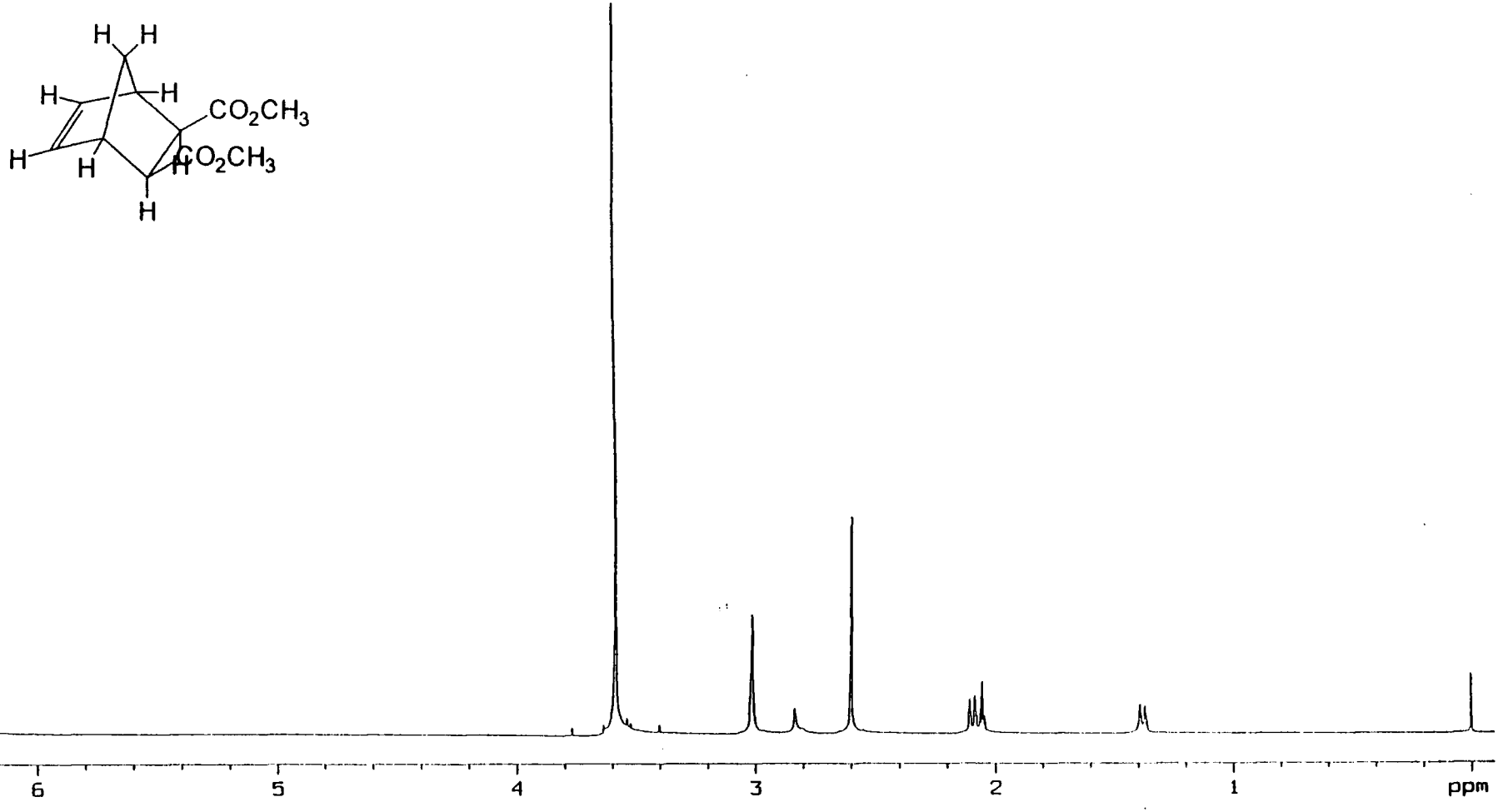

Appendix A13: ^{1}H NMR spectrum of *endo,endo*-bicyclo[2.2.1]hept-5-ene-2,3 dicarboxylic acid dimethyl ester. (monomer 2)
Recorded at 400MHz in d_6-acetone.

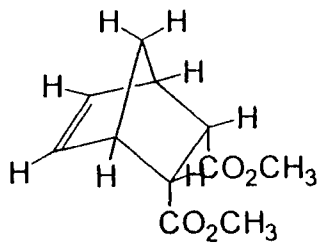

Appendix A14: ^{1}H NMR spectrum of 2-*endo*-3-*exo*-bicyclo[2.2.1]hept-5-ene-2,3-dicarboxylic acid dimethyl ester. (monomer 3).
Recorded at 400MHz in d_6-acetone.

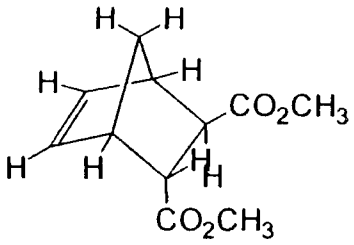

Appendix A15: ^{1}H NMR spectrum of poly(*exo,exo*-bicyclo[2.2.1]hept-5-ene-2,3-dicarboxylic acid dimethyl ester). (Poly-1S)
Recorded at 400MHz in $CDCl_3$.

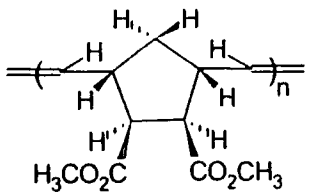

Appendix A16: [1]H NMR spectrum of hydrogenated poly(*exo,exo*-bicyclo [2.2.1]hept-5-ene-2,3-dicarboxylic acid dimethyl ester). (Poly-1P) Recorded at 400MHz in $CDCl_3$.

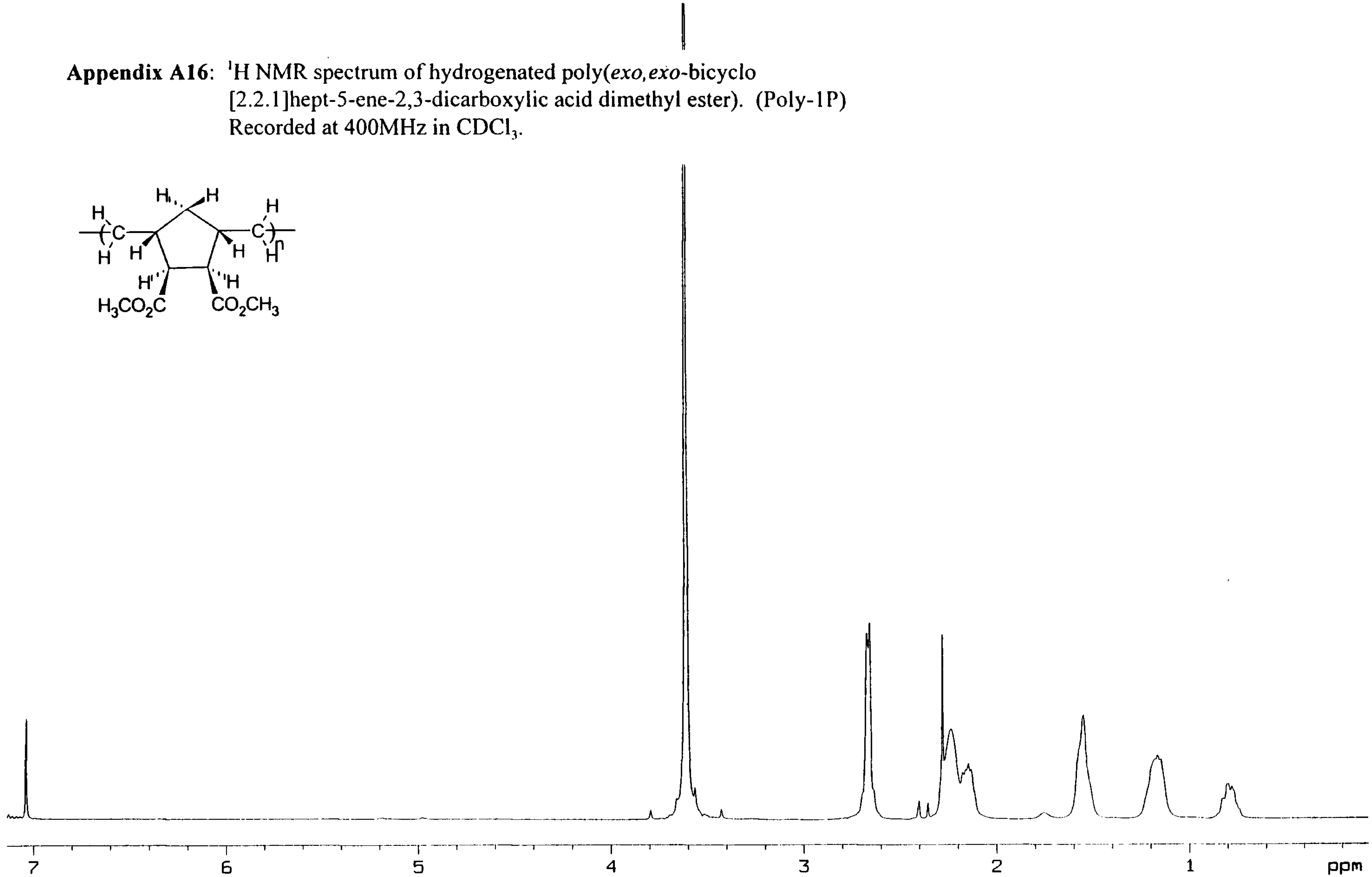

Appendix A17: ^{1}H NMR spectrum of hydrogenated, hydrolysed poly(*exo,exo*-bicyclo [2.2.1]hept-5-ene-2,3-dicarboxylic acid dimethyl ester). (Poly-1F) Recorded at 400MHz in D_2O.

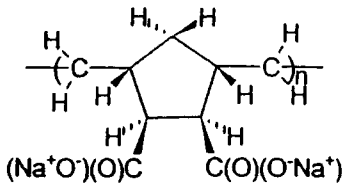

Appendix A18: ^{1}H NMR spectrum of poly(*endo,endo*-bicyclo[2.2.1]hept-5-ene-2,3-dicarboxylic acid dimethyl ester). (Poly-2S)
Recorded at 400MHz in $CDCl_3$.

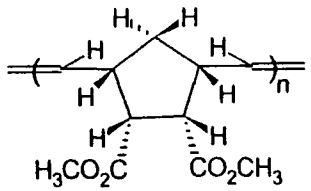

Appendix A19: ^{1}H NMR spectrum of hydrogenated poly(*endo,endo*-bicyclo [2.2.1]hept-5-ene-2,3-dicarboxylic acid dimethyl ester). (Poly-2P) Recorded at 400MHz in $CDCl_3$.

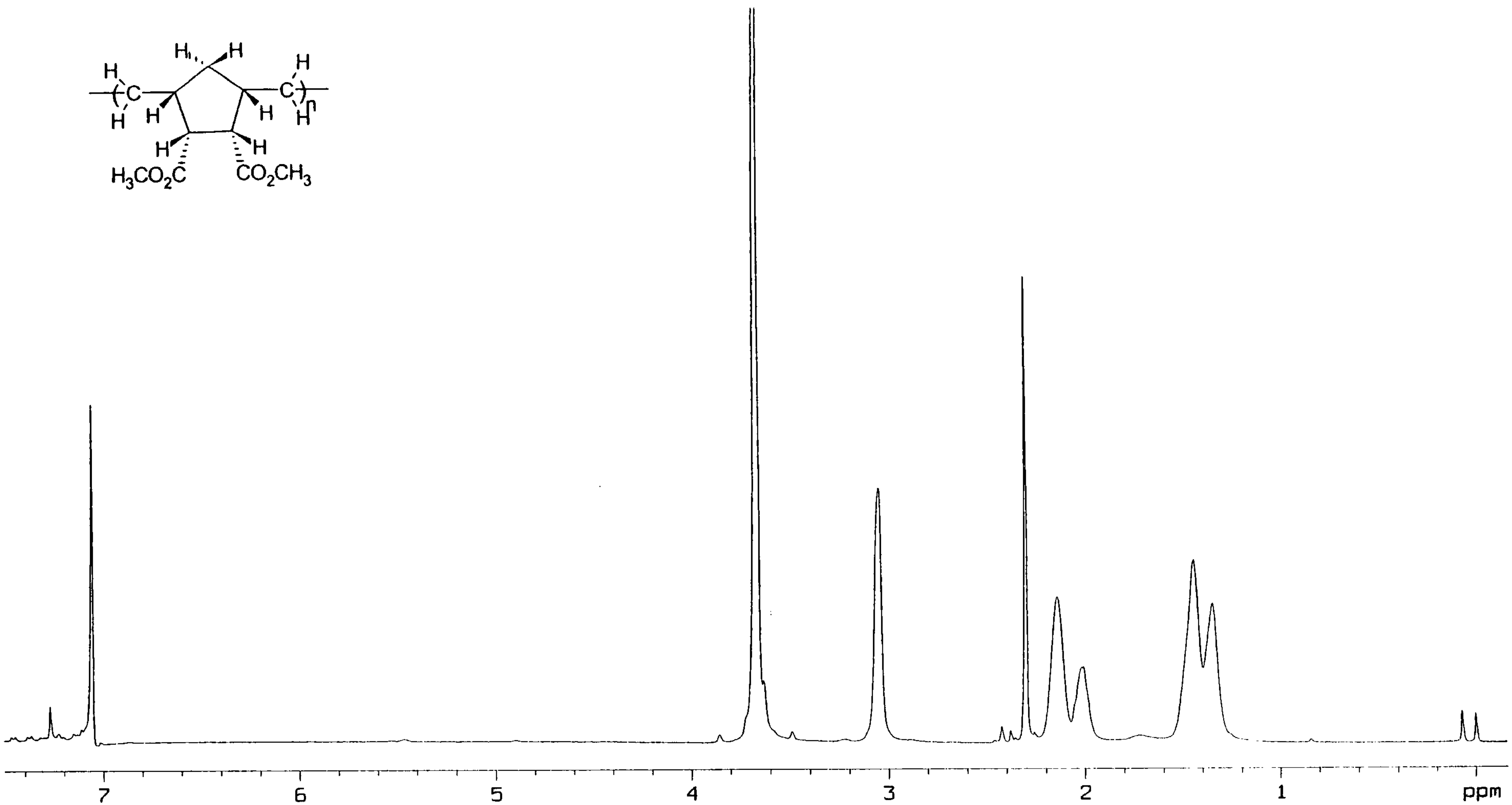

Appendix A20: ^{1}H NMR spectrum of hydrogenated, hydrolysed poly(*endo,endo*-bicyclo [2.2.1]hept-5-ene-2,3-dicarboxylic acid dimethyl ester). (Poly-2F) Recorded at 400MHz in D_2O.

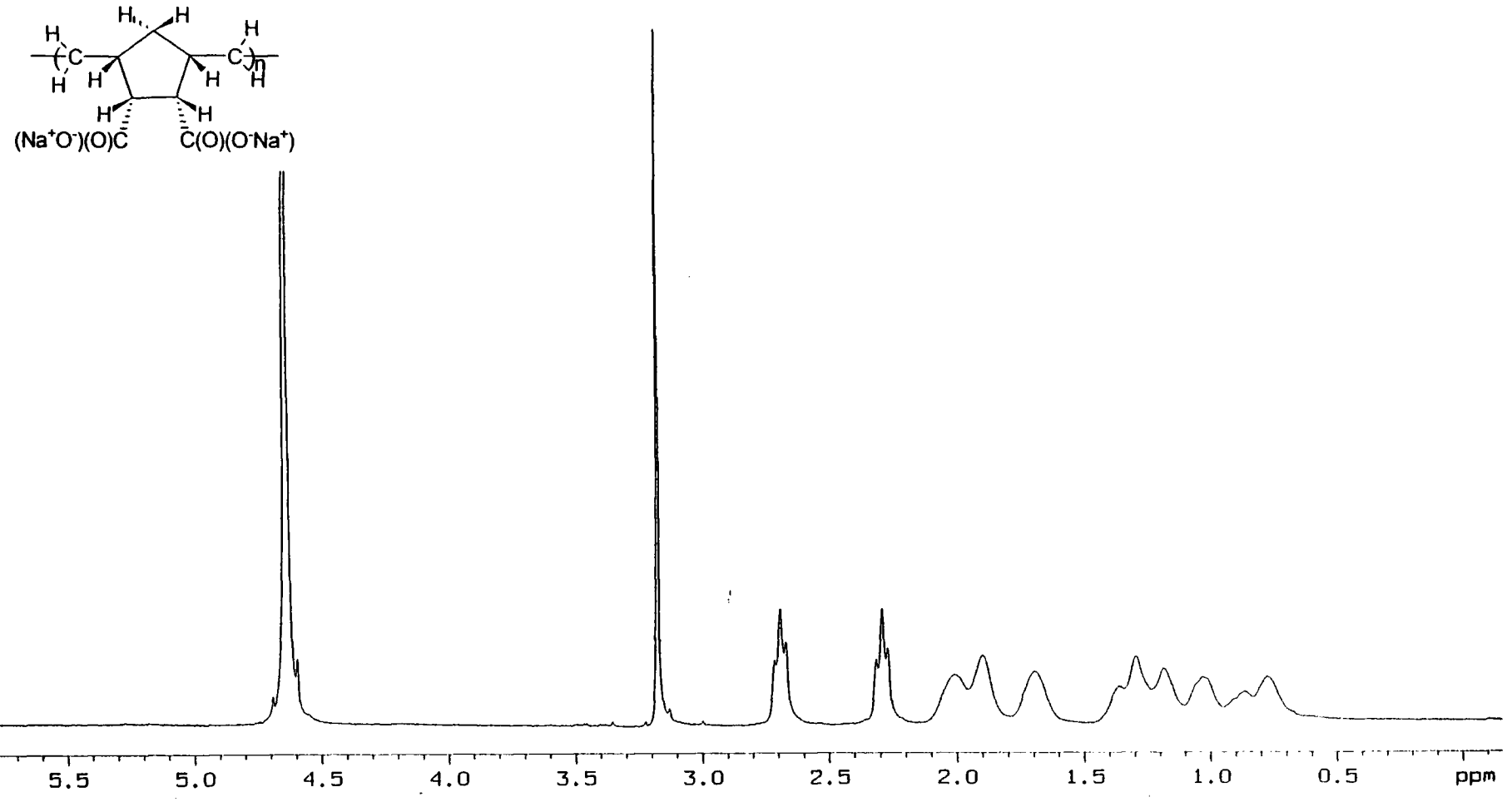

Appendix A21: ^{1}H NMR spectrum of poly(*2-endo-3-exo*-bicyclo[2.2.1]hept-5-ene-2,3- dicarboxylic acid dimethyl ester). (Poly-3S)
Recorded at 400MHz in $CDCl_3$.

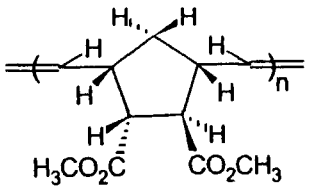

Appendix A22: ^{1}H NMR spectrum of hydrogenated poly(*2-endo-3-exo*-bicyclo [2.2.1]hept-5-ene-2,3-dicarboxylic acid dimethyl ester). (Poly-3P) Recorded at 400MHz in $CDCl_3$.

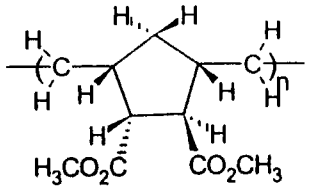

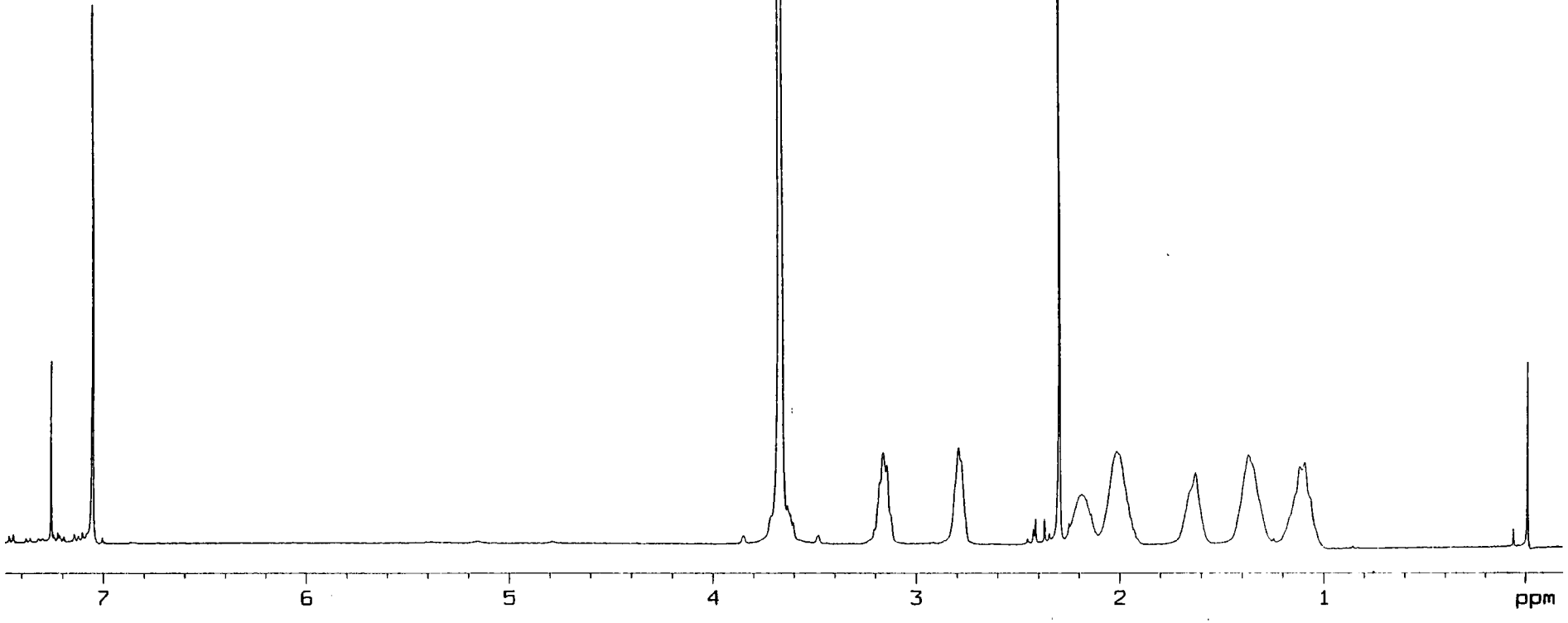

Appendix A23: ^{1}H NMR spectrum of hydrogenated, hydrolysed poly(*2-endo-3-exo*-bicyclo [2.2.1]hept-5-ene-2,3-dicarboxylic acid dimethyl ester). (Poly-3F) Recorded at 400MHz in D_2O.

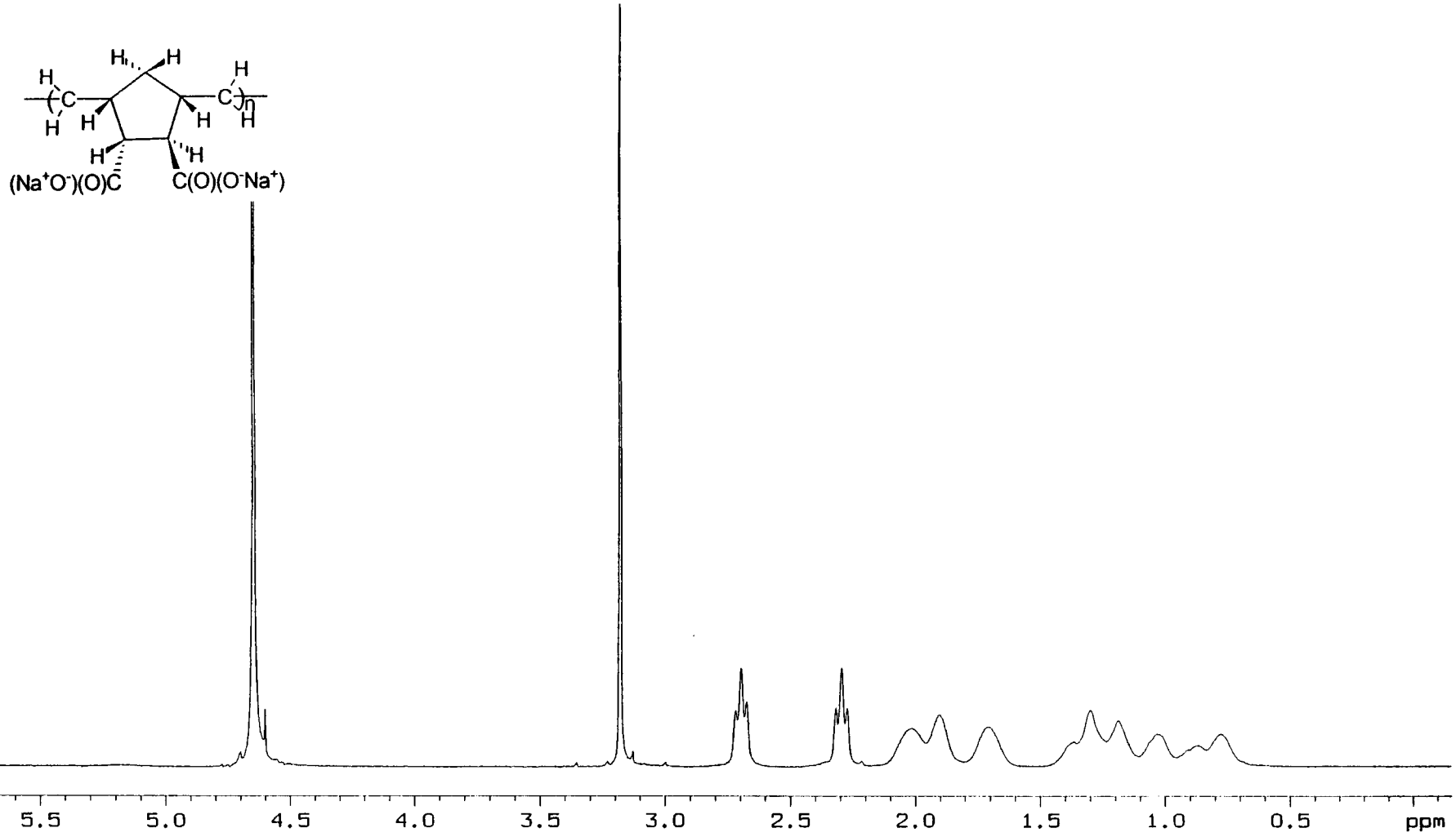

APPENDIX B

^{13}C NMR SPECTRA

Appendix B1: ^{13}C NMR spectrum of *exo*-bicyclo[2.2.1]hept-5-ene-2,3-dicarboxy anhydride.
Recorded at 100.58 MHz in d_6-acetone.

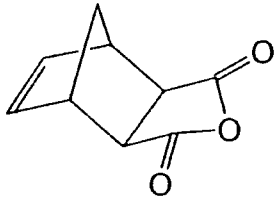

Appendix B2: ^{13}C NMR spectrum of *exo,exo*-bicyclo[2.2.1]hept-5-ene-2,3-dicarboxylic acid.
Recorded at 100.58 MHz in d_6-acetone.

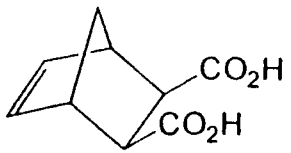

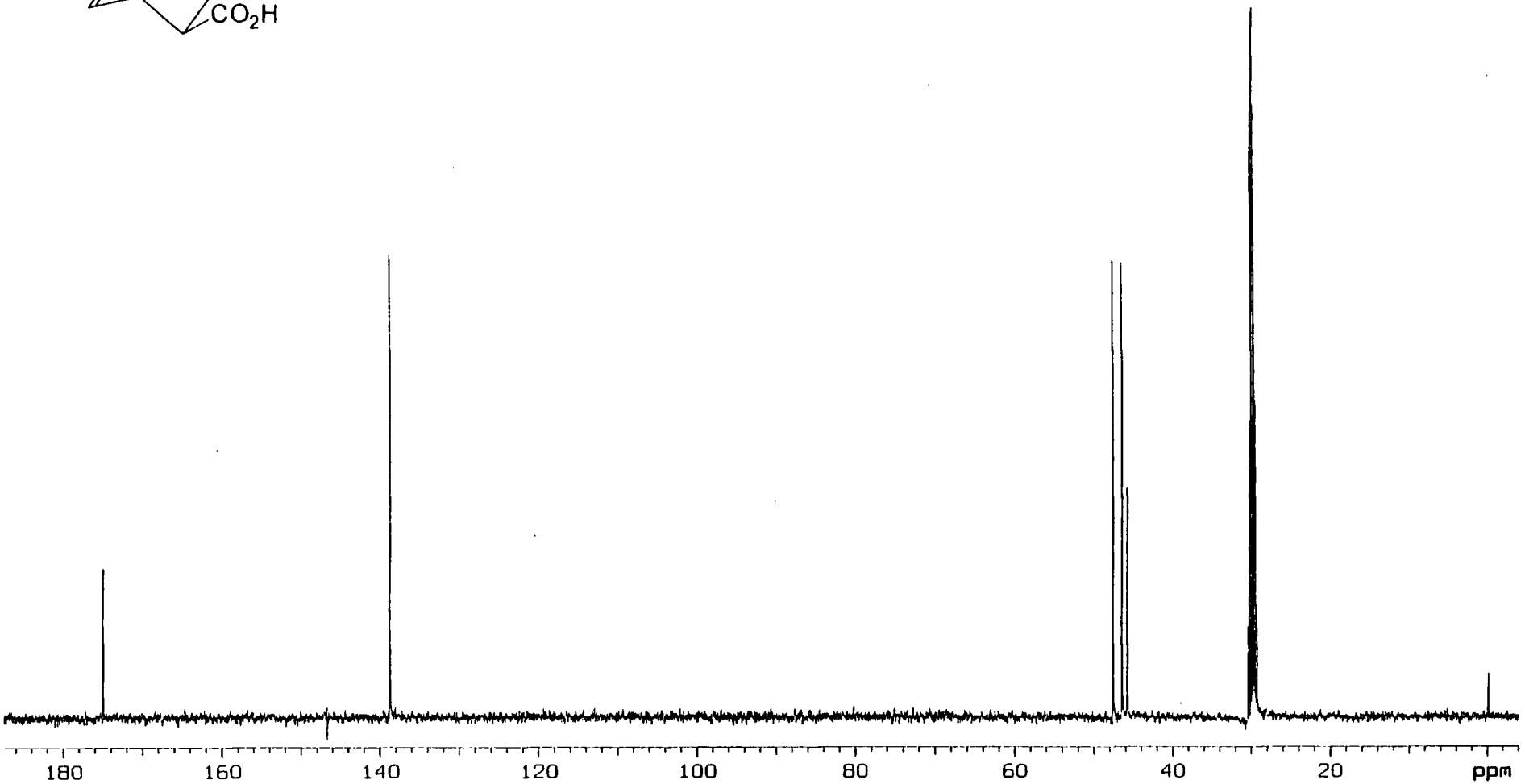

Appendix B3: ^{13}C NMR spectrum of *exo,exo*-bicyclo[2.2.1]heptane-2,3-dicarboxylic acid.
Recorded at 100.58 MHz in d_6-acetone.

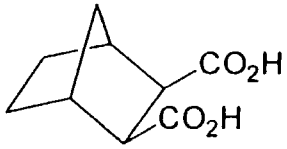

Appendix B4: ^{13}C NMR spectrum of *endo*-bicyclo[2.2.1]hept-5-ene-2,3-dicarboxy anhydride.
Recorded at 100.58 MHz in d_6-acetone.

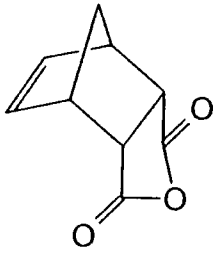

Appendix B5: ^{13}C NMR spectrum of *endo,endo*-bicyclo[2.2.1]heptane-2,3-dicarboxylic acid.
Recorded at 100.58 MHz in d_6-acetone.

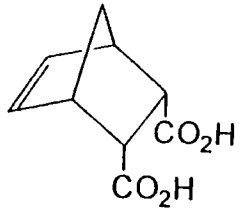

Appendix B6: ^{13}C NMR spectrum of *endo,endo*-bicyclo[2.2.1]heptane-2,3-dicarboxylic acid.
Recorded at 100.58 MHz in d_6-acetone.

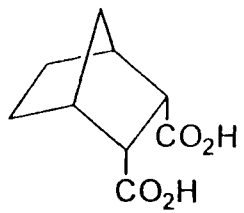

Appendix B7: ^{13}C NMR spectrum of 2-*endo*-3-*exo*-bicyclo[2.2.1]hept-5-ene-2,3-dicarboxylic acid.
Recorded at 100.58 MHz in d_6-acetone.

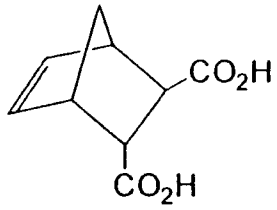

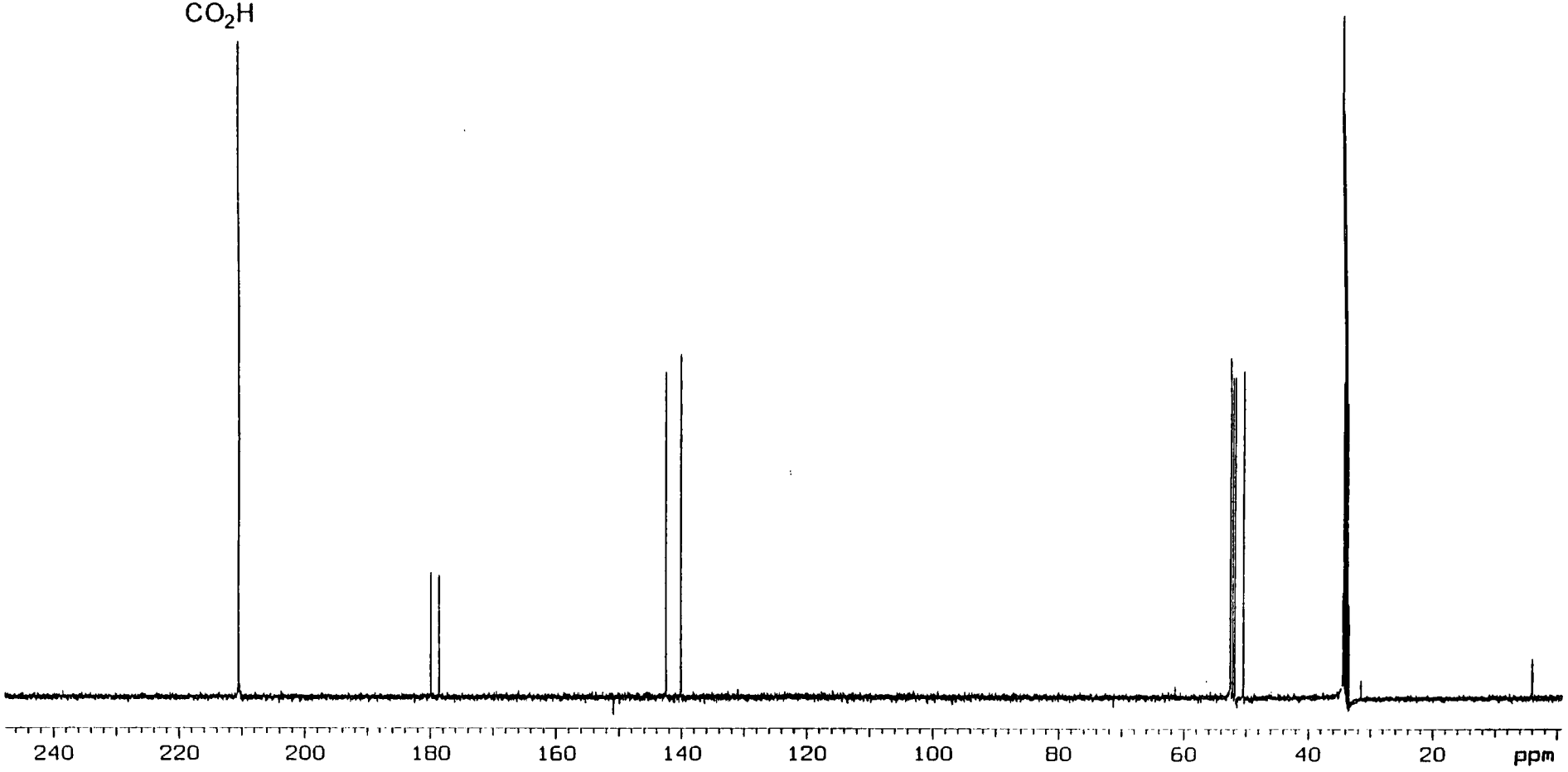

Appendix B8: ^{13}C NMR spectrum of 2-*endo*-3-*exo*-bicyclo[2.2.1]heptane-2,3-dicarboxylic acid.
Recorded at 100.58 MHz in d_6-acetone.

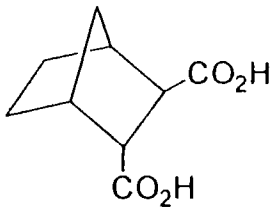

Appendix B9: ^{13}C NMR spectrum of *exo*-7-oxabicyclo[2.2.1]hept-5-ene-2,3-dicarboxy anhydride.
Recorded at 100.58 MHz in d_6-acetone.

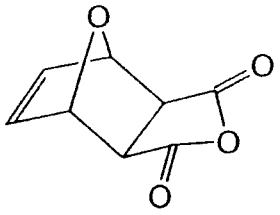

Appendix B10: ^{13}C NMR spectrum of *exo,exo*-7-oxabicyclo-[2.2.1]hept-5-ene-2,3-bis(carboxylic acid).
Recorded at 100.58 MHz in D_2O.

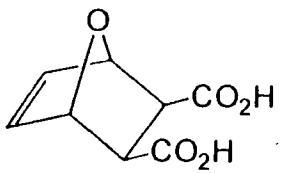

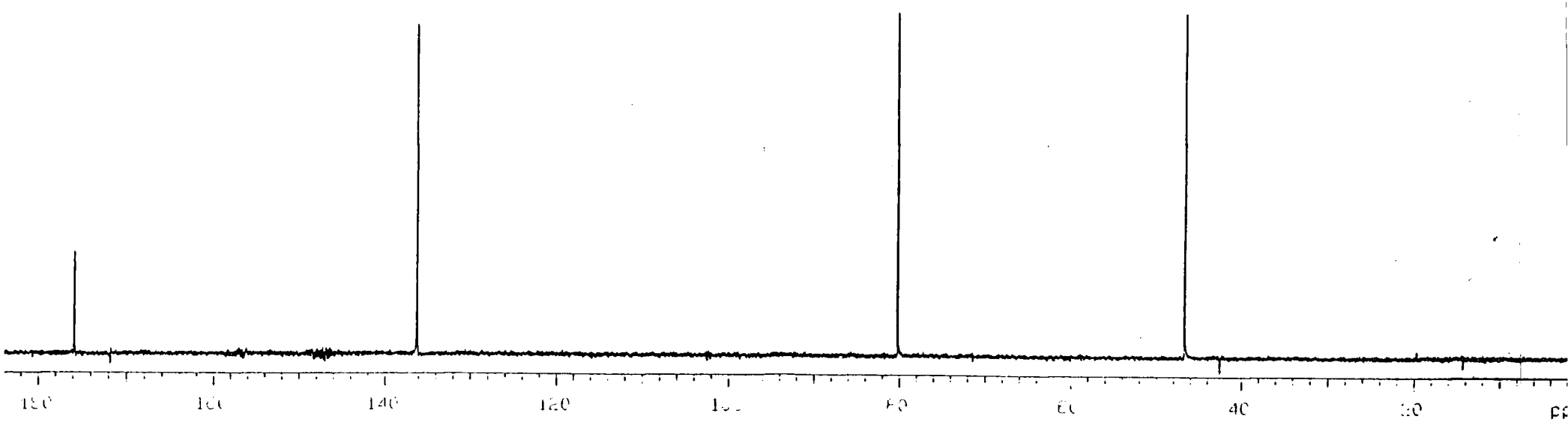

Appendix B11: ^{13}C NMR spectrum of *exo,exo*-7-oxabicyclo-[2.2.1]heptane-2,3-bis(carboxylic acid).
Recorded at 100.58 MHz in d_6-acetone.

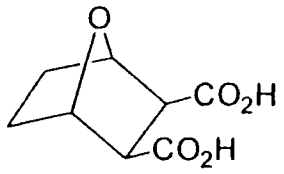

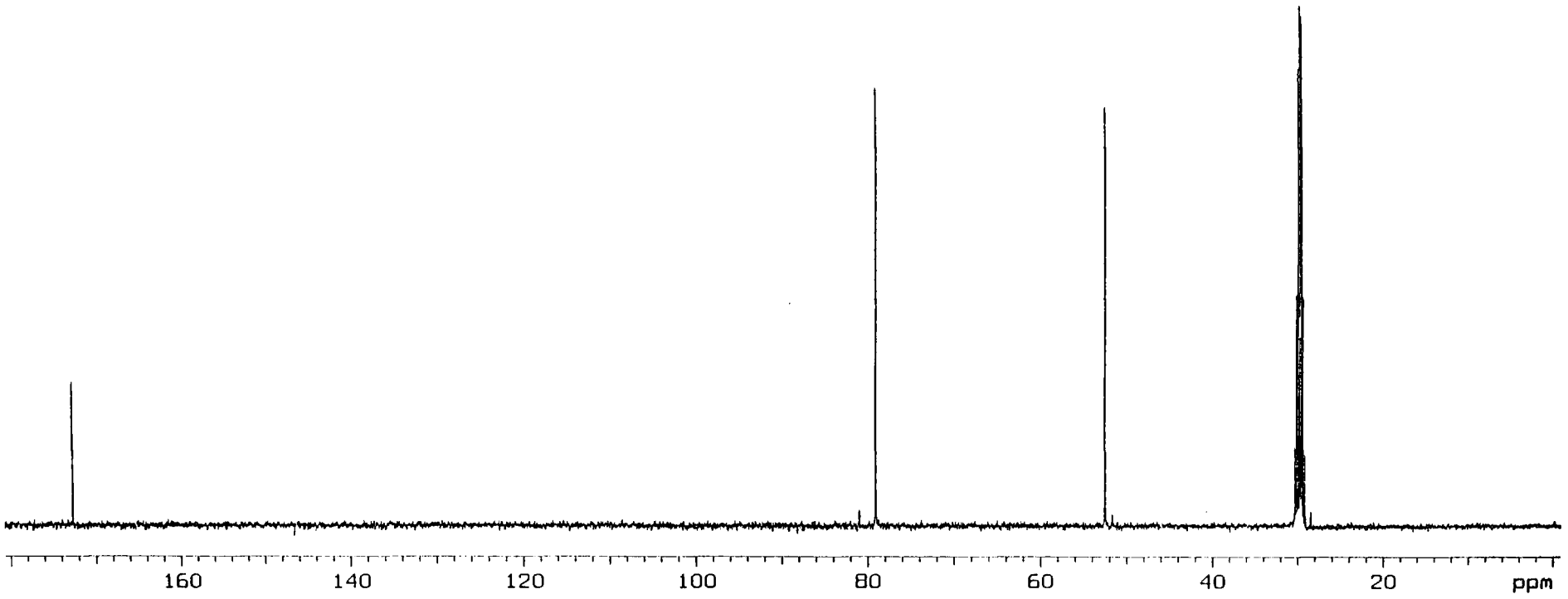

Appendix B12: ^{13}C NMR spectrum of *exo,exo*-bicyclo[2.2.1]hept-5-ene-2,3 dicarboxylic acid dimethyl ester. (monomer 1)
Recorded at 100.58 MHz in d_6-acetone.

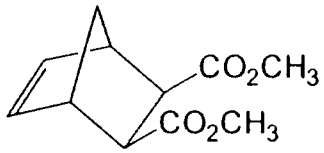

Appendix B13: ^{13}C NMR spectrum of *endo,endo*-bicyclo[2.2.1]hept-5-ene-2,3 dicarboxylic acid dimethyl ester. (monomer 2).
Recorded at 100.58 MHz in d_6-acetone.

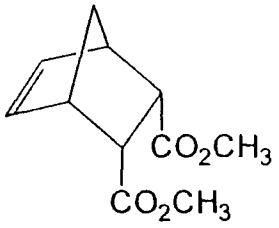

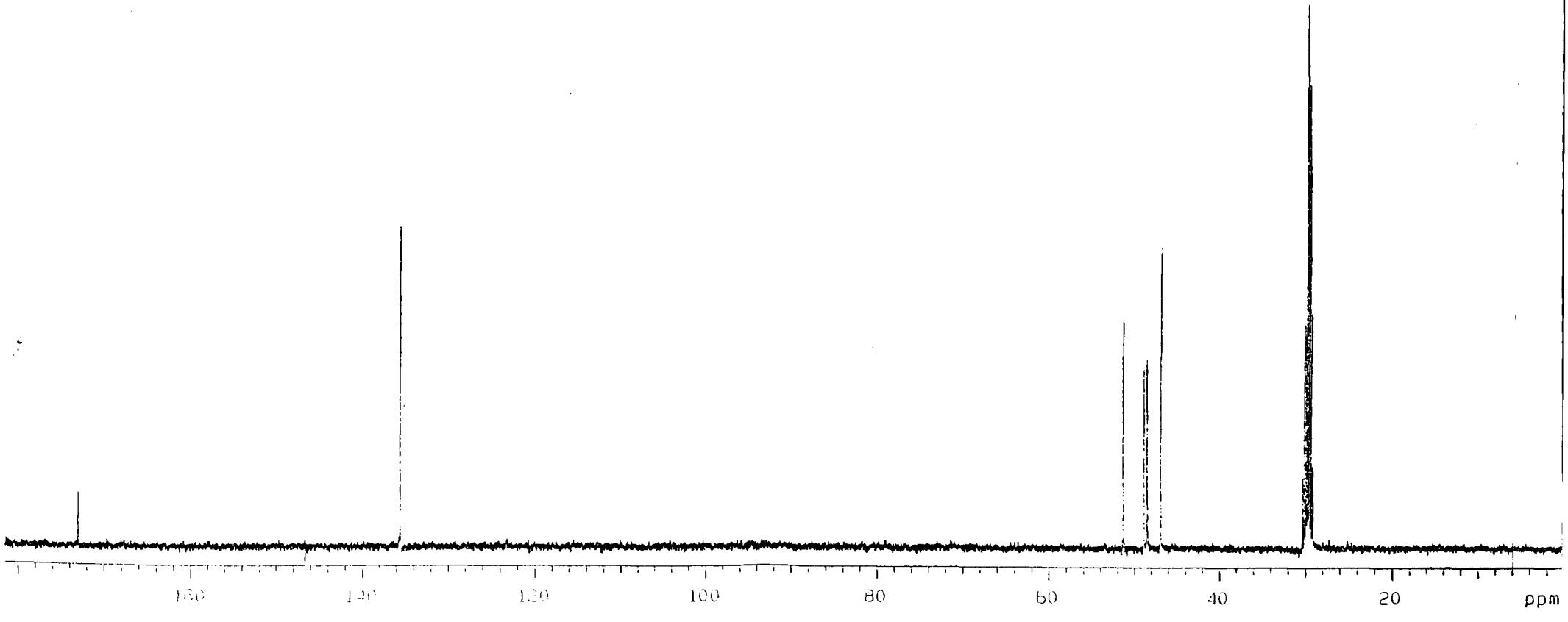

Appendix B14: ^{13}C NMR spectrum of 2-*endo*-3-*exo*-bicyclo[2.2.1]hept-5-ene-2,3-dicarboxylic acid dimethyl ester. (monomer 3).
Recorded at 100.58 MHz in d_6-acetone.

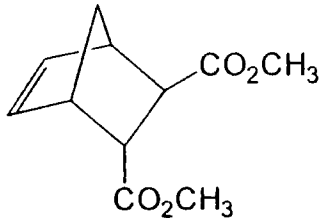

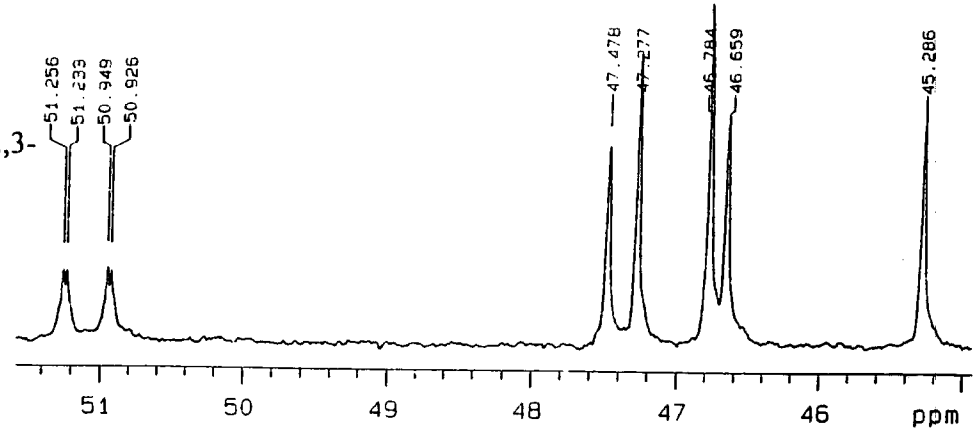

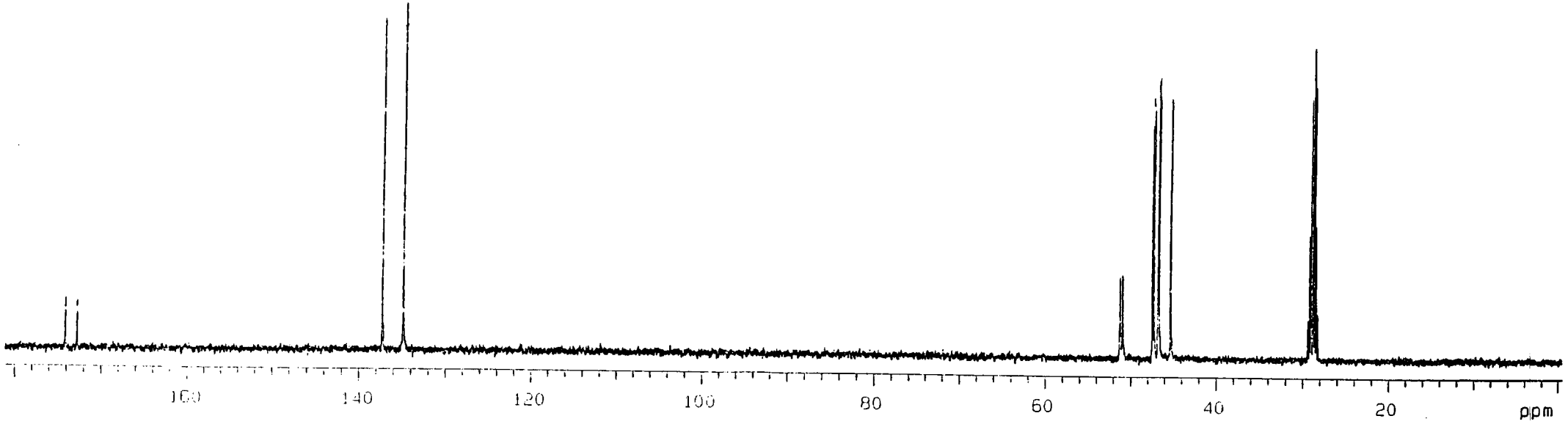

Appendix B15: ^{13}C NMR spectrum of poly(*exo,exo*-bicyclo[2.2.1]hept-5-ene-2,3-dicarboxylic acid dimethyl ester). (Poly-1S)
Recorded at 100.58 MHz in $CDCl_3$.

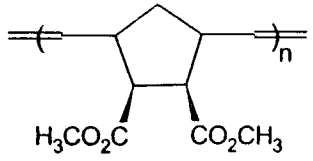

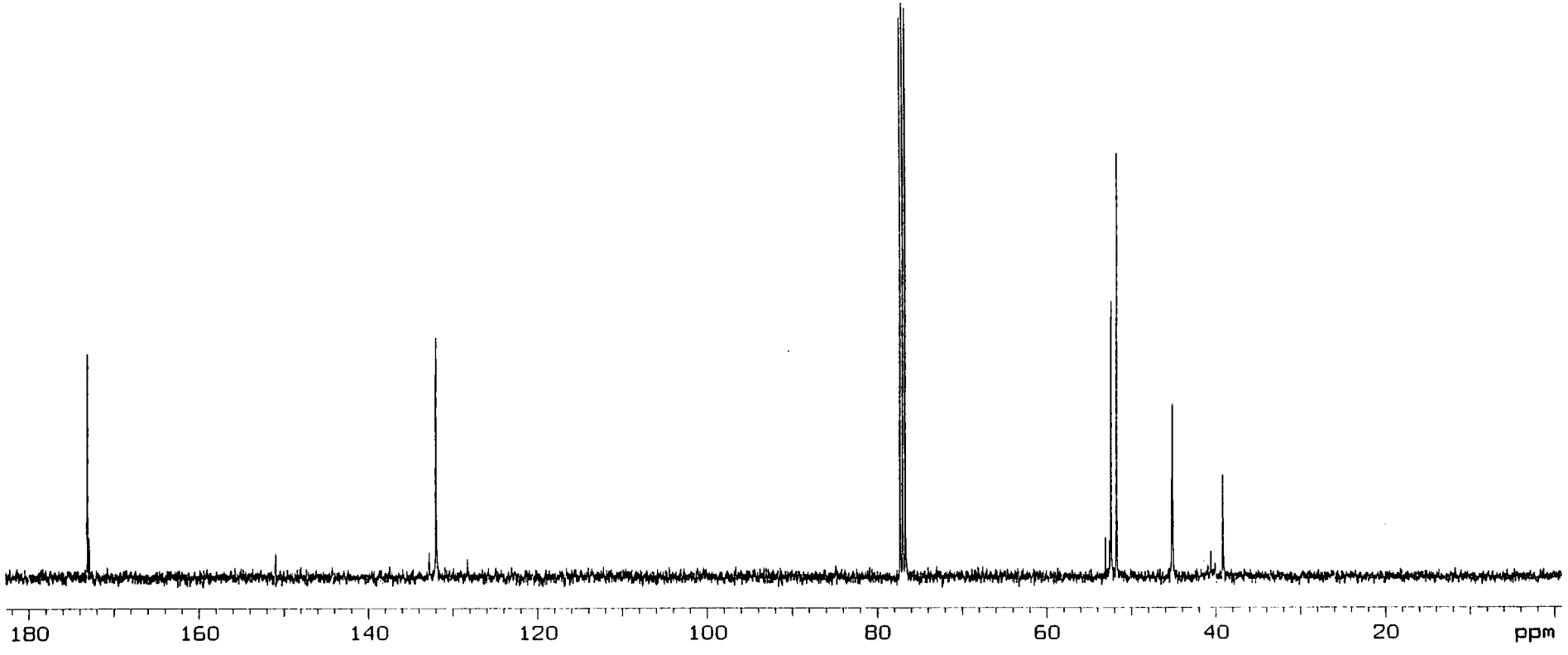

Appendix B16: ^{13}C NMR spectrum of hydrogenated poly(*exo,exo*- bicyclo [2.2.1]hept-5-ene-2,3-dicarboxylic acid dimethyl ester). (Poly-1P) Recorded at 100.58 MHz in $CDCl_3$.

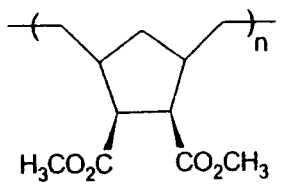

Appendix B17: ^{13}C NMR spectrum of hydrogenated, hydrolysed poly(*exo,exo*-bicyclo [2.2.1]hept-5-ene-2,3-dicarboxylic acid dimethyl ester). (Poly-1F) Recorded at 100.58 MHz in D_2O.

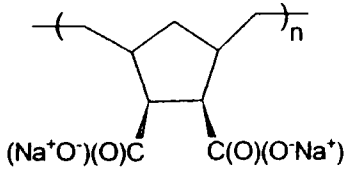

Appendix B18: ^{13}C NMR spectrum of poly(*endo,endo*-bicyclo[2.2.1]hept-5-ene-2,3-dicarboxylic acid dimethyl ester). (Poly-2S)
Recorded at 100.58 MHz in $CDCl_3$.

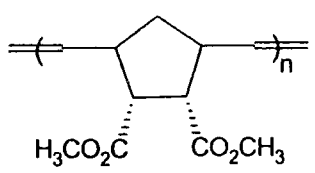

Appendix B19: ^{13}C NMR spectrum of hydrogenated poly(*endo,endo*- bicyclo [2.2.1]hept-5-ene-2,3-dicarboxylic acid dimethyl ester). (Poly-2P) Recorded at 100.58 MHz in $CDCl_3$.

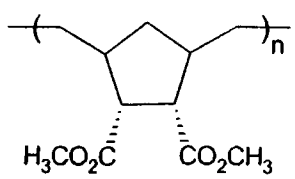

Appendix B20: ^{13}C NMR spectrum of hydrogenated, hydrolysed poly(*endo,endo*-bicyclo [2.2.1]hept-5-ene-2,3-dicarboxylic acid dimethyl ester). (Poly-2F) Recorded at 100.58 MHz in D_2O.

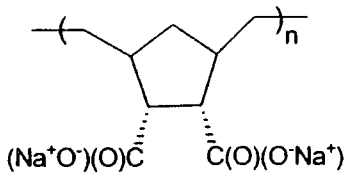

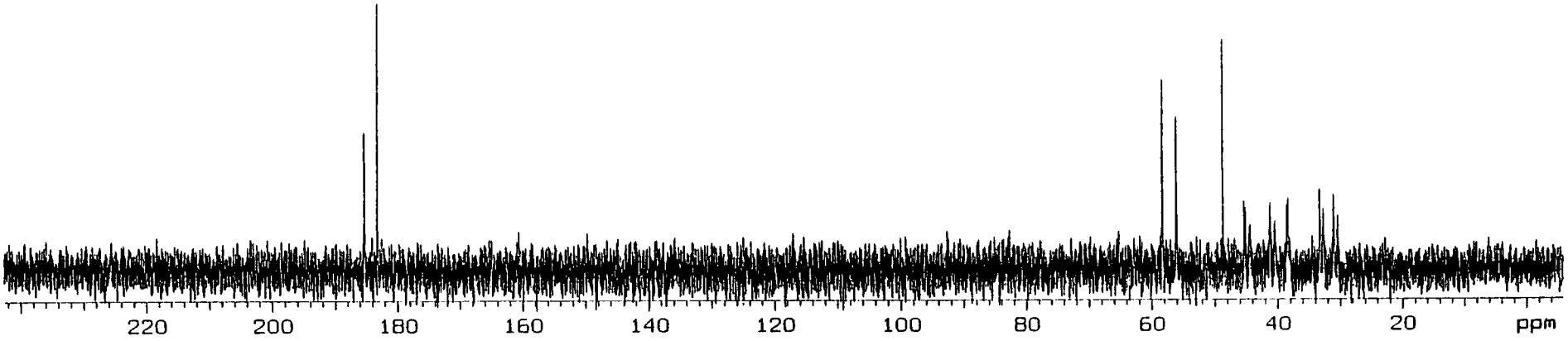

Appendix B21: ^{13}C NMR spectrum of poly(*2-endo-3-exo*-bicyclo[2.2.1]hept-5-ene-2,3-dicarboxylic acid dimethyl ester). (Poly-3S)
Recorded at 100.58 MHz in $CDCl_3$.

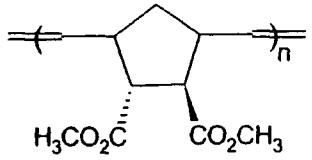

Appendix B22: ^{13}C NMR spectrum of hydrogenated poly(*endo,endo*-bicyclo [2.2.1]hept-5-ene-2,3-dicarboxylic acid dimethyl ester). (Poly-3P) Recorded at 100.58 MHz in $CDCl_3$.

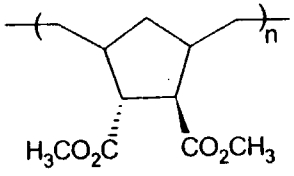

Appendix B23: ^{13}C NMR spectrum of hydrogenated, hydrolysed poly(*2-endo-3-exo*-bicyclo [2.2.1]hept-5-ene-2,3-dicarboxylic acid dimethyl ester). (Poly-3F) Recorded at 100.58 MHz in D_2O.

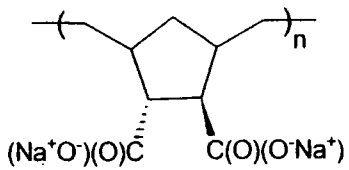

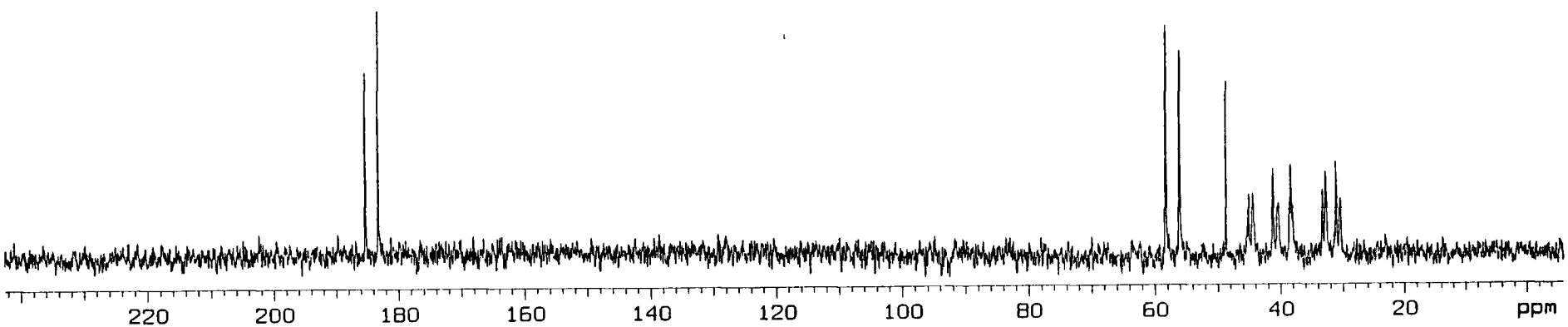

APPENDIX C

FTIR SPECTRA

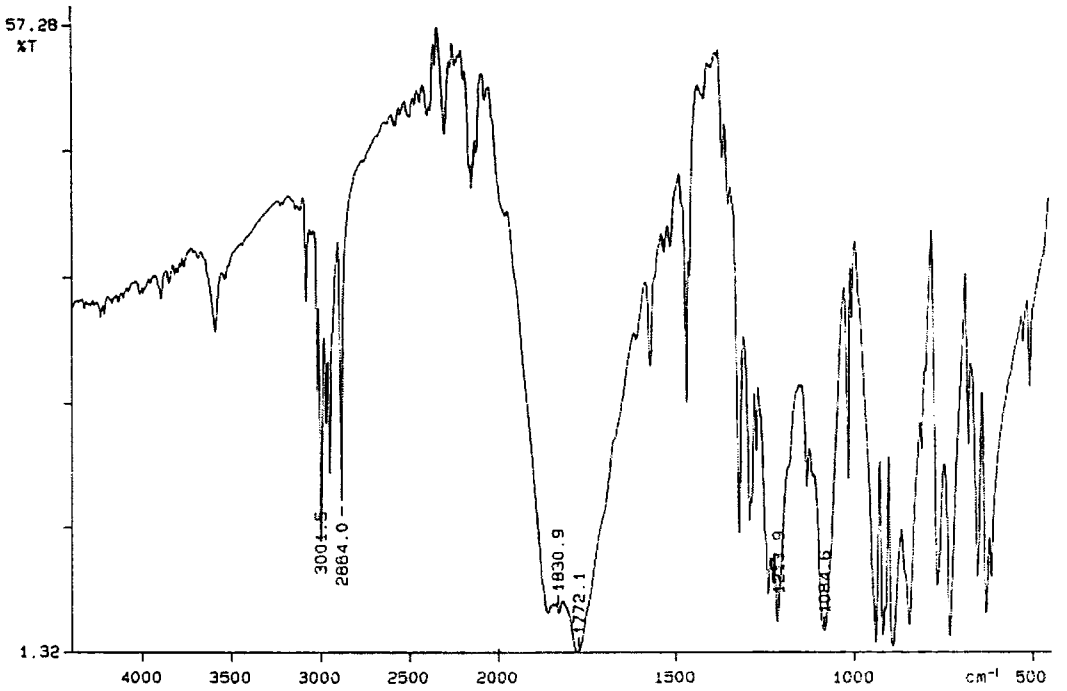

Appendix C1 : FTIR spectrum of *exo*-bicyclo[2.2.1]hept-5-ene-2,3-dicarboxy anhydride. (compound 1a)

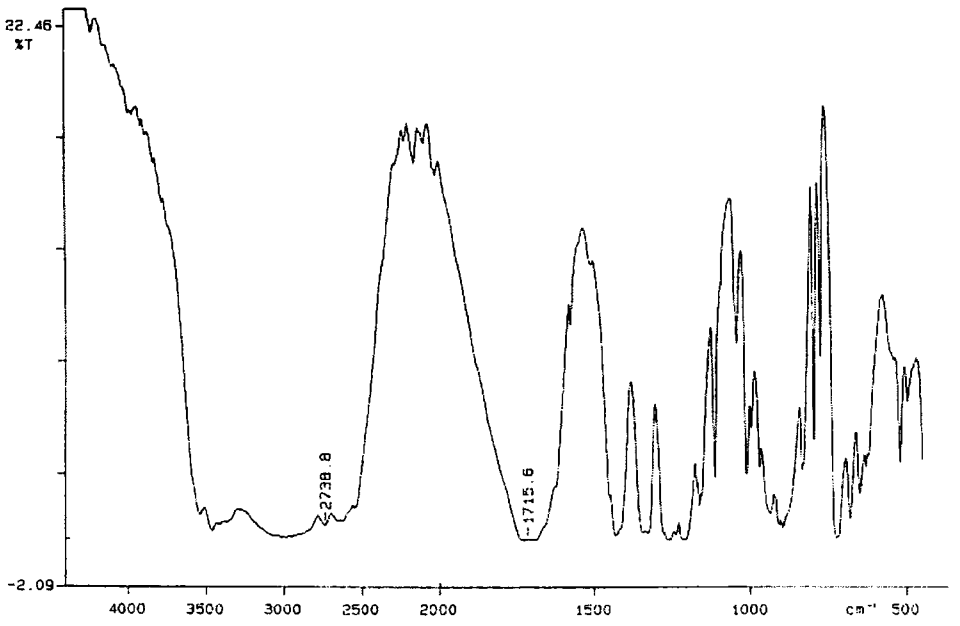

Appendix C2 : FTIR spectrum of *exo,exo*-bicyclo[2.2.1]hept-5-ene-2,3-dicarboxylic acid. (model compound 1b)

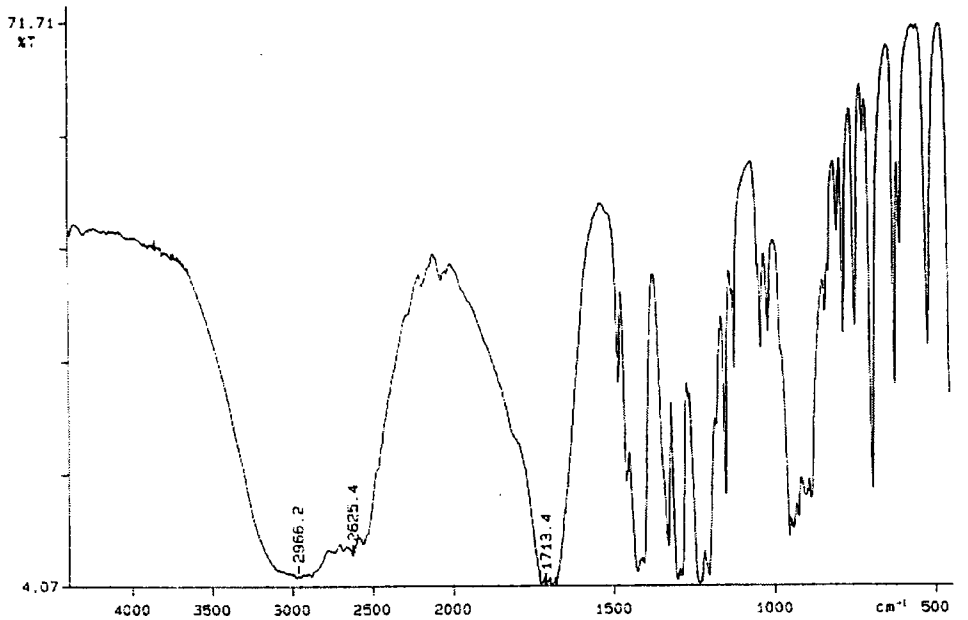

Appendix C3 : FTIR spectrum of *exo,exo*-bicyclo[2.2.1]heptane-2,3-dicarboxylic acid. (model compound 1c)

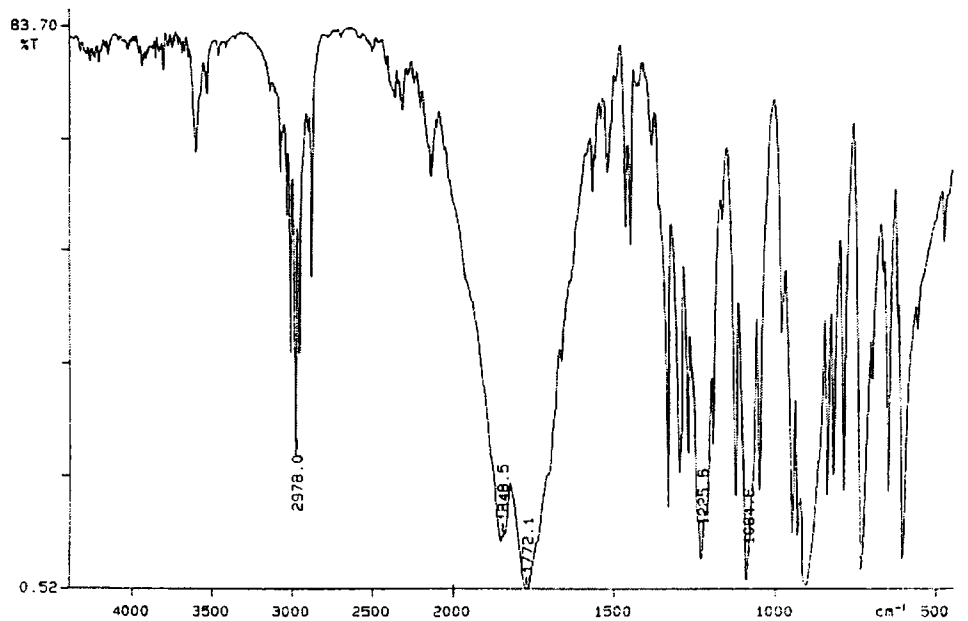

Appendix C4 : FTIR spectrum of *endo*-bicyclo[2.2.1]hept-5-ene-2,3-dicarboxy anhydride. (compound 2a)

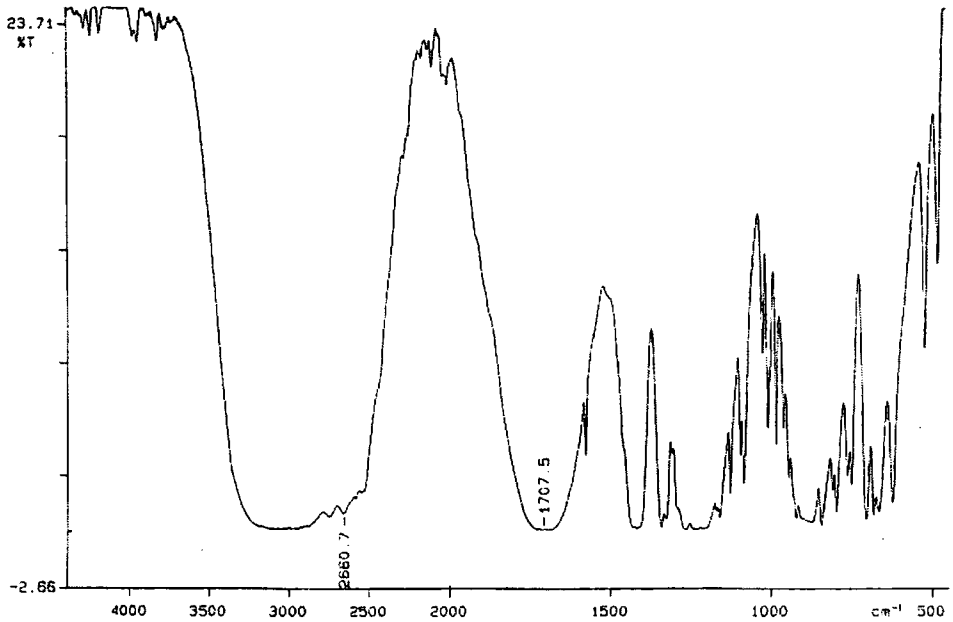

Appendix C5 : FTIR spectrum of *endo,endo*-bicyclo[2.2.1]heptane-2,3-dicarboxylic acid. (model compound 2b)

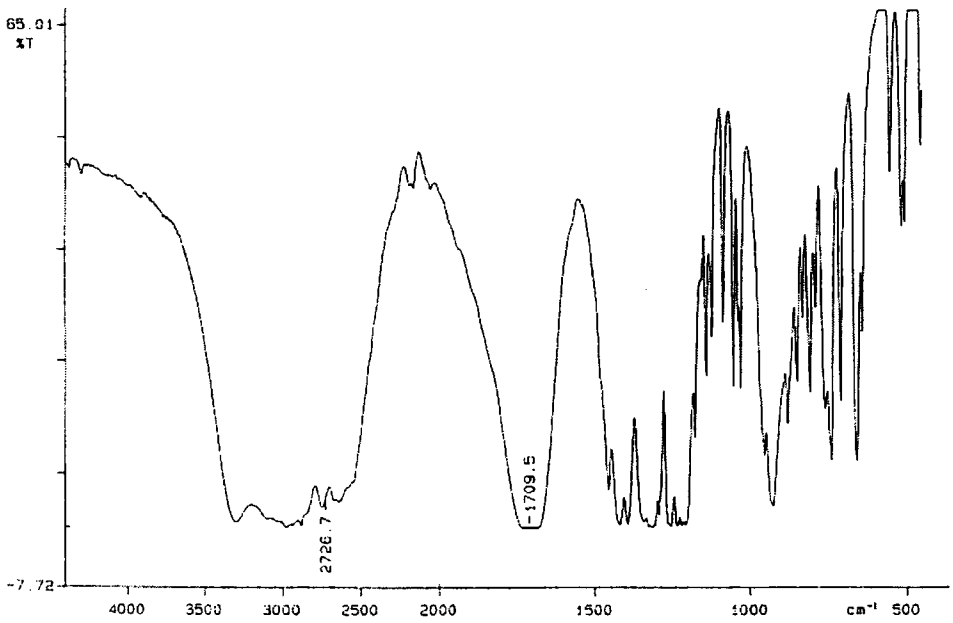

Appendix C6 : FTIR spectrum of *endo,endo*-bicyclo[2.2.1]heptane-2,3-dicarboxylic acid. (model compound 2c)

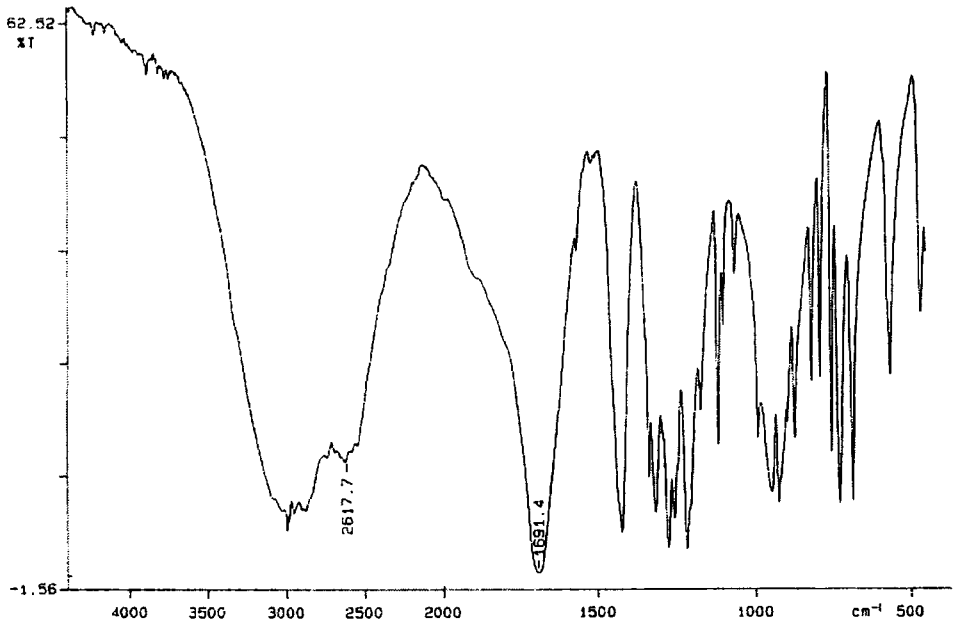

Appendix C7 : FTIR spectrum of 2-*endo*-3-*exo*-bicyclo[2.2.1]hept-5-ene-2,3-dicarboxylic acid. (model compound 3a)

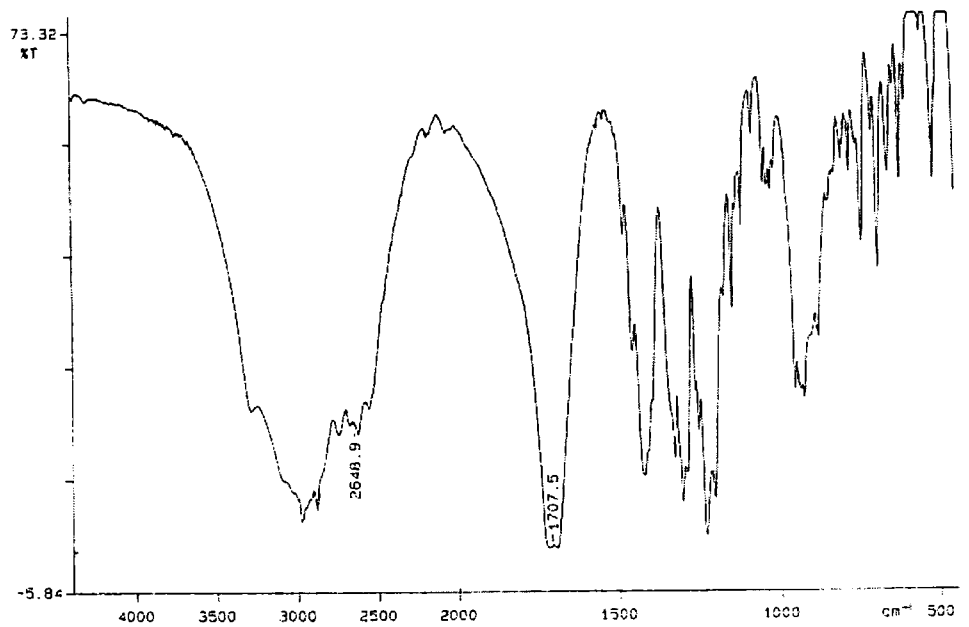

Appendix C8 : FTIR spectrum of 2-*endo*-3-*exo*-bicyclo[2.2.1]heptane-2,3-dicarboxylic acid. (model compound 3b)

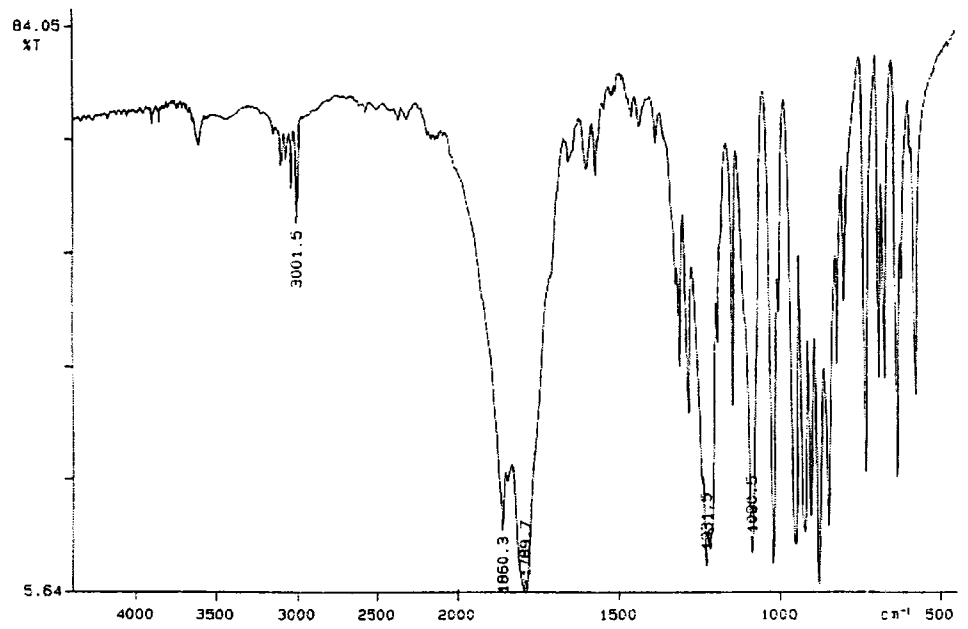

Appendix C9 : FTIR spectrum of *exo*-7-oxabicyclo[2.2.1]hept-5-ene-2,3-dicarboxy anhydride. (compound 4a)

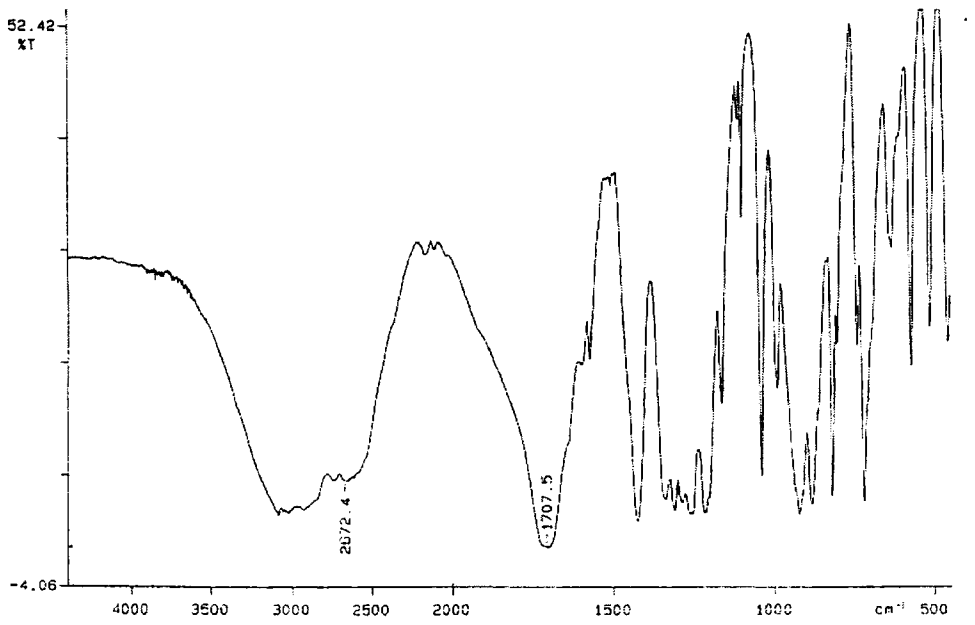

Appendix C10: FTIR spectrum of *exo,exo*-7-oxabicyclo-[2.2.1]hept-5-ene-2,3-bis(carboxylic acid). (model compound 4b)

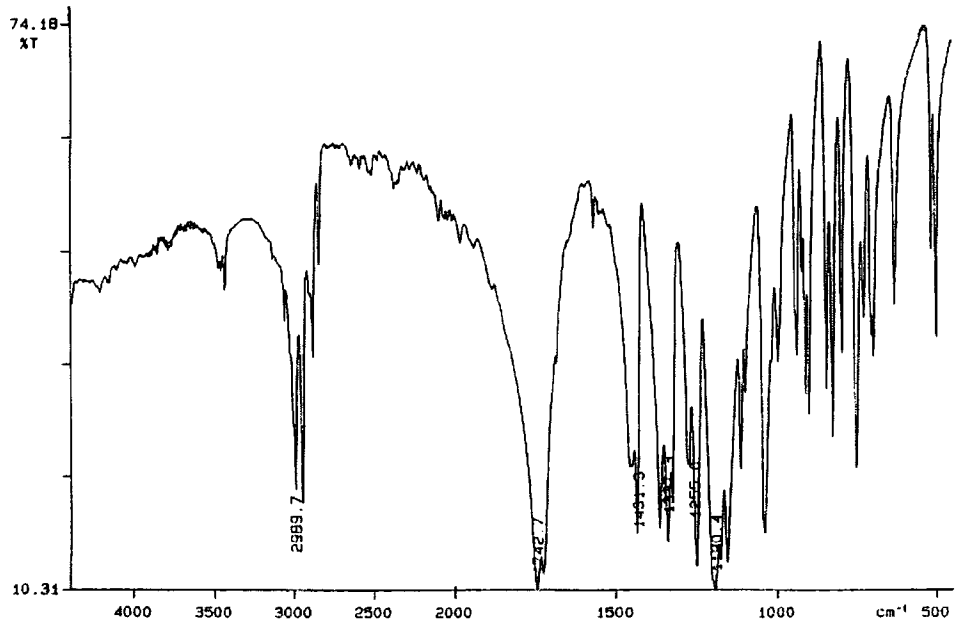

Appendix C11: FTIR spectrum of *exo,exo*-bicyclo[2.2.1]hept-5-ene-2,3-dicarboxylic acid dimethyl ester. (monomer 1)

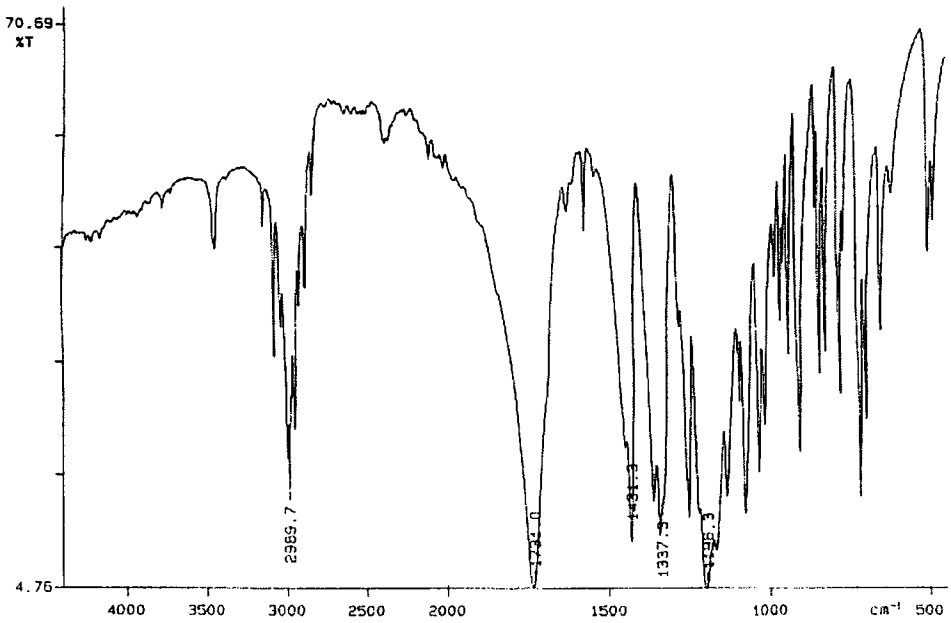

Appendix C12: FTIR spectrum of *endo,endo*-bicyclo[2.2.1]hept-5-ene-2,3 dicarboxylic acid dimethyl ester. (monomer 2)

APPENDIX D

GPC TRACES

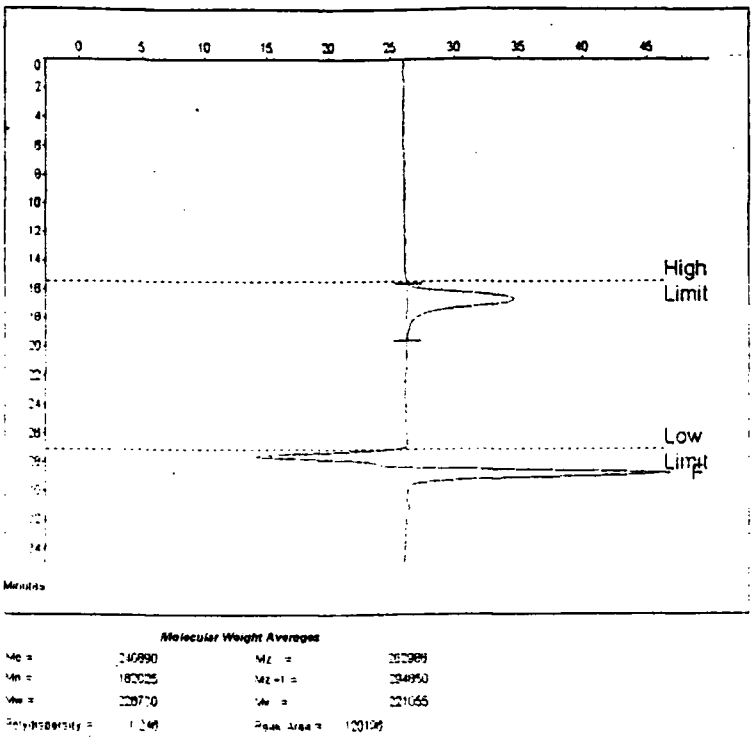

Appendix D1 : GPC trace of Poly 1S (*exo,exo*- repeat units, starting polymer).

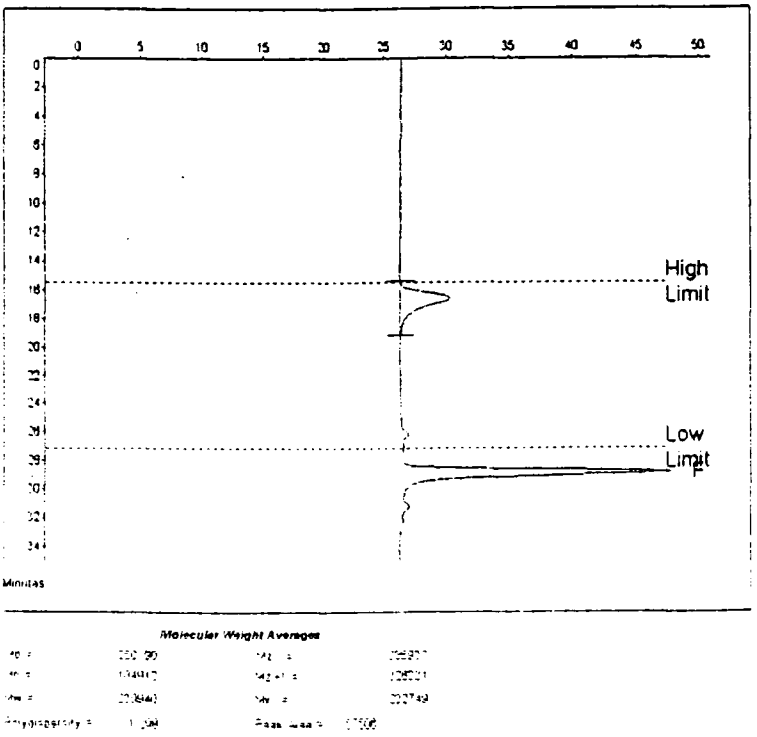

Appendix D2 : GPC trace of Poly 1P (*exo,exo*- repeat units, hydrogenated, precursor polymer).

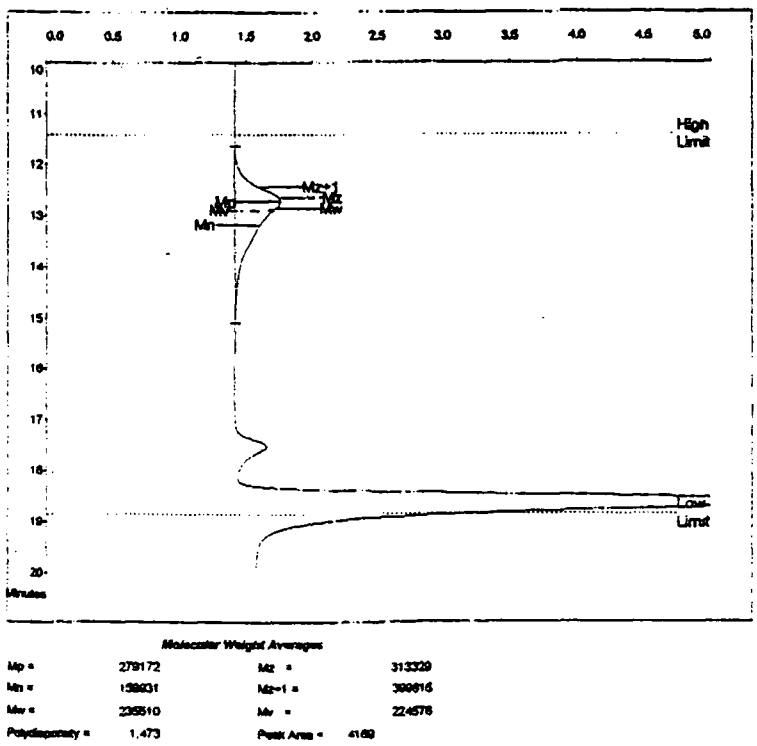

Appendix D3 : GPC trace of Poly 1F (*exo,exo-* repeat units, hydrogenated hydrolysed, final polymer).

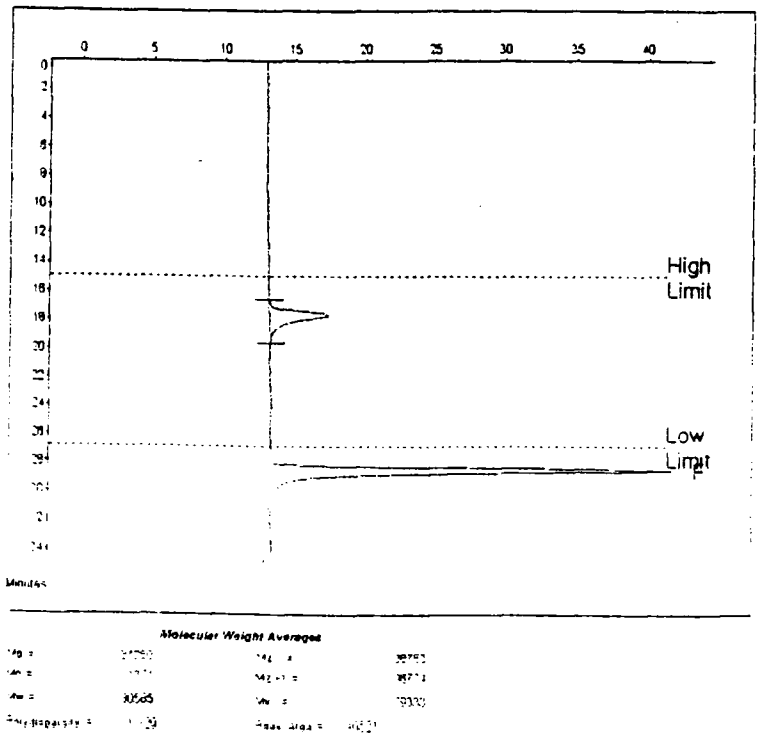

Appendix D4 : GPC trace of Poly 1S' (*exo,exo-* repeat units, starting polymer).

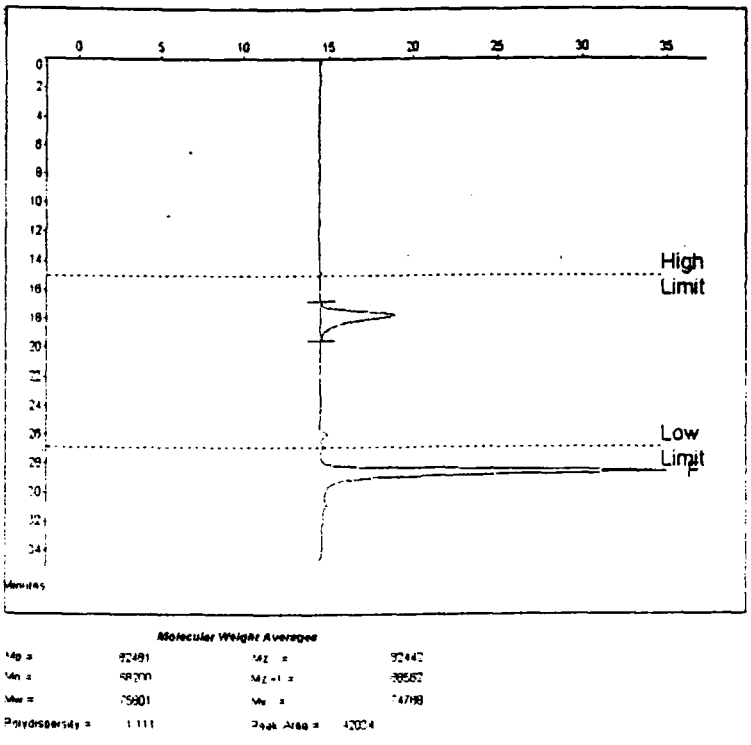

Appendix D5 : GPC trace of Poly 1P' (*exo,exo-* repeat units, hydrogenated, precursor polymer).

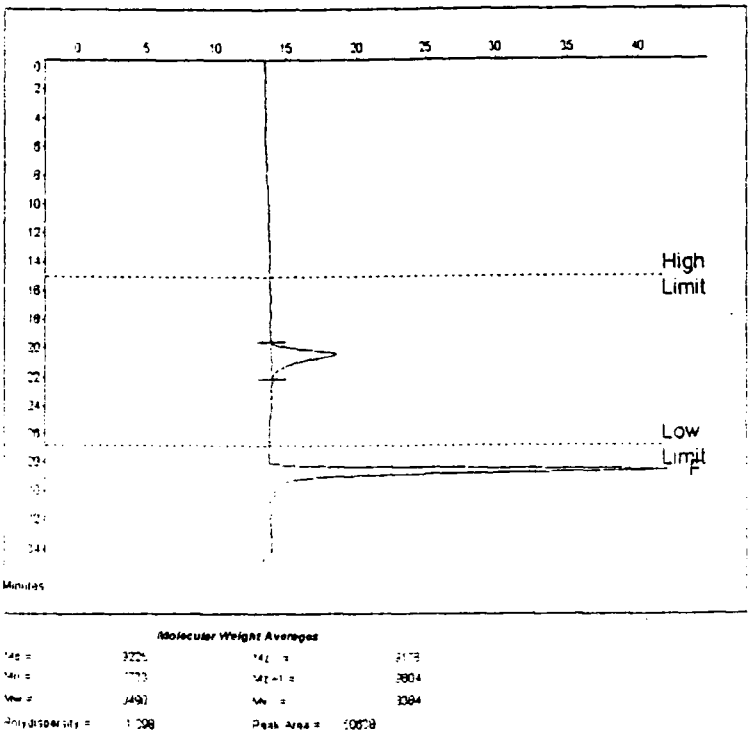

Appendix D6 : GPC trace of Poly 1S'' (*exo,exo-* repeat units, starting polymer).

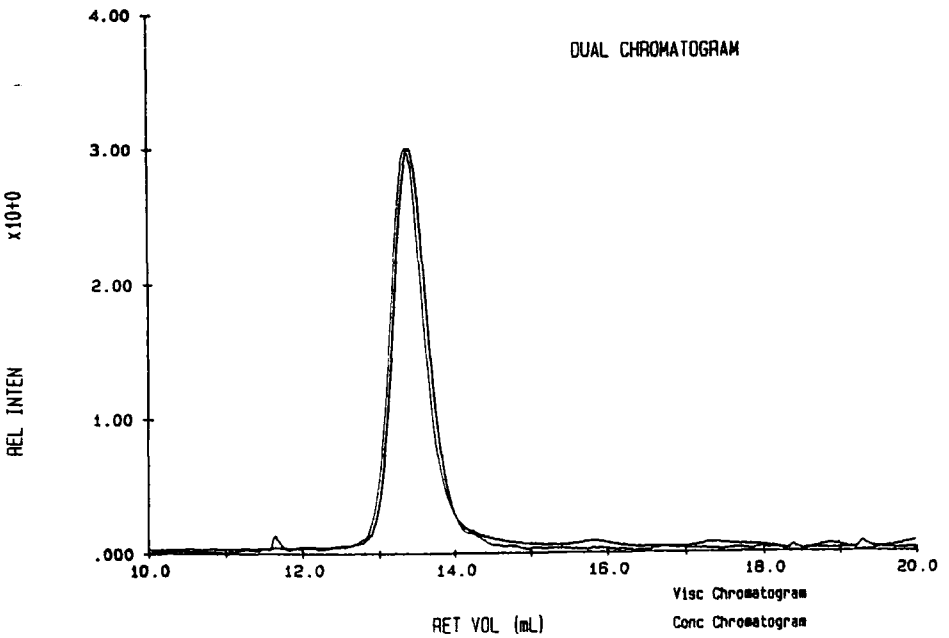

Appendix D7 : GPC trace of Poly 2S (*endo,endo*- repeat units, starting polymer).

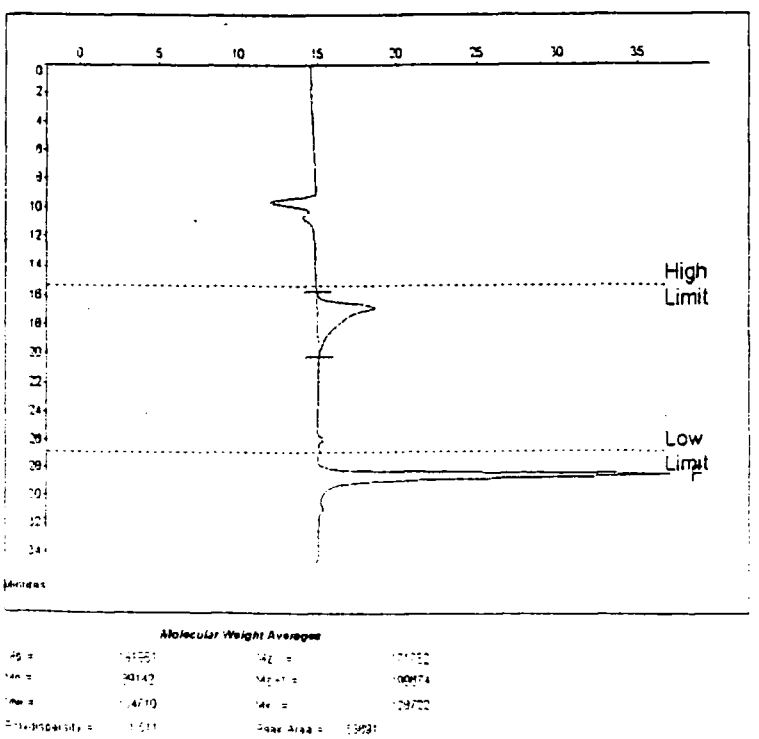

Appendix D8 : GPC trace of Poly 2P (*endo,endo*- repeat units, hydrogenated, precursor polymer).

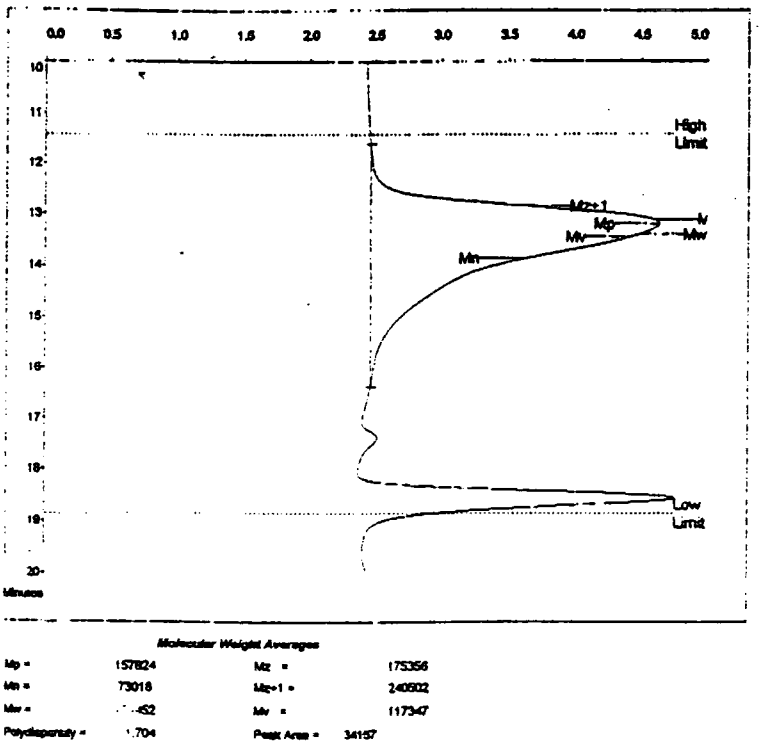

Appendix D9 : GPC trace of Poly 2F (*endo,endo*- repeat units, hydrogenated, hydrolysed, final polymer).

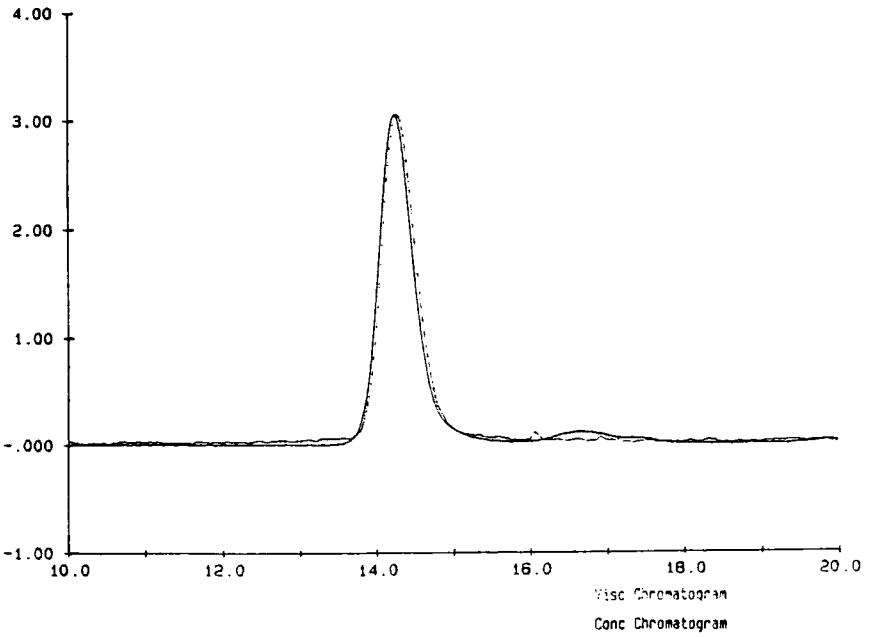

Appendix D10 : GPC trace of Poly 2S' (*endo,endo*- repeat units, hydrogenated, precursor polymer).

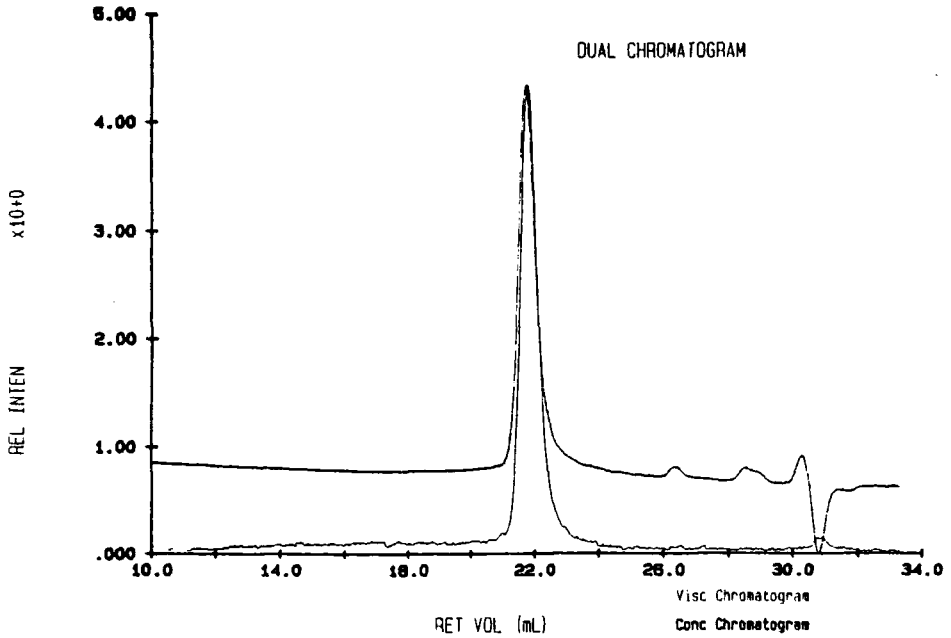

Appendix D11 : GPC trace of Poly 2P' (*endo,endo*- repeat units, hydrogenated, precursor polymer).

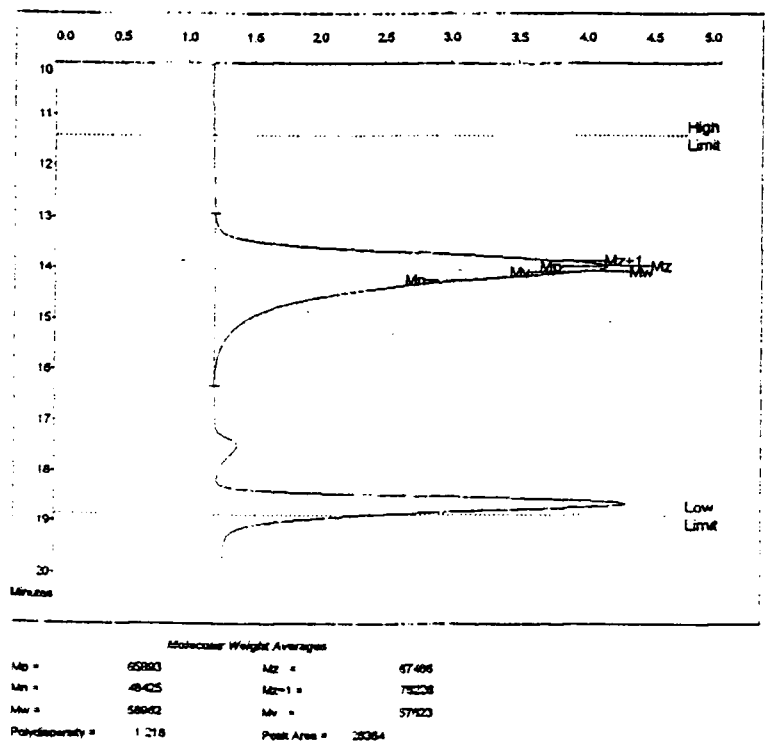

Appendix D12 : GPC trace of Poly 2F' (*endo,endo*- repeat units, hydrogenated, hydrolysed, final polymer).

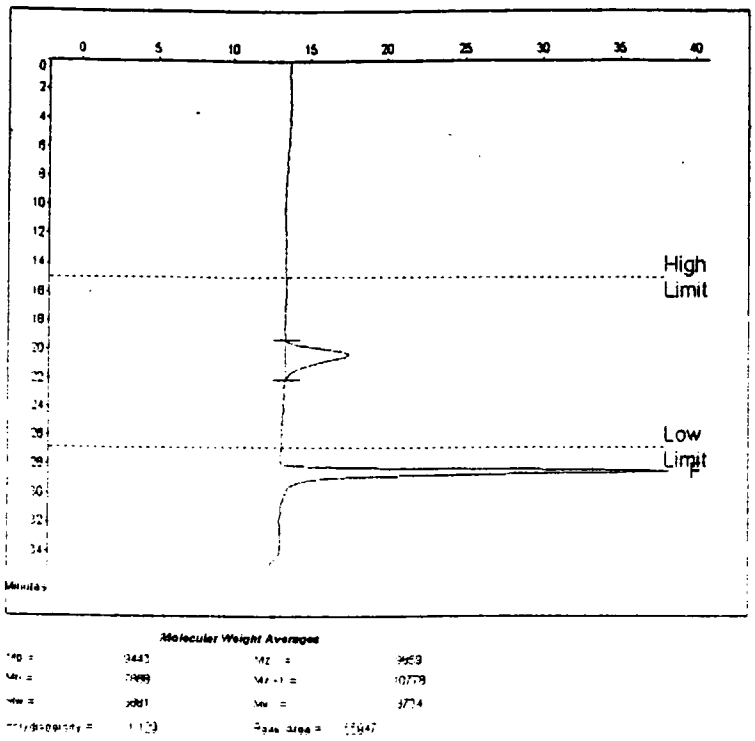

Appendix D13 : GPC trace of Poly 2S'' (*endo,exo-* repeat units, starting polymer).

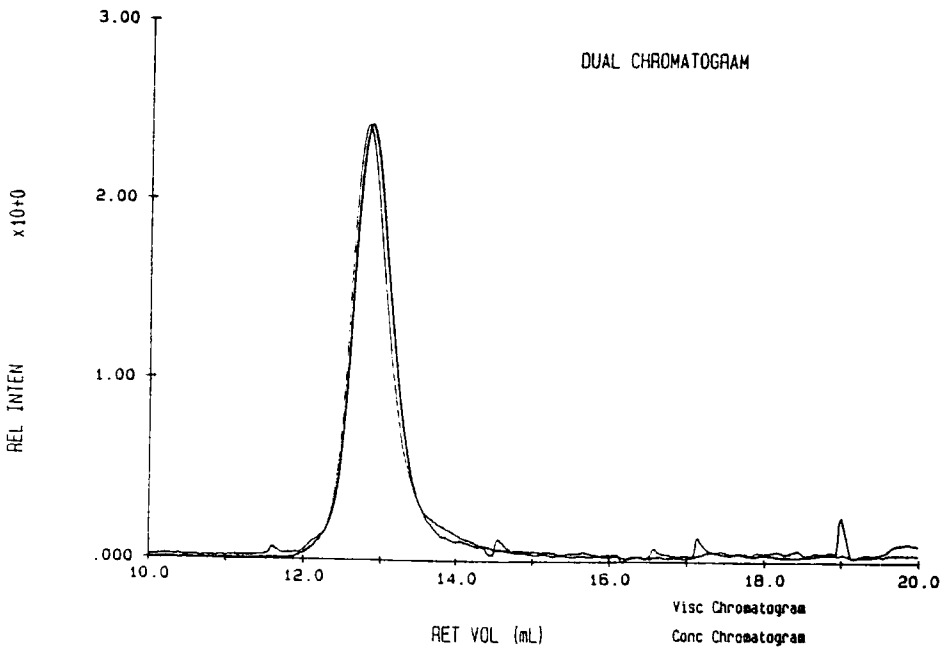

Appendix D14 : GPC trace of Poly 3S (*2-exo-3-endo-* repeat units, starting polymer).

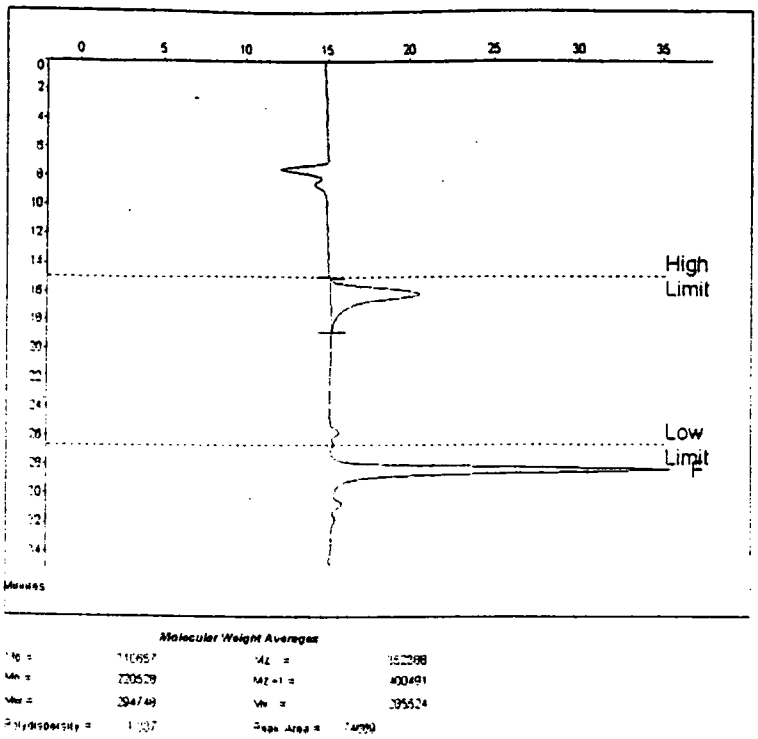

Appendix D15 : GPC trace of Poly 3P (*2-exo-3-endo-* repeat units, hydrogenated, precursor polymer).

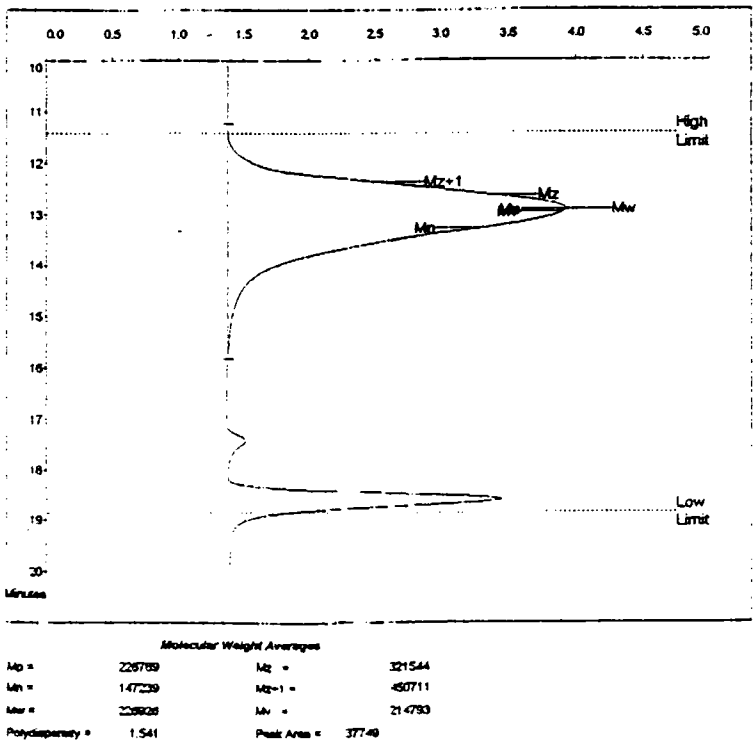

Appendix D16: GPC trace of Poly 3F (2-*exo-3-endo-* repeat units, hydrogenated, hydrolysed, final polymer).

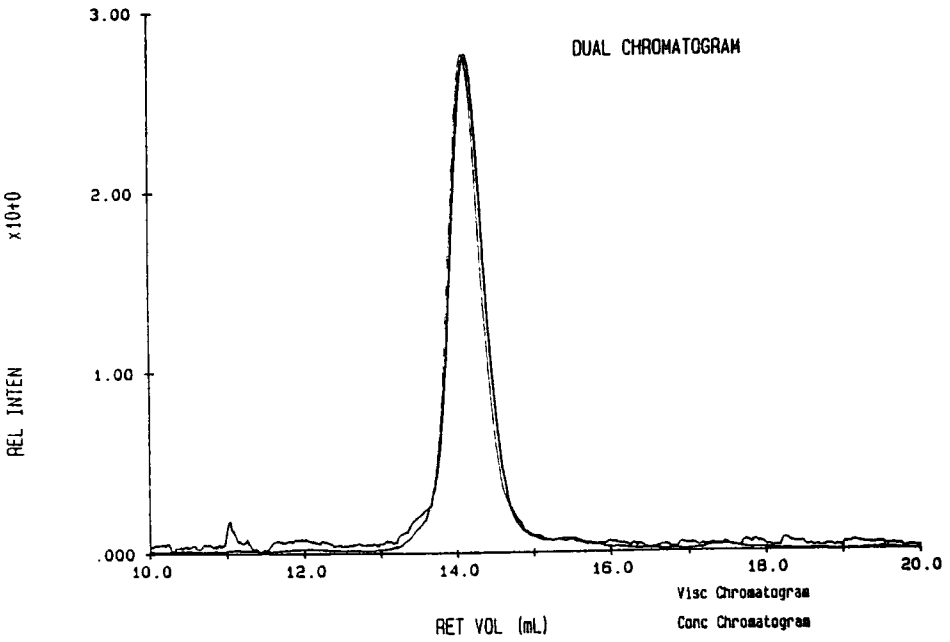

Appendix D17 : GPC trace of Poly 3S' (*2-exo-3-endo-* repeat units, starting polymer).

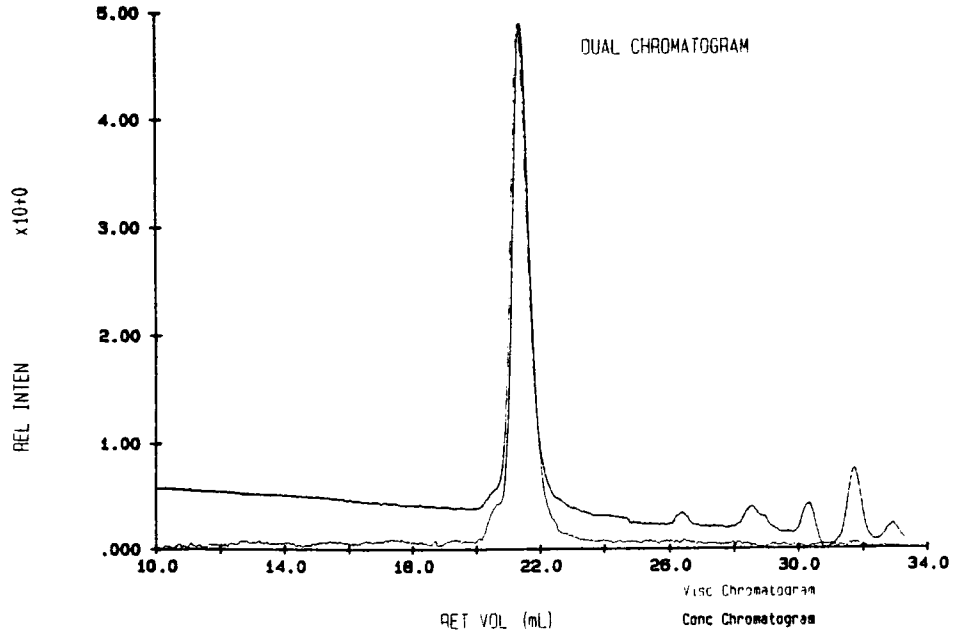

Appendix D18 : GPC trace of Poly 3P' (*2-exo-3-endo-* repeat units, hydrogenated, precursor polymer).

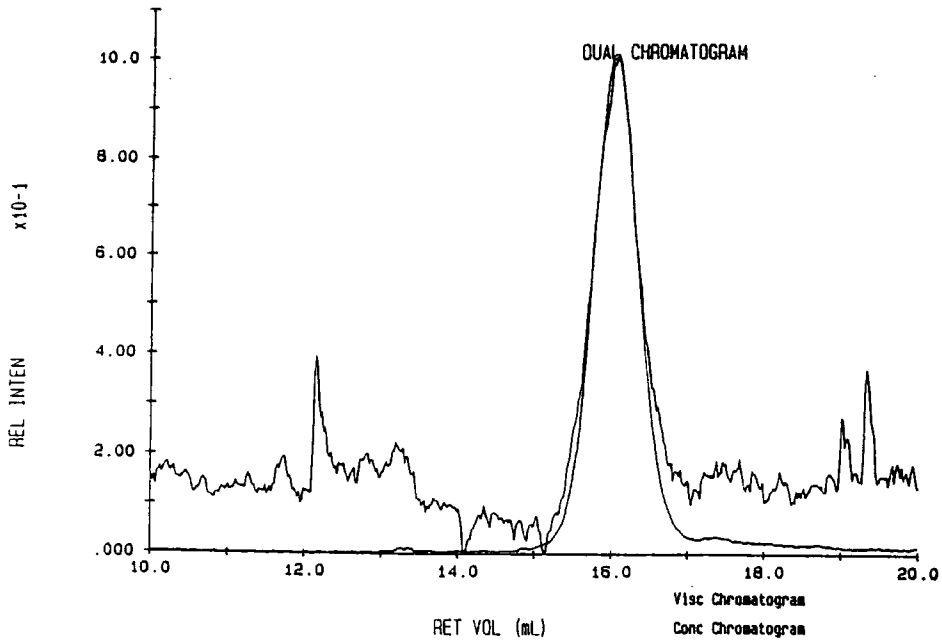

Appendix D19 : GPC trace of Poly 3S'' (*2-exo-3-endo-* repeat units, starting polymer).

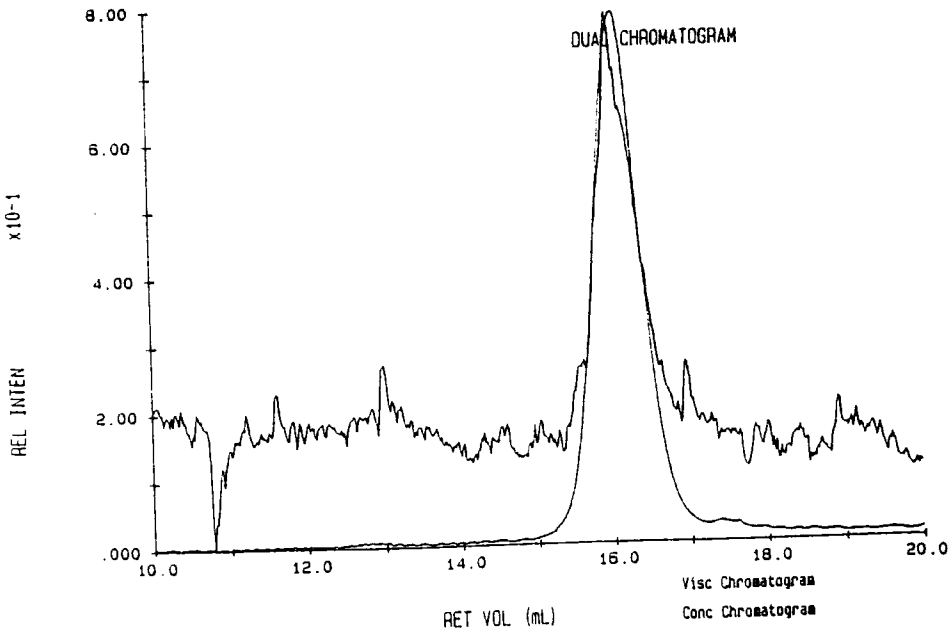

Appendix D20 : GPC trace of Poly 3P'' (*2-exo-3-endo-* repeat units, hydrogenated, precursor polymer).

APPENDIX E

CRYSTALLOGRAPHIC DATA

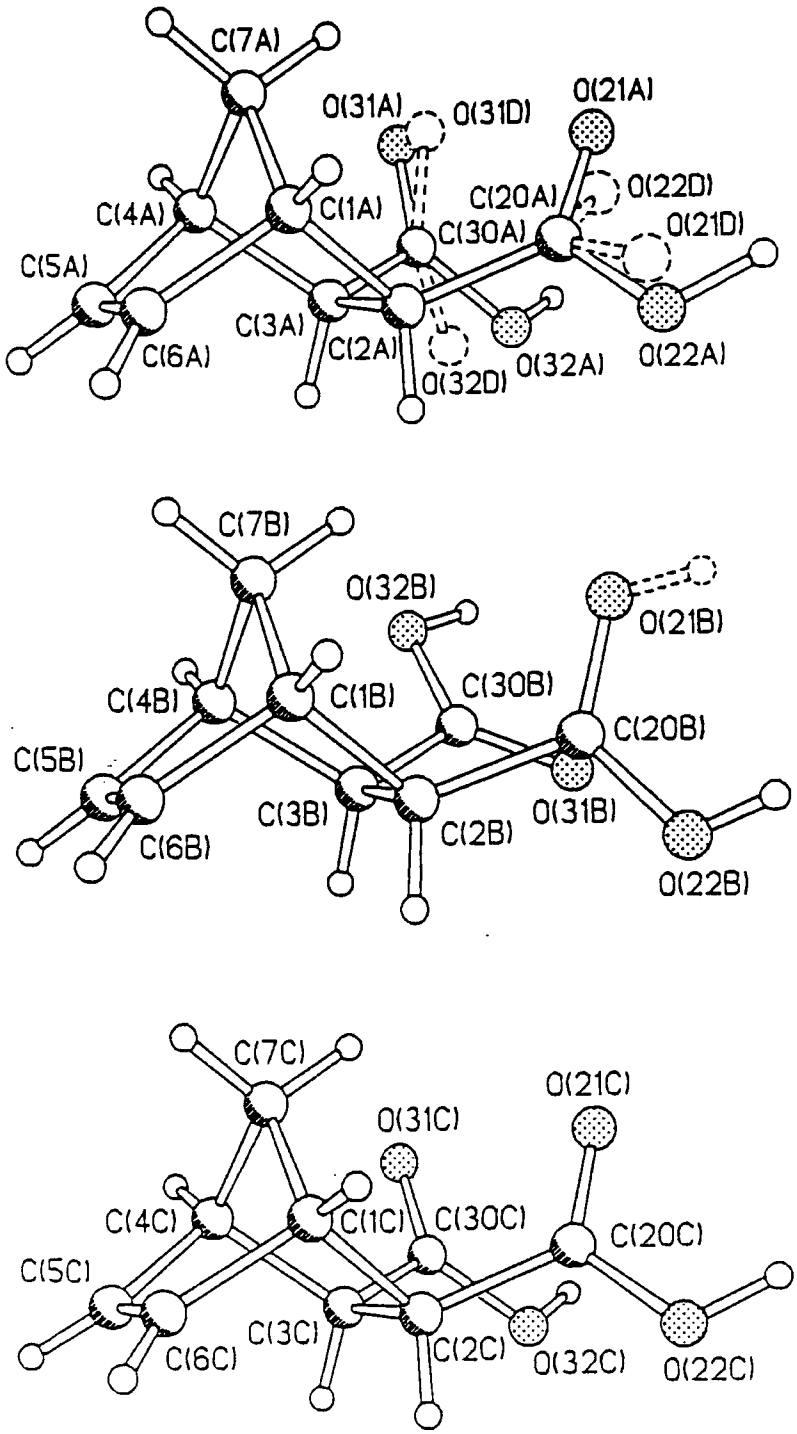

Appendix E1 : The crystal structures of *exo,exo*-bicyclo[2.2.1]hept-5-ene-2,3-dicarboxylic acid.

Table 1. Crystal data and structure refinement for 1.

Identification code	97srv123
Empirical formula	C9 H10 O4
Formula weight	182.17
Temperature	150(2) K
Wavelength	0.71073 A
Crystal system	Triclinic
Space group	P-1
Unit cell dimensions	a = 11.305(1) A alpha = 114.22(1) deg b = 11.505(1) A beta = 97.44(1) deg. c = 11.725(1) A gamma = 101.93(1) deg
Volume	1320.9(3) A^3
Z	6
Density (calculated)	1.374 g/cm^3
Absorption coefficient	0.109 mm^-1
F(000)	576
Crystal size	0.4 x 0.3 x 0.2 mm
Theta range for data collection	1.9 to 27.5 deg.
Index ranges	-14<=h<=12, -14<=k<=14, -10<=l<=15
Reflections collected	9582
Independent reflections	5970 [R(int) = 0.0236]
Observed reflections, I>2sigma(I)	4833
Absorption correction	None
Refinement method	Full-matrix least-squares on F^2
Data / restraints / parameters	5923 / 0 / 493
Goodness-of-fit on F^2	1.153
Final R indices [I>2sigma(I)]	R1 = 0.0487, wR2 = 0.0908
R indices (all data)	R1 = 0.0673, wR2 = 0.1122
Extinction coefficient	0.0201(9)
Largest diff. peak and hole	0.313 and -0.206 e.A^-3

Table 2. Atomic coordinates (x 10^4) and equivalent isotropic displacement parameters (A^2 x 10^3) for 1. U(eq) is defined as one third of the trace of the orthogonalized Uij tensor.

	x	y	z	U(eq)
C(1A)	2072(2)	2594(2)	8860(2)	21.4(4)
C(2A)	1386(2)	1421(2)	7477(2)	21.3(4)
C(3A)	1275(2)	2203(2)	6651(2)	22.9(4)
C(4A)	1906(2)	3685(2)	7663(2)	24.6(4)
C(5A)	1019(2)	3988(2)	8544(2)	28.0(4)
C(6A)	1112(2)	3341(2)	9253(2)	24.8(4)
C(7A)	2962(2)	3540(2)	8518(2)	22.4(4)
C(20A)	2108(2)	417(2)	7056(2)	25.5(4)
O(21A)	3036(2)	561(2)	6631(2)	34.5(4)
O(22A)	1684(3)	-634(3)	7256(3)	35.1(5)
O(21D)	2058(28)	-343(34)	7476(34)	33(9)
O(22D)	2532(23)	295(24)	6053(23)	42(6)
C(30A)	1825(2)	1745(2)	5489(2)	26.9(4)
O(31A)	2758(3)	2413(3)	5384(3)	23.7(5)
O(32A)	1171(2)	542(2)	4587(2)	42.6(5)
O(31D)	2920(41)	2202(42)	5290(44)	31(11)
O(32D)	892(21)	1067(23)	4452(22)	36(6)
C(1B)	2612(2)	4284(2)	2690(2)	25.9(4)
C(2B)	2782(2)	4912(2)	4200(2)	21.2(4)
C(3B)	3808(2)	6273(2)	4664(2)	21.0(4)
C(4B)	4140(2)	6186(2)	3383(2)	23.4(4)
C(5B)	4715(2)	5037(2)	2901(2)	27.2(4)
C(6B)	3809(2)	3914(2)	2479(2)	28.1(4)
C(7B)	2840(2)	5528(2)	2461(2)	27.3(4)
C(20B)	1557(2)	4999(2)	4554(2)	24.4(4)
O(21B)	903(2)	5573(2)	4151(2)	38.5(4)
O(22B)	1225(2)	4410(2)	5225(2)	42.4(4)
C(30B)	3415(2)	7495(2)	5424(2)	25.5(4)
O(31B)	3015(2)	7634(2)	6380(1)	36.1(4)
O(32B)	3584(2)	8408(2)	5010(2)	34.8(4)
C(1C)	3848(2)	-1663(2)	1277(2)	29.6(4)
C(2C)	3609(2)	-329(2)	1356(2)	22.4(4)
C(3C)	2739(2)	-842(2)	-17(2)	21.2(4)
C(4C)	2599(2)	-2364(2)	-668(2)	26.2(4)
C(5C)	3889(2)	-2461(2)	-855(2)	33.0(4)
C(6C)	4626(2)	-2050(2)	294(2)	35.8(5)
C(7C)	2574(2)	-2665(2)	491(2)	30.2(5)
C(20C)	3038(2)	276(2)	2470(2)	23.4(4)
O(21C)	1994(1)	-257(2)	2502(1)	38.9(4)
O(22C)	3769(1)	1386(1)	3419(1)	31.4(3)
C(30C)	1508(2)	-518(2)	-8(2)	21.1(4)
O(31C)	492(1)	-1358(1)	-484(1)	25.6(3)
O(32C)	1651(1)	778(1)	534(1)	28.0(5)

Table 3. Bond lengths [A] and angles [deg] for 1.

C(1A)-C(6A)	1.523(3)	C(1A)-C(7A)	1.538(3)
C(1A)-C(2A)	1.581(2)	C(1A)-H(1A)	0.96(2)
C(2A)-C(20A)	1.507(3)	C(2A)-C(3A)	1.577(3)
C(2A)-H(2A)	0.95(2)	C(3A)-C(30A)	1.512(3)
C(3A)-C(4A)	1.563(3)	C(3A)-H(3A)	0.98(2)
C(4A)-C(5A)	1.521(3)	C(4A)-C(7A)	1.538(3)
C(4A)-H(4A)	0.97(2)	C(5A)-C(6A)	1.331(3)
C(5A)-H(5A)	0.96(2)	C(6A)-H(6A)	0.99(2)
C(7A)-H(71A)	1.01(2)	C(7A)-H(72A)	1.00(2)
C(20A)-O(21D)	1.16(4)	C(20A)-O(21A)	1.227(3)
C(20A)-O(22D)	1.29(2)	C(20A)-O(22A)	1.330(3)
O(22A)-H(22A)	0.98(3)	C(30A)-O(31A)	1.223(4)
C(30A)-O(32D)	1.32(2)	C(30A)-O(32A)	1.324(3)
C(30A)-O(31D)	1.33(5)	O(32A)-H(32A)	0.92(4)
C(1B)-C(6B)	1.521(3)	C(1B)-C(7B)	1.539(3)
C(1B)-C(2B)	1.580(3)	C(1B)-H(1B)	0.98(2)
C(2B)-C(20B)	1.508(3)	C(2B)-C(3B)	1.574(3)
C(2B)-H(2B)	0.98(2)	C(3B)-C(30B)	1.516(3)
C(3B)-C(4B)	1.564(3)	C(3B)-H(3B)	0.97(2)
C(4B)-C(5B)	1.525(3)	C(4B)-C(7B)	1.536(3)
C(4B)-H(4B)	0.97(2)	C(5B)-C(6B)	1.327(3)
C(5B)-H(5B)	0.95(2)	C(6B)-H(6B)	0.98(2)
C(7B)-H(71B)	1.00(2)	C(7B)-H(72B)	0.97(2)
C(20B)-O(21B)	1.254(2)	C(20B)-O(22B)	1.275(2)
O(21B)-H(21B)	0.81(7)	O(22B)-H(22B)	0.79(5)
C(30B)-O(31B)	1.225(2)	C(30B)-O(32B)	1.317(2)
O(32B)-H(32B)	0.92(3)	C(1C)-C(6C)	1.517(3)
C(1C)-C(7C)	1.533(3)	C(1C)-C(2C)	1.581(3)
C(1C)-H(1C)	0.97(2)	C(2C)-C(20C)	1.506(3)
C(2C)-C(3C)	1.574(3)	C(2C)-H(2C)	0.96(2)
C(3C)-C(30C)	1.513(2)	C(3C)-C(4C)	1.559(3)
C(3C)-H(3C)	0.97(2)	C(4C)-C(5C)	1.522(3)
C(4C)-C(7C)	1.537(3)	C(4C)-H(4C)	0.99(2)
C(5C)-C(6C)	1.326(3)	C(5C)-H(5C)	0.96(2)
C(6C)-H(6C)	0.96(3)	C(7C)-H(71C)	0.99(3)
C(7C)-H(72C)	1.01(2)	C(20C)-O(21C)	1.226(2)
C(20C)-O(22C)	1.308(2)	O(22C)-H(22C)	0.92(3)
C(30C)-O(31C)	1.224(2)	C(30C)-O(32C)	1.322(2)
O(32C)-H(32C)	0.93(3)		

C(6A)-C(1A)-C(7A)	101.2(2)	C(6A)-C(1A)-C(2A)	104.0(2)
C(7A)-C(1A)-C(2A)	101.13(14)	C(6A)-C(1A)-H(1A)	115.7(12)
C(7A)-C(1A)-H(1A)	117.8(13)	C(2A)-C(1A)-H(1A)	114.7(13)
C(20A)-C(2A)-C(3A)	115.6(2)	C(20A)-C(2A)-C(1A)	110.8(2)
C(3A)-C(2A)-C(1A)	101.62(14)	C(20A)-C(2A)-H(2A)	106.9(12)
C(3A)-C(2A)-H(2A)	111.0(12)	C(1A)-C(2A)-H(2A)	110.8(11)
C(30A)-C(3A)-C(4A)	114.3(2)	C(30A)-C(3A)-C(2A)	114.4(2)
C(4A)-C(3A)-C(2A)	103.02(14)	C(30A)-C(3A)-H(3A)	104.6(12)
C(4A)-C(3A)-H(3A)	111.8(12)	C(2A)-C(3A)-H(3A)	108.9(12)
C(5A)-C(4A)-C(7A)	100.9(2)	C(5A)-C(4A)-C(3A)	103.9(2)
C(7A)-C(4A)-C(3A)	101.1(2)	C(5A)-C(4A)-H(4A)	117.9(13)
C(7A)-C(4A)-H(4A)	117.1(13)	C(3A)-C(4A)-H(4A)	113.6(13)
C(6A)-C(5A)-C(4A)	107.9(2)	C(6A)-C(5A)-H(5A)	127.2(14)
C(4A)-C(5A)-H(5A)	124.4(14)	C(5A)-C(6A)-C(1A)	107.2(2)
C(5A)-C(6A)-H(6A)	128.4(13)	C(1A)-C(6A)-H(6A)	123.9(13)
C(1A)-C(7A)-C(4A)	93.91(14)	C(1A)-C(7A)-H(71A)	112.1(12)
C(4A)-C(7A)-H(71A)	112.3(12)	C(1A)-C(7A)-H(72A)	113.8(12)
C(4A)-C(7A)-H(72A)	113.1(12)	H(71A)-C(7A)-H(72A)	111(2)
O(21D)-C(20A)-O(22D)	124(2)	O(21A)-C(20A)-O(22A)	122.1(2)
O(21D)-C(20A)-C(2A)	119(2)	O(21A)-C(20A)-C(2A)	124.6(2)

O(22D)-C(20A)-C(2A)	115.6(11)	O(22A)-C(20A)-C(2A)	113.2(2)
C(20A)-O(22A)-H(22A)	108(2)	C(20A)-O(21D)-H(22A)	120(4)
O(31A)-C(30A)-O(32A)	123.7(2)	O(32D)-C(30A)-O(31D)	116(2)
O(31A)-C(30A)-C(3A)	124.0(2)	O(32D)-C(30A)-C(3A)	107.7(10)
O(32A)-C(30A)-C(3A)	112.3(2)	O(31D)-C(30A)-C(3A)	133(2)
C(30A)-O(32A)-H(32A)	112(2)	C(30A)-O(32D)-H(32A)	94(2)
C(6B)-C(1B)-C(7B)	100.3(2)	C(6B)-C(1B)-C(2B)	104.3(2)
C(7B)-C(1B)-C(2B)	101.9(2)	C(6B)-C(1B)-H(1B)	117.2(13)
C(7B)-C(1B)-H(1B)	118.7(13)	C(2B)-C(1B)-H(1B)	112.3(13)
C(20B)-C(2B)-C(3B)	116.3(2)	C(20B)-C(2B)-C(1B)	111.0(2)
C(3B)-C(2B)-C(1B)	101.73(14)	C(20B)-C(2B)-H(2B)	107.6(12)
C(3B)-C(2B)-H(2B)	109.5(12)	C(1B)-C(2B)-H(2B)	110.6(12)
C(30B)-C(3B)-C(4B)	114.7(2)	C(30B)-C(3B)-C(2B)	114.5(2)
C(4B)-C(3B)-C(2B)	102.87(14)	C(30B)-C(3B)-H(3B)	103.6(13)
C(4B)-C(3B)-H(3B)	111.5(13)	C(2B)-C(3B)-H(3B)	109.8(13)
C(5B)-C(4B)-C(7B)	100.4(2)	C(5B)-C(4B)-C(3B)	106.0(2)
C(7B)-C(4B)-C(3B)	100.4(2)	C(5B)-C(4B)-H(4B)	117.1(12)
C(7B)-C(4B)-H(4B)	118.3(13)	C(3B)-C(4B)-H(4B)	112.6(12)
C(6B)-C(5B)-C(4B)	107.7(2)	C(6B)-C(5B)-H(5B)	128.3(13)
C(4B)-C(5B)-H(5B)	123.8(13)	C(5B)-C(6B)-C(1B)	107.4(2)
C(5B)-C(6B)-H(6B)	128.4(14)	C(1B)-C(6B)-H(6B)	123.8(14)
C(4B)-C(7B)-C(1B)	93.9(2)	C(4B)-C(7B)-H(71B)	111.8(12)
C(1B)-C(7B)-H(71B)	113.9(12)	C(4B)-C(7B)-H(72B)	112.4(13)
C(1B)-C(7B)-H(72B)	112.0(13)	H(71B)-C(7B)-H(72B)	112(2)
O(21B)-C(20B)-O(22B)	123.7(2)	O(21B)-C(20B)-C(2B)	120.5(2)
O(22B)-C(20B)-C(2B)	115.8(2)	C(20B)-O(21B)-H(21B)	113(4)
C(20B)-O(22B)-H(22B)	113(3)	O(31B)-C(30B)-O(32B)	123.0(2)
O(31B)-C(30B)-C(3B)	121.9(2)	O(32B)-C(30B)-C(3B)	115.0(2)
C(30B)-O(32B)-H(32B)	109(2)	C(6C)-C(1C)-C(7C)	100.9(2)
C(6C)-C(1C)-C(2C)	105.5(2)	C(7C)-C(1C)-C(2C)	101.0(2)
C(6C)-C(1C)-H(1C)	115.8(14)	C(7C)-C(1C)-H(1C)	120.7(14)
C(2C)-C(1C)-H(1C)	111.0(14)	C(20C)-C(2C)-C(3C)	115.2(2)
C(20C)-C(2C)-C(1C)	109.9(2)	C(3C)-C(2C)-C(1C)	101.1(2)
C(20C)-C(2C)-H(2C)	108.6(12)	C(3C)-C(2C)-H(2C)	110.8(13)
C(1C)-C(2C)-H(2C)	111.1(13)	C(30C)-C(3C)-C(4C)	113.6(2)
C(30C)-C(3C)-C(2C)	114.8(2)	C(4C)-C(3C)-C(2C)	103.5(2)
C(30C)-C(3C)-H(3C)	103.5(12)	C(4C)-C(3C)-H(3C)	112.4(12)
C(2C)-C(3C)-H(3C)	109.3(12)	C(5C)-C(4C)-C(7C)	100.4(2)
C(5C)-C(4C)-C(3C)	104.8(2)	C(7C)-C(4C)-C(3C)	100.7(2)
C(5C)-C(4C)-H(4C)	117.1(13)	C(7C)-C(4C)-H(4C)	118.4(13)
C(3C)-C(4C)-H(4C)	113.3(13)	C(6C)-C(5C)-C(4C)	107.8(2)
C(6C)-C(5C)-H(5C)	128.8(14)	C(4C)-C(5C)-H(5C)	123.1(14)
C(5C)-C(6C)-C(1C)	107.3(2)	C(5C)-C(6C)-H(6C)	127(2)
C(1C)-C(6C)-H(6C)	126(2)	C(1C)-C(7C)-C(4C)	93.9(2)
C(1C)-C(7C)-H(71C)	110.6(14)	C(4C)-C(7C)-H(71C)	111.3(14)
C(1C)-C(7C)-H(72C)	113.8(12)	C(4C)-C(7C)-H(72C)	114.3(12)
H(71C)-C(7C)-H(72C)	112(2)	O(21C)-C(20C)-O(22C)	123.0(2)
O(21C)-C(20C)-C(2C)	122.5(2)	O(22C)-C(20C)-C(2C)	114.4(2)
C(20C)-O(22C)-H(22C)	112(2)	O(31C)-C(30C)-O(32C)	123.6(2)
O(31C)-C(30C)-C(3C)	123.9(2)	O(32C)-C(30C)-C(3C)	112.5(2)
C(30C)-O(32C)-H(32C)	110(2)		

able 4. Anisotropic displacement parameters (A^2 x 10^3) for 1.
he anisotropic displacement factor exponent takes the form:
2 pi^2 [h^2 a*^2 U11 + ... + 2 h k a* b* U12]

	U11	U22	U33	U23	U13	U12
:(1A)	23(1)	22(1)	17(1)	7(1)	4(1)	5(1)
:(2A)	20(1)	20(1)	21(1)	7(1)	6(1)	4(1)
:(3A)	19(1)	26(1)	18(1)	8(1)	1(1)	3(1)
:(4A)	28(1)	22(1)	24(1)	11(1)	6(1)	7(1)
:(5A)	26(1)	24(1)	29(1)	6(1)	5(1)	10(1)
:(6A)	24(1)	24(1)	20(1)	4(1)	9(1)	5(1)
:(7A)	21(1)	20(1)	20(1)	5(1)	4(1)	4(1)
:(20A)	31(1)	18(1)	22(1)	5(1)	5(1)	5(1)
)(21A)	33(1)	23(1)	49(1)	13(1)	19(1)	11(1)
)(22A)	50(2)	28(1)	40(1)	21(1)	24(1)	17(1)
:(30A)	25(1)	30(1)	18(1)	8(1)	0(1)	1(1)
)(31A)	23(1)	22(1)	25(1)	9(1)	8(1)	7(1)
)(32A)	37(1)	43(1)	20(1)	-2(1)	9(1)	-14(1)
:(1B)	25(1)	23(1)	23(1)	6(1)	6(1)	3(1)
:(2B)	21(1)	22(1)	25(1)	13(1)	8(1)	9(1)
:(3B)	21(1)	21(1)	22(1)	9(1)	5(1)	8(1)
:(4B)	26(1)	20(1)	25(1)	10(1)	11(1)	7(1)
:(5B)	27(1)	27(1)	31(1)	13(1)	14(1)	10(1)
:(6B)	33(1)	23(1)	30(1)	10(1)	15(1)	11(1)
:(7B)	32(1)	31(1)	20(1)	11(1)	7(1)	11(1)
:(20B)	24(1)	28(1)	26(1)	15(1)	9(1)	10(1)
)(21B)	31(1)	58(1)	56(1)	42(1)	23(1)	27(1)
)(22B)	35(1)	69(1)	60(1)	52(1)	28(1)	28(1)
:(30B)	28(1)	24(1)	23(1)	9(1)	5(1)	9(1)
)(31B)	58(1)	32(1)	29(1)	16(1)	22(1)	24(1)
)(32B)	51(1)	27(1)	40(1)	20(1)	24(1)	22(1)
:(1C)	32(1)	31(1)	29(1)	16(1)	2(1)	13(1)
:(2C)	20(1)	22(1)	25(1)	10(1)	5(1)	4(1)
:(3C)	22(1)	24(1)	22(1)	12(1)	7(1)	9(1)
C(4C)	26(1)	24(1)	27(1)	8(1)	6(1)	12(1)
C(5C)	34(1)	33(1)	36(1)	12(1)	14(1)	20(1)
C(6C)	30(1)	37(1)	45(1)	17(1)	9(1)	20(1)
C(7C)	34(1)	21(1)	37(1)	14(1)	7(1)	9(1)
C(20C)	24(1)	22(1)	23(1)	11(1)	3(1)	4(1)
O(21C)	29(1)	42(1)	24(1)	1(1)	10(1)	-8(1)
O(22C)	27(1)	24(1)	28(1)	2(1)	6(1)	-2(1)
C(30C)	24(1)	22(1)	21(1)	12(1)	7(1)	8(1)
O(31C)	22(1)	22(1)	32(1)	10(1)	6(1)	7(1)
O(32C)	23(1)	20(1)	40(1)	12(1)	8(1)	8(1)

Table 5. Hydrogen coordinates (x 10^4) and isotropic displacement parameters (A^2 x 10^3) for 1.

	x	y	z	U(eq)
H(1A)	2425(19)	2320(21)	9462(20)	26(5)
H(2A)	587(18)	961(19)	7479(18)	16(5)
H(3A)	392(20)	2044(20)	6293(19)	23(5)
H(4A)	2143(20)	4278(22)	7280(21)	29(6)
H(5A)	427(22)	4460(23)	8493(22)	37(6)
H(6A)	588(21)	3234(22)	9841(21)	31(6)
H(71A)	3425(20)	4409(22)	9300(21)	29(6)
H(72A)	3553(19)	3131(21)	8035(20)	25(5)
H(22A)	2219(31)	-1218(33)	6977(31)	66(10)
H(32A)	1464(33)	304(35)	3850(36)	81(12)
H(1B)	1824(21)	3574(22)	2225(21)	30(6)
H(2B)	3105(19)	4367(20)	4544(19)	22(5)
H(3B)	4521(21)	6333(21)	5265(21)	28(6)
H(4B)	4617(20)	7037(22)	3477(20)	26(5)
H(5B)	5585(21)	5153(21)	2986(20)	27(6)
H(6B)	3876(22)	3003(25)	2182(23)	42(7)
H(71B)	2257(20)	6067(21)	2753(20)	26(5)
H(72B)	2868(20)	5315(22)	1573(22)	31(6)
H(21B)	238(60)	5520(55)	4346(55)	30(15)
H(22B)	532(49)	4366(45)	5293(44)	42(13)
H(32B)	3406(28)	9143(31)	5573(29)	69(9)
H(1C)	4207(21)	-1555(23)	2123(23)	35(6)
H(2C)	4369(20)	302(21)	1473(20)	24(5)
H(3C)	3136(18)	-394(19)	-468(19)	18(5)
H(4C)	1897(22)	-2874(23)	-1435(23)	36(6)
H(5C)	4101(21)	-2705(23)	-1677(23)	36(6)
H(6C)	5511(24)	-1915(24)	491(24)	44(7)
H(71C)	2605(22)	-3587(25)	268(23)	43(7)
H(72C)	1865(20)	-2460(21)	914(20)	27(6)
H(22C)	3395(30)	1711(32)	4095(32)	75(10)
H(32C)	873(28)	930(28)	495(27)	63(9)

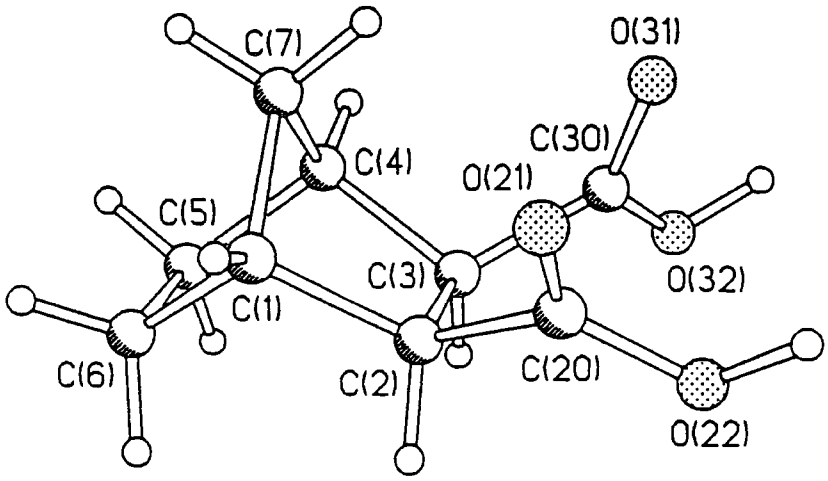

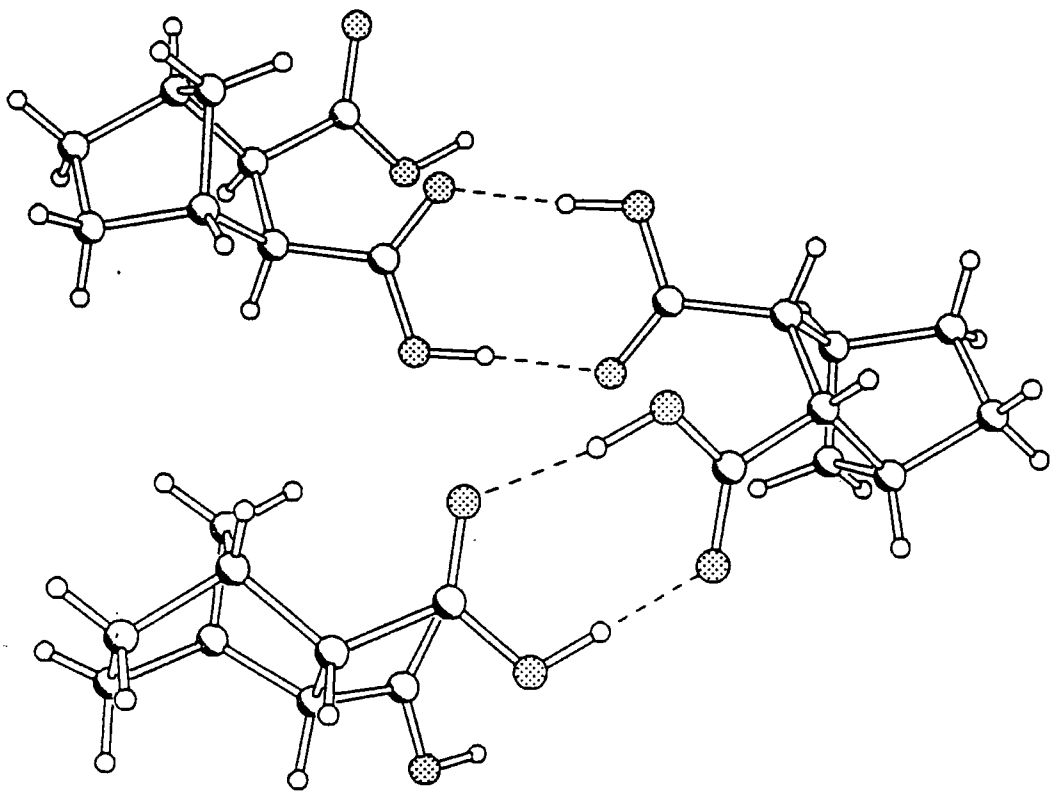

Appendix E2 : The crystal structure of *exo,exo*-bicyclo[2.2.1]heptane-2,3-dicarboxylic acid.

Table 1. Crystal data and structure refinement for 1.

Identification code	97srv127
Empirical formula	C9 H12 O4
Formula weight	184.19
Temperature	295(2) K
Wavelength	0.71073 A
Crystal system	Monoclinic
Space group	C2/c
Unit cell dimensions	a = 15.358(1) A alpha = 90 deg. b = 11.526(1) A beta = 107.57(1) deg. c = 10.664(1) A gamma = 90 deg.
Volume	1799.6(3) A^3
Z	8
Density (calculated)	1.360 g/cm^3
Absorption coefficient	0.107 mm^-1
F(000)	784
Crystal size	0.40 x 0.26 x 0.22 mm
Theta range for data collection	2.25 to 30.25 deg.
Index ranges	-18<=h<=21, -15<=k<=16, -15<=l<=15
Reflections collected	7010
Independent reflections	2481 [R(int) = 0.0298]
Observed reflections, I>2sigma(I)	1964
Absorption correction	None
Refinement method	Full-matrix least-squares on F^2
Data / restraints / parameters	2464 / 0 / 167
Goodness-of-fit on F^2	1.122
Final R indices [I>2sigma(I)]	R1 = 0.0457, wR2 = 0.1013
R indices (all data)	R1 = 0.0623, wR2 = 0.1259
Extinction coefficient	0.017(1)
Largest diff. peak and hole	0.273 and -0.171 e.A^-3

Table 2. Atomic coordinates (x 10^4) and equivalent isotropic displacement parameters (A^2 x 10^3) for 1. U(eq) is defined as one third of the trace of the orthogonalized Uij tensor.

	x	y	z	U(eq)
C(1)	2867(1)	2162(2)	8281(2)	46.2(4)
C(2)	2086(1)	2493(1)	7042(1)	36.3(3)
C(3)	2042(1)	1433(1)	6098(1)	36.1(3)
C(4)	2796(1)	623(2)	6954(2)	48.8(4)
C(5)	3725(1)	1166(2)	7035(2)	60.6(5)
C(6)	3769(1)	2237(2)	7930(2)	56.8(5)
C(7)	2736(1)	851(2)	8344(2)	54.5(5)
C(20)	1184(1)	2769(1)	7278(1)	39.5(3)
O(21)	1097(1)	2775(1)	8395(1)	55.8(4)
O(22)	532(1)	3040(1)	6226(1)	56.0(4)
C(30)	1137(1)	805(1)	5637(1)	37.1(3)
O(31)	721(1)	491(1)	6396(1)	58.5(4)
O(32)	865(1)	600(1)	4382(1)	58.4(4)

Table 3. Bond lengths [A] and angles [deg] for 1.

C(1)-C(7)	1.529(3)	C(1)-C(2)	1.541(2)
C(1)-C(6)	1.543(2)	C(1)-H(1)	0.96(2)
C(2)-C(20)	1.515(2)	C(2)-C(3)	1.571(2)
C(2)-H(2)	0.99(2)	C(3)-C(30)	1.511(2)
C(3)-C(4)	1.552(2)	C(3)-H(3)	0.99(2)
C(4)-C(7)	1.535(3)	C(4)-C(5)	1.537(2)
C(4)-H(4)	1.00(2)	C(5)-C(6)	1.550(3)
C(5)-H(51)	1.01(2)	C(5)-H(52)	0.99(2)
C(6)-H(61)	0.96(2)	C(6)-H(62)	1.00(2)
C(7)-H(71)	0.97(2)	C(7)-H(72)	1.00(2)
C(20)-O(21)	1.239(2)	C(20)-O(22)	1.297(2)
O(22)-H(22)	0.98(3)	C(30)-O(31)	1.228(2)
C(30)-O(32)	1.297(2)	O(32)-H(32)	0.96(3)
C(7)-C(1)-C(2)	101.75(12)	C(7)-C(1)-C(6)	101.9(2)
C(2)-C(1)-C(6)	107.54(13)	C(7)-C(1)-H(1)	116.2(12)
C(2)-C(1)-H(1)	112.7(12)	C(6)-C(1)-H(1)	115.3(12)
C(20)-C(2)-C(1)	115.05(12)	C(20)-C(2)-C(3)	113.93(11)
C(1)-C(2)-C(3)	103.26(13)	C(20)-C(2)-H(2)	103.7(10)
C(1)-C(2)-H(2)	112.1(10)	C(3)-C(2)-H(2)	108.9(10)
C(30)-C(3)-C(4)	110.66(13)	C(30)-C(3)-C(2)	115.99(12)
C(4)-C(3)-C(2)	102.13(12)	C(30)-C(3)-H(3)	106.7(10)
C(4)-C(3)-H(3)	110.7(10)	C(2)-C(3)-H(3)	110.6(10)
C(7)-C(4)-C(5)	101.6(2)	C(7)-C(4)-C(3)	102.36(14)
C(5)-C(4)-C(3)	107.66(14)	C(7)-C(4)-H(4)	119.0(12)
C(5)-C(4)-H(4)	113.6(12)	C(3)-C(4)-H(4)	111.4(12)
C(4)-C(5)-C(6)	103.0(2)	C(4)-C(5)-H(51)	108.4(14)
C(6)-C(5)-H(51)	110.3(14)	C(4)-C(5)-H(52)	112.4(13)
C(6)-C(5)-H(52)	112.8(14)	H(51)-C(5)-H(52)	110(2)
C(1)-C(6)-C(5)	103.28(14)	C(1)-C(6)-H(61)	109.8(13)
C(5)-C(6)-H(61)	110.7(14)	C(1)-C(6)-H(62)	111.1(12)
C(5)-C(6)-H(62)	112.8(12)	H(61)-C(6)-H(62)	109(2)
C(1)-C(7)-C(4)	94.59(13)	C(1)-C(7)-H(71)	112.8(13)
C(4)-C(7)-H(71)	112.2(13)	C(1)-C(7)-H(72)	113.9(11)
C(4)-C(7)-H(72)	114.2(11)	H(71)-C(7)-H(72)	109(2)
O(21)-C(20)-O(22)	123.51(14)	O(21)-C(20)-C(2)	122.06(13)
O(22)-C(20)-C(2)	114.39(13)	C(20)-O(22)-H(22)	110(2)
O(31)-C(30)-O(32)	123.83(13)	O(31)-C(30)-C(3)	122.49(13)
O(32)-C(30)-C(3)	113.65(12)	C(30)-O(32)-H(32)	110(2)

able 4. Anisotropic displacement parameters (A^2 x 10^3) for 1.
he anisotropic displacement factor exponent takes the form:
2 pi^2 [h^2 a*^2 U11 + ... + 2 h k a* b* U12]

	U11	U22	U33	U23	U13	U12
:(1)	35(1)	67(1)	33(1)	1(1)	4(1)	-10(1)
:(2)	35(1)	41(1)	32(1)	-1(1)	9(1)	-9(1)
:(3)	33(1)	42(1)	35(1)	0(1)	12(1)	-7(1)
:(4)	37(1)	47(1)	60(1)	5(1)	12(1)	0(1)
:(5)	34(1)	81(1)	67(1)	4(1)	15(1)	0(1)
:(6)	33(1)	81(1)	51(1)	4(1)	4(1)	-16(1)
:(7)	38(1)	70(1)	50(1)	24(1)	6(1)	-2(1)
:(20)	39(1)	43(1)	35(1)	-3(1)	10(1)	-7(1)
)(21)	44(1)	87(1)	37(1)	-11(1)	13(1)	-6(1)
)(22)	42(1)	80(1)	45(1)	13(1)	11(1)	8(1)
:(30)	37(1)	39(1)	35(1)	-1(1)	11(1)	-7(1)
)(31)	53(1)	83(1)	41(1)	-5(1)	16(1)	-35(1)
)(32)	53(1)	84(1)	39(1)	-15(1)	16(1)	-30(1)

Table 5. Hydrogen coordinates (x 10^4) and isotropic displacement parameters (A^2 x 10^3) for 1.

	x	y	z	U(eq)
H(1)	2852(13)	2598(17)	9045(20)	59(5)
H(2)	2225(11)	3201(15)	6619(16)	43(4)
H(3)	2192(11)	1680(14)	5295(16)	40(4)
H(4)	2723(14)	-186(19)	6610(20)	63(6)
H(51)	4218(17)	596(21)	7475(23)	81(7)
H(52)	3775(15)	1374(21)	6160(23)	77(7)
H(61)	4278(16)	2179(19)	8717(22)	71(6)
H(62)	3812(14)	2987(19)	7478(20)	65(6)
H(71)	3228(16)	478(18)	9018(22)	69(6)
H(72)	2141(14)	621(16)	8473(19)	58(5)
H(22)	-59(22)	3048(27)	6409(28)	123(11)
H(32)	291(21)	205(26)	4153(28)	110(9)

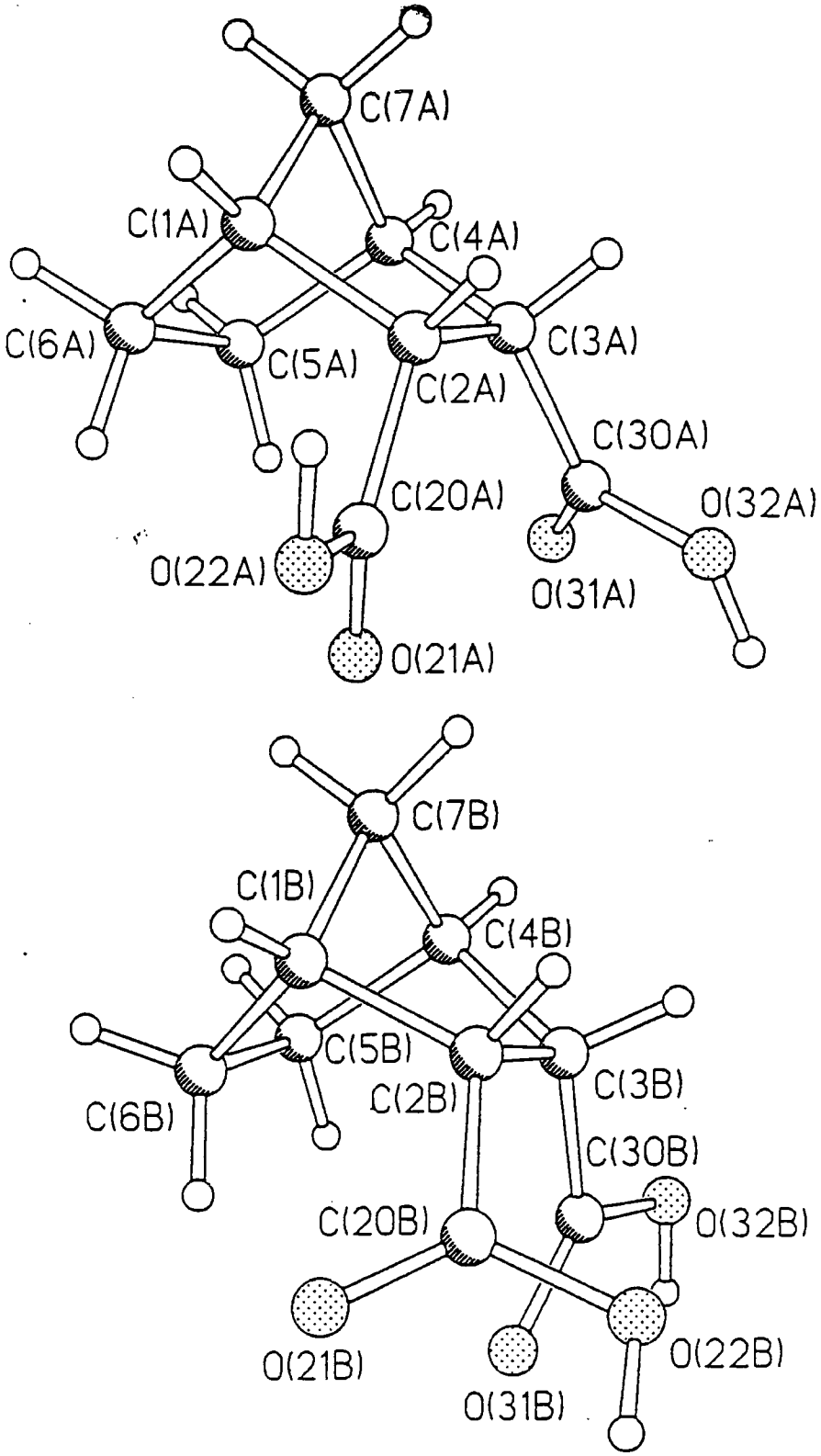

Appendix E3 : The crystal structures of *endo,endo*-bicyclo[2.2.1]heptane-2,3-dicarboxylic acid.

Table 1. Crystal data and structure refinement for 1.

Identification code	97srv129
Empirical formula	C9 H12 O4
Formula weight	184.19
Temperature	150(2) K
Wavelength	0.71073 A
Crystal system	Monoclinic
Space group	P2(1)/c
Unit cell dimensions	a = 20.778(1) A alpha = 90 deg. b = 9.329(1) A beta = 92.59(1) deg. c = 9.021(1) A gamma = 90 deg.
Volume	1746.8(3) A^3
Z	8
Density (calculated)	1.401 g/cm^3
Absorption coefficient	0.110 mm^-1
F(000)	784
Crystal size	0.45 x 0.35 x 0.15 mm
Theta range for data collection	0.98 to 27.5 deg.
Index ranges	-27<=h<=29, -10<=k<=13, -12<=l<=12
Reflections collected	11797
Independent reflections	4003 [R(int) = 0.0472]
Observed reflections, I>2sigma(I)	3200
Absorption correction	None
Refinement method	Full-matrix least-squares on F^2
Data / restraints / parameters	3929 / 0 / 331
Goodness-of-fit on F^2	1.122
Final R indices [I>2sigma(I)]	R1 = 0.0452, wR2 = 0.1017
R indices (all data)	R1 = 0.0627, wR2 = 0.1236
Largest diff. peak and hole	.281 and -.341 e.A^-3

Table 2. Atomic coordinates (x 10^4) and equivalent isotropic displacement parameters (A^2 x 10^3) for 1. U(eq) is defined as one third of the trace of the orthogonalized Uij tensor.

	x	y	z	U(eq)
C(1A)	4250.3(8)	4493(2)	1298(2)	18.6(3)
C(2A)	3543.9(7)	4209(2)	1765(2)	15.7(3)
C(3A)	3355.4(7)	5683(2)	2462(2)	16.2(3)
C(4A)	3989.6(8)	6540(2)	2481(2)	17.8(3)
C(5A)	4505.5(8)	5849(2)	3541(2)	22.1(3)
C(6A)	4715.1(8)	4490(2)	2676(2)	24.8(3)
C(7A)	4222.8(8)	6105(2)	946(2)	21.1(3)
C(20A)	3524.5(8)	2933(2)	2783(2)	20.3(3)
O(21A)	3529.0(7)	3011(1)	4130(1)	28.0(3)
O(22A)	3530.2(7)	1643(1)	2149(2)	33.8(3)
C(30A)	2983.8(7)	5631(2)	3858(2)	18.2(3)
O(31A)	3158.8(5)	6224(1)	5023(1)	23.6(3)
O(32A)	2426.4(6)	4953(1)	3666(1)	25.5(3)
C(1B)	769.3(8)	4291(2)	9500(2)	20.8(3)
C(2B)	773.6(7)	5527(2)	8372(2)	17.9(3)
C(3B)	1483.6(8)	6089(2)	8518(2)	19.1(3)
C(4B)	1758.8(8)	5250(2)	9917(2)	24.6(3)
C(5B)	1910.2(9)	3695(2)	9467(2)	29.7(4)
C(6B)	1230.2(9)	3083(2)	9041(2)	25.4(4)
C(7B)	1151.6(8)	5013(2)	10800(2)	26.1(4)
C(20B)	475.0(8)	5231(2)	6849(2)	20.5(3)
O(21B)	203.0(6)	4102(1)	6523(1)	26.9(3)
O(22B)	482.4(6)	6352(1)	5953(1)	28.5(3)
C(30B)	1896.4(8)	5840(2)	7210(2)	20.5(3)
O(31B)	1757.4(5)	5046(1)	6167(1)	27.9(3)
O(32B)	2448.0(6)	6545(2)	7345(2)	30.4(3)

Table 3. Bond lengths [A] and angles [deg] for 1.

C(1A)-C(7A)	1.538(2)	C(1A)-C(6A)	1.540(2)
C(1A)-C(2A)	1.568(2)	C(1A)-H(1A)	0.99(2)
C(2A)-C(20A)	1.505(2)	C(2A)-C(3A)	1.569(2)
C(2A)-H(2A)	0.99(2)	C(3A)-C(30A)	1.507(2)
C(3A)-C(4A)	1.541(2)	C(3A)-H(3A)	0.97(2)
C(4A)-C(7A)	1.542(2)	C(4A)-C(5A)	1.545(2)
C(4A)-H(4A)	0.97(2)	C(5A)-C(6A)	1.561(2)
C(5A)-H(51A)	1.00(2)	C(5A)-H(52A)	1.01(2)
C(6A)-H(61A)	1.00(2)	C(6A)-H(62A)	0.98(2)
C(7A)-H(71A)	0.98(2)	C(7A)-H(72A)	0.99(2)
C(20A)-O(21A)	1.217(2)	C(20A)-O(22A)	1.333(2)
O(22A)-H(22A)	0.90(3)	C(30A)-O(31A)	1.228(2)
C(30A)-O(32A)	1.324(2)	O(32A)-H(32A)	0.95(3)
C(1B)-C(2B)	1.538(2)	C(1B)-C(7B)	1.542(2)
C(1B)-C(6B)	1.547(2)	C(1B)-H(1B)	0.99(2)
C(2B)-C(20B)	1.508(2)	C(2B)-C(3B)	1.566(2)
C(2B)-H(2B)	1.00(2)	C(3B)-C(30B)	1.508(2)
C(3B)-C(4B)	1.570(2)	C(3B)-H(3B)	0.98(2)
C(4B)-C(7B)	1.538(2)	C(4B)-C(5B)	1.543(3)
C(4B)-H(4B)	1.00(2)	C(5B)-C(6B)	1.556(3)
C(5B)-H(51B)	1.02(2)	C(5B)-H(52B)	1.02(2)
C(6B)-H(61B)	0.99(2)	C(6B)-H(62B)	0.96(2)
C(7B)-H(71B)	1.01(2)	C(7B)-H(72B)	0.99(2)
C(20B)-O(21B)	1.225(2)	C(20B)-O(22B)	1.322(2)
O(22B)-H(22B)	0.92(3)	C(30B)-O(31B)	1.222(2)
C(30B)-O(32B)	1.322(2)	O(32B)-H(32B)	0.93(3)

C(7A)-C(1A)-C(6A)	100.63(13)	C(7A)-C(1A)-C(2A)	101.19(12)
C(6A)-C(1A)-C(2A)	110.06(13)	C(7A)-C(1A)-H(1A)	115.7(11)
C(6A)-C(1A)-H(1A)	115.1(11)	C(2A)-C(1A)-H(1A)	112.7(11)
C(20A)-C(2A)-C(1A)	110.41(13)	C(20A)-C(2A)-C(3A)	115.74(13)
C(1A)-C(2A)-C(3A)	102.33(12)	C(20A)-C(2A)-H(2A)	109.8(11)
C(1A)-C(2A)-H(2A)	107.1(11)	C(3A)-C(2A)-H(2A)	110.9(11)
C(30A)-C(3A)-C(4A)	118.55(13)	C(30A)-C(3A)-C(2A)	116.96(13)
C(4A)-C(3A)-C(2A)	103.29(12)	C(30A)-C(3A)-H(3A)	102.7(11)
C(4A)-C(3A)-H(3A)	107.9(11)	C(2A)-C(3A)-H(3A)	106.7(11)
C(3A)-C(4A)-C(7A)	99.06(12)	C(3A)-C(4A)-C(5A)	111.08(13)
C(7A)-C(4A)-C(5A)	102.07(13)	C(3A)-C(4A)-H(4A)	113.4(10)
C(7A)-C(4A)-H(4A)	115.4(11)	C(5A)-C(4A)-H(4A)	114.3(10)
C(4A)-C(5A)-C(6A)	103.33(13)	C(4A)-C(5A)-H(51A)	112.0(10)
C(6A)-C(5A)-H(51A)	113.0(11)	C(4A)-C(5A)-H(52A)	109.3(11)
C(6A)-C(5A)-H(52A)	111.4(11)	H(51A)-C(5A)-H(52A)	108(2)
C(1A)-C(6A)-C(5A)	102.90(13)	C(1A)-C(6A)-H(61A)	112.4(11)
C(5A)-C(6A)-H(61A)	113.4(12)	C(1A)-C(6A)-H(62A)	110.2(12)
C(5A)-C(6A)-H(62A)	112.4(13)	H(61A)-C(6A)-H(62A)	106(2)
C(1A)-C(7A)-C(4A)	94.71(12)	C(1A)-C(7A)-H(71A)	113.1(12)
C(4A)-C(7A)-H(71A)	112.6(12)	C(1A)-C(7A)-H(72A)	111.4(12)
C(4A)-C(7A)-H(72A)	111.9(12)	H(71A)-C(7A)-H(72A)	112(2)
O(21A)-C(20A)-O(22A)	118.87(14)	O(21A)-C(20A)-C(2A)	124.26(14)
O(22A)-C(20A)-C(2A)	116.81(14)	C(20A)-O(22A)-H(22A)	111(2)
O(31A)-C(30A)-O(32A)	123.44(14)	O(31A)-C(30A)-C(3A)	123.87(14)
O(32A)-C(30A)-C(3A)	112.55(13)	C(30A)-O(32A)-H(32A)	108(2)
C(2B)-C(1B)-C(7B)	99.05(13)	C(2B)-C(1B)-C(6B)	110.33(13)
C(7B)-C(1B)-C(6B)	102.58(14)	C(2B)-C(1B)-H(1B)	112.0(11)
C(7B)-C(1B)-H(1B)	118.0(11)	C(6B)-C(1B)-H(1B)	113.6(11)
C(20B)-C(2B)-C(1B)	116.80(13)	C(20B)-C(2B)-C(3B)	119.04(13)
C(1B)-C(2B)-C(3B)	103.23(13)	C(20B)-C(2B)-H(2B)	102.5(11)
C(1B)-C(2B)-H(2B)	108.3(11)	C(3B)-C(2B)-H(2B)	106.3(11)
C(30B)-C(3B)-C(2B)	116.73(13)	C(30B)-C(3B)-C(4B)	110.67(13)
C(2B)-C(3B)-C(4B)	102.02(13)	C(30B)-C(3B)-H(3B)	106.5(11)

C(2B)-C(3B)-H(3B)	111.6(11)	C(4B)-C(3B)-H(3B)	109.2(11)
C(7B)-C(4B)-C(5B)	100.54(14)	C(7B)-C(4B)-C(3B)	102.15(13)
C(5B)-C(4B)-C(3B)	109.17(14)	C(7B)-C(4B)-H(4B)	117.0(13)
C(5B)-C(4B)-H(4B)	114.5(12)	C(3B)-C(4B)-H(4B)	112.2(12)
C(4B)-C(5B)-C(6B)	102.49(14)	C(4B)-C(5B)-H(51B)	113.0(13)
C(6B)-C(5B)-H(51B)	115.1(12)	C(4B)-C(5B)-H(52B)	108.6(13)
C(6B)-C(5B)-H(52B)	111.0(13)	H(51B)-C(5B)-H(52B)	107(2)
C(1B)-C(6B)-C(5B)	103.46(14)	C(1B)-C(6B)-H(61B)	111.1(11)
C(5B)-C(6B)-H(61B)	112.2(12)	C(1B)-C(6B)-H(62B)	109.8(12)
C(5B)-C(6B)-H(62B)	111.1(12)	H(61B)-C(6B)-H(62B)	109(2)
C(4B)-C(7B)-C(1B)	94.30(13)	C(4B)-C(7B)-H(71B)	115.3(13)
C(1B)-C(7B)-H(71B)	113.1(12)	C(4B)-C(7B)-H(72B)	110.9(13)
C(1B)-C(7B)-H(72B)	112.5(13)	H(71B)-C(7B)-H(72B)	110(2)
O(21B)-C(20B)-O(22B)	123.5(2)	O(21B)-C(20B)-C(2B)	122.9(2)
O(22B)-C(20B)-C(2B)	113.37(14)	C(20B)-O(22B)-H(22B)	109(2)
O(31B)-C(30B)-O(32B)	123.1(2)	O(31B)-C(30B)-C(3B)	124.95(14)
O(32B)-C(30B)-C(3B)	111.87(13)	C(30B)-O(32B)-H(32B)	111(2)

Table 4. Anisotropic displacement parameters (A^2 x 10^3) for 1. The anisotropic displacement factor exponent takes the form: -2 pi^2 [h^2 a*^2 U11 + ... + 2 h k a* b* U12]

	U11	U22	U33	U23	U13	U12
C(1A)	18(1)	20(1)	18(1)	-1(1)	3(1)	2(1)
C(2A)	19(1)	16(1)	12(1)	0(1)	0(1)	1(1)
C(3A)	18(1)	16(1)	15(1)	0(1)	0(1)	2(1)
C(4A)	20(1)	15(1)	19(1)	-1(1)	3(1)	-1(1)
C(5A)	19(1)	26(1)	22(1)	-3(1)	-2(1)	0(1)
C(6A)	18(1)	26(1)	30(1)	-2(1)	-3(1)	6(1)
C(7A)	23(1)	21(1)	20(1)	2(1)	6(1)	-2(1)
C(20A)	26(1)	18(1)	16(1)	1(1)	2(1)	-1(1)
O(21A)	46(1)	24(1)	14(1)	4(1)	4(1)	1(1)
O(22A)	66(1)	16(1)	20(1)	0(1)	6(1)	-2(1)
C(30A)	17(1)	17(1)	20(1)	-2(1)	1(1)	1(1)
O(31A)	22(1)	29(1)	20(1)	-7(1)	5(1)	-6(1)
O(32A)	21(1)	34(1)	22(1)	-8(1)	5(1)	-9(1)
C(1B)	20(1)	22(1)	20(1)	1(1)	3(1)	-2(1)
C(2B)	17(1)	18(1)	19(1)	-1(1)	3(1)	1(1)
C(3B)	20(1)	18(1)	19(1)	-3(1)	2(1)	-2(1)
C(4B)	23(1)	29(1)	22(1)	-1(1)	-4(1)	-3(1)
C(5B)	24(1)	31(1)	35(1)	3(1)	0(1)	6(1)
C(6B)	27(1)	21(1)	28(1)	2(1)	1(1)	2(1)
C(7B)	32(1)	29(1)	17(1)	1(1)	3(1)	-1(1)
C(20B)	18(1)	21(1)	23(1)	2(1)	1(1)	0(1)
O(21B)	31(1)	23(1)	26(1)	4(1)	-7(1)	-8(1)
O(22B)	36(1)	22(1)	27(1)	6(1)	-9(1)	-7(1)
C(30B)	20(1)	19(1)	23(1)	-2(1)	3(1)	-4(1)
O(31B)	26(1)	33(1)	26(1)	-12(1)	8(1)	-11(1)
O(32B)	25(1)	36(1)	31(1)	-14(1)	11(1)	-14(1)

Table 5. Hydrogen coordinates (x 10^4) and isotropic displacement parameters (A^2 x 10^3) for 1.

	x	y	z	U(eq)
H(1A)	4378(9)	3862(21)	474(22)	25(5)
H(2A)	3281(9)	4017(19)	848(20)	19(5)
H(3A)	3055(9)	6137(20)	1763(21)	21(5)
H(4A)	3931(8)	7559(20)	2629(19)	14(4)
H(51A)	4331(9)	5618(20)	4534(21)	19(4)
H(52A)	4876(10)	6540(22)	3710(22)	29(5)
H(61A)	4688(10)	3582(23)	3264(22)	28(5)
H(62A)	5162(11)	4549(23)	2377(24)	33(5)
H(71A)	3909(10)	6345(21)	135(22)	26(5)
H(72A)	4657(10)	6494(23)	770(22)	31(5)
H(22A)	3541(13)	1728(30)	1154(33)	63(8)
H(32A)	2221(14)	4966(29)	4587(32)	62(8)
H(1B)	327(9)	3953(20)	9672(20)	20(5)
H(2B)	496(10)	6317(22)	8738(22)	28(5)
H(3B)	1500(9)	7123(21)	8726(21)	23(5)
H(4B)	2127(11)	5767(23)	10434(24)	36(6)
H(51B)	2234(11)	3634(23)	8655(24)	35(6)
H(52B)	2112(11)	3176(24)	10367(25)	38(6)
H(61B)	1175(9)	2872(21)	7963(23)	28(5)
H(62B)	1147(9)	2228(22)	9592(22)	25(5)
H(71B)	940(11)	5913(25)	11162(24)	37(6)
H(72B)	1241(10)	4353(24)	11638(24)	35(6)
H(22B)	257(14)	6124(30)	5079(32)	65(8)
H(32B)	2716(14)	6319(30)	6575(32)	64(8)

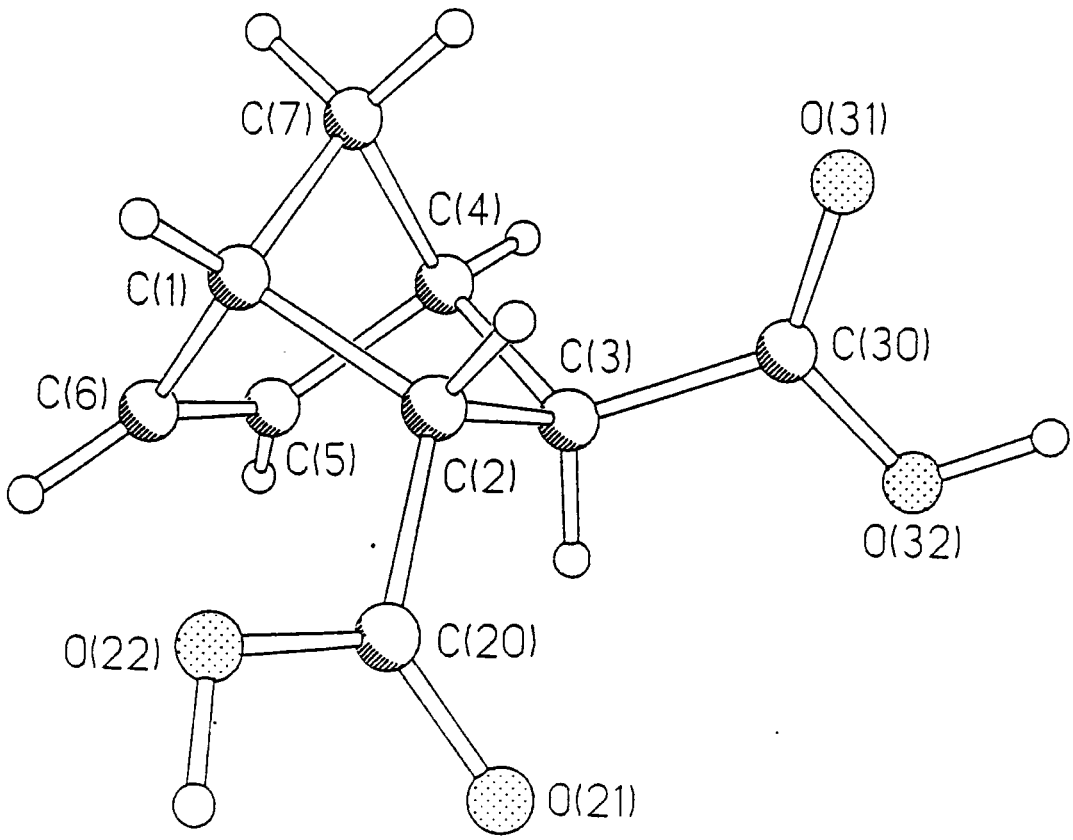

Appendix E4 : The crystal structure of 2-*endo*-3-*exo*-bicyclo[2.2.1]hept-5-ene-2,3-dicarboxylic acid.

Table 1. Crystal data and structure refinement for 1.

Identification code	97srv124
Empirical formula	C9 H10 O4
Formula weight	182.17
Temperature	150(2) K
Wavelength	0.71073 A
Crystal system	Monoclinic
Space group	P2(1)/c
Unit cell dimensions	a = 12.724(1) A alpha = 90 deg. b = 5.4014(3) A beta = 92.56(1) deg. c = 12.178(1) A gamma = 90 deg.
Volume	836.1(1) A^3
Z	4
Density (calculated)	1.447 g/cm^3
Absorption coefficient	0.115 mm^-1
F(000)	384
Crystal size	0.40 x 0.22 x 0.16 mm
Theta range for data collection	1.6 to 30.4 deg.
Index ranges	-13<=h<=17, -7<=k<=6, -16<=l<=15
Reflections collected	6317
Independent reflections	2301 [R(int) = 0.0396]
Observed reflections, I>2sigma(I)	1842
Absorption correction	None
Refinement method	Full-matrix least-squares on F^2
Data / restraints / parameters	2289 / 0 / 159
Goodness-of-fit on F^2	1.110
Final R indices [I>2sigma(I)]	R1 = 0.0465, wR2 = 0.0977
R indices (all data)	R1 = 0.0639, wR2 = 0.1153
Extinction coefficient	0.023(3)
Largest diff. peak and hole	0.320 and -0.241 e.A^-3

Table 2. Atomic coordinates (x 10^4) and equivalent isotropic displacement parameters (A^2 x 10^3) for 1. U(eq) is defined as one third of the trace of the orthogonalized Uij tensor.

	x	y	z	U(eq)
C(1)	2990(1)	1374(3)	2477(1)	19.6(3)
C(2)	2818(1)	2821(3)	3572(1)	16.9(3)
C(3)	2004(1)	4852(3)	3221(1)	17.2(3)
C(4)	1715(1)	4121(3)	1985(1)	21.7(3)
C(5)	2696(1)	4829(3)	1390(1)	25.8(3)
C(6)	3453(1)	3228(3)	1690(1)	23.9(3)
C(7)	1837(1)	1274(3)	2029(1)	22.8(3)
C(20)	3796(1)	3847(3)	4145(1)	19.0(3)
O(21)	3829(1)	5890(2)	4583(1)	28.5(3)
O(22)	4599(1)	2297(2)	4163(1)	27.4(3)
C(30)	1078(1)	4889(3)	3949(1)	18.3(3)
O(31)	574(1)	3043(2)	4181(1)	32.0(3)
O(32)	869(1)	7105(2)	4327(1)	33.4(3)

Table 3. Bond lengths [A] and angles [deg] for 1.

C(1)-C(6)	1.523(2)	C(1)-C(7)	1.543(2)
C(1)-C(2)	1.569(2)	C(1)-H(1)	0.99(2)
C(2)-C(20)	1.505(2)	C(2)-C(3)	1.556(2)
C(2)-H(2)	0.98(2)	C(3)-C(30)	1.506(2)
C(3)-C(4)	1.583(2)	C(3)-H(3)	0.98(2)
C(4)-C(5)	1.520(2)	C(4)-C(7)	1.547(2)
C(4)-H(4)	0.99(2)	C(5)-C(6)	1.333(2)
C(5)-H(5)	0.97(2)	C(6)-H(6)	0.99(2)
C(7)-H(71)	0.99(2)	C(7)-H(72)	0.99(2)
C(20)-O(21)	1.226(2)	C(20)-O(22)	1.320(2)
O(22)-H(22)	0.93(3)	C(30)-O(31)	1.225(2)
C(30)-O(32)	1.314(2)	O(32)-H(32)	0.94(3)
C(6)-C(1)-C(7)	100.84(13)	C(6)-C(1)-C(2)	106.28(12)
C(7)-C(1)-C(2)	98.71(12)	C(6)-C(1)-H(1)	116.7(11)
C(7)-C(1)-H(1)	117.8(11)	C(2)-C(1)-H(1)	114.1(11)
C(20)-C(2)-C(3)	113.22(12)	C(20)-C(2)-C(1)	115.69(12)
C(3)-C(2)-C(1)	103.54(11)	C(20)-C(2)-H(2)	105.1(11)
C(3)-C(2)-H(2)	110.1(11)	C(1)-C(2)-H(2)	109.2(11)
C(30)-C(3)-C(2)	112.07(12)	C(30)-C(3)-C(4)	114.12(12)
C(2)-C(3)-C(4)	102.07(11)	C(30)-C(3)-H(3)	107.2(11)
C(2)-C(3)-H(3)	110.4(11)	C(4)-C(3)-H(3)	110.9(11)
C(5)-C(4)-C(7)	100.56(13)	C(5)-C(4)-C(3)	103.26(12)
C(7)-C(4)-C(3)	101.30(12)	C(5)-C(4)-H(4)	118.8(11)
C(7)-C(4)-H(4)	117.0(11)	C(3)-C(4)-H(4)	113.4(11)
C(6)-C(5)-C(4)	107.74(14)	C(6)-C(5)-H(5)	127.0(12)
C(4)-C(5)-H(5)	125.0(12)	C(5)-C(6)-C(1)	107.75(14)
C(5)-C(6)-H(6)	127.9(12)	C(1)-C(6)-H(6)	123.8(12)
C(1)-C(7)-C(4)	94.01(12)	C(1)-C(7)-H(71)	113.9(11)
C(4)-C(7)-H(71)	114.0(11)	C(1)-C(7)-H(72)	112.7(12)
C(4)-C(7)-H(72)	112.7(12)	H(71)-C(7)-H(72)	109(2)
O(21)-C(20)-O(22)	123.55(14)	O(21)-C(20)-C(2)	123.02(14)
O(22)-C(20)-C(2)	113.39(13)	C(20)-O(22)-H(22)	108(2)
O(31)-C(30)-O(32)	122.92(14)	O(31)-C(30)-C(3)	123.82(14)
O(32)-C(30)-C(3)	113.26(13)	C(30)-O(32)-H(32)	111(2)

Table 4. Anisotropic displacement parameters (A^2 x 10^3) for 1. The anisotropic displacement factor exponent takes the form: -2 pi^2 [h^2 a*^2 U11 + ... + 2 h k a* b* U12]

	U11	U22	U33	U23	U13	U12
C(1)	22(1)	18(1)	19(1)	-3(1)	1(1)	-1(1)
C(2)	17(1)	18(1)	16(1)	1(1)	1(1)	-1(1)
C(3)	17(1)	17(1)	18(1)	1(1)	0(1)	0(1)
C(4)	24(1)	23(1)	17(1)	2(1)	-3(1)	0(1)
C(5)	38(1)	25(1)	15(1)	0(1)	5(1)	-4(1)
C(6)	28(1)	26(1)	18(1)	-5(1)	6(1)	-5(1)
C(7)	25(1)	21(1)	22(1)	-3(1)	-4(1)	-2(1)
C(20)	17(1)	24(1)	16(1)	-2(1)	1(1)	0(1)
O(21)	24(1)	25(1)	35(1)	-10(1)	-8(1)	3(1)
O(22)	19(1)	31(1)	32(1)	-12(1)	-7(1)	5(1)
C(30)	17(1)	19(1)	19(1)	0(1)	-2(1)	1(1)
O(31)	31(1)	22(1)	44(1)	-7(1)	18(1)	-6(1)
O(32)	37(1)	20(1)	45(1)	-4(1)	21(1)	0(1)

Table 5. Hydrogen coordinates (x 10^4) and isotropic displacement parameters (A^2 x 10^3) for 1.

	x	y	z	U(eq)
H(1)	3370(14)	-206(35)	2581(15)	21(5)
H(2)	2516(14)	1697(36)	4107(16)	24(5)
H(3)	2328(14)	6487(36)	3265(15)	22(5)
H(4)	1027(15)	4778(34)	1710(15)	23(5)
H(5)	2766(16)	6291(41)	937(17)	33(5)
H(6)	4206(16)	3313(37)	1537(16)	28(5)
H(71)	1354(15)	446(35)	2528(16)	24(5)
H(72)	1764(16)	497(37)	1296(17)	30(5)
H(22)	5148(19)	3003(46)	4586(20)	49(7)
H(32)	316(23)	7035(55)	4813(24)	73(9)

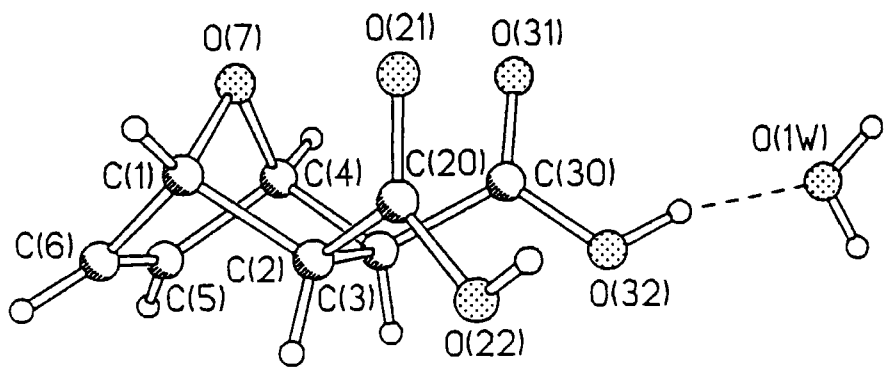

Appendix E5 : The crystal structure of *exo,exo*-7-oxabicyclo-[2.2.1]hept-5-ene-2,3-bis(carboxylic acid).

Table 1. Crystal data and structure refinement for 1.

Identification code	97srv125
Empirical formula	C8 H10 O6
Formula weight	202.16
Temperature	150(2) K
Wavelength	0.71073 A
Crystal system	Monoclinic
Space group	P2(1)/n
Unit cell dimensions	a = 7.348(1) A alpha = 90 deg. b = 8.913(1) A beta = 96.59(1) deg c = 13.277(1) A gamma = 90 deg.
Volume	863.8(2) A^3
Z	4
Density (calculated)	1.554 g/cm^3
Absorption coefficient	0.136 mm^-1
F(000)	424
Crystal size	0.4 x 0.4 x 0.3 mm
Theta range for data collection	2.76 to 25.99 deg.
Index ranges	-10<=h<=10, -11<=k<=12, -18<=l<=18
Reflections collected	5382
Independent reflections	1689 [R(int) = 0.0322]
Observed reflections, I>2sigma(I)	1442
Absorption correction	None
Refinement method	Full-matrix least-squares on F^2
Data / restraints / parameters	1674 / 0 / 168
Goodness-of-fit on F^2	1.069
Final R indices [I>2sigma(I)]	R1 = 0.0361, wR2 = 0.0744
R indices (all data)	R1 = 0.0467, wR2 = 0.0833
Extinction coefficient	0.036(3)
Largest diff. peak and hole	0.252 and -0.161 e.A^-3

Table 2. Atomic coordinates (x 10^4) and equivalent isotropic displacement parameters (A^2 x 10^3) for 1. U(eq) is defined as one third of the trace of the orthogonalized Uij tensor.

	x	y	z	U(eq)
C(1)	7188(2)	2335(2)	2709(1)	20(1)
C(2)	5307(2)	1526(2)	2420(1)	17(1)
C(3)	3949(2)	2830(2)	2637(1)	17(1)
C(4)	5332(2)	4059(2)	3062(1)	22(1)
C(5)	6267(2)	3510(2)	4072(1)	27(1)
C(6)	7424(2)	2449(2)	3856(1)	26(1)
O(7)	6758(1)	3865(1)	2408(1)	22(1)
C(20)	5100(2)	938(2)	1346(1)	18(1)
O(21)	5872(2)	1480(1)	662(1)	25(1)
O(22)	4027(2)	-257(1)	1217(1)	24(1)
C(30)	2711(2)	3420(2)	1730(1)	19(1)
O(31)	3003(2)	4608(2)	1312(1)	38(1)
O(32)	1272(2)	2591(1)	1470(1)	32(1)
O(1W)	-1490(2)	3797(2)	355(1)	45(1)

Table 3. Bond lengths [A] and angles [deg] for 1.

C(1)-O(7)	1.445(2)
C(1)-C(6)	1.517(2)
C(1)-C(2)	1.567(2)
C(1)-H(1)	0.98(2)
C(2)-C(20)	1.512(2)
C(2)-C(3)	1.580(2)
C(2)-H(2)	0.96(2)
C(3)-C(30)	1.517(2)
C(3)-C(4)	1.556(2)
C(3)-H(3)	0.95(2)
C(4)-O(7)	1.447(2)
C(4)-C(5)	1.516(2)
C(4)-H(4)	0.98(2)
C(5)-C(6)	1.325(2)
C(5)-H(5)	0.99(2)
C(6)-H(6)	0.96(2)
C(20)-O(21)	1.223(2)
C(20)-O(22)	1.325(2)
O(22)-H(22)	0.90(2)
C(30)-O(31)	1.226(2)
C(30)-O(32)	1.303(2)
O(32)-H(32)	0.89(3)
O(1W)-H(1W)	0.84(3)
O(1W)-H(2W)	0.80(3)
O(7)-C(1)-C(6)	102.17(12)
O(7)-C(1)-C(2)	102.00(11)
C(6)-C(1)-C(2)	105.80(12)
O(7)-C(1)-H(1)	111.2(10)
C(6)-C(1)-H(1)	117.9(9)
C(2)-C(1)-H(1)	115.9(10)
C(20)-C(2)-C(1)	112.35(12)
C(20)-C(2)-C(3)	115.48(12)
C(1)-C(2)-C(3)	100.07(11)
C(20)-C(2)-H(2)	107.6(10)
C(1)-C(2)-H(2)	111.7(10)
C(3)-C(2)-H(2)	109.6(10)
C(30)-C(3)-C(4)	110.57(13)
C(30)-C(3)-C(2)	116.37(12)
C(4)-C(3)-C(2)	100.61(11)
C(30)-C(3)-H(3)	107.2(10)
C(4)-C(3)-H(3)	112.2(10)
C(2)-C(3)-H(3)	110.0(10)
O(7)-C(4)-C(5)	101.90(13)
O(7)-C(4)-C(3)	100.69(11)
C(5)-C(4)-C(3)	107.74(13)
O(7)-C(4)-H(4)	109.9(10)
C(5)-C(4)-H(4)	120.5(10)
C(3)-C(4)-H(4)	113.7(10)
C(6)-C(5)-C(4)	106.04(14)
C(6)-C(5)-H(5)	129.5(11)
C(4)-C(5)-H(5)	124.2(11)
C(5)-C(6)-C(1)	105.2(2)
C(5)-C(6)-H(6)	129.8(12)
C(1)-C(6)-H(6)	124.7(12)
C(1)-O(7)-C(4)	95.59(11)
O(21)-C(20)-O(22)	122.79(14)
O(21)-C(20)-C(2)	123.96(14)
O(22)-C(20)-C(2)	113.22(13)
C(20)-O(22)-H(22)	110(2)

O(31)-C(30)-O(32)	123.2(2)
O(31)-C(30)-C(3)	122.60(14)
O(32)-C(30)-C(3)	114.08(13)
C(30)-O(32)-H(32)	111(2)
H(1W)-O(1W)-H(2W)	106(2)

Symmetry transformations used to generate equivalent atoms:

Table 4. Anisotropic displacement parameters (A^2 x 10^3) for 1. The anisotropic displacement factor exponent takes the form: -2 pi^2 [h^2 a*^2 U11 + ... + 2 h k a* b* U12]

	U11	U22	U33	U23	U13	U12
C(1)	19(1)	18(1)	25(1)	0(1)	1(1)	0(1)
C(2)	18(1)	15(1)	18(1)	2(1)	2(1)	0(1)
C(3)	18(1)	17(1)	17(1)	1(1)	4(1)	-1(1)
C(4)	24(1)	17(1)	25(1)	-3(1)	4(1)	-1(1)
C(5)	31(1)	27(1)	22(1)	-5(1)	-1(1)	-8(1)
C(6)	26(1)	25(1)	25(1)	1(1)	-7(1)	-6(1)
O(7)	22(1)	18(1)	26(1)	1(1)	5(1)	-3(1)
C(20)	17(1)	15(1)	22(1)	0(1)	1(1)	2(1)
O(21)	33(1)	23(1)	19(1)	-2(1)	6(1)	-8(1)
O(22)	26(1)	24(1)	23(1)	-7(1)	7(1)	-9(1)
C(30)	20(1)	17(1)	21(1)	0(1)	5(1)	2(1)
O(31)	41(1)	32(1)	38(1)	16(1)	-2(1)	-3(1)
O(32)	28(1)	29(1)	37(1)	3(1)	-10(1)	-2(1)
O(1W)	26(1)	59(1)	50(1)	26(1)	7(1)	-3(1)

Table 5. Hydrogen coordinates (x 10^4) and isotropic displacement parameters (A^2 x 10^3) for 1.

	x	y	z	U(eq)
H(1)	8215(22)	1953(19)	2380(12)	16(4)
H(2)	5150(22)	692(19)	2863(12)	18(4)
H(3)	3178(22)	2511(19)	3126(13)	18(4)
H(4)	4844(23)	5076(21)	2994(13)	20(4)
H(5)	5934(26)	3839(22)	4739(15)	36(5)
H(6)	8173(27)	1794(23)	4300(15)	36(5)
H(22)	4019(30)	-610(26)	578(18)	53(7)
H(32)	485(41)	3068(35)	1017(22)	89(10)
H(1W)	-2425(39)	3452(32)	575(21)	74(9)
H(2W)	-1842(31)	4259(28)	-150(18)	50(7)

APPENDIX F

CALCITE CRYSTAL DATA

Appendix F1: Tables of Calcite Crystal Data.

Monomer / $[Ca^{+2}]$: [monomer]	Nucleation density (mm^{-2})	Mean size (μm)	Standard deviation (±)
1b / 10:1	334	28.8	9.2
1b / 100:1	128	26.5	5.5
1b / 1000:1	160	35.1	8.1
2b / 10:1	320	29.0	9.3
2b / 100:1	92	39.7	14.3
2b / 1000:1	108	38.3	12.4
3a / 10:1	160	35.7	10.0
3a / 100:1	130	39.0	10.0
3a / 1000:1	84	39.7	9.3
4b / 10: 1	193	52.6	11.9
4b / 100:1	124	43.3	11.0
4b / 1000:1	60	41.5	10.4
control	136	27.8	10.9
1c / 10:1	516	9.6	3.9
2c / 10:1	496	13.0	6.2
3b / 10:1	432	10.0	5.1
4c / 100:1	627	9.9	3.8
control	644	10.1	6.2

Nucleation densities and size measurements of $CaCO_3$ crystals grown from supersaturated solutions of $Ca(HCO_3)_2$ with monomer additives.

Polymer / $[Ca^{+2}]$: [repeat unit]	Nucleation density (mm^{-2})	Mean size (μm)	Standard deviation (±)
Poly3F''	76	39.3	7.7
Poly3F'	236	29.2	6.3
Poly 3F	336	33.9	8.7
Poly1F'	108	29.5	7.0
Poly1F	864	37.2	7.7
control	268	36.6	13.85

Nucleation densities and size measurements of $CaCO_3$ crystals grown from supersaturated solutions of $Ca(HCO_3)_2$ with polymer additives.

Appendix F2: A molecular model of the crystal lattice structure of calcite.

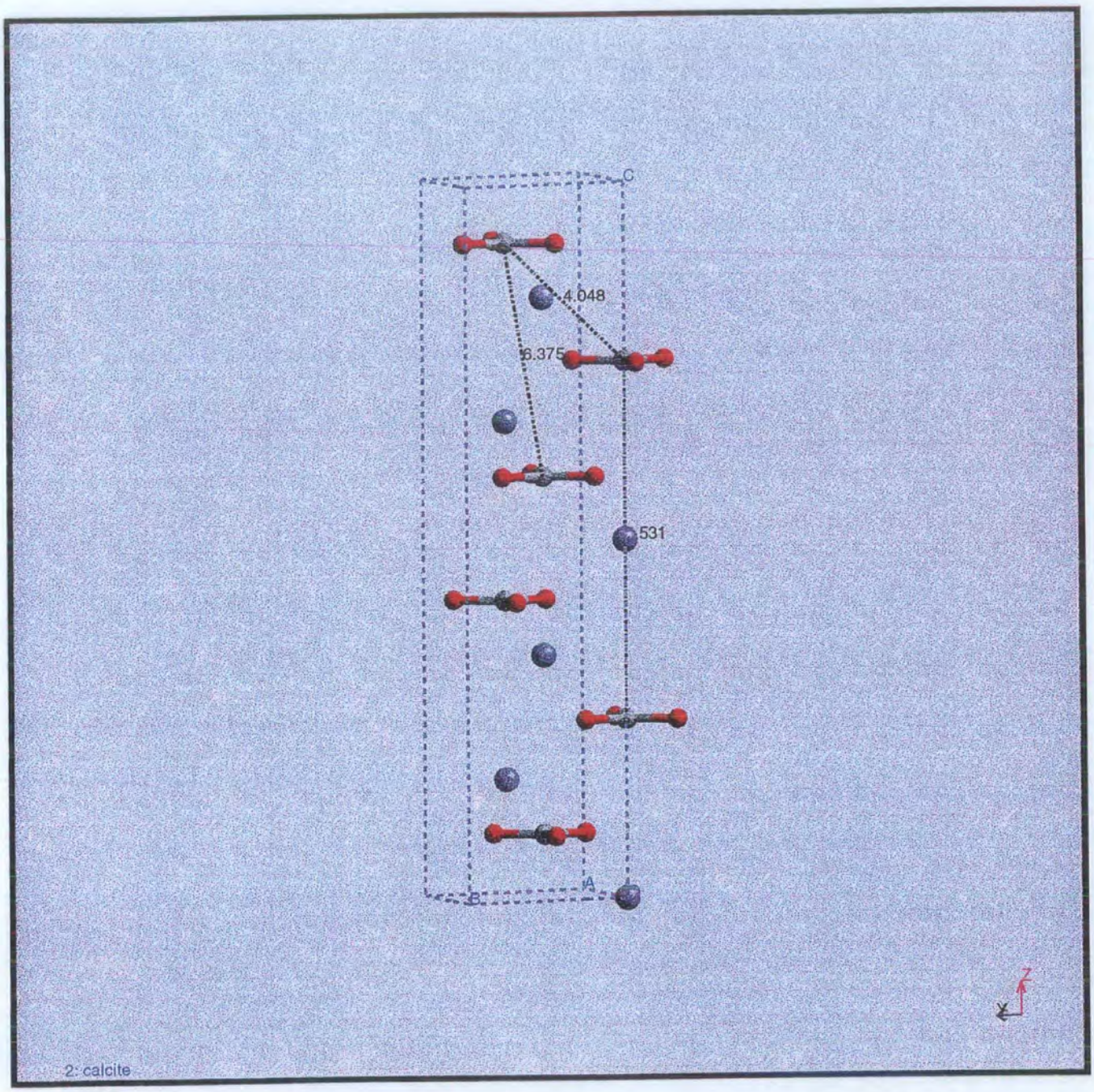

Appendix F3: A molecular model of the crystal lattice structure of aragonite.

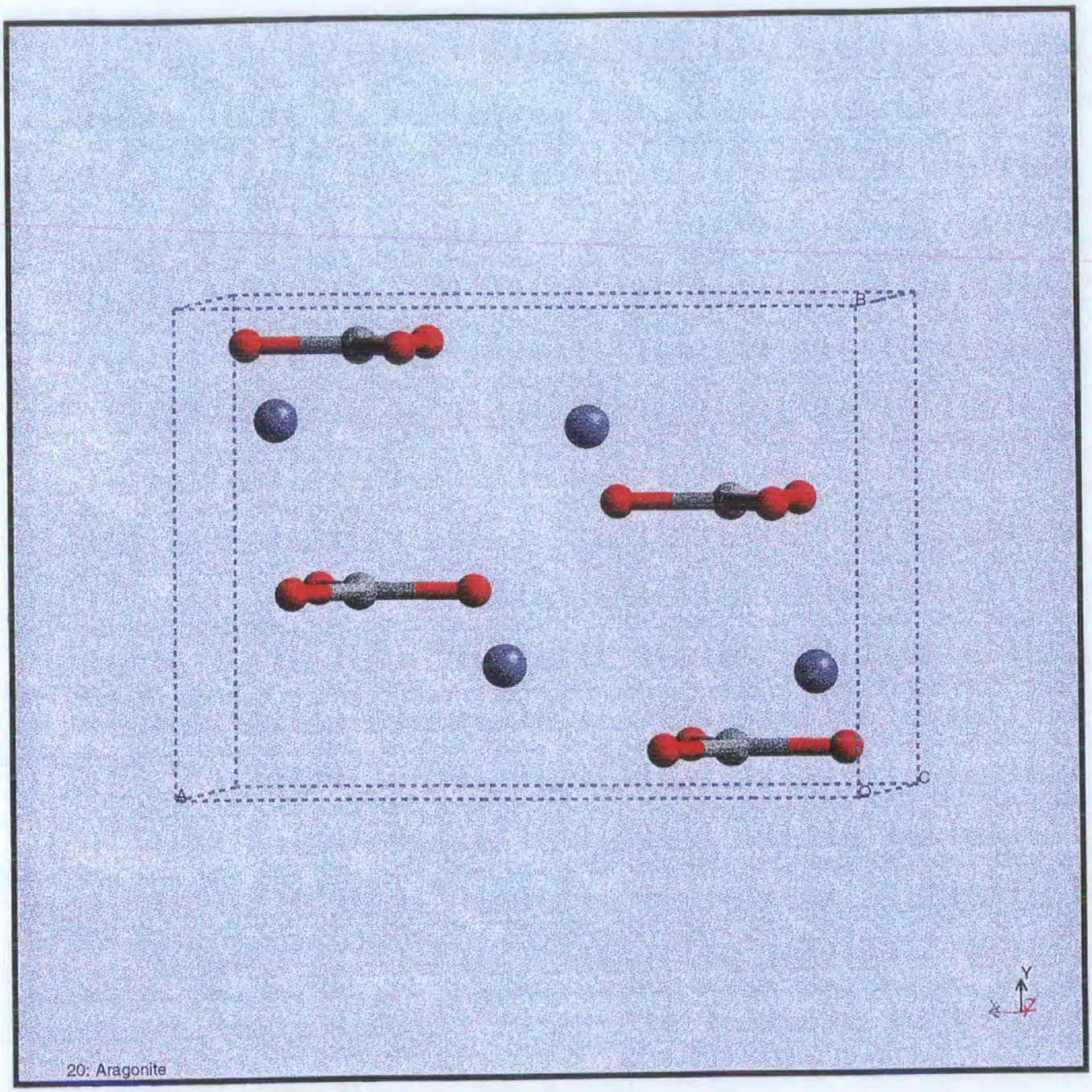

Appendix F4: A 3D molecular projection of the structure of a calcite rhomb viewed approximately perpendicularly to the (1 0 4) face.

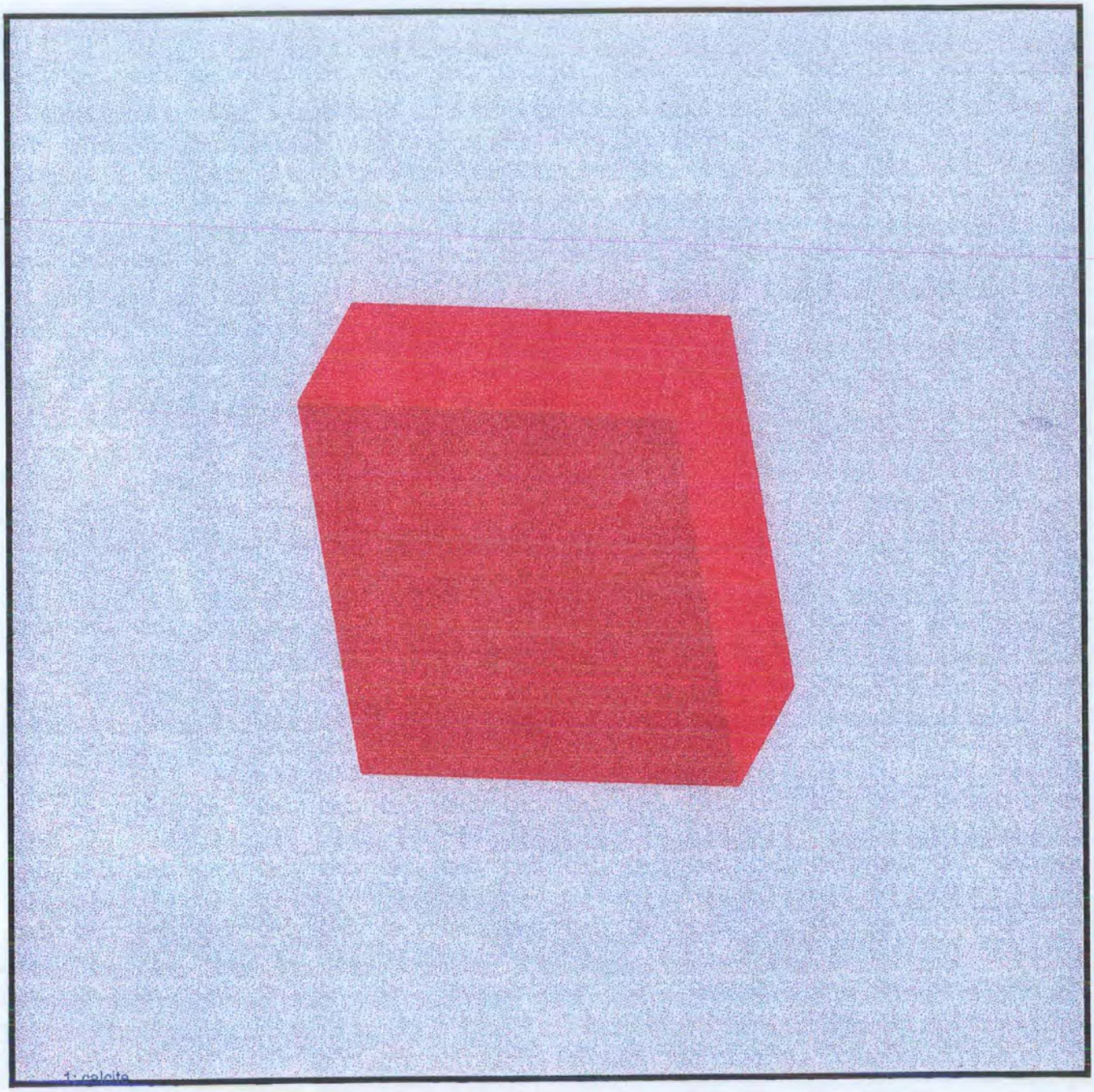

Appendix F5: A 3D molecular projection of the structure of a calcite rhomb viewed approximately parallel to the c-axis.

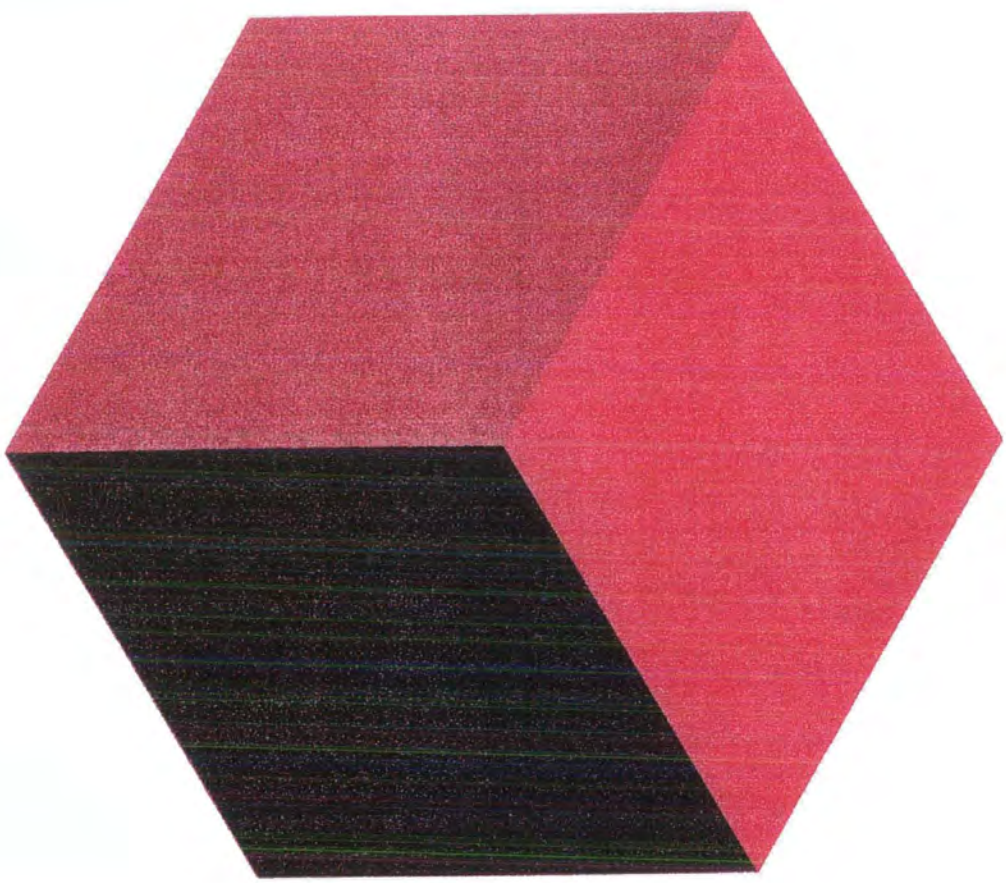

15: calcite

COLLOQUIA ATTENDED

1994

October 5 Prof. N. L. Owen, Brigham Young University, Utah, USA
Determining Molecular Structure - the INADEQUATE NMR way

November 2 Dr P. G. Edwards, University of Wales, Cardiff
The Manipulation of Electronic and Structural Diversity in Metal Complexes - New Ligands

November 9 Dr G. Hogarth, University College, London
New Vistas in Metal-imido Chemistry

November 10 Dr M. Block, Zeneca Pharmaceuticals, Macclesfield
Large-scale Manufacture of ZD 1542, a Thromboxane Antagonist Synthase Inhibitor

November 16 Prof. M. Page, University of Huddersfield
Four-membered Rings and b-Lactamase

November 23 Dr J. M. J. Williams, University of Loughborough
New Approaches to Asymmetric Catalysis

1995

January 18 Dr G. Rumbles, Imperial College, London
Real or Imaginary Third Order Non-linear Optical Materials

January 25 Dr D. A. Roberts, Zeneca Pharmaceuticals
The Design and Synthesis of Inhibitors of the Renin-angiotensin System

February 1 Dr T. Cosgrove, Bristol University
Polymers do it at Interfaces

February 8 Dr D. O'Hare, Oxford University
Synthesis and Solid-state Properties of Poly-, Oligo- and Multidecker Metallocenes

March 1 Dr M. Rosseinsky, Oxford University
Fullerene Intercalation Chemistry

March 22 Dr M. Taylor, University of Auckland, New Zealand
Structural Methods in Main-group Chemistry

April 26 Dr M. Schroder, University of Edinburgh

Redox-active Macrocyclic Complexes : Rings, Stacks and Liquid Crystals

May 4 Prof. A. J. Kresge, University of Toronto
The Ingold Lecture Reactive Intermediates : Carboxylic-acid Enols and Other Unstable Species

October 11 Prof. P. Lugar, Frei Univ Berlin, FRG
Low Temperature Crystallography

October 18 Prof. A. Alexakis, Univ. Pierre et Marie Curie, Paris,
Synthetic and Analytical Uses of Chiral Diamines

November 1 Prof. W. Motherwell, UCL London
New Reactions for Organic Synthesis

November 3 Dr B. Langlois, University Claude Bernard-Lyon
Radical Anionic and Psuedo Cationic Trifluoromethylation

November 8 Dr. D. Craig, Imperial College, London
New Strategies for the Assembly of Heterocyclic Systems

November 15 Dr Andrea Sella, UCL, London
Chemistry of Lanthanides with Polypyrazoylborate Ligands

November 17 Prof. David Bergbreiter, Texas A&M, USA
Design of Smart Catalysts, Substrates and Surfaces from Simple Polymers

November 22 Prof. I Soutar, Lancaster University
A Water of Glass? Luminescence Studies of Water-Soluble Polymers.

1996

January 10 Dr Bill Henderson, Waikato University, NZ
Electrospray Mass Spectrometry - a new sporting technique

January 24 Dr Alan Armstrong, Nottingham Univesity
Alkene Oxidation and Natural Product Synthesis

February 14 Dr J. Rohr, Univ Gottingen, FRG
Goals and Aspects of Biosynthetic Studies on Low Molecular Weight Natural Products

February 28 Prof. E. W. Randall, Queen Mary & Westfield College
New Perspectives in NMR Imaging

March 12 RSC Endowed Lecture - Prof. V. Balzani, Univ of Bologna
Supramolecular Photochemistry

October 16 Professor Ojima, Guggenheim Fellow, State University of New York at Stony Brook, Silylformylation and Silylcarbocyclisations in Organic Synthesis

October 22 Professor B. J. Tighe, Department of Molecular Sciences and Chemistry, University of Aston. Making Polymers for Biomedical Application - can we meet Nature's Challenge? Joint lecture with the Institute of Materials

November 6 Dr Melinda Duer, Chemistry Department, Cambridge
Solid-state NMR Studies of Organic Solid to Liquid-crystalline Phase Transitions

November 12 Professor R. J. Young, Manchester Materials Centre, UMIST
New Materials - Fact or Fantasy?
Joint Lecture with Zeneca & RSC

November 18 Professor G. A. Olah, University of Southern California, USA
Crossing Conventional Lines in my Chemistry of the Elements

November 20 Professor J. Earnshaw, Deptartment of Physics, Belfast
Surface Light Scattering: Ripples and Relaxation

November 27 Dr Richard Templer, Imperial College, London
Molecular Tubes and Sponges

1997

January 29 Dr Julian Clarke, UMIST
What can we learn about polymers and biopolymers from computer-generated nanosecond movie-clips?

February 12 Dr Geert-Jan Boons, University of Birmingham
New Developments in Carbohydrate Chemistry

February 18 Professor Sir James Black, Foundation/King's College London
My Dialogues with Medicinal Chemists

February 26 Dr Tony Ryan, UMIST
Making Hairpins from Rings and Chains

March 5 Dr J. Staunton FRS, Cambridge University
Tinkering with biosynthesis: towards a new generation of antibiotics

CONFERENCES ATTENDED

June 1995	Schloβmann Seminar in Biology and Materials Science, Mainz, Germany
July 1995	ISOM 95, University of Durham
Sept. 1995	IRC Club Meeting, University of Durham
Sept. 1996	IRC Club Meeting, University of Bradford
July/Aug 1996	The Macrogroup UK International Conference on 'Recent Advances in Polymer Synthesis', University of York
July 1997	ISOM 12, St. Augustine, Florida, USA

MODEL COMPOUNDS

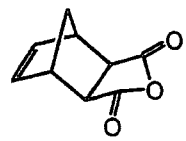

1a

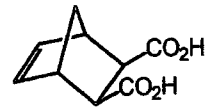

1b

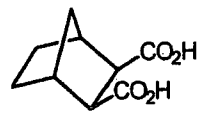

1c

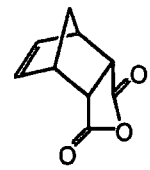

2a

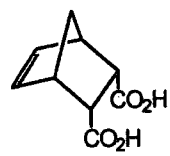

2b

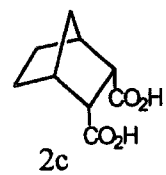

2c

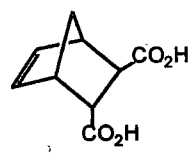

3a

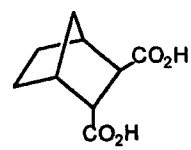

3b

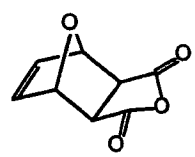

4a

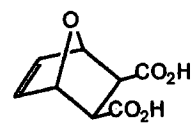

4b

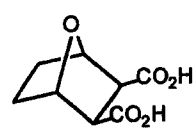

4c

POLYMERS

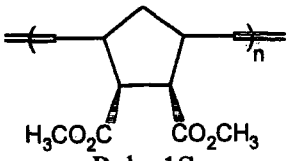

Poly-1S

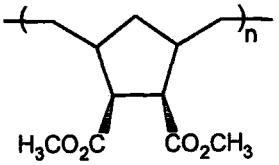

Poly-1P

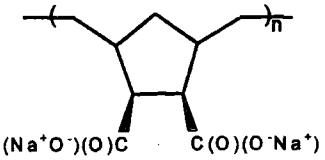

Poly-1F

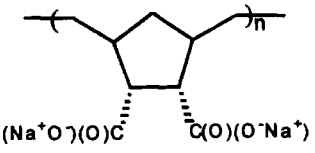

Poly-2F

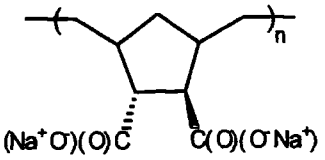

Poly-3F